ABSTRACT

Title of Document:	Structural Health Monitoring of Nonlinear Beam under Combined Translational and Rotational Vibration
	Ed Habtour, Doctorate of Philosophy, 2015
Directed By:	Professor Abhijit Dasgupta, Department of Mechanical Engineering

This study presents a nonlinear dynamic methodology for detecting fatigue damage precursor in an isotropic metallic cantilever beam exposed to harmonic transverse, rotation or combined – transverse and rotation – base excitations. The methodology accounts for important dynamic nonlinearities due to the complex loading generated by uniaxial and multiaxial nonlinear oscillations. These nonlinearities include: 1) structural stiffening due to gyroscopic motion and high-response amplitude at the structure fundamental mode, 2) structural softening due to inertial forces and gyroscopic loads, and localized evolution in the material microstructure due to fatigue damage and 3) cross-axis coupling due to multiaxial loading. The loading intensity and number of vibration cycles intensified these nonlinearities. The damage precursor feature is acquired by quantifying the reduction in the nonlinear stiffness term in the equation of motion due to localized evolution in the material micromechanical properties at high stress concentration regions. Nanoindentation studies near high stress concentration sites confirmed the evolution in the local micromechanical properties, as a function of loading cycles. The

nonlinear analytical approach tracks the degradation in the structural stiffness as a function of the nonlinear dynamic response for the uniaxial transverse or rotation base excitation. The change in the dynamic response due to damage precursor is captured experimentally. The nonlinear stiffness terms are found to be sensitive to fatigue damage precursor for translational or rotational excitation. Therefore, the nonlinear stiffness sensitivity to fatigue damage precursor appeared to be a promising metric for structural health monitoring applications. This method is applicable to a cantilever beam only. Additional investigations will be required to extend its applicability to more complex structures.

For the combined transverse and rotation base excitation, the experimental and analytic results demonstrated the importance of cross-axis coupling. The Experiments are performed using a unique multiaxial electrodynamic shaker with high controllability of phase and base excitation frequencies. The analytical model captures the modulation in the nonlinear dynamic response behavior seen in the experiments as a function of cross-axis coupling and the phase relation between the axes. Although the model is successful in capturing these general trends, it does not agree with the beam deflection absolute values obtained from the experiments. The discrepancy is due to fatigue damage accumulation during the experiments, which is manifested by a shift in the resonance frequency and an increase in the response amplitude.

STRUCTURAL HEALTH MONITORING OF NONLINEAR BEAM UNDER COMBINED TRANSLATIONAL AND ROTATIONAL VIBRATION

By

Ed Habtour

Dissertation submitted to the Faculty of the Graduate School of the
University of Maryland, College Park, in partial fulfillment
of the requirements for the degree of
Doctorate of Philosophy
2015

Advisory Committee:
Professor Abhijit Dasgupta, Mechanical Engineering, Chair
Professor Balakumar Balachandran
Professor Amr Baz
Professor Hugh Bruck
Professor Charles Schwartz

© Copyright by
Ed Habtour
2015

Acknowledgements

I would to express my gratitude to my advisor Professor Abhijit Dasgupta for taking the time to work with me on an Army relevant project. I am thankful for his guidance and suggestions in pursuing my PhD. I would also like to thank my committee members Balakumar Balachandran, Amr Baz, Hugh Bruck, and Charles Schwartz for their valuable suggestions.

I thank my management at the US Army, Dr. Mark Valco, Director of the Vehicle Technology Directorate at the Army Research Laboratory (ARL), Mr. Dy Le, Mechanics Division Chief at ARL, and Dr. David Mortin, Reliability Branch Chief at the Army Materiel System Activity Analysis, for their support throughout this project. Their support was instrumental in my ability to complete this project. I would like to thank Dr. Daniel Cole for providing nanoindentation measurements, which were performed at the US Army Research Laboratory (ARL). Dr. Samuel Stanton at the Army Research Office checked the derivations and for that I am very grateful. I would like to thank Mr. Roman Sridharan for help me navigating the control software for the Multiaxial vibration shaker. I would also like to express my appreciation to the following individuals at the US Army for their invaluable prospective and insights about Army's applications, environmental standards, reliability guidelines, and testing methodologies: Mr. William (Skip) Connon, Mr. Michael Pohland, Dr. Jarret Riddick, Dr. Mark Robeson and Prof. Volker Weiss.

Table of Contents

List of Tables

List of Figures

Chapter 1 Introduction

Complex multiaxial vibration environments have been the cause of many fatigue-induced failures, in part due to nonlinear dynamic response of flexible structures. As such, nonlinear vibration has long been an area of study. This work will extend on the available knowledge base to bridge nonlinear vibration with fatigue damage by exploiting the sensitivity of dynamic nonlinearities to damage precursors (incubators), under both uniaxial and multiaxial vibration.

1.1 Research Objectives

The motivation for the multiaxial vibration research efforts is prompted by the serious need to understand "real-world" complex dynamic systems operating in multiaxial vibratory environments such as helicopter blades, aircraft wings, ground vehicles, accelerometers, sensors, MEMS, energy harvesters and electronics. There is also a need to understand the nonlinear interactions and amplification of the response of structures exposed to simultaneous multiaxial dynamic loads that can be only simulated with multiaxial excitation shaker [1, 2]. The effects of vibration-induced fatigue damage and damage precursors and their effects on the structural nonlinear dynamic response (uniaxial and multiaxial response) are equally important.

Uniaxial shakers have been the prevailing tools for performing vibration testing because multiaxial shakers are not commonly available. Military and commercial standards were developed to mitigate this equipment limitation by proposing sequential uniaxial excitation as a compromise for simultaneous multiaxial excitation. When qualifying products subject to vibration, it is common therefore to test under uniaxial excitation, sequentially along different axes. The vibration profiles used for such uniaxial tests are provided in standards such as MIL-STD-810G. Current standards do not provide vibration methodologies for simultaneous

multiaxial vibration, and uniaxial excitations are applied to test products even though most field operational data indicate that these products are exposed to multiaxial dynamic loading environments. Sequential vibration testing along various orthogonal axes may be an acceptable proxy for the ideal of simultaneous multiaxial testing for linear systems, but is inadequate when it comes to nonlinear response. Unfortunately, uniaxial sequential testing may provide overly optimistic fatigue durability results [2, 3]. However, uniaxial excitations are applied to test products even though most field operational data indicate that these products are exposed to multiaxial dynamic loading environments. Thus, serious compromises must be made in the experimental design to perform meaningful tests on a uniaxial electrodynamic shaker, which are discussed in Chapter 3. For example, to simulate multiaxial vibrations, the MIL-STD-810G recommends performing the vibration tests by sequentially applying uniaxial excitation to a test article along three orthogonal axes (X, Y and Z), which can be accomplished by exciting the structure one axis at a time. Subsequently, the principle of superposition is employed, where the system outputs are added [4]:

$$X_{combined} = X_{out}(X_{input}) + X_{out}(Y_{input}) + X_{out}(Z_{input})$$

where $X_{out}(X_{input})$, $X_{out}(Y_{input})$, and , $X_{out}(Z_{input})$ are the output response as a function of X_{input}, Y_{input}, and Z_{input} inputs, respectively. Such superposition assumes that the structural dynamic response is linear.

Realistically, mechanical systems are not rigorously linear, and consequently linear models have limitations. In general, linear models are applicable only in restrictive conditions such as very low vibration amplitude. The multiaxial excitation environment introduces additional complexity to the structural response and thus enhances the nonlinear behavior. Thus, the principle of linear superposition may generate misleading results. Furthermore, increasing the

amplitude of oscillations along multiple axes amplifies the nonlinearity and exacerbates the inaccuracy of the superposition approach. To accurately estimate the dynamic response of a structure under multiaxial base excitations, it is important to include the nonlinearities in the analysis.

Typically, Hooke's law is a very good approximation for structures exhibiting linear elastic response to external forces. In long slender structures, most materials are capable of enduring reasonably large deformations before their intrinsic stress-strain characteristic shows any significant departure from the linear regime. Nonetheless, it is common to encounter dynamic nonlinearities in slender mechanical structures long before the intrinsic material nonlinearity is reached. For example, kinematic nonlinearity produces nonlinear hardening (stiffening) effect that appears in many engineering applications. The most noticeable nonlinear stiffening effect is in the form of a force that is proportional to the cube of displacement, x, in the equation of motion [5]. Thus, the restoring force becomes a function that combines linear and nonlinear stiffness components. For a stiffness element with linear and nonlinear (cubic) components, the force can be expressed as a function of displacement as follows:

$$F(x) = kx + \alpha k x^3$$

The element stiffness and nonlinear stiffness coefficients are k and α, respectively. Consequently, the linear equation of motion with nonlinear restoring force becomes the Duffing equation, which contains an additional nonlinear geometric term [6]. If α is positive, it can assist the linear restoring force, thus making the structure stiffer (hardening effect) and increasing its natural frequency. Unlike in the case of a linear system, the maximum value of the amplitude occurs at an excitation frequency higher than the structure natural frequency [5]. If α is negative, it will oppose the linear restoring force, thus making the structure softer (softening effect) and

reducing its natural frequency [7].

Furthermore, inertial nonlinearities often add to the damping mechanisms. Whenever forces acting on a structure are expanded up to the cubical displacement, they should be expected to add to the linear damping (which is proportional to the response velocity of the structure), a nonlinear damping term in the equation of motion [8]. The added nonlinear damping term (due to nonlinear inertial forces) increases with the motion amplitude. The nonlinear inertial damping effect is included in the dynamic analysis in this research effort. Additional sources of nonlinearity may appear due to practical reasons such as the manner in which the beam is clamped by its boundaries to the surrounding material and the multiaxial base loading. The prior will not be an issue in this study since our test article is a slender deformable cantilever beam clamped to a rigid fixture. The multiaxial loading contribution is a major focus in this research, and is discussed in Chapter 6.

Several researchers have investigated structures under nonlinear oscillatory loading, which are detailed in the Chapter 3. In these investigations dynamic models were developed in a consistent manner through the formulation of energy expressions and application of Hamilton's principle. The models included nonlinear dynamic stiffening and inertial softening terms. However, most of the research reported in the literature on these systems is focused on either transverse excitation or constant spin velocity with various combinations of free, clamped, and simply-supported boundaries [9, 10]. What is absent in the structural dynamics and structural health monitoring literature is a comprehensive theory for predicting the nonlinear response of structures exposed to simultaneous combinations of varying rotation and base excitation that includes all of the following nonlinearities: 1) geometric gyroscopic stiffening, 2) inertial and gyroscopic softening, 3) coupling between the rotational excitation (primary motion at the base),

and local displacement (secondary motion), and 4) cross-axis nonlinear coupling. These nonlinearities become important when modeling fast and flexible robot manipulators, robotic arms, and adaptive structures.

Furthermore, high cycle vibrations in these structures may lead to fatigue, and instability. Thus, monitoring structural health of the system is important in aiding vibration control to correct the system's operational drift due to fatigue damage accumulation and to prolong the life cycle.

The objective of this study is to develop a fatigue damage precursor detection method for monitoring the structural degradation of an isotropic cantilever beam prior to crack initiation. *Fatigue damage precursor* is defined here as any observable early degradation of the material microstructural morphology and resulting changes in or the physical properties of a structure, prior to any detectable fatigue crack initiation. Examples of measurable precursors to fatigue crack development may involve, but are not restricted to, changes in the microstructure, chemical composition, electrical signal, acoustic response, thermal signature or mechanical response of a structure. Recognizing a damage precursor requires classifying and recognizing damage incubators and initiators such as residual or compressive stress, phase changes, and microvoids. This study presents a nonlinear vibration methodology to detect fatigue damage precursor by exploiting the sensitivity of the nonlinear stiffness term in the equations of motion to material fatigue degradation. This approach appears to be promising health monitoring metric for predicting fatigue damage precursor. This study shows that the nonlinear vibration-based measurement techniques can successfully sense the development of fatigue damage precursor too well in advance of actual fatigue crack initiation. Localized material evolution due to accumulative damage (change in the apparent material stiffness as a function of loading cycles)

at high stress concentration sites is confirmed through nanoindentation.

1.2 Research Objectives

The objectives of this research are as follows:

- Experimentally demonstrate the sensitivity nonlinear stiffness to fatigue damage precursor in a cantilever metallic beam exposed to transverse harmonic base excitation.
- Experimentally demonstrate the sensitivity nonlinear stiffness to damage evolution in a cantilever metallic beam exposed to rotational harmonic base excitation.
- Develop uniaxial nonlinear analytical dynamic model for transverse excitation to model the effect of damage precursor on the structural response of a cantilever beam, which includes inertial and geometric nonlinearities.
- Develop uniaxial nonlinear analytical dynamic model for rotational excitation to model the effect of damage precursor on the structural response of a cantilever beam, which includes inertial and geometric nonlinearities and gyroscopic effects.
- Experimentally study the nonlinear dynamic response of a cantilever beam under combined rotation and transverse base vibration using multiaxial electrodynamic shaker
- Develop a model to study the nonlinear response of a cantilever beam due to varying phase angle between rotation and transverse excitation, while holding the rotation and transverse base amplitudes constants. The model includes inertial and geometric nonlinearities, gyroscopic effects and cross-axes contribution.

1.3 Dissertation Overview

The focus of this research effort is on studying the nonlinear dynamic response of structures under transverse, rotation and combined multiaxial vibration loading. An additional focus is on developing a nonlinear dynamic methodology for detecting and quantifying fatigue

damage precursor in isotropic metallic cantilever beam, prior to fatigue crack initiation, based on measurement of the structure nonlinear response to harmonic base excitation. The effort that instigated this research is document in Appendix A, where a notched cantilever beam was exposed to broadband stationary random vibration excitation. Linear mechanics principles were applied to determine the time to failure in the frequency domain. However, the major focus of this research is to study the nonlinear dynamic response of structures under transverse, rotation and combined multiaxial vibration loading. A damage precursor feature is extracted for cantilever beams by quantifying the reduction in the nonlinear stiffness due to localized microscopic material softening. The reason for using a cantilever beam in this research effort is because the beam is one of the fundamental elements of an engineering structure. The dynamics of a beam can be used as an approximate idealization of complex structures such a helicopter rotor blades, spacecraft antennae, flexible satellites, airplane wings, robotic arms, and electronic interconnects. In other words, studying the dynamic response, both analytically and experimentally, of a simple structural element under various base excitation conditions may provide insights into the behavior of complex structures under similar loading.

This dissertation is structured into individual chapters, with each chapter comprising a stand-alone publication with multiple authors. Consequently, there is some amount of necessary redundancy across the chapters, in the interest of completeness, to make each chapter self-contained. The contribution of each other is stated in the beginning of each chapter. Chapter 2 was published in the *ASM Journal of the Failure Prevention and Analysis*, and it describes a modified computational approach to model large electronic components exposed to multiaxial random vibrations using Spectral Finite Element Method (S-FEM). The approach uses a multiscale approach with local 3-dimensional S-FEM and global 2-Dimensional FEM model to reduce computational time. Chapter 3 is a comprehensive review of the response and damage of linear and nonlinear systems under

multiaxial vibrations, and includes the experimental results for the durability and nonlinear response of large electronic components exposed to multiaxial random. The paper was published in *the Journal of Shock and Vibration*. Chapter 4 is an article currently under review in the *Journal of Structural Control and Health Monitoring (SCHM)*. The paper contains a nonlinear vibration-based methodology for exploiting the sensitivity of the nonlinearities in the equation of motion to damage precursor in isotropic cantilever beam, prior to fatigue crack initiation, based on measurement of the structure nonlinear response to transverse base excitation. The experimental results are utilized to update the nonlinear stiffness in the equation of motion. Chapter 5 is an article currently under review in the *International Journal of nonlinear Mechanics (IJNM)*, which provides a promising analytical approach to model and predict the response of cantilever beam exposed to a varying rotation base excitation. This type of dynamic load reveals interesting nonlinearities due to the gyroscopic effects due to the harmonic base rotation. The model takes into account the evolution of the material due to damage accumulation. Chapter 6 is an article being prepared for publication in *Shock and Vibration* Journal. The article presents analytical and experimental results that show structural dependency on the phase difference between different axes of excitation, when a structure is exposed to multiaxial vibration. Results show that cross-axis coupling between rotation and simultaneous transverse excitations promoted nonlinear amplification/attenuation in the response of the structure, depending on the phase relationship between the rotational and the translational excitations. Chapter 7 presents the overall conclusions and contributions of this dissertation, discusses its limitations and suggests relevant future work. The complete mathematical derivations of the models are provided in Appendices B and C.

1.4 References

[1] E. Habtour, C. Choi, G. Drake, A. Dasgupta, and M. Al- Bassyiouni, “Improved reliability testing with multiaxial electrodynamics vibration,” in *Proceedings of the 56th Annual Reliability and Maintainability Symposium*, San Jose, Ca, USA, 2010.

[2] Ernst, M., E. Habtour, A. Dasgupta, M. Pohland, M. Robeson, and M. Paulus. "Comparison of Electronic Component Durability Under Uniaxial and Multiaxial Random Vibrations." *Journal of Electronics Packaging* 137.1, 2015.

[3] W. E. Whiteman and M. S. Berman, “Fatigue failure results for multi-axial versus uniaxial stress screen vibration testing,” *Shock and Vibration*, vol. 9, no. 6, pp. 319–328, 2002.

[4] Nayfeh, A. H. *Introduction to Perturbation Techniques*. New York: Wiley, 1981.

[5] Balachandran, B., and E. B. Magrab. *Vibrations*. 2nd ed. Toronto, Canada: Cengage Learning, 2009.

[6] Virgin, L. N. *Introduction to Experimental Nonlinear Dynamics: A Case Study in Mechanical Vibration*. Cambridge, U.K.: Cambridge UP, 2000.

[7] L. G. Villanueva, R. B. Karabalin, M. H. Matheny, D. Chi, J. E. Sader, and M. L. Roukes, “Nonlinearity in nanomechanical cantilevers,” *Physical Review B*, vol. 87, Article ID 024304, 2013.

[8] Hamdan, M. N., and M. H. F. Dado. "Large Amplitude Free Vibrations Of A Uniform Cantilever Beam Carrying An Intermediate Lumped Mass And Rotary Inertia." *Journal of Sound and Vibration* 206.2 (1997): 151-168.

[9] Habtour, E., W. Connon, M. F. Pohland, S. C. Stanton, and M. Paulus. "Review of Response and Damage of Linear and Nonlinear Systems under Multiaxial Vibration." *Shock and Vibration*, vol. 2014, Article ID 294271, 2014-a. doi:10.1155/2014/294271.

[10] Habtour, E., Cole, D. P., Riddick, J. C., Weiss, V., Robeson, Sridharan, R., and Dasgupta, A., "Detection of Fatigue Damage Precursor Using a Nonlinear Vibration Approach", *Journal of Structural Health Monitoring*, (under review).

Chapter 2 Approach To Improve Electronics Reliability Under Complex Vibration Conditions

Published in ASM International Journal of Failure Analysis and Prevention, 2012

This was published in the *ASM Journal of the Failure Prevention and Analysis*, and it describes a modified computational approach to model large electronic components exposed to multiaxial random vibrations using Spectral Finite Element Method (S-FEM). The approach uses a multiscale approach with local 3-dimensional S-FEM and global 2-Dimensional FEM model to reduce computational time. The authors are Mr. Ed Habtour, Mr. Cholmin Choi, Dr. Michael Osterman and Professor Abhijit Dasgupta. Mr. Ed Habtour (first author) conducted the analytical and FEM modeling. Mr. Mr. Cholmin Choi provided the multiaxial shaker table response. Dr. Michael Osterman provided assistance designing the circuit cards. Professor Dasgupta provided technical and academic guidance in this effort.

Abstract:

The functionality of next-generation the US Army's platforms, such as the Small Unmanned Ground Vehicles (SUGV) and Small Unmanned Arial Vehicles (SUAV), is strongly dependent on the reliability of electronically-rich devices. Thus, the performance and accuracy of these systems will be dependent on the life cycle of electronics. These electronic systems and the critical components in them experience extremely harsh environments such as shock and vibration. Therefore, it is imperative to identify the failure mechanisms of these components through experimental and virtual failure assessment. One of the key challenges in re-creating life-cycle vibration conditions during design and qualification testing in the lab is the re-creation of simultaneous multi-axial excitation that the product experiences in the field. Instead, the

common practice is to use sequential single-axis excitation in different axes or uncontrolled multi-axial vibration on repetitive shock shakers. Consequently, the dominant failure modes in the field are sometimes very difficult to duplicate in a laboratory test.

This chapter presents the joint effort by the US Army Materiel Systems Analysis Activity (AMSAA) and the Center of Advanced Life Cycle Engineering (CALCE) at the University of Maryland to develop test methods and analytic models that better capture unforeseen design defects prior to the qualification phase, by better replication of the life-cycle vibration conditions. One approach was to utilize a novel Multi-Degrees of Freedom (M-DoF) electrodynamic shaker to ruggedize designs for fatigue damage due to multi-directional random vibration. The merits of vibration testing methods with six-DoF shaker and cost saving associated with such an approach will be addressed in this chapter. There is a potential for M-DoF to detect critical design flaws earlier in the development cycle than has been traditionally possible with existing shaker technologies; and therefore produce more cost effective, reliable and safe systems for the warfighters.

2.1 Introduction

In military applications, electronic devices play a vital role in mission success. These devices, which provide control, guidance, communication, and reconnaissance, are vital components in modern unmanned vehicular applications. This trend in modern warfare has increased the complexity of electronic equipment, especially in low volume, highly sophisticated, and dense electronic systems. Figure 2-1 and Figure 2-2 show the SUGV and SUAV [1]. These modern systems take advantage of the remarkable advances made in low cost commercial electronics. It is becoming progressively more beneficial to use such components in military applications for improved computational performance, on-demand availability,

addressing obsolescence, and providing state-of-the-art capabilities. This current movement of using commercial-off-the-shelf (COTS) electronics and devices for military applications has led to concerns about their reliability in harsh battlefield environments. Typically, these types of systems are subjected to various complex loadings, including shock and vibration, during their life-cycle. These loads may impose significant stresses on the PCB substrate, component packages, leads and solder joints [1]. These stresses can be due to a combination of bending moments in the PCB and/or inertias of components. They may lead to several failures such as delamination in the PCB, solder joint fatigue, lead fracture or structural damage to components.

Figure 2-1. Small Unmanned Ground Vehicle (SUGV)

Figure 2-2. Small Unmanned Aerial Vehicle (SUAV)

When conducting PoF analysis of electronic systems, the large variety of package types is perhaps one of the main challenges to consider, since failure may occur due to one of several failure drivers. One of the most frequent failures in electronics is the package to board interconnect in heavy components with large center of mass (CM) and low profile surface mount packages (SMT). The failure in heavy components with large CM can be predominantly due to inertial loads. While in light low-profile SMT packages, the dominant stress source can be due to

board deflection. Both of these failure drivers may compete in heavy and large electronic components such as inductors and transformers. Depending on the architecture of these components, they can also significantly alter the local vibration response. It is common to increase the board stiffness to reduce the overall response of the PCB. However, increasing the board stiffness may increase local bending moments.

The current available vibration fatigue life prediction methods for large/heavy components force reliability engineers to use one of two extremes. One method is to construct a detailed 3-D FEA. This approach may be impractical when dealing with large circuit card assemblies (CCA) containing many components; each with multiple leads and solder joints. Further, these methods can be computationally expensive and their accuracy may be compromised due to assumptions in material properties and support conditions. The other extreme is to use simple empirical equations. Probably the best-known empirical method to estimate component life under vibration is Steinberg's model [2]. However, these models are also limited to a defined set of boundary conditions and package structures. Therefore, they cannot be the only design tool to evaluate new products or emerging technologies with a high level of confidence.

This chapter is concerned with a rapid analytical technique for analyzing heavy/large components that can provide an engineer high fidelity assessment while reducing the computational time. A PoF approach was developed that may improve the reliability assessment of CCAs containing large/heavy components. This approach is a hybrid-method that combines 2-D and 3-D FEA where the mechanical and inertial properties of the components at the local level are taken into consideration. These properties may be used to extract an accurate natural

frequency value for the CCA. Nonetheless, this approach may not eliminate the need to address the components inertial effects.

2.2 Physics of Failure Approach

2.2.1 Simplified Single Degree of Freedom Approach

As mentioned above one of the most known simplified models for analysis of PCB vibration fatigue is Steinberg's model [2]. Steinberg model defines a critical maximum vibration induced displacement for components as [2]:

$$d = \frac{0.00022\,B}{C\,h\,r\,\sqrt{L}} \qquad \text{Eq. 2-1}$$

where B is the length of the PCB edge parallel to the component located at the center of the board in units of inches. L and h are the length of the component and the thickness of the PCB in inches, respectively. C is a constant coefficient, which depends on the component type, and r is the relative position factor of the component relative to the PCB. The Steinberg model assumes a dynamic single-amplitude displacement for the PCB This model is valid only for single-degree-of-freedom (SDOF) systems. The out-of-plane root-mean-square (rms) displacement is calculated as follows [2]:

$$Z_{rms} = \frac{9.8\,G_{rms}}{f_n^2} \qquad \text{Eq. 2-2}$$

where f_n is the natural frequency and G_{rms} is the root-mean-square output acceleration. The G_{rms} can be estimated using Miles' equation:

$$G_{rms} = \sqrt{\frac{\pi\,P f_n Q}{2}} \text{ and } Q = \sqrt{f_n} \qquad \text{Eq. 2-3}$$

where P is the input Power Spectral Density and Q is the transmissibility. Steinberg states when the dynamic single-amplitude displacement at the center of the PCB is limited to the critical value d, the component is expected to achieve a fatigue life of 20 million stress reversals in a random vibration environment and 10 million stress reversals under sinusoidal vibration. One must be cautious when using this model since Steinberg's empirical approach is based on a specific experimental data set from a particular collection of specimen architectures and boundary conditions. Thus, this empirical approach may be more accurate when applied to PCBs assembled in exactly the same manner. The drawback of his model is that it cannot be used outside the range and configuration of the assembly used in the derivation of the model. It cannot be used to evaluate new products or emerging technologies with high confidence. Nonetheless, this approach may help designers obtain a rough estimate of the acceleration factors for accelerated vibration durability tests and for comparing the relative dynamic robustness of competing designs.

Electronically dense military platforms have to endure severe and complex dynamical loading conditions during the life cycle, resulting in high-cycle fatigue. For complex structure and dynamic loading the Steinberg's model alone may not be an adequate approach for assessing the survivability of military devices.

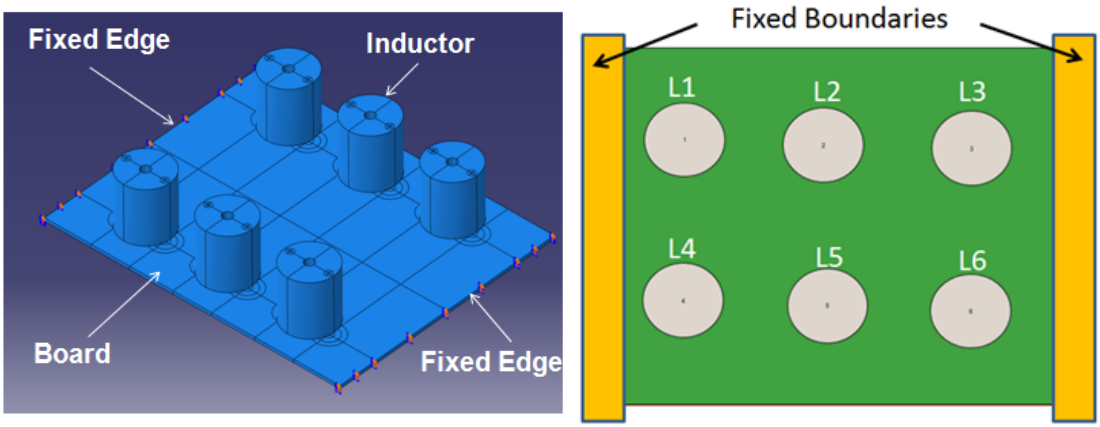

Figure 2-3 CAD model of PCB with large components

In this study a 127x101.6 mm^2 PCB with six large/heavy inductors was designed, as shown in Figure 2-3. The inductor geometry is shown in Figure 2-4. The PCB was assumed to be fixed (clamped) along the short edges of the board, as illustrated in Figure 2-4 with the red dots. The objective is to evaluate 2-D and 3-D FEA approaches to assess the reliability of large electronic components. A more cost effective approach combining 2-D and 3-D FEA was developed to extract the natural frequency of the PCB and more accurately determine the maximum deflection, curvature, and stress. The goal is to evaluate whether this approach can detect critical failure risks early in the development cycle. The modeling also provides effective guidance for future vibration testing using a multi-degree-of-freedom (M-DoF) electrodynamic (ED) shaker. The test results will be used in the future to evaluate the accuracy of this modeling approach and to assess the effect of the local inertia of large/heavy components on the fatigue life of interconnects.

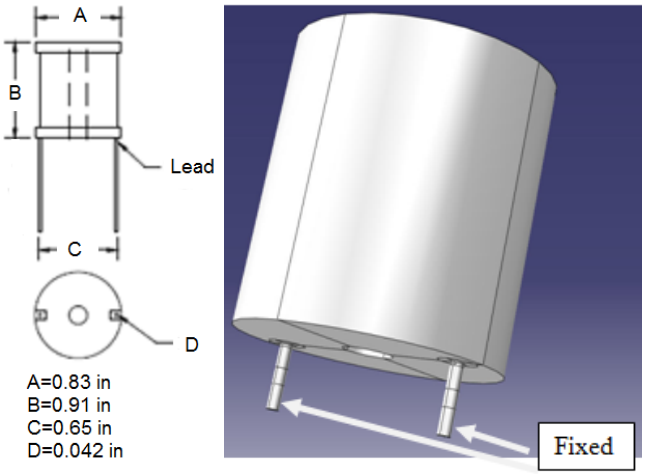

Figure 2-4 Large inductor used in this study

2.2.2 Two-Dimensional Approach

A more detailed approach than the Steinberg model when conducting PoF analysis is a simplified 2-D (plate or shell) FEA of a PCB. The mass of the components are "smeared" over their PCB footprints to reduce computational time and cost. This method was developed by Pitarresi and Primaver where they performed experimental and FEA modeling work to characterize the natural frequencies, mode shape, and transmissibility at the board level [3]. Later, they used the simple plate vibration models, using the property smearing approaches, as well as detailed finite element modeling. In the case where the local inertias are significant, a traditional 3-D FEA might be necessary. Transforming a 3-D PCB model in Figure 2-3 to 2-D FEA using the smeared technique is shown in Figure 2-5. The PCB was discretized into rectangular shell elements, as shown in Figure 2-5. The individual elements were defined by four nodes. Typically in traditional FEA, the shell element nodes in a continuum structure have six-DoF. For PCB PoF analysis, the number of degrees of freedom was reduced to three plate DOFs, which includes one out of plane displacement, u_z, and two rotations about the two orthogonal

axes in the plane of the board. The displacement of each node is driven by the element's stiffness matrix. The element stiffness matrix is a function of the element geometry and the constitutive material properties. Because PCBs have multilayer composite construction, laminated plate theory was used to calculate the element stiffness matrix. The layers' geometric and material properties were designed symmetrically about the middle surface of the board. Therefore, the bending-extension coupling effect was not a cause for concern and the extension and the coupling matrixes were eliminated [4]. This led to a simplified plate equation with only the bending stiffness:

$$\begin{Bmatrix} M_x \\ M_y \\ M_{xy} \end{Bmatrix} = \begin{bmatrix} D_{11} & D_{12} & 0 \\ D_{12} & D_{22} & 0 \\ 0 & 0 & D_{33} \end{bmatrix} \begin{Bmatrix} \kappa_{xx} \\ \kappa_{yy} \\ 2\kappa_{xy} \end{Bmatrix} \quad \text{Eq. 2-4}$$

where $\{M\}$ and $\{\kappa\}$ are the moment resultant and board curvature written as vectors in reduced Voigt notation. The flexural (or bending) rigidity matrix, $[D]$, is the measure of how easily the board bends. $[D]$ can be calculated as follows:

$$D_{ij} = \frac{1}{3}\sum_{k=1}^{n} Q_{ij}^{k}(h_k^3 - h_{k-1}^3) \quad for\ i\ ,j = 1,2,3 \quad \text{Eq. 2-5}$$

where i and j coincide with the natural axes of the material and n is the number of layers in the PCB. The distance of the outermost fiber of the k^{th} layer from the mid-surface of the plate is h_k. Q^k_{ij} is the material stiffness matrix for the material in layer k [4] for additional information on how to calculate Q_{ij}. For a uniform, symmetrical, homogeneous composite construction the board rigidity, $D_{11}=D_{22}=D$, may be approximated as:

$$D = \frac{E\,t^3}{12(1-\nu^2)} \qquad \text{Eq. 2-6}$$

where E is the elastic modulus, t is the board thickness and ν is the Poisson's ratio. After obtaining the [D] matrix, the board curvature can be calculated from the simplified plate equation (4). The smeared-technique was then implemented using 2-D shell elements.

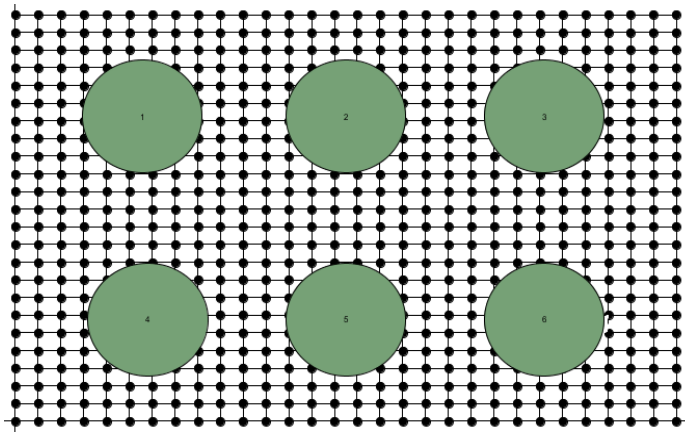

Figure 2-5. 2-D FEA of PWB and inductors, using smearing method

The smeared technique includes the mass of the board and components by simply increasing the mass of the shell element under the footprint of each component. However, the component stiffness is not included in this simplified smearing approach. The first mode natural frequency for this board, using this smearing approach, is 108 Hz.

However, for large/heavy thru-hole components, some 2-D codes may approximately include the stiffening effect of the components. In this approach, the mass and stiffening effects are included by locally increasing the PCB's density and Young's modulus, respectively. Unfortunately, such an approach does not address the inertias and radius of gyration of large components with high stand-off. These effects can cause additional stresses in the leads and interconnects and a traditional 3-D FEA might be necessary to analyze this effect.

Table 2-1 Inductor modal response for various standoff heights

Standoff Height (mm)	Mode I (Hz)	Mode II (Hz)	Mode III (Hz)
0.5	108	1733	3266
1.0	102	1657	3161
1.5	98	1560	2682
2.0	94	1430	2200

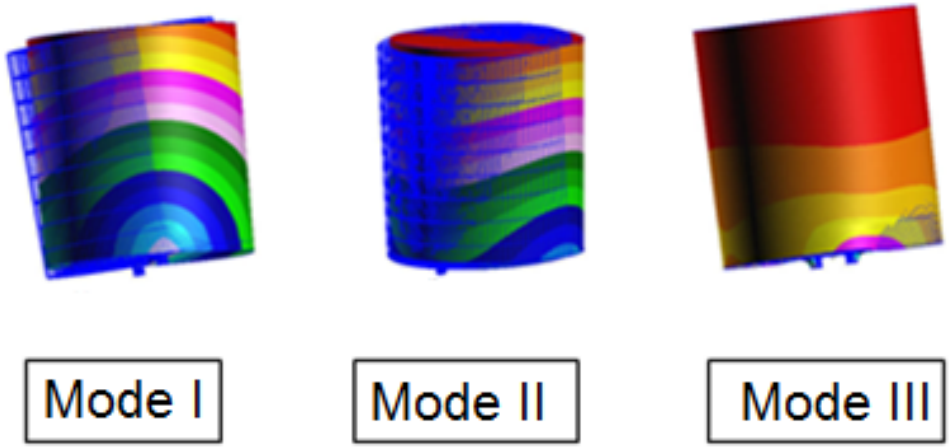

Figure 2-6. Inductor modal shapes when lead base is fixed

2.2.3 Three Dimensional Approach

In this study, modal analyses were first conducted on just the inductor with various standoff heights as shown in Table 2-1. In this task, the component leads were assumed to be "fixed" at the interface with the PWB, as shown in Figure 2-4. As expected the modal frequency dropped as the standoff height increased, due to the component's significant inertia. Resulting mode shapes are shown in Figure 2-6. This additional motion will clearly have a significant impact on the stresses induced in the interconnects but these effects are typically neglected in the smeared properties technique.

To more accurately model the system, a 3-D model of the board with attached inductors was constructed and analyzed. In this analysis, the modal frequencies of the inductors dropped significantly because of the compliance of the PWB attached to the lead foot. The first mode response of the middle inductors is depicted in Figure 2-7. The inductor standoff height in this analysis was 2.0 mm and the maximum response occurred in the components located at the middle of the PCB. The frequency for the first vibration mode for the middle components and the components closer to the fixed edges was approximately 71 Hz, which is approximately 20% lower than the frequency for a rigidly clamped lead foot. The PCBs first vibration mode was 159 Hz, which was about 45% higher than that predicted by the smeared 2-D model, because of the additional stiffening effect of the components. The first mode shape of the PCB is shown in Figure 2-8.

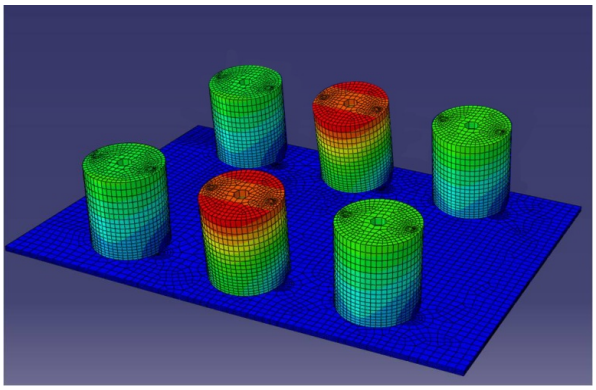

Figure 2-7 Middle inductor's first modal response

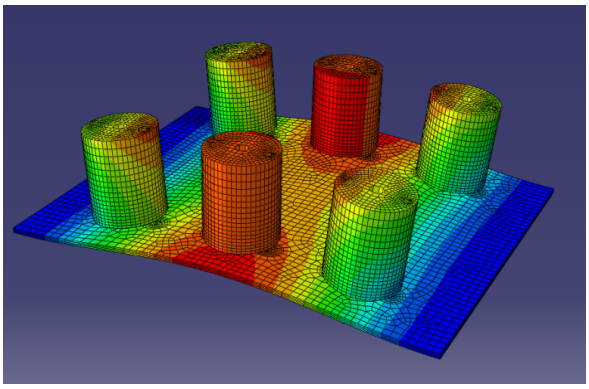

Figure 2-8 PCB first modal response

In typical vibration fatigue analysis, the PCB is treated as a thin plate. Therefore, many researchers reasoned that the PCB's natural frequency is dependent upon the geometry and the material of the board and not necessarily on the components [5]. This might be valid for microelectronic components with low mass and low stand-off, where the drop in natural

frequency due to the added mass of the components is compensated for by the increase in the natural frequency due to the local increase in stiffness from component mounting. However, for large/heavy components the scheme may not be applicable since the increase in the component mass and the leads stiffness might not cancel each other. The first vibration mode for the PCB described above when neglecting both the inertial and stiffness effects of the components was approximately 310 Hz. Clearly, neglecting the mass and stiffness effects of the inductor over estimated the natural frequency of the PCB. If the mass effect of the components was included only in this particular PCB, the natural frequency was108 Hz, while inclusion of the stiffening effects also, (using the 3-D global FEA model) increases the frequency to 159 Hz.

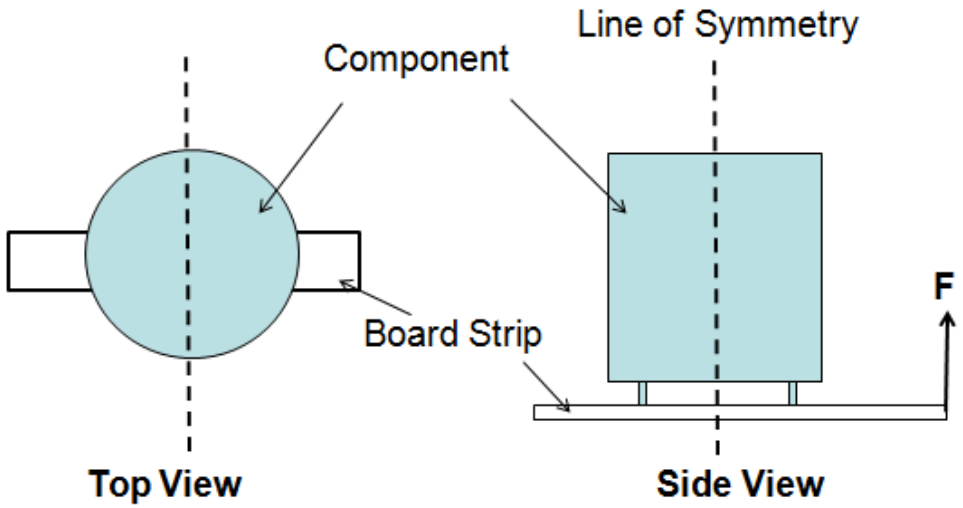

Figure 2-9. Local FEA model

2.2.4 Combined Two and Three-Dimensional Approach

In this study the simplicity of the global 2-D FEA was combined with a more detailed local 3-D FEA. The advantages of this approach are significant cost and time reduction without resorting to full 3-D FEA. In this approach, the local 3D FEA model was considered first. Based on the knowledge of the effective moment-curvature relationship near the component of interest,

a local effective stiffness was determined. The warpage was evaluated by simply applying a local unit load to the local model, as shown in Figure 2-9. This caused the PCB to experience small dynamic deflection or warpage. The local deformation was modeled with two radii of curvature. This was accomplished through the use of Kirchhoff-plate moment-curvature equations, where the local radii of curvature and the local applied bending moments are related as follows:

$$\begin{Bmatrix} M_{xx} \\ M_{yy} \\ M_{xy} \end{Bmatrix} = \begin{bmatrix} D_{11} & D_{12} & 0 \\ D_{12} & D_{22} & 0 \\ 0 & 0 & D_{33} \end{bmatrix} \begin{Bmatrix} \kappa_{xx} \\ \kappa_{yy} \\ 2\kappa_{xy} \end{Bmatrix} \quad \text{Eq. 2-7}$$

$$\begin{Bmatrix} M_{x} \\ M_{y} \\ M_{xy} \end{Bmatrix} = \frac{h^3}{12} \begin{bmatrix} E_{11} & E_{12} & 0 \\ E_{12} & E_{22} & 0 \\ 0 & 0 & E_{33} \end{bmatrix} \begin{Bmatrix} \kappa_{xx} \\ \kappa_{yy} \\ 2\kappa_{xy} \end{Bmatrix} \quad \text{Eq. 2-8}$$

where, $D_{ij}=E_{ij}h^3/12$ for i, j = 1, 2, 3. Assuming an isotropic Poisson's ratio for simplicity, the local effective stiffness due to the presence of the component can be calculated as follows:

$$D_{11} = \frac{M_x - \nu M_y}{\kappa_x(1-\nu^2)} \quad \text{Eq. 2-9}$$

Similarly,

$$D_{22} = \frac{M_y - \nu M_x}{\kappa_y(1-\nu^2)} \quad \text{Eq. 2-10}$$

The curvature can be calculated from the PWB deflection of the local 3D FEA model, by the relationship below:

$$\kappa_x = \frac{\frac{d^2y}{dx^2}}{(1+\frac{d^2y}{dx^2})^{3/2}} \quad \text{Eq. 2-11}$$

where, the elastic deflected curve was expressed mathematically as $y=f(x)$. The component was assumed to remain rigid and all the deformation was assumed to occur in the PWB and the leads. This assumption was made in the local model to make the displacement calculation more manageable.

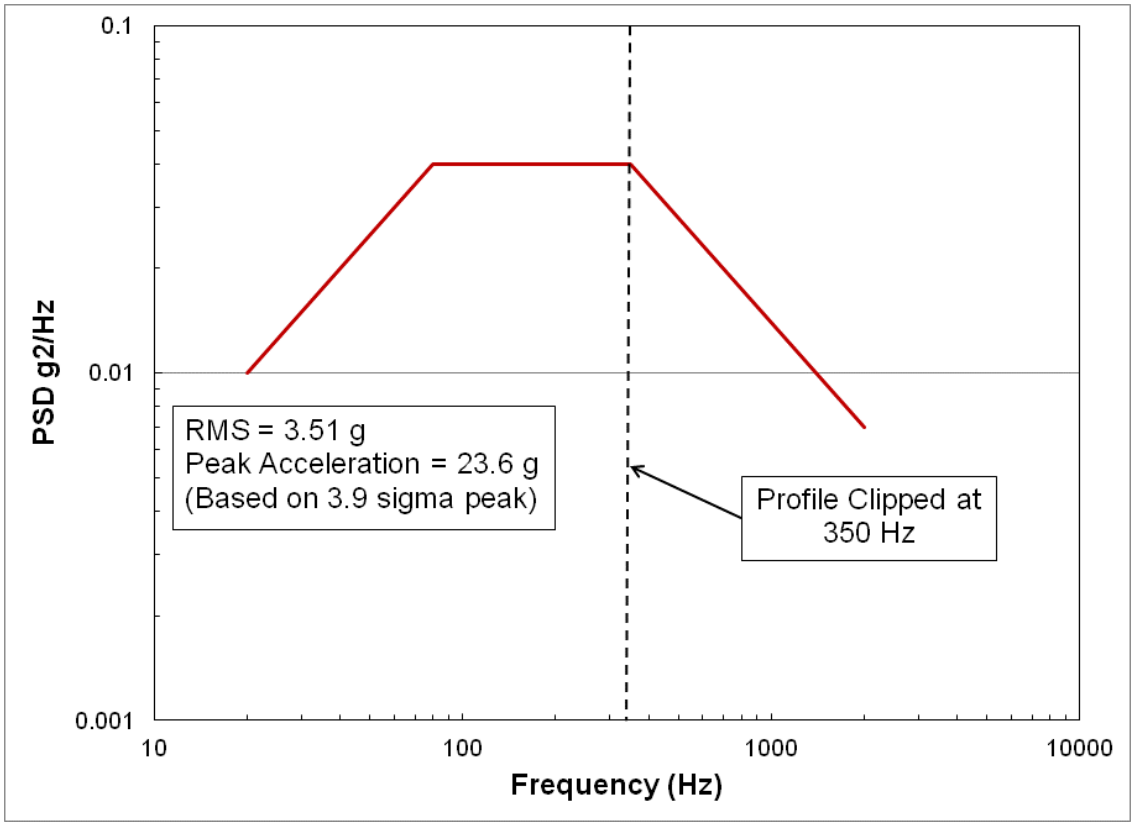

Figure 2-10. NAVMAT P9492 ASD/PSD

The global 2-D FEA model was constructed in the manner discussed above. However, the local flexural rigidity matrix, [*D*], was replaced at the footprint of each component, with the ones calculated from the local 3-D FEA model. The first vibration mode was then obtained from the 2-D global model, which was 160 Hz. This value was close to that obtained from the full 3-D FEA model discussed above. Therefore, one may use a combined two-three-dimensional

approach to reach similar results to a full 3-D FEA with the advantages of less computational time and cost reduction.

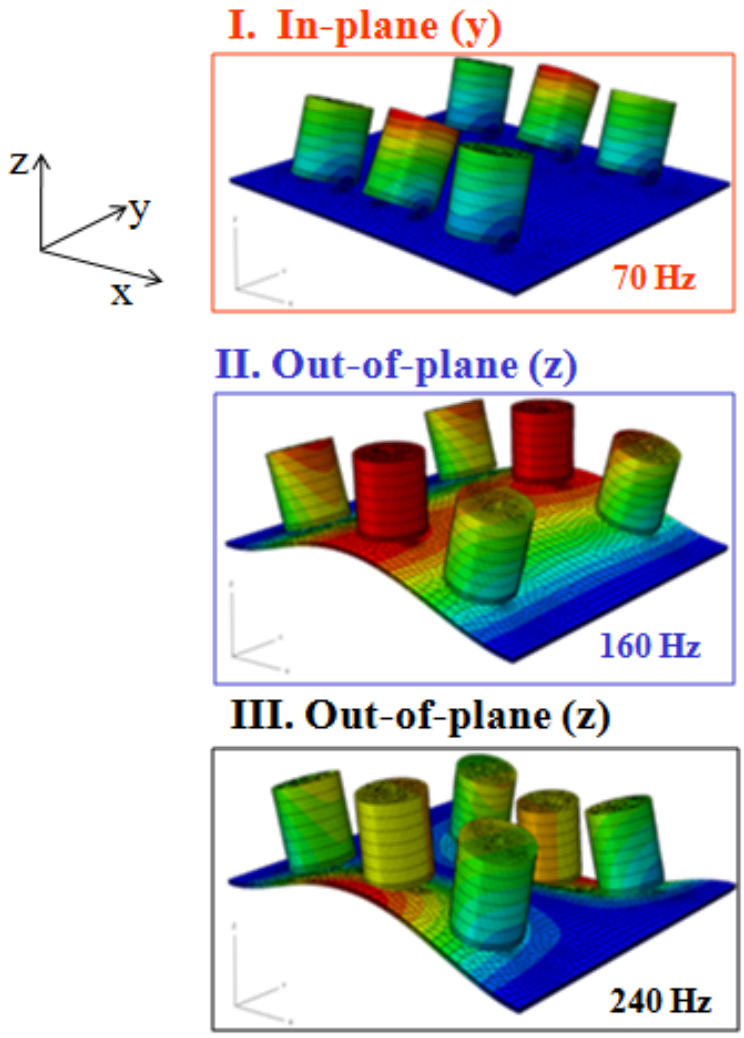

Figure 2-11. Response Analysis

Although this approach may improve the prediction of the first mode of the CCA, it does not take into account the inertial effect of the large components. Therefore, a spectral response analysis was conducted using the global 3-D FEA model, for the NAVMAT P9492 Acceleration/Power Spectral Density (ASD/PSD) profile, Figure 2-10. The profile was clipped at 350Hz, meaning the analysis was performed for 0-350 Hz range. This was done to study the first

two modes of the assembly. A base motion excitation was used at the boundary for each in-plane direction (x and y directions) and out-of-plane (z direction) individually. The direction of the excitations and responses are shown in Figure 2-11. This analysis was followed by combined excitation in all directions: x, y and z. The PSD acceleration responses are given in Figure 2-12. It can be seen from Figure 2-13 that the center component experienced the highest excitation in the in-plane y direction as well as a slightly lower excitation in the out-of-plane direction at the first mode frequency of the component, 70 Hz. Another interesting observation is the component is excited in the out-of-plane direction at the first frequency mode of the board. In terms of the PWB, the dominant mode is the first mode of the board, as expected. Nonetheless there were dynamic effects due to the excitation in the y direction that caused an acceleration peak in the PWB at the component natural frequency, 70 Hz. This peak is generated by the component's high inertia, which produces a rocking motion as shown in Figure 2-11.

Finally, the PSD of the analyzed lead stress due to the combined dynamic loading is shown in Figure 2-13. The maximum stresses were located at the leads of the center components, as illustrated in Figure 2-14. The stresses shown in this figure were the z-component stresses. This stress component represents the bending stresses in the leads, caused by combination of inertial loads and the board deflection. Because of the board architecture and the components' inertial effect there might be alteration in the local vibration response. As mentioned above, it is a common practice to increase the board stiffness under the footprint of the component, to reduce the overall response of the PCB but this may increase local bending moments and stresses in the PWB.

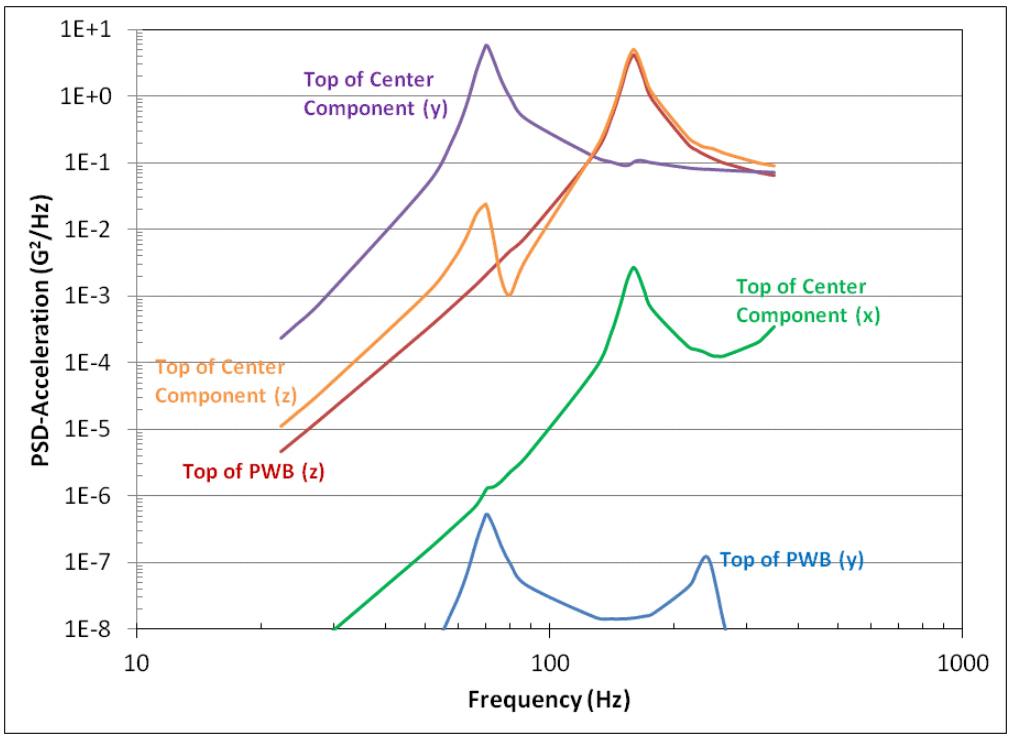

Figure 2-12. Spectral Response Analysis

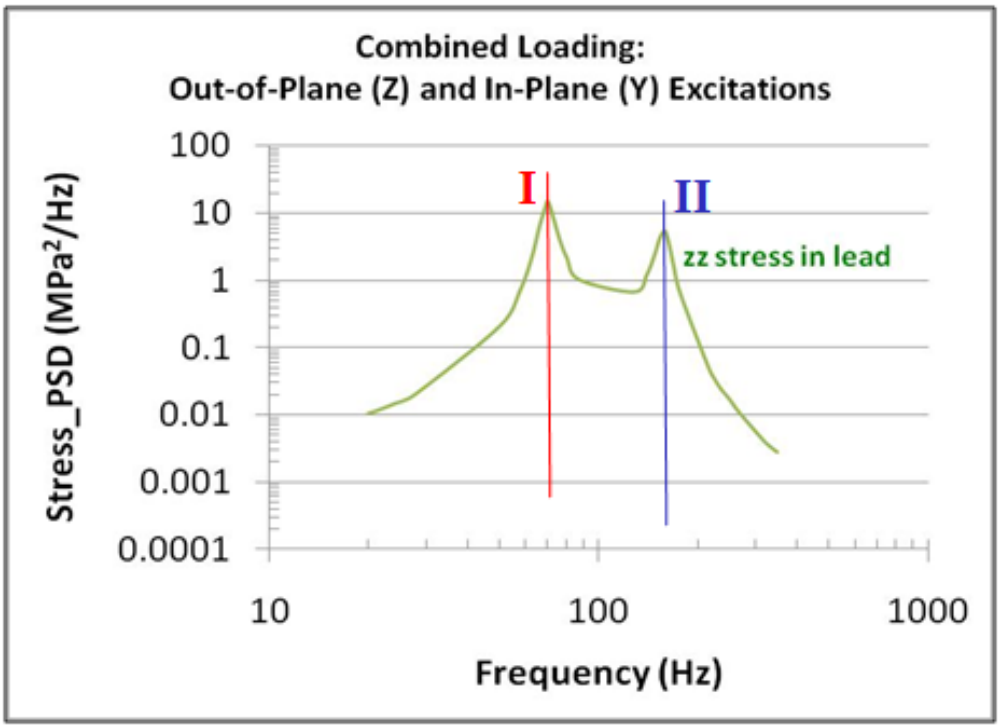

Figure 2-13. Stress Due to Combined Loading

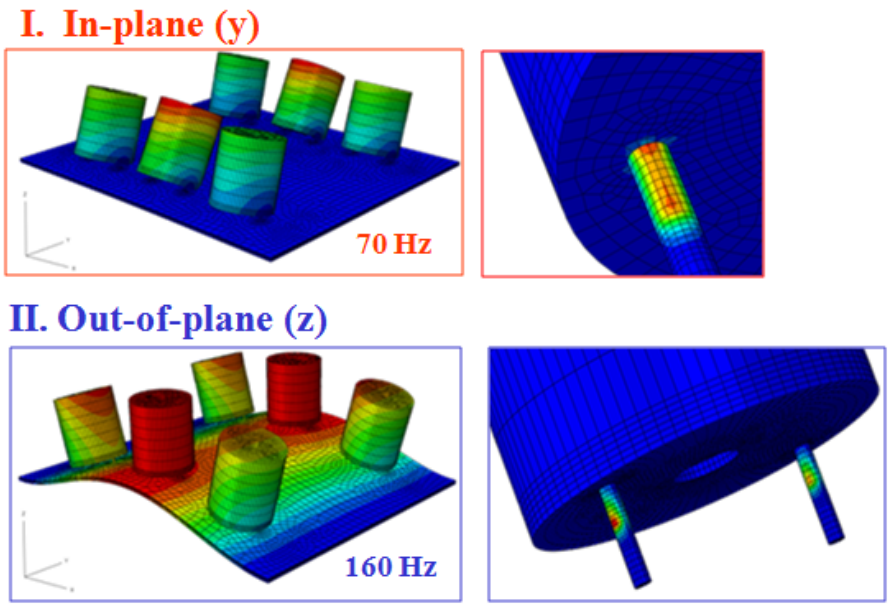

Figure 2-14. Maximum Stresses at Component Leads

Clearly, the modified smeared technique may address the overall stiffness of the CCA and produce an accurate PWB first mode frequency, however, it doesn't tackle failure in heavy components. Therefore, the best practice is to conduct a M-DoF accelerated vibration test to assess the actual damage accumulation rates in the components, leads and PWB; followed by full 3-D FEA modeling to generate acceleration factors that can be used to extrapolate the test results to various life cycle conditions and mission profiles. In practice, engineers often use one of these two approaches (i.e. modeling or testing) to qualify the product. The next section addresses the testing methodology.

2.3 Testing Approach

When considering PoF of electronics in ground vehicles, there are two types of motion that should be considered. One motion is the induced curvature or bending in the PCB as the assembly moves in a vibratory manner (global motion). The other motion is the movement of individual components with respect to the PCB due to the compliance of the components'

attachment (local motion). To accurately assess how the excitations are transmitted from the vehicle to the electronic component level, some researchers have suggested modeling the dynamic response of the vehicle subsystems. This approach, however, can be an arduous task [6]. The main reason for this lies in the fact that the vehicle chassis and body are complex systems. The reaction forces and vibration velocities depend not only on the strength of excitation within the chassis but also on the coupling of the chassis and the subsystems. Thus, one has no choice but to count on engineering judgment in estimating the boundary conditions and system inputs. A more practical approach perhaps is using experimental Frequency Response Function (FRF) data to represent the vehicle then combine it with the FEA models of the subassembly.

Figure 2-15. Typical RS Shaker Architecture

Two approaches utilized in this study for M-DoF testing are based on a Repetitive Shock (RS) shaker and a M-DoF ED shaker. A typical RS shaker, as depicted in Figure 2-15, utilizes a collection of pneumatic actuators to impart impact energy to a specially designed vibration table that transmits the resulting multiaxial vibration energy to test specimens mounted on the table. The RS shaker is often used in the industry to identify marginal designs and design weaknesses that, due to statistical variability, would eventually result in premature field failures when

production quantities of the product are exposed to life cycle conditions. This method relies on the use of elevated stresses to determine the operating and destruct limits of the design.

The test is performed in a chamber, which typically has a broad spectrum of vibration energy from 10 to 5,000 Hz and runs from 1 to 150 G_{rms}. The RS testing typically does not provide quantitative information of acceleration factors for precipitated failure mechanisms, due to two major limitations [7]. First, the only input that can be controlled during vibration testing is the G_{rms} in the vertical direction (or Z direction). Thus, it is impossible to control the shape of the PSD profile. Secondly, since the chamber employs pneumatically driven hammers, it is impossible to independently control each DoF. It is difficult to determine the acceleration of failure and/or the DoF that instigates the most damage to the components. Therefore, a quantitative relationship between performance in the field and performance in the test is difficult to establish.

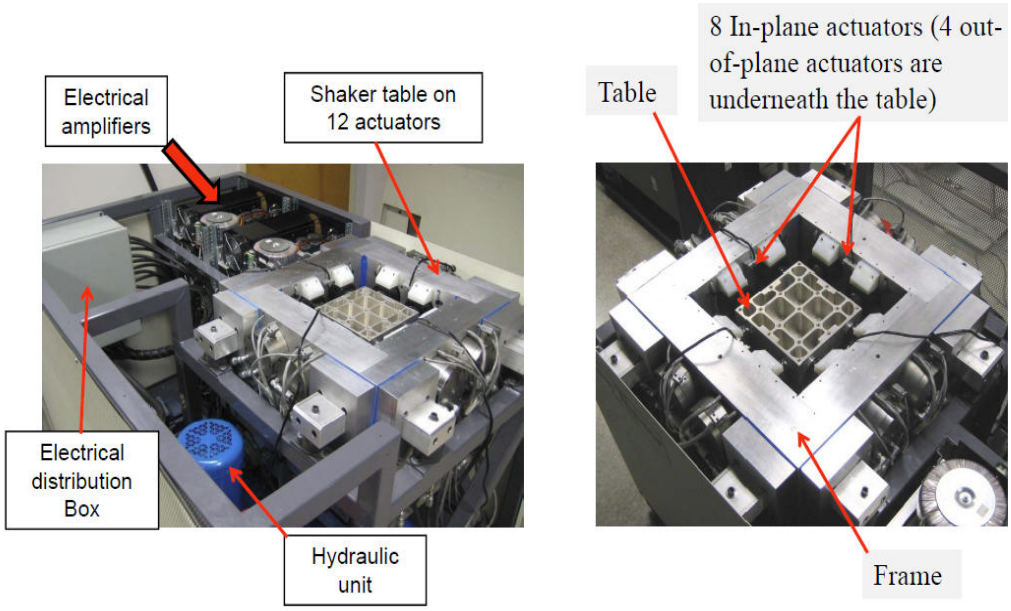

Figure 2-16. Multiaxial six-DoF ED Shaker

Due to these limitations of RS shakers in M-DoF vibration testing, this team is investigating the possibility of utilizing multiaxial electrodynamic (M-DoF ED) shakers. The objective is to study the differences in failure modes and fatigue life for simultaneous multi-axis excitation versus single-axis excitation.

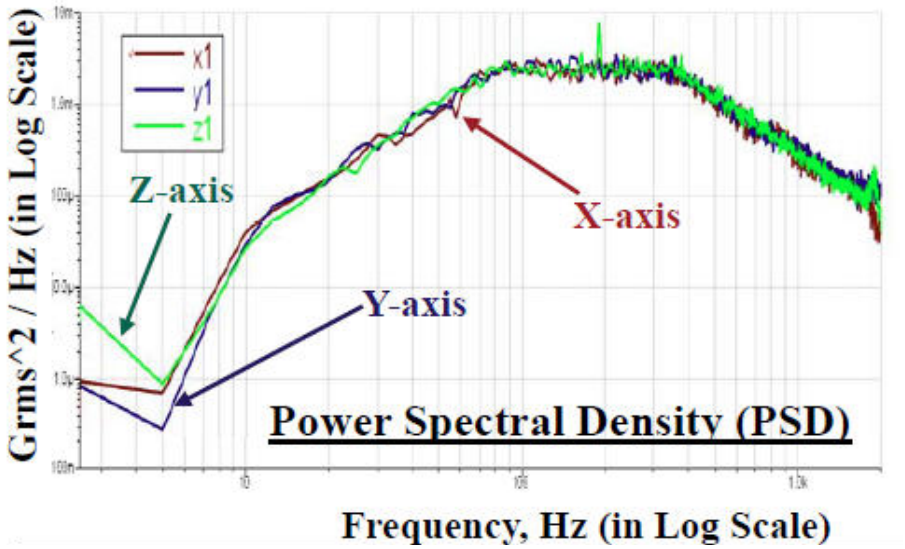

Figure 2-17. PSD in M-DoF ED Shaker [7]

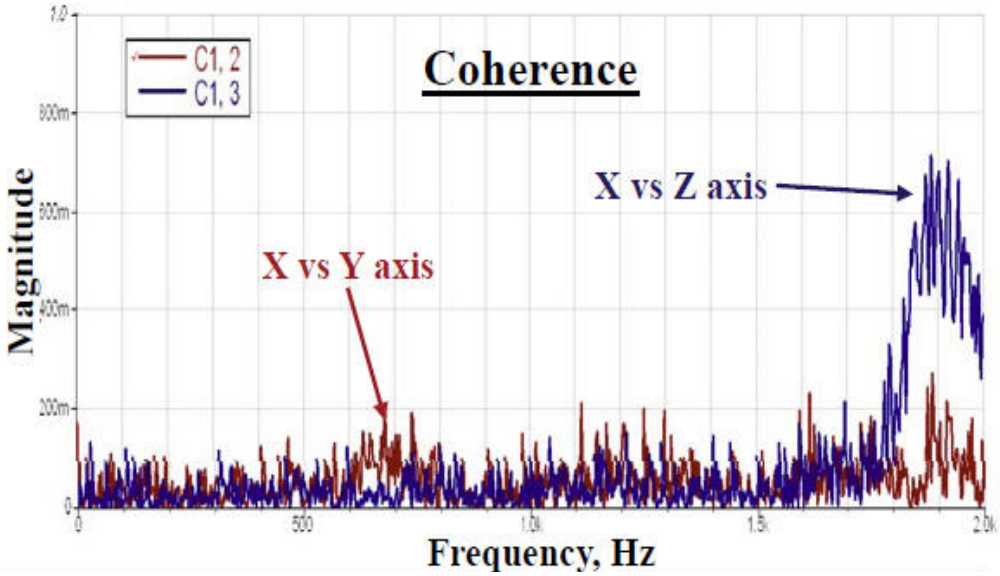

Figure 2-18. Coherence in M-DoF ED Shaker [7]

The M-DoF ED shaker used in this study consists of 12 electrodynamic actuators; 4 for each of the three orthogonal excitation axes. Eight are in-plane and four out of plane (underneath the shaker table), as shown in Figure 2-16. The twelve ED shakers are mechanically coupled to the table via self-aligning hydrodynamically lubricated bearings. The four actuators in each axis can be run in-phase or out-of-phase to produce translation in that axis or rotation about transverse axes. This architecture allows the shaker to produce a true M-DoF vibration environment. The actuators can exert up to 200lbf force per axis with max translation of ±0.25 inches and max rotation of $\pm 5^{o}$. The excitation limit is up to 30Gs with 0-3000Hz for a 10lb payload. Unlike other testing methodologies, multiaxial ED shakers provide a more controlled simultaneous loading along different axes of a test specimen, thus, allowing controlled exploration of cross-axis interactions that could not be easily explored with single-axis excitation or with RS shakers. The input PSDs and coherences can be controlled for all axes, as demonstrated by CALCE, Figure 19 [7]. Figure 2-17 shows excellent control of the shape of the excitation PSD profile. CALCE has also shown that the coherence between the axes is excellent as shown in Figure 2-18. Therefore, it is possible to identify the most dominant failure mechanisms or the DoF that instigates the most damage to the components.

The M-DoF ED shaker at CALCE will be utilized to excite the test PWB with large insertion-mount components, to levels seen on the battlefield, such as the NAVMAT P9492 PSD profile. The FRF experimental data will be combined with the FEA model where the interconnect fatigue results would be extracted with the aid of FEA.

This approach may help in establishing a quantitative relationship between performance in the battlefield and performance in the test. It may also produce a modified smeared modeling

approach that addresses inertial effects of large/heavy components without the need to resort to a fully 3-dimensional detailed FEA model.

2.4 Outcomes

As discussed above, the fatigue damage in the interconnects can be due to a combination of flexural deformations in PCBs and/or due to inertial forces caused by the mass of large/heavy components with high stand-off. When conducting electronics PoF, a hybrid two/three-dimensional FEA approach may provide natural frequency results closer to full 3-D FEA while reducing cost and computational time. However, failures predominantly due to inertial loads may require full 3-D FEA, testing, or both.

It is essential to understand the structural characteristics of large/heavy components in electronics devices in order to correlate the defects with the dynamic responses. As mentioned above, the main challenge in electronics packaging is the prediction of the reliability and lifetime of the critical components. Therefore, it is imperative to identify the failure mechanisms of the components through experimental analysis. However, the experimental approach has to emulate the real world operational conditions, which includes simulating M-DoF dynamic loads. This involves experimentally measuring the transient in-plane and out-of-plane displacement responses, which can be accomplished with the aid of a multiaxial shaker.

2.5 References

[1] Erwin, S., I., "In Damage Control Mode, Army Builds Future Network of Combat Brigades", National Defense, (Jul.) 2010.

[2] Steinberg, D., *Vibration Analysis for Electronic Equipment*, 3rd Edition, Wiley Inter-Science, New York, NY, 2000.

[3] Pitarresi J. and Primavera A., "Comparison of Vibration Modeling Techniques for Printed Circuit Cards", *ASME Journal of Electronic Packaging,* 1991, **114**, 378–383.

[4] Jones, R. M., *Mechanics of Composite Materials*, 2nd Edition, Taylor and Francis Group, New York, NY, 1999.

[5] Barker, D. B., and Chen, Y. S., "Modeling Vibration Restrain of Wedge Lock Card Guides", *ASME Annual Meeting,* 92-WA/EEP-16, (Nov.) 1992, Anaheim, CA.

[6] Li, R. S., "A Methodology for Fatigue Prediction of Electronic Components under Random Vibration Load," *Journal of Electronic Packaging, ASME,* 2001, Vol. 123, pp. 394-400.

[7] C. Choi, M. Al-Bassyiouni, A. Dasgupta and M. Osterman, "PoF Issues in Multi-DoF Vibration Testing: ED Shakers and RS Shakers", *IEEE ASTR09 Workshop*, New Jersey, Oct. 2009.

Chapter 3 Review of Response and Damage of Linear and Nonlinear Systems under Multiaxial Vibration

Published in Shock and Vibration, 2014

This chapter contains a comprehensive review of the response and damage of linear and nonlinear systems under multiaxial vibrations, and includes the experimental results for the durability and nonlinear response of large electronic components exposed to multiaxial random. The paper was published in *the Journal of Shock and Vibration*. Authors are Mr. Ed Habtour, Mr. William (Skip) Connon, Mr. Michael F. Pohland, Dr. Samuel C. Stanton, Dr. Mark Paulus, and Professor Abhijit Dasgupta. Mr. Ed Habtour (first author) conducted the literature review and all the multiaxial vibration experiments and analysis conducted at University of Maryland. Skip Connon, Michael Pohland, Dr. Samuel Stanton, and Mark Paulus provided insights about the US Department of Defense guidelines, and standards related to multiaxial vibrations, test and evaluation and reliability. They also provided reports and publications related to the topic. Professor Dasgupta provided technical and academic guidance in this effort.

Abstract:

A review of past and recent developments in multiaxial excitation of linear and nonlinear structures is presented. The objective is to review some of the basic approaches used in the analytical and experimental methods for kinematic and dynamic analysis of flexible mechanical systems, and to identify future directions in this research area. In addition, comparison between uniaxial and multiaxial excitations and their impact on a structure's life-cycles is provided. The importance of understanding failure mechanisms in complex structures has led to the development of a vast range of theoretical, numerical, and experimental techniques to address

complex dynamical effects. Therefore, it is imperative to identify the failure mechanisms of structures through experimental and virtual failure assessment based on correctly identified dynamic loads. For that reason, techniques for mapping the dynamic loads to fatigue were provided. Future research areas in structural dynamics due to multiaxial excitation are identified as (i) effect of dynamic couplings, (ii) modal interaction, (iii) modal identification and experimental methods for flexible structures, and (iv) computational models for large deformation in response to multiaxial excitation.

3.1 Introduction

The study of fatigue failure was instigated in the 19th century following several catastrophic train accidents [1]. This field has evolved drastically to include substantial scientific efforts to gain an understanding of failure mechanisms in structures under dynamic loading [2–10]. The scientific studies of fatigue accelerated in the 1940s to mitigate fatigue failures seen in military systems during World War II. These studies began to include multiaxial loading in the 1960s; such studies increased significantly in the 1990s due to the proliferation of complex components in the electronics, military, aerospace and automotive platforms [2]. In spite of the significant accomplishments achieved in the twentieth century the introduction of sophisticated and high precision devices in the 2000s, such as micro/nano-electromechanical systems (MEMS/NEMS) and electronics has exposed the limitation of our knowledge of fatigue due to multiaxial vibration. Researchers are still struggling to systematically model high-cycle fatigue of linear and nonlinear structures under multi- axial loading; thus, prediction methods for high-cycle fatigue life remain somewhat immature. Life-cycle prediction under multiaxial dynamic loading has been shown to be extremely complex and more intractable than uniaxial models [11]. This is primarily because the validation of multiaxial models is extremely difficult since

multiaxial vibration shakers, shown in Figure 3-1.

The initial assumption at the beginning of this literature review was that there would be an abundance of research performed in multiaxial vibration since most mechanical and electronics products are universally subject to multi-degrees of freedom (MDoF) dynamic loading. However, only limited life-cycle modeling studies focusing on multiaxial vibration have been published in the literature. Analytical and experimental investigations of structures exposed to multiaxial harmonics and random loading are also scarce. Most studies found in the literature are focused on uniaxial loading. Furthermore, military and commercial standards were developed to mitigate the testing limitations by proposing sequential uniaxial excitation as a compromise and proxy for simultaneous multiaxial excitation. In qualifying products subject to vibration, it is common to test sequential uniaxial vibration profiles found in standards such as MIL-STD-810G. Unfortunately, current standards do not provide vibration profiles for simultaneous multiaxial vibration. Single axis electrodynamic and hydraulic shakers have been the prevailing tools for performing harmonic and random vibration testing. Unfortunately, uniaxial sequential testing may provide overly optimistic fatigue durability results [10, 13].

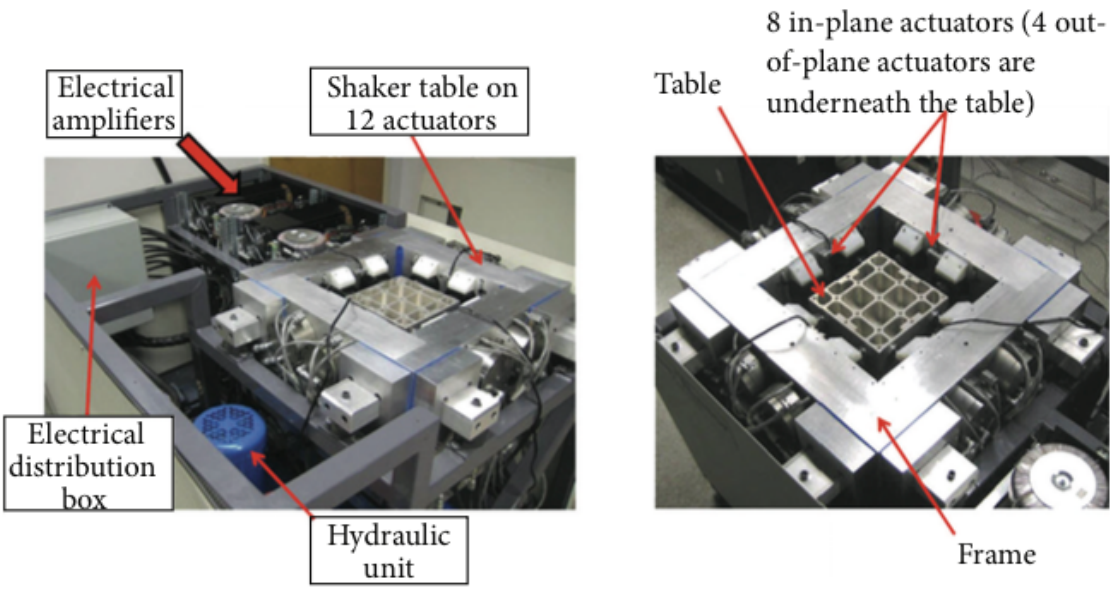

Figure 3-1. Six-DoF electrodynamic shaker at CALCE (with TEAM Inc. permission)

While several different schemes are widely used to test devices sequentially in the various axes, it is understood that they are rough approximations to the ideal of simultaneous multiaxial testing and must be in the linear regime. Uniaxial excitations are applied to test products even though most field operational data indicate that these products are exposed to multiaxial dynamic loading environments. Examples include a spacecraft launch, a military ground vehicle over rough terrains, a helicopter blade during instability, and an aircraft wing exposed to turbulent flow. Thus, serious compromises must be made in the experimental design to perform meaningful tests on a single-axis electrodynamic shaker. For example, to simulate multiaxial vibrations, the MIL-STD-810G recommends performing the vibration tests by sequentially applying single axis excitation to a test article along three orthogonal axes (*X*, *Y*, and *Z*). This can be accomplished by exciting the structure in one direction then repeating the procedure twice after rotating the structure 90^{o} each time. Depending on the complexity of the structure, this procedure may require designing a different fixture for each rotation.

Understanding the failure mechanisms due to complex vibration loading is becoming increasingly important for current systems that are progressively complex and electronically rich [14]. These failure mechanisms can be exploited through accelerated multiaxial vibration testing, which may provide reliability improvements at significantly lower cost [15]. Unfortunately, difficulties encountered in this approach have limited its application and acceptance. Some of these difficulties can be traced, in part, to a lack of understanding of the propagation of multiaxial dynamic loads from the system level to individual components. To appreciate a particular failure mechanism by means of testing, it is important to resolve the dynamic loads by simulating the actual vibration conditions, which can be accomplished with a multiaxial shaker.

The objective of this literature review is to provide engineers and researchers with an overview of the work that has been done in the area of uniaxial and multiaxial vibration. The review provides most of the significant accomplishments in the past century in uniaxial and multiaxial vibration and high-cycle fatigue. State-of-the-current technologies and state-of-the-art technologies are provided. The review is broken into four major parts: the first section focuses on the industrial studies and research in complex dynamic loading and high-cycle fatigue, whereas the second part focuses on the theoretical and experimental aspects. The third section discusses mapping fatigue to multiaxial dynamic loading. The final portion of this chapter summarizes proposed and future efforts in the field of multiaxial vibration.

3.2 Physics of Failure Approach

3.2.1 Automotive Applications

The automotive industry has produced an abundance of publications on the use of uniaxial and multiaxial excitation for durability and qualification testing, to meet warranty and reliability requirements demanded by consumers. A typical automobile prototype is subjected to

a variety of vibration profiles that simulate operational conditions in a laboratory environment. According to Dodds and Ward [16] and Awate et al. [17] automotive manufacturers utilize accelerated life testing for critical components to meet the life-cycle requirement while reducing the testing cost. This can be accomplished by driving on various road surfaces (proving grounds) similar to those seen in the field. During testing, acceleration data are collected for the critical components. The measured conditions are then simulated on shakers in the test laboratory, where the critical components are exposed to similar dynamic conditions, but accelerated. Another approach that automotive manufacturers rely on is the four-post hydraulic shaker. This is a common testing tool for validating vehicle durability [17]. It is a relatively simple and cost effective configuration for performing a complete vehicle vibration evaluation. A typical four-post hydraulic shaker consists of four vertical servohydraulic actuators for a simple shaker to four actuators in the vertical direction and eight actuators in the transverse direction for more advanced shakers (total of twelve actuators, three actuators per post) to simulate a multiaxial environment A simple four-vertical servohydraulic shaker, which excites a vehicle through its tires, is shown in Figure 3-1. Similar to the component accelerated life testing, the wheels' accelerations and forces and the wheel-to-body displacements data obtained from the proving ground can be reproduced by such a shaker. The dynamic loading produced by the shaker induces stresses on the vehicle and its components. However, using a four- or twelve-hydraulic actuator shaker introduces two major limitations [17, 18]. The first limitation is the inability to simulate the effect of rolling tires on the overall stiffness and damping of the suspension system and vehicle structure. The second issue is that hydraulic shakers have limited frequency range, in general 1–80 Hz [16].

Figure 3-2. Four-post hydraulic simulator, from Awate *et al*. [17]

Because of these limitations, estimating and modeling vibration fatigue for components in higher frequency ranges can be an arduous task. High-frequency dynamic loading, especially random loading, is a major contributor to fatigue in vehicular components [19]. These high frequencies can easily generate other high frequencies caused by rotating speeds, random vibration, and noise radiation that can potentially augment the severity of damages. These high-frequency loads are transmitted from the chassis to the vehicle body and eventually to the components [20]. One of the common multiscale hierarchical approaches for modeling fatigue in vehicular components is to model global dynamic responses of the vehicle and progressively generate the effect of these responses on the vehicle subsystems and eventually on individual components, which can be an expensive and time consuming approach. Another common approach is to rely on engineering judgment in assuming realistic boundary conditions and loads directly at the subsystem or component level. Subsequently, finite element methods (FEM) are used for stress and fatigue assessment, based on these assumptions and on linearizing approximations of the structure, which may lead to erroneous results and vehicle recalls. Liu [20]

suggested a more practical approach where FEM is coupled with experimental transfer functions. Liu detailed a methodology for extracting an experimental frequency response function (FRF) that represents the body and then combining it with the FEM models.

As mentioned above, random vibration in automobiles is one of the major contributors to fatigue damage. Typically, automotive fatigue researchers rely on power spectral densities (PSDs) to represent stochastic dynamic behaviors [18, 21–24]. A detailed approach to estimating fatigue life due to random vibration loading for a truck was provided by Bonte et al. [22]. They developed an analytic model where symmetric in-phase road excitations were applied to all wheels of a full truck. They also applied asymmetric excitations (180-degree phase difference) to the left and right tracks to generate out- of-phase conditions. Biaxial stress power spectral densities (PSDs) were calculated from multiple random excitations and equivalent von Mises' stress PSDs were derived. Later, Bonte et al. [23] developed a new analytical approach to estimating the equivalent von Mises' stress PSDs from several random vibration inputs while accounting for phase differences. The damage ratio was then calculated based on a uniaxial fatigue analysis approach based on the Dirlik method [25]. This approach provided qualitative results for design improvements to linear structures that can be implemented as a fast tool to evaluate different design concepts and the effect of dynamic loading on fatigue life.

Unfortunately, these tests and analytical tools are not always successful in producing failures observed in the field. The Ford Corporation found that a module could pass the qualification test but fail in the field [26]. A test or health monitoring system that could capture every failure or intermittent in real time does not exist. In spite of the great wealth of fatigue research generated by the automotive industry, the industry continues to maintain the same practice of qualifying their products by subjecting them to uniaxial vibration with the option of

sequential vibration testing. However, there seems to be consensus in the literature that such an approach can be both time consuming and cost ineffective and may result in the acceptance of unreliable components.

3.2.2 Aerospace Applications

Surprisingly, studies published in the open literature pertaining to uniaxial and multiaxial vibration testing for aerospace applications are somewhat limited. This is due to the proprietary nature of the aerospace industry. In aeronautic applications, the majority of the dynamic loads stem from turbulent flow and during landing and takeoff, which are multiaxial in nature. Aircraft wings, for example, are constantly exposed to multiaxial dynamic loading since the wings are connected to a flexible support, such as the fuselage. In addition to bending in the wing, the root of the wing experiences dynamic rotation because of the inherent flexibility at the point of attachment [27]. In astronautic applications, one of the most critical and persistent spacecraft design problems is the launch survivability of sensitive and expensive systems. The acceleration levels input to a typical spacecraft are over a wide frequency range from about 30 Hz to 2000 Hz or higher [15]. Billions of dollars in lost satellites or degraded performances of payloads are attributed to damage accumulated from vibration due to launch loads [28].

In spite of the lack of specificity of multiaxial vibration and fatigue in aerospace applications, most of the multiaxial loading investigations performed by aerospace researchers have focused on the dynamics of beam-like structures as idealization of the of helicopter blades, aircraft wings, or deployable solar panels in satellites [27, 29–32]. Only two major studies, at the system level, are reviewed in this section. The first study is an early investigation of the dynamics of a blade in a compressor [33]. The other is a more recent study of fatigue assessment of a military helicopter flare- dispenser bracket [34]. In the study performed by Whithead [33],

experimental the power spectra of vibration response were measured for blades in axial compressors exposed to turbulent flow. In deriving the equations of motion, the effect of aerodynamic coupling between the blades was assumed to be a minor effect and thus neglected. Aykan and Celik [34] compared fatigue damage accumulated under uniaxial and multiaxial broadband random excitation. The PSD of the dynamic response was obtained for a military helicopter flare-dispenser aluminum bracket during flight. The PSD profile was used as an input for uniaxial excitation testing. However, due to lack of multiaxial excitation testing capability, the simultaneous three-axial loading was modeled using FEM to calculate the structural response. Similar to most studies found in the literature, Aykan and Celik assumed that sequential uniaxial loadings were equivalent to multiaxial loadings. Thus, the fatigue analysis was performed in frequency domain with the assumption of linear structural behavior. They concluded that the cumulative fatigue damage in multiaxial excitations was higher than adding the damage for sequential axes even for linear structures. It is important to point out that, for military aircraft, the MIL-STD-810G provides single-axis PSD profiles for simulating the dynamic inputs in various fixed-wing aircrafts and in rotorcrafts.

3.2.3 Electronics Applications

One of the predominant failure modes in electronics is solder joint fatigue due to vibrations [35, 36]. Analyses of solder joint stresses associated with uniaxial vibration are widely seen in the literature: Lau et al. [37– 39], Liu et al. [40], Yang et al. [41], and Zhou et al. [42]. One of the most detailed methodologies for monitoring, recording, and analyzing life-cycle vibration loads of electronics was developed by Gu et al. [43]. They developed this methodology by exciting circuit card assemblies (CCAs) in the out-of-plane direction using broadband PSD profiles. Strain data was collected for different PSD levels from a series of experiments. FEM

simulation was then conducted and calibrated based on the experimental responses of the CCAs. A strain transfer function was calculated to predict the damage ratio in the solder where the structure was assumed to be linear. Unfortunately, literature does not provide any methodology that con- siders multiaxial vibration in electronics systems. Zhou et al. [36, 42] estimated vibration fatigue of Sn3.0Ag0.5Cu and Sn37Pb solders for CCAs exposed to linear harmonic uniaxial excitation. The analysis was conducted in the time domain to quantify the fatigue damage caused by harmonic excitation at the first natural frequency. In their study, they observed two competing failure sites in the solder interconnect and in the printed wiring board (PWB) copper trace just below the failed components. Several researchers studied high-cycle fatigue in CCAs exposed uniaxial harmonic and random excitations in the range of 10 Hz to 10 kHz [36, 42, 44-48]. Based on this extensive literature review, there are two multiaxial vibration fatigue studies in electronics components. The first study by Habtour et al. [15] provided a rapid analytical technique for analyzing the response of heavy/large components under biaxial random vibration excitation. A modified 2-D FEM smeared technique was used to model the CCA, which was coupled with a detailed local 3D FEM for heavy components. Based on the knowledge of the effective moment-curvature relationship near the component of interest, a local effective stiffness was calculated. This was accomplished through the use of Kirchhoff-plate moment-curvature equations. The modified smeared technique correctly predicted the overall stiffness of the CCA and produced an accurate PWB first mode frequency; however, the model does not take into account the inertial effect of the large component on the overall response of the CCA. The second study by Ernst et al. [49] is the only experimental study that exposed heavy/large electronic components to biaxial planar random excitations. This study is discussed in detail later in this chapter in the section titled “Mapping Dynamic Loads to Fatigue.”

3.3 Theoretical Approach

3.3.1 Beam Vibrations

The beam has many characteristics of typical aeronautical and astronomical structures. Indeed, high aspect ratio aircraft wings, spacecraft deployable solar panels, and helicopter rotor blades are frequently idealized as beams. Even for low aspect ratio wings, the bending and torsional deformation can be approximated by use of beam theory with an adjusted stiffness [27].

3.3.2 Stochastic Vibrations

There have been significant scientific contributions in stochastic vibrations since the 1950's. During that time, random vibration received significant attention due to its importance in fatigue damage in aircraft and naval ships. One of the earlier studies in random vibration of beams was performed by Eringen [50], where he derived a closed-form solution for space-time correlation functions of a simply supported beam. Eringen employed generalized harmonic vibration analysis of damped beams exposed to one-dimensional randomly distributed external pressure loads. His approach provided cross-correlation functions for displacements and stresses in terms of the external pressure cross-correlation function. Herbert [51] applied Markoff process and Fokker-Planck equations to investigate large vibration of a simply supported elastic beam exposed to broadband white noise external pressure acting on the entire beam surface. He obtained the joint probability density function (PDF) of the modal amplitudes using the Fokker-Planck equation. An approximate expression for the mean-squared displacement of the beam was derived and was then compared to numerical computation, which indicated a reduction in the mean-square displacement due to the nonlinearity. Herbert [51] also showed that when the deflection was sufficiently large, the first mode still represented a good estimate of the total mean-squared deflection; however, the effect of the higher modes must be considered in

calculating the response of the first mode. The studies reported by Herbert lacked experimental validation. Elishakoff and Livshits [52] utilized Eringen's and Herbert's findings to produce closed-form solutions for a simply sup- ported Euler-Bernoulli beam under random vibration with different damping mechanisms. The excitation was spatially and temporally random stationary white noise induced on the entire bottom surface of the beam. Elishakoff stated that using a span averages approach instead of the maximum random vibration responses could yield an underestimate of the stresses. In a different study, Elishakoff [3] generalized the Eringen problem to include the effect of axial loading on a beam exposed to a random transverse load. Later, Elishakoff et al. [53] employed a stochastic linearization to investigate large amplitude random vibrations of simply supported and clamped beams on an elastic foundation under a stochastic loading. He stated that, for different boundary conditions and the loading patterns, the stochastic linearization method was superior to the classical stochastic technique, especially in nonlinear structures. Ibrahim and Somnay [54] investigated the response of an elastic Euler-Bernoulli beam with one frictional support at each end, which was exposed to single point harmonic and stochastic excitations (randomized only in time). The beam was allowed to slide on the two frictional supports. A Monte Carlo simulation was utilized to estimate the beam mean-square response for the stochastic excitation case. For the harmonic excitation case, the quality factor improved as the excitation frequency increased beyond the resonance frequency. The friction in the random excitation case caused a significant reduction of the system mean-square response.

3.3.3 Nonlinear Vibrations

Substantial attention has been devoted to nonlinear dynamics and vibrations of beams because of their vital importance in many engineering applications and fatigue problems. One of

the most cited studies in nonlinear dynamics is the work of Hodges and Dowell [32], where they developed the multiaxial equations of motion for a rotor blade, idealized as a cantilevered beam, using Hamilton's principle. They maintained the cubic nonlinear terms and included the effect of warping. Ho et al. [55, 56] examined free and forced nonplanar oscillations of fixed- fixed and cantilever inextensional beams, respectively. Ho et al. reduced the nonlinear partial-differential equations of motion to two coupled nonlinear ordinary-differential equations using separation of variables, where they assumed only one mode in each plane. They also ignored the axial inertial and Poisson effects. It was concluded that whirling oscillations might occur for significantly large excitation amplitude. Crespo da Silva and Glynn [57, 58] developed a set of partial-differential equations for flexural-flexural- torsional motions of inextensional beams, which contained geometric and inertial nonlinearities. It was found that the geometric nonlinearities were critical for low modes and must not be neglected. Later, Da Silva [29] extended the above approach to extensional beams where he constructed partial- differential equations for flexural-flexural-torsional motions. The axial displacement due to warping was considered in the derivations. These equations were then applied to study the nonlinear response of an extensional cantilever beam to a fundamental resonant excitation [59]. Crespo da Silva concluded that the nonlinear terms due to midplane stretching were predominant in extensional beams. Nayfeh and Pai [60] and Pai and Nayfeh [61] also investigated nonlinear nonplanar responses of inextensional cantilever beams to parametric and resonant excitations using the partial-differential equations of motion developed by Crespo da Silva and Glynn [58]. The method of multiple scales was utilized to construct nonlinear first-order ordinary- differential equations governing the modulation of the amplitudes and phases of the interacting modes in each plane. They conclude that the geometric nonlinear terms had a stiffening effect, whereas the inertial

terms had a softening effect. Crespo da Silva and Zaretzky [30] and Zaretzky and Crespo da Silva [62] continued to study the nonlinear response of an inextensional beam exposed to one of the flexural modes resonant excitation. The method of multiple scales was applied to the governing partial-differential equations to produce the equations of motion that provide the capability for modulating the amplitudes and phases of the beam interacting modes. Arafat et al. [63] showed that the partial- differential equations of motion of Crespo da Silva and Glynn [57, 58] can be derived using Hamilton's extended principle. Nayfeh and Arafat used the method of multiple scales to the Lagrangian terms to derive the modulation equations for amplitudes and phases of the two interacting modes [64]. Nayfeh and Arafat [65] and Arafat [66] derived the Lagrangian equations of motion for nonlinear flexural- flexural-tensional vibrations of symmetric laminate composite and isotropic metallic long slender cantilever beams with nearly square cross-sections under uniaxial harmonic excitation of the base. Perturbation procedure was then applied to establish approximate solutions for the weakly nonlinear equations of motion. The beam was assumed to be inextensible with negligible torsional inertia, leading to two partial-differential equations governing the motions of the beam. Banerjee [67] provided a methodology for deriving exact expressions for the mode shapes of free vibration of composite beams. The effect of material coupling between the bending and torsional modes was considered. The equations of motion of the bending-torsion were solved analytically for bending and torsion. Malatkar and Nayfeh [68, 69] and Malatkar [70] extended Arafat's equations of motion development to their experimental and theoretical study of the response of a flexible long cantilever beam exposed to external single axis harmonic plane excitation near the beam third mode. They observed that the beam response contained significant contributions from the first mode when the beam third mode amplitude and phase were slowly modulated. The energy

leakage between these modes depended on how close the modulation frequency was to the frequency of the first mode.

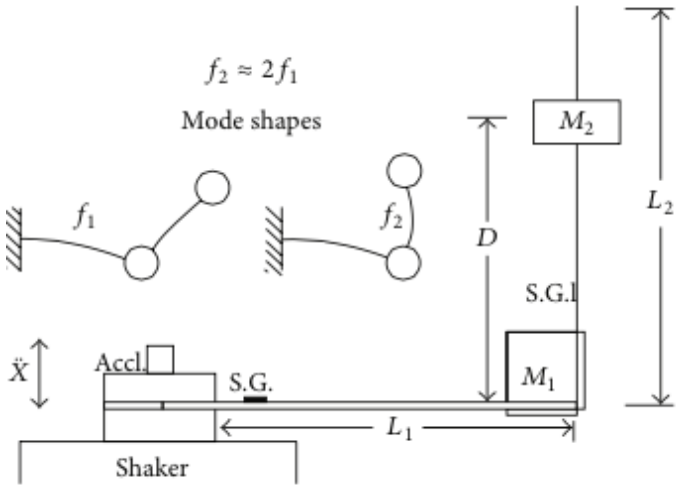

Figure 3-3. L-shape structure excitation, Balachandran and Nayfeh [77]

Anderson et al. [71] experimentally investigated the response of a thin steel cantilever beam with an initial curvature to a combination parametric excitation exposed to uniaxial base excitation. The first four natural frequencies were 0.65, 5.65, 16.19, and 31.91 Hz. Their study suggested that over a range of forcing frequency above 32 Hz, the first and fourth modes were initiated by a combination parametric resonance with the first mode dominating the response. The experimental results confirm the occurrence of external subcombination resonances in structures found in the study by Dugundji and Mukhopadhyay [72]. These resonances can be utilized as mechanisms for instigating large amplitude low- frequency modes with high-frequency excitations.

The dynamics of nonlinear beams with complicated boundary conditions were also investigated. Dowell [31] per- formed an analytical study of large motion of axially sliding beams with dry friction damping. In Dowell's study, an Euler- Bernoulli beam pinned at both

ends was considered; however, the beam was fixed at one end against the axial motion and with a sliding restraint. Coulomb dry friction damping was assumed. The Galerkin modal solution method was applied for a single mode. Dowell concluded that, for large beam response, damping was created due to dry friction and equivalent to a linear viscous damper. Tang and Dowell [73] performed a numerical and experimental study to support Dowell's analytical work [31] using a pinned-pinned beam under single axial harmonic excitation for slip and no-slip conditions. Their model was more reliable for the first mode than higher modes and can be applied to a beam with well- separated modes.

Sophistications were added to beam models to idealize more complex structures such as antenna and radar structures and aircraft wings. This can be achieved with cantilever beams or L-shape beams models with tip mass under a base excitation. To [74] analyzed the dynamics of an antenna by deriving the natural frequencies and mode shapes of a cantilever beam with an eccentric tip mass under a base excitation. To assumed small deflection and neglected the effect of the axial deflection due to the heavy mass at the tip. The model was appropriate only for linear structures with uniaxial excitation. Later, Cartmell and Roberts [75] conducted theoretical and experimental investigations of the stability of a cantilever beam with tip mass having two simultaneous combination parametric bending and torsion resonances. The multiple scales method was utilized. It was possible to reach an agreement between theoretical and experimental results within limited ranges of excitation frequency, but unattainable in periodic modulation regions. Cartmell and Roberts did not consider the effect of inherent nonlinearities in the system. In 1990, Balachandran and Nayfeh [76] reported the planar response of a flexible L- shaped beam-mass structure with the second natural frequency twice the first natural frequency of the structure, as shown in Figure 3-3. They showed that weakly nonlinear analysis can be used to

qualitatively and quantitatively predict the response of an internally resonant structural system subjected to small primary resonant excitations. Balachandran and Nayfeh developed the Lagrangian for weakly nonlinear motions of the L-shape structure where they assumed that the structure was undamped. It was possible through their approach to identify the Hopf bifurcations, thereby ascertaining the parameters that control the possibility of periodic and chaotic modulated motions. Later, Balachandran and Nayfeh [77] presented experimental results on the influence of modal interactions on the nonlinear response of the L- shape structure. The major conclusion was that the frequency relationships between the different modes of oscillation in the structures led to modal interactions during the resonant excitations and nonlinear responses. Jaworski and Dowell [78] performed a theoretical and experimental investigation of the free vibration of a cantilevered beam with multiple cross-section steps. The natural frequencies were obtained experimentally using modal impact testing. The experimental results were then compared against Euler-Bernoulli beam theory solutions from Rayleigh-Ritz FEM results, where the asymptotic approximation was utilized for higher modes to avoid numerical error. A detectable difference in the first in-plane bending natural frequency was noted between the beam theory results and those of the higher-dimensional FEM models and experimental observation.

3.3.4 Microsystems Vibrations

For the past two decades, consumers' demand for miniaturized smart devices has continued to increase at a considerable pace. As a result, microsystems devices have become ubiquitous in almost every product that humans interact with on daily bases such as smart phones, computers, medical devices, and automobiles. Recent advancements in microsystems fabrication have allowed for new possibilities in designing an assortment of microstructures such as piezoelectric energy harvesters, sensors, accelerometers, bistable piezoelectric devices,

microgyroscopes, and MEMS [79, 80]. Fortunately, these microstructural components' behavior can be formulated based on the Euler-Bernoulli beam or Timoshenko beam theory [81– 85]. Researchers have investigated both linear and nonlinear vibration based energy harvesting devices, in which these devices were modeled using beam theory [84, 86–90]. Beam theory was also extended to nanomechanical cantilevers, such as the efforts performed by Villanueva et al. [91]. Some of these microstructures are submerged in fluids with various viscosities to achieve optimal performance, such as the work presented by Green and Sader [86]. They developed a theoretical model for the torsional response of a linear cantilevered beam excited by an arbitrary driving force while submerged in a viscous fluid. Esmaeili et al. [84] developed equations of motions for a microgyroscope, which was modeled as a linear cantilever beam with a tip mass exposed to excitation at the base. Their governing equations were derived from Hamilton's principle with a 6-DoF base motion where the torsion was neglected. Esmaeili et al. resolved the measurement error in oscillating gyroscopes due to cross-axis effects resulting from a combination of lateral rotation and longitudinal speeds in the linear regime.

Ansari et al. [79] developed an exact frequency analysis of a rotating beam with an attached tip mass while the beam undergoes coupled torsional-bending vibrations, where the base angular velocity was the instigator of the coupling. The extended Hamilton principle was utilized to derive the coupled equations of motion and the associated boundary condition. Ansari et al. demonstrated that the undamped structure experiencing base rotation has complex eigenvalues, which revealed a damping behavior. They also showed analytically that increases in the rotational velocity cause an increase in the frequencies. Later, Ansari et al. [81] presented a more complex vibration and parametric sensitivity analysis of a vibrating gyroscopic microdevice. The device consists of four beams attached to a stiff substrate with a mass at the

center, as shown in Figure 3-4. Thus, the device experienced coupled flexural and torsional responses. The results obtained from their analysis revealed that an increase in the base rotation increased the real and imaginary components of the eigenvalues.

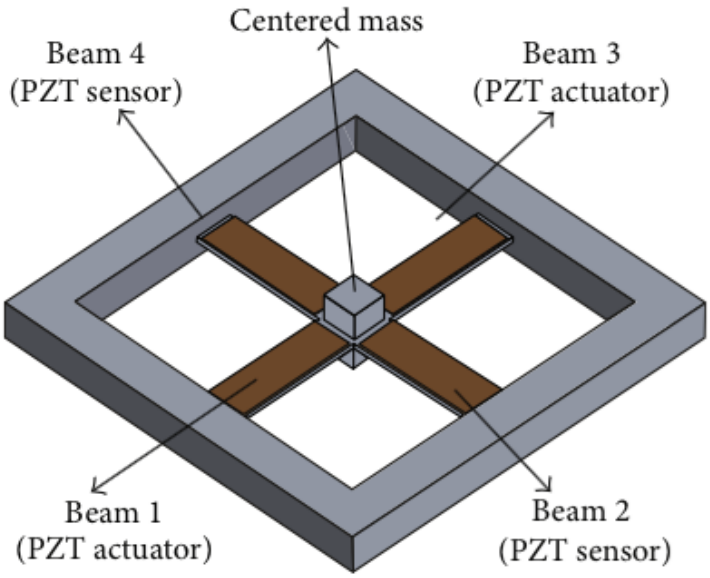

Figure 3-4. Schematic of a rocking-mass gyroscope Ansari et al. [79]

Kumar et al. [92] studied the effects of structural and inertial nonlinearities on near resonant response for a flexible cantilever inextensional beam exposed to base excitation combined with simultaneous parametric excitation. They conducted base excitation experiments for a cantilevered spring steel beam: $190\times19\times0.5$ mm^3, which was oriented at 80^o angle to induce both direct and parametric excitations. The energy method was utilized to derive the governing equations for their structure, where the rotational inertia and the torsion were assumed negligible [93]. Kumar et al. claimed that this work provided a baseline understanding of the effect of nonlinearities on parametrically excited systems.

It was apparent during this literature review that resonant energy harvesters were analyzed and designed for uniaxial base excitation at a single frequency, whereas many real-

world applications encompass multiaxial excitations, broadband spectrum, and time varying dynamic loading. In terms of multiaxial excitations for microsystems, the only study that can be found in the open literature is the work of Esmaeili et al. [84]. Limited studies were found in the literature that investigated energy harvesters for time varying broadband random excitations [80, 85, 94]. Ali et al. [94] employed a linearized stochastic methodology to a cantilever beam configuration energy harvester exposed to uniaxial stationary Gaussian broadband base excitations. Wickenheiser [80] developed an optimization methodology for designing linear and nonlinear vibration energy harvesters for maximizing power production by vibrations due to uniaxial broadband random loading environments at low frequencies. Wickenheiser [80] also linearized his approach by employing a close form approximation. Stanton et al. [85] investigated the nonlinear dynamics and stability of a broadband energy harvester under broadband random excitation. The harvester was modeled analytically and numerically as a cantilever beam with tip mass under uniaxial broadband base excitation, which were validated experimentally. Stanton et al. [85] considered the bifurcation parameter within the harvester as either a fixed or an adaptable tuning mechanism for enhanced sensitivity to broadband random excitation. Later, Stanton et al. [87] modeled nonlinear damping of uniaxial weakly excited piezoelectric actuators, which included nonconservative piezoelectric constitutive relations. In their analysis, a piezoelectric actuator was idealized as a cantilever beam with tip mass. Stanton et al. showed that the tip mass precipitated nonlinear resonances at lower base excitations. Stanton et al. [88] extended the method of harmonic balance to estimate the presence and impact of a bistable piezoelectric inertial generator. In their model, they included nonlinear dissipation and cubic softening influences in the electroelastic laminates. Westra et al. [89] investigated the interactions between a directly and a parametrically excited mode of a clamped- clamped

micromechanical beam resonator. They were able to detect the motion of a parametrically excited mode that provoked a change in another mode of the same structure. They demonstrated that the parametric excitation of one mode instigated a change in the fundamental frequency of the other modes.

3.3.5 Nanosystems Vibration

Nanomechanical cantilevers recently received increased consideration in biomedical sensing and prognostics and diagnostics applications. The biomolecular community deserves the majority of the credit for accelerating the research in nanomechanical cantilevers by generating applications that ranged from high-throughput biomolecular detection to bioactuation [95]. Biomolecular researchers and physicists suggested that the cantilever motion of DNA can be manipulated by controlling the entropy change during DNA hybridization [95]. Later scientists were able to measure the resonant frequency shift based on a nanomechanical cantilever augmented with an actuating layer for the detection of a prostate-specific antigen in fluid setting [96]. Dorignac et al. [97] estimated the stochastic dynamic response of biofunctionalized structures by utilizing the nanomechanical cantilever beam idealization. Their model assumed that the structure was linear and immersed in viscous fluid, where random excitations are generated by biomolecular interactions only; the model ignored any inertial loading. Salehi-Khojin et al. [98] presented a modeling approach to dynamic characterization of nanomechanical cantilevers with geometrical discontinuities. The linear analysis provided eigenvectors and eigenvalues for the first three modes and compared them with those obtained from the experiment and theory for uniform beams. The uniform beam theory was unsuccessful in predicting the system's response, while the discontinuous beam model provided better estimates. Seena et al. [99] studied the mechanical and dynamic characteristics of highly sensitive

piezoresistive nanomechanical cantilever sensors in detecting explosives in vapor phase, where the system was assumed to be linear. There were limited studies that investigated the nonlinear dynamic characterization of nanomechanical cantilever beams. Villanueva et al. [91] investigated the fidelity of Euler-Bernoulli's beam theory in estimating the dynamic response of nanomechanical cantilever beams in the nonlinear domain, where the beam was exposed to single axial harmonic base excitations. They showed that the Euler-Bernoulli's beam theory predictions differ significantly from their measurements for the nonlinearity of the first fundamental mode.

3.4. High-Cycle Fatigue

The main objective of this section is to provide a general overview of the available literature on high-cycle fatigue, with an emphasis on uniaxial and multiaxial harmonic and random dynamic loading. A brief review of early fatigue studies is provided; however, the core of this review is focused on recent theoretical, experimental, and computational advancements. The railway industry deserves the credit for instigating serious scientific studies for understanding, analyzing, classifying, and mitigating cyclic fatigue in the late 1800's. One of these early studies was by Wohler, who is considered one of the earliest pioneers of fatigue, for investigating fatigue failures in railway carriage axles [2]. Industrial investment in fatigue studies in the early 20th century led to the popular exponential relationships between stress amplitude and loading cycles by Dowling and the secondary effect on life due to mean stresses by Suresh [2, 100]. In many of these efforts, the focus was on stresses due to a constant amplitude sinusoidal loading, which led to the sinusoidal fatigue equations found in many fatigue textbooks [2, 101]. Significant considerations were dedicated to examining the mean stress effects for fatigue in welds due to harmonic and random loading [102, 103].

3.4.1 Uniaxial Loading

There are many circumstances in fatigue problems where it is unrealistic to always consider a constant amplitude sinusoidal loading. Examples of such cases are components in an off-road vehicle, electronic components in a rotorcraft, and an aircraft wing exposed to turbulent flow. Methods and standards were developed to determine the time to failure (TTF) with constant and variable loading amplitudes. The most well known is the "linear cumulative damage rule" for variable amplitude loading, which was attributed to Palmgren [104] and later popularized by Miner [105]. The Palmgren-Miner rule reasoned that fatigue damage is cumulative; thus, each stress cycle contributed to damage as a function of the number of cycles to failure for that cycle amplitude. Their linear cumulative damage approach neglected any sequence effects that may change fatigue life, that is, low amplitude stress followed by high amplitude versus the opposite sequence. Later, Miles [106] utilized the Palmgren-Miner cumulative damage rule for analyzing narrowband random vibration fatigue. The linear summation of damage was extended to an integral of stress peaks scaled by the PDF of the peaks for a narrowband random vibration fatigue problem. The resulting damage equation was a function of the sinusoidal stress versus the number of fatigue cycles (known as S- N curve), the material fatigue constants, and the standard deviation of stress. Crandall [107] and Lin [108] produced influential studies on nonlinear response PDFs and their effect on fatigue. Crandall developed equations for the rates of zero crossings for nonlinear non-Gaussian systems for structures with nonlinear restoring forces. The analytical relationship that Lin developed for nonlinear stress PDFs was based on a quadratic displacement to stress equation, where the displacement PDF was assumed to be nonlinear.

The narrowband random vibration loading case, deservingly, received significant

attention in the 1960's. Bendat [109] proposed the first significant step towards a method of determining fatigue life from the PSDs. For a narrowband time history loading, Bendat assumed that corresponding depressions of comparable size would follow positive peaks in the time history. Using this method, it was shown that the PDF of peaks for a narrowband signal tended towards a Rayleigh distribution. Bendat used a series of equations derived by Rice [110] to estimate the expected number of peaks using moments of area under the PSD. The narrowband solution was extremely conservative when broadband time history profiles were used. This was due to the assumption that peaks were matched with corresponding troughs of similar magnitude. The narrowband random vibration loading case was extended to arbitrary stress cycles using loading cycle versus amplitude counting methods. The narrowband time-domain approach emerged as the standard method in estimating the fatigue life of structures, widely known as the "rainflow" cycle counting method and attributed to Matsuishi and Endo [2].

To overcome the conservatism in the narrowband method of Bendat, Dirlik [25] proposed an important and extensive fatigue model that corrected for Bendat's method. Dirlik's model was based on a closed-form expression for the PDF of rainflow ranges using a Monte Carlo technique. For a given set of material properties, life estimates may be made for any number of different component geometries of load histories. Bishop [111] and Bishop and Sherratt [112] enhanced the rainflow cycle counting method by adding more mathematical rigor to improve its robustness and accuracy. The time-domain based theoretical approach formulated by Bishop was computationally intensive and showed little improvement on the accuracy over Dirlik's empirical model. Currently, the Dirlik's approach is widely applied to fatigue problems and fatigue codes such as HBM nCode and MSC-NASTRAN [21–23, 113].

Stochastic FEM provided high accuracy for antisymmetric laminates with different

boundary conditions under transverse random loading. Sweitzer [9] developed statistical methods for determining TTF for nonlinear clamped steel beam subjected to random loading. Broadband uniaxial base acceleration was applied with a frequency range from 20 to 500Hz for 0.5, 1, 2, 4, and 8 G_{rms}. The total strain was predicted by summing the strains from the linear, square, and cubic displacements. Sweitzer observed that the displacement PDF became skewed, that is, kurtosis less than 3.0, while the acceleration PDF was skewed in an opposite direction, but the velocity remained Gaussian. Sweitzer was unable to explain kurtosis behavior of the displacement, velocity, and acceleration as the system became more nonlinear.

Most recent work in high-cycle fatigue with application to random loads was the development of an analytic model by Paulus et al. [11] to predict the remaining life of a cantilever beam with notches experiencing random vibration excitation. The model utilized Paris' law to estimate fatigue life, where only the input power spectral density and damping factor were required. The model applied linear elastic fracture mechanics for crack propagation and included the shift in frequency that resulted from the crack growth. Habtour et al. [114] developed an FEM model to predict the stress intensity and natural frequency during damage accumulation. The analytic model developed by Paulus et al. was coupled with the FEM to predict TTF for complex geometries for which stress intensity values were not available.

3.4.2 Multiaxial Loading

The autoregressive moving average (ARMA) model was applied in fatigue problems by scientists. Leser et al. [4] discussed the use of ARMA for stationary variations and Fourier series model for nonstationary variations. They obtained strain history of an automotive front suspension component driven through proving ground maneuvers. Critical fatigue damage plane

was selected, followed by rainflow cycle counting of the strain data. The critical plane approach involves obtaining the maximum shear strain and the plane that acts on it, then using the maximum normal stress acting on the plane to calculate an effective stress [2]. A multiaxial fatigue model, valid for proportional loading, was employed, and two fatigue failure modes due to normal strain and shear strain were considered. Reconstructions using the ARMA model introduced a number of large cycles that are not present in the original loading; all reconstructions were tending to be biased toward shorter lives. Lu [115] applied the ARMA model to higher-order nonlinear beams and composite plates subjected to stochastic loading. A fourth-order nonlinear beam equation was examined to study the effect of rotary inertia and shear deformation on the root mean square (RMS) values of displacement response. A linearly coupled equivalent linearization method was applied to the simulated data of nonlinear beams. Reasonable estimations of both the nonlinear frequencies and the power spectral densities were shown. However, Lu stated that accurate result for MDoF systems and other linearization techniques need to be explored for the higher-order beams.

The usability of the energy parameter, being the sum of the elastic and plastic strain energies in the critical plane, for structures experiencing cyclical loading received significant attention from fatigue experts. Lagoda et al. [116] experimentally evaluated its use by exposing steel specimens to biaxial nonproportional random tension and compression loads. They developed an algorithm to predict fatigue life under a biaxial stress state in high-cycle regimes using the energy parameter. Lagoda et al. concluded that normal strain energy density in the critical plane seemed to be an efficient parameter for fatigue life prediction under random and cyclic nonproportional loading conditions in high-cycle fatigue. Pitoiset et al. [6] studied multiaxial fatigue of structures exposed to random vibration. They developed frequency- domain

methods for estimating the high-cycle fatigue life of metallic structures [117]. The cycle counting concept was extended to multiaxial random processes. The multiaxial rainflow method consisted of counting rainflow cycles on all possible linear combinations of the random vector components. Pitoiset and Preumont frequency domain methods were computationally more efficient than the time-domain approach and with reasonable correlation with the time- domain method in terms of localizing the critical areas in the structure. They also proposed the frequency domain implementation of Crossland's failure criterion, which also was found in very good agreement and much faster than its time-domain counterpart. Pitoiset et al. [118] showed that a mean value other than zero determined the presence of a very low frequency component that did not exist in the real process. This incoherence was mitigated by the construction of a process having the same RMS of von Mises stress, but with correct frequency content. This approach did not take into account phase differences between the multiaxial stress components. Carpinteri et al. [119, 120] investigated theoretical and experimental application of the weight function method to estimate the principal stress directions under multiaxial random loading. The stress tensor and its eigenvectors (principle direction cosines) changed at each time increment. The Euler angles were calculated from the matrix of the eigenvectors for a generic time instant and then the angles were averaged by employing suitable weight functions. The experimental data were successfully correlated with the theoretical model using the maximum principal stress direction estimated by the weight function method. Liu and Mahadevan [5] developed a model where a multiaxial high-cycle fatigue principle based on the critical plane was correlated with the fatigue crack plane. They introduced an adjustment factor to consider the effect of the mean stress, which can be calibrated by utilizing experimental fatigue results. Liu and Mahadevan [121] extended the model to predict the fatigue life of a composite beam under off-axis loading,

which caused proportional multiaxial stress within the material. Later, Liu [122] extended the same model for composite beams under uniaxial and biaxial fatigue loading at a frequency of 10 Hz. The results of the proposed fatigue model were validated experimentally for low frequency loading.

In high-cycle fatigue, probabilistic methodology is common in assessing the reliability of structures subject to multiaxial random loading. Lambert et al. [123] developed a probabilistic approach for structures exposed to Gaussian random loading with a nonzero mean. This approach was used to estimate the octahedral shear stress distribution for stationary random stresses. A Monte Carlo simulation was then employed to characterize the octahedral shear stress distribution. According to the authors, the experimental results were not available; thus, errors may have occurred due to the quality of the random process generator and the limited frequency range of the PSD input load, which was approximately 5–100Hz. Braccesi et al. [124] reduced multiaxial stress analysis to an equivalent uniaxial process that defined random process in the time and frequency domains. This analytical approach was based on the energy contents of the shear stress acting on the planes belonging to the octahedral cone [125]. Allegri and Zhang [126] applied the inverse power laws to assess the fatigue damage of structures exposed to accelerated broadband Gaussian random vibration. A scaling law was used to relate the test time in a laboratory to the actual operational life. Allegri and Zhang stated that fatigue accumulation in a random multiaxial loading environment was more rapid than for constant amplitude loading; that is, the *S-N* curve slope was larger in the case of random loading. This implied that the correct value of the exponent, which appears in the inverse power scaling law, was estimated by random fatigue tests on representative material samples. Zhou et al. have also pointed the same observations for uniaxial random vibration [42].

One of the most common approaches found in the literature was the application of stochastic analysis that combined structural failure models with linear FEM to develop a methodology for the reliability assessment [127, 128]. Segalman et al. [7] provided an approach for calculating the RMS von Mises stresses for structures loaded randomly. Segalman et al. estimated the RMS von Mises stresses from stress component transfer functions that were extracted from the FEM. The RMS stresses were calculated directly from the linear stress and displacement modes and compared to the traditional Miles' approach, which uses a spectrum of root mean square acceleration response to a random PSD applied to a single degree-of-freedom system [101]. Lei and Qiu [127] developed dynamic stochastic FEM to study the dynamic response of frame structures with stochastic parameters to dynamic excitation. The dynamic response of random structure was analyzed using a perturbation approach and modal superposition. They provided linear numerical examples to indicate that using dynamic stochastic FEM reduced the computation time while improving accuracy of the solution for the dynamic analysis of structures with stochastic parameters of dynamic excitation. However, the randomization was applied to the structural parameters, that is, mass and stiffness, but not for the excitation. Similarly, Lagoda et al. [129] developed an algorithm for estimation of fatigue life under multiaxial random vibration using spectral methods based on fatigue experiments performed on steel samples. The method retained the accuracy of the linear FEM model and modal analysis. Tibbits [130] extended the approached developed by Segalman et al. to calculate the percentiles of von Mises stress in linear structures subjected to random loads having nonzero mean values. He constructed von Mises stress statistics as a series of noncentral Chi-square distributions. The desired precision of the model was based on the number of terms in the series. Guechichi et al. [131] proposed a method for predicting the fatigue life for different materials

subjected to constant amplitude multiaxial proportional loading that covered high- cyclic fatigue. FEM was developed to evaluate the fatigue life and to localize the critical region. Two cases were solved: the first case was a rectangular plate with low thickness under single axial and alternating bending loads; the second case was a circular cross-section rod subjected to uniaxial load and alternating torsion moment. The Crossland criterion and FEM analysis were used to compute the maximum equivalent stress. McNeill [128] provided statistical failure prediction of orthotropic composite plates under random loading. Stochastic FEM solutions of damaging load of the structures were obtained with layerwise plate theory. First- order perturbation technique was utilized to estimate the mean and variance of failure.

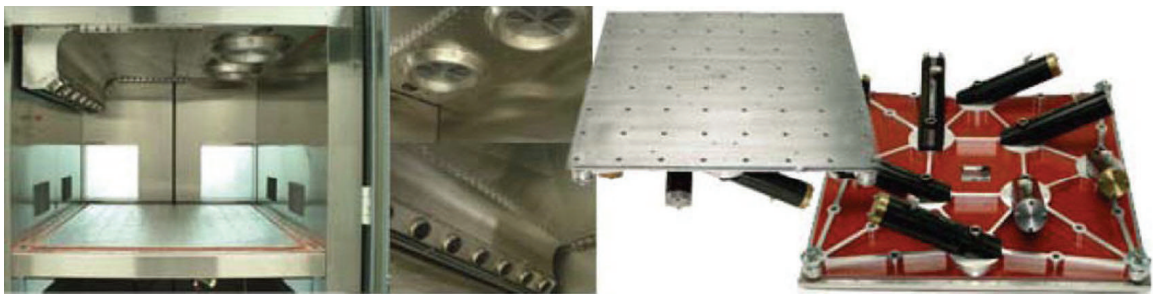

Figure 3-5. High accelerated life testing (HALT) chamber [15]

3.5 Experimental MDoF Vibration Studies

The typical product development approach is an iterative cycle known as design-prototype-test-fix [45]. Unfortunately, this process is time consuming and requires expensive physical prototyping and testing. The lack of reliability prediction capability of a product leads to deficiency in its development. To overcome this impediment, the design-prototype- test-fix approach was greatly modified in the electronics industries, with the introduction of high-accelerated life testing (HALT) methodology during the prototyping and qualification stages. This can be accomplished by utilizing a HALT shaker table/chamber, shown in Figure 3-5. A

typical HALT chamber has a broad frequency spectrum between 10 and 10kHz and runs from 1 to 150 G_{rms}. The intent of HALT is to accelerate the failures in electronic devices by applying a higher than normal stress to failure while assessing the design robustness through rigorous root cause failure analyses. The basic idea of HALT is to produce repetitive shocks to the shaker table using multiple pneumatic actuators at different locations of the table, thus producing multiaxial energy. Thus, the device under test is exposed to uncontrolled broadband multiaxial random excitation, with the exception of the RMS acceleration value. Furthermore, the HALT chambers are capable of exposing the test article to thermal stresses, and in some cases to humidity while it is under vibration. Designers and quality engineers have utilized HALT testing to expose design weaknesses that would eventually emerge as field failures [14]. Unfortunately, HALT provides only a qualitative rather than a quantitative understanding of the failure modes and mechanisms due to two limitations [14]. First, the only acceleration input to the actuators that can be controlled is an acceleration RMS, G_{rms}; thus, the only excitation that can be achieved is a quasi-random vibration. The second limitation is the fact that HALT uses pneumatic actuators; consequently, it is impossible to control the energy input to each axis individually. Due to these limitations, it is nearly impossible to ascertain the most dominant failure mode or the axial load that initiates the damage. It is also impossible to precisely correlate structural failure during HALT to life-cycle seen in the field.

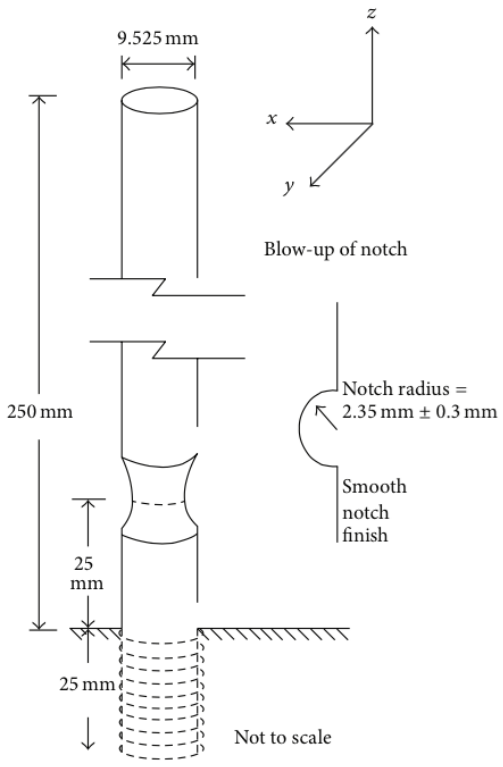

Figure 3-6. Dimensions of samples tested by Whiteman and Burman [10]

Due to the limitations of single axis electrodynamic shakers, hydraulic actuators, and HALT shakers, researchers are currently investigating the utility of multiaxial electro- dynamic shakers to understand the response of structures exposed to multiaxial vibrations and subsequently the failures due to these complex dynamics. However, studies evaluating the merits of multiaxial vibration testing using multiaxial electrodynamic shakers are very limited. This deficit is attributed to high cost constraints associated with these shakers. Only a few investigators such as Whiteman and Burman [10, 13], French et al. [12], Gregory et al. [132], and Ernst et al. [49] have pointed out the shortcomings of the sequential single axis vibration method. They have also reported evidence of differences in failure modes and fatigue life for multiaxial loadings versus single-axis inputs by utilizing multiaxial electrodynamic shakers. These studies are discussed in detail below.

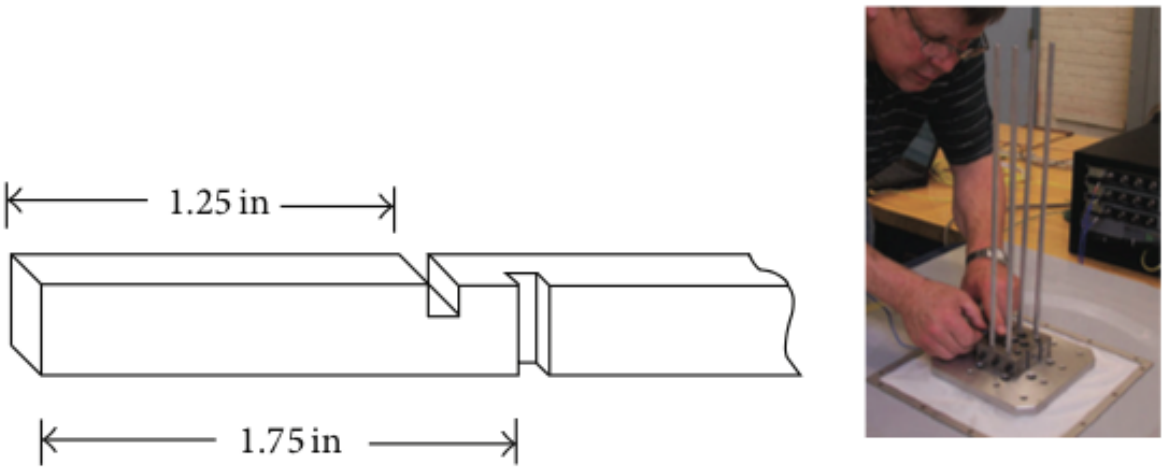

Figure 3-7. Dimensions of samples tested by French et al. and test setup [12]

Some of the limited work performed using multiaxial shakers was by Fullekrug [133], who characterized the modal response in the frequency and time domains of a structure under base excitation using a hydraulic shaker that had limited frequency range from 0 to 120 Hz. Fullekrug developed kinematic relationships between loads at the base and structural responses due to these loads. The primary conclusion was that the frequency domain was best suited for a general and reliable modal identification of linear systems, whereas the time-domain method was more suited for analyzing transient vibration. Whiteman and Burman [13] investigated the differences between fatigue mechanisms and the effects of uniaxial versus triaxial testing. The samples used in this study were 250mm long aluminum beams with a 9.5 mm diameter and a 0.235 cm radius notch stress concentrator around the entire circumference of each specimen as shown in Figure 3-6. Whiteman and Burman [10] performed a uniaxial random excitation experiment in the transverse direction and then repeated the same test for sequential excitation in the axial direction followed by the transverse direction. The random vibration acceleration inputs were 3.0, 3.5, 4.0, and 4.5 G_{rms} with a frequency range from 15 to 85Hz. The tests were then repeated using simultaneous triaxial excitation. It was found that the excitation in the axial

direction did not weaken the specimens; on the contrary, it increased the samples' fatigue life. Whiteman and Burman [10] believed that work or strain hardening took place during the axial excitation portion of the second set of tests, which increased the fatigue failure resistance in the transverse direction. In the triaxial vibration experiments, the stresses that eventually caused fatigue failure were predominantly in the axial direction. However, simultaneous triaxial excitation accelerated the crack initiation more rapidly. By comparison, the TTF for the single axis experiments was appreciably longer than the triaxial experiments for the same input energy level. French et al. [12] performed durability experiments on notched beam specimens using both sequential uniaxial and simultaneous biaxial testing on a TEAM tensor triaxial shaker, which was electrodynamically driven. The specimens were $19\times0.25\times0.25$ in^3 aluminum beams with notches located at two adjoining sides of the beam, as shown in Figure 3-7. One notch was normal to a transverse excitation (*x*-direction) while the other notch was normal to the other transverse excitation (*y*-direction). The notches were introduced to act as stress concentrators with depth of 0.08 in. The notch normal to *y*-direction was 0.5in above the notch normal to the *x*-direction, as shown in Figure 3-7. The base excitation signal was a sine chirp from 10 to 35Hz over 30s. The peak-to-peak acceleration amplitude was held constant at 4G. The sequential uniaxial and simultaneous biaxial experiments produced different TTF, different failure distributions, and different failure modes. French et al. concluded that sequential uniaxial testing generally takes longer time to conduct than simultaneous multiaxial testing. Furthermore, the results from the sequential uniaxial testing are prone to produce questionable results. Unfortunately, the bandwidth in this study was limited and inapplicable to realistic structures.

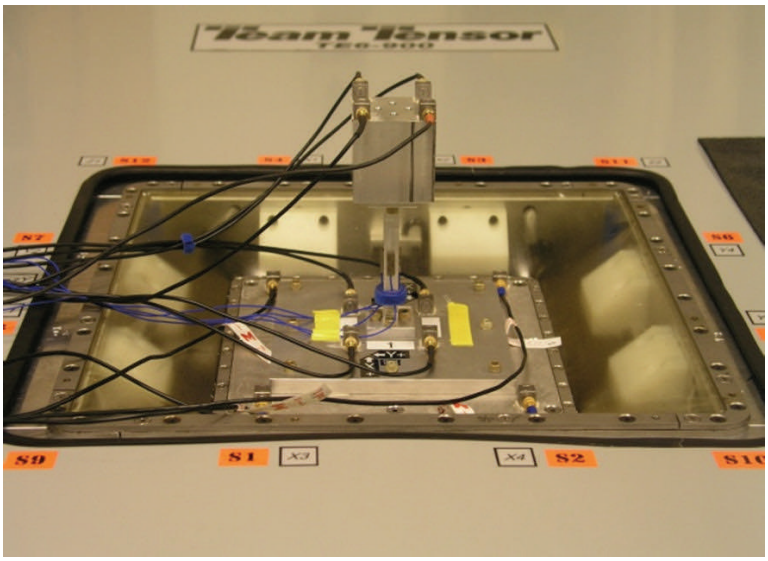

Figure 3-8. Simple structure under multiaxial loads [132]

At Sandia National Laboratories, Gregory et al. [132] investigated the prospect of using a six-DoF multiaxial electrodynamic shaker, developed by TEAM Inc., to illustrate the importance of multiaxial excitations in performing realistic tests. Dynamic characterization experiments were performed in uniaxial and multiaxial modes to compare the responses of a structure under the different loadings with bandwidth of 10–2000Hz. The specimen used for this experiment was a short rectangular aluminum beam with a lumped mass mounted at the tip, as shown in Figure 3-8. Acceleration PSD input level of $0.0032G^2/Hz$ was chosen to yield an overall level of $2.5G_{rms}$ for the *X*, *Y*, and *Z* translations. A spectral FEM model of the structure was constructed to investigate the differences in the calculated von Mises stresses. According to Gregory et al., the control system was configured for a full six-DoF random vibration input from 20 to 2000Hz with zero coherence between the inputs. The experiment was then configured for uniaxial translation for each DoF. The PSD levels were selected to be the same as for the previous six-DoF tests to allow comparison of responses for uniaxial versus multiaxial excitations. The experimental results showed significant differences in the acceleration response of the mass as well as the

strain measured in the beam. The modal participations were different for the multiaxial experiment, and the resulting instantaneous stresses and accelerations states were different, not only in magnitude, but also in location and direction. This indicated that the potential failure modes would be different.

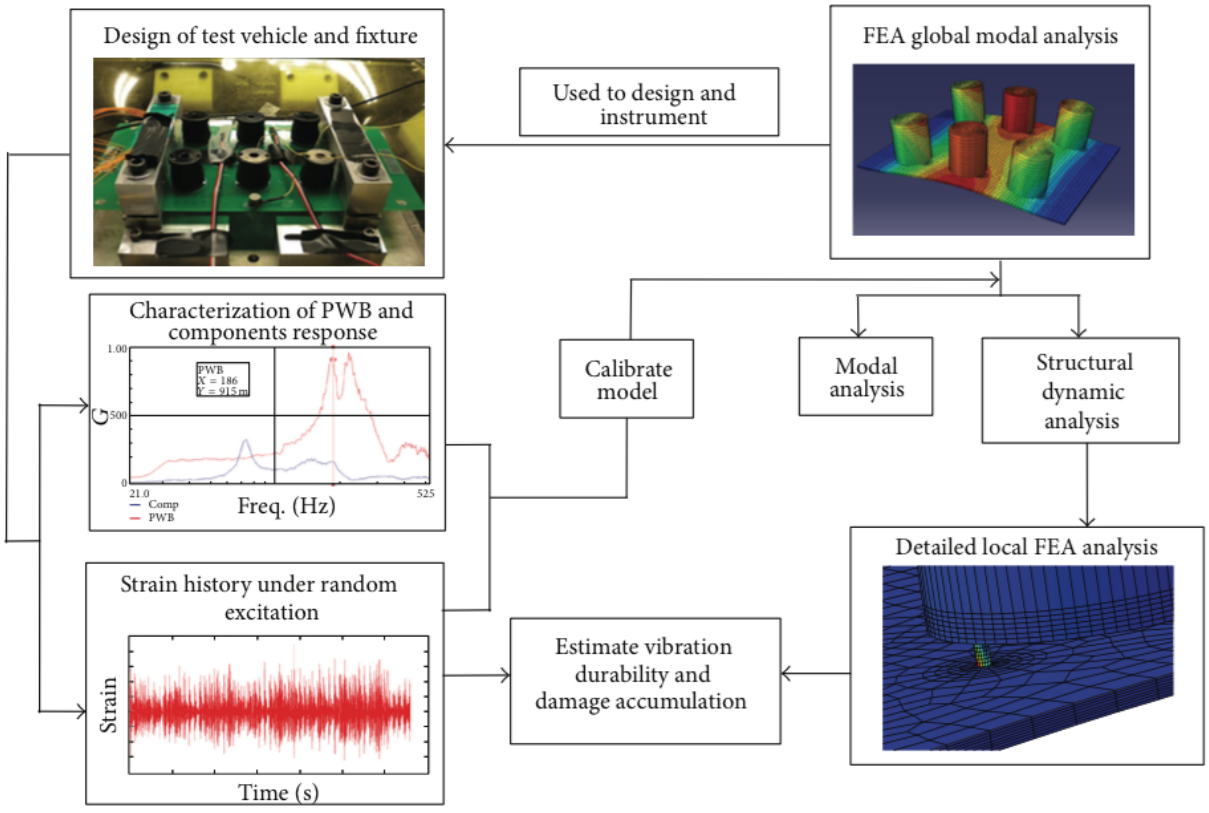

Figure 3-9. Approach for mapping dynamic loads to fatigue [136]

3.6 Mapping Dynamic Loads to Fatigue

Some fatigue specialists maintain that the stress levels caused by vibration are usually too low to contribute to fatigue damage and that fatigue cracks start because of higher stresses present in the loading history [2]. It is also commonly known that the substantial number of stress cycles produced by high-frequency excitations can considerably contribute to fatigue damage and may cause failure without reaching high load levels [5, 134]. Special analysis is

often required in these situations since the vibration data is not in a form that can be used directly in a common fatigue damage model such as the Palmgren-Miner rule. A common approach in mapping stationary random dynamic loads to fatigue is through performing a summation of all modal spectral densities and determining the response standard deviations in a broadband frequency range, covering all resonance frequencies of the structure within broadband frequency range. The modal cross-spectral densities are typically neglected [135]. Nonetheless, Dahlberg states that lightly damped structures with well-separated fundamental frequencies are not a sufficient reason to neglect modal cross-spectral densities even if the random excitation of the structure is broadband where several modes of the structure are excited [135].

To accurately estimate multiaxial vibration durability and damage accumulation, the dynamics response model of the structure must be coupled with experimental data, as illustrated in Figure 3-9 [136]. This approach requires an iterative and arduous development. The reason for this is that the reaction forces and vibration velocities in complex structures depend not only on the strength of excitation, but also on the coupling between structures and their components, as shown in Figure 3-9. The computational and experimental coupling is necessary since the FEM cannot model structures adequately up to mid frequency range due to the higher modal density. The experimental tasks provide FRF dynamic characterization of the structure and its components as well as time history data. A more practical approach is to utilize the experimental FRF data to represent the structure and then combine it with the FEM models as shown in Figure 3-9. However, this approach is not applicable if the structure is exposed to high amplitude excitation that could generate nonlinear behavior. Thus, the time history data must be combined with the FEM models. This approach is intended to yield accurate results but is time consuming to set up and is computationally expensive.

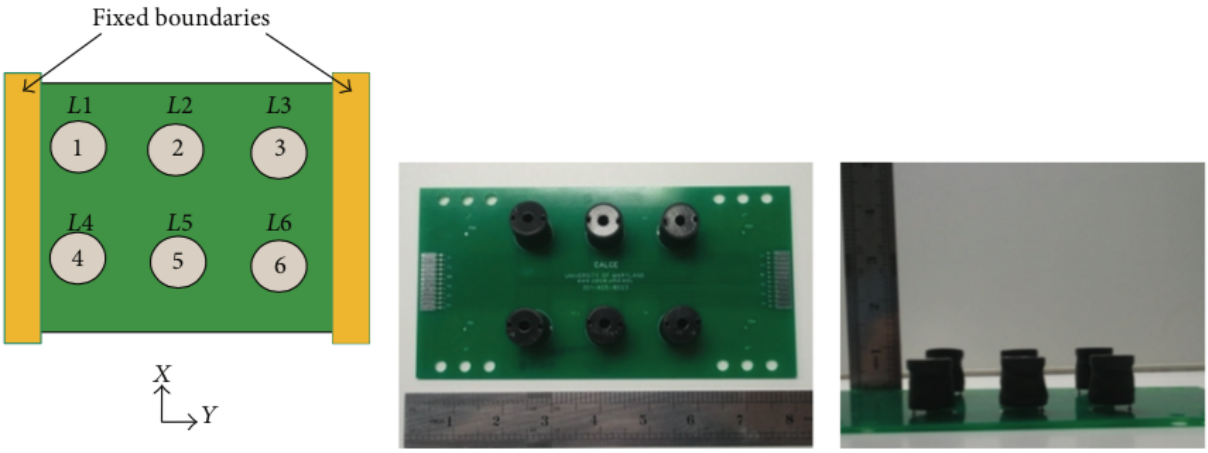

Figure 3-10. CCA with six large inductors, dimensions are in inches

Currently, the Center for Advanced Life Cycle Engineering (CALCE) at the University of Maryland and the US Army Research Laboratory (ARL) are investigating the utility of multiaxial electrodynamic shakers. The objective is to study the differences in failure modes and fatigue life for multiaxial versus single-axial excitations by utilizing multiaxial electrodynamic shakers. The multiaxial electrodynamic shaker used for this study was developed by TEAM Inc. It consists of eight plane actuators and four out-of- plane actuators underneath the shaker table, as shown in Figure 3-10. The twelve electrodynamic shakers are mechanically coupled to the table. This architecture allows the shaker to produce a true six-DoF vibration environment. Each axis has four shakers with 200lbf rotation per axis. The excitation limit is up to 30Gs with 0–3000Hz. The objective is to establish a quantitative and qualitative relationship between complex random multiaxial dynamic loading and the failure mechanisms. In this study, CALCE performed two sets of three random excitation experiments on CCAs. The first set was for low amplitude broadband stationary random excitations, which consisted of the following single-axis in- plane, single-axis out-of-plane and combined in-plane and out-of-plane excitations. Each CCA was clamped along the two short edges while it was free along the two long edges, as

shown in Figure 3-10. The CCA contained six large heavy inductors with high center of mass and with high standoff, as shown in Figure 3-10. Each inductor was attached to the CCA via two leads to instigate bending motion in the in-plane direction and a gyroscopic motion. In the first set of tests, the excitation was a uniform broadband random stationary profile at low PSD acceleration input of 0.0025 g^2 /Hz and 0.78G_{rms}.

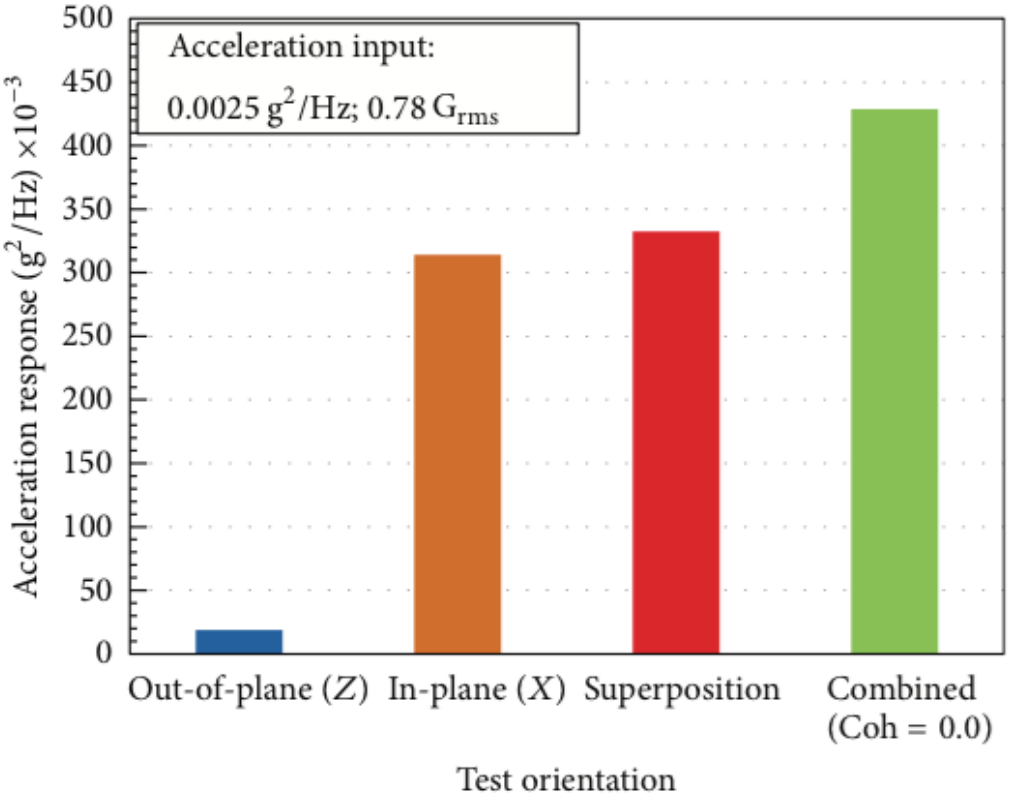

Figure 3-11. Component 2 acceleration response in the *x*-direction 0.78G_{rms}

The acceleration responses of the middle component for the three different excitations mentioned above are shown in Figure 3-11 and compared to the superposition technique. The same sets of tests were repeated for higher PSD acceleration input of 0.04g^2 /Hz and 3.14G_{rms}. The acceleration responses in the in-plane direction (*X*) of the middle component for the three different excitations mentioned above are shown in Figure 3-11 and Figure 3-12 and compared to

the superposition technique. Figure 3-11 and Figure 3-12 show the component response due to multiaxial excitations is equivalent to the linear superposition of corresponding uniaxial responses. Furthermore, as the acceleration input increases, the deviation between the actual component response due to multiaxial vibration and the linear superposition of uniaxial responses increases as well. This deviation may be justified based on three reasons. First, the modal participation and nonlinear interactions between components and PWB could be the major contributors to this deviation. Second, the geometry of each component may create gyroscopic forces, which are proportional to the velocities consistent with viscous damping forces; however, they are conservative forces [137]. Finally, the material non- linearity of the PWB and the solder joints may augment the drastic difference in TTF between multiaxial excitations and sequential uniaxial superposition, as shown in Figure 3-13. Further studies are needed to quantify these contributions. The fatigue damage in the components' interconnects site, shown in Figure 3-14, is due to a combination of flexural deformations in PCBs and inertial forces (translation and gyroscopic motions). The inertial forces are generated by the mass of large/heavy components with high standoff. Thus, simultaneous multiaxial vibration may have the potential to generate higher stresses through nonlinear cross-axis interactions at the component level.

In this study, the change of the natural frequencies of a middle component (L5) and an edge component (L1) were monitored during the experiments mentioned above. Ernst et al. [49] showed that the frequencies shifted linearly across all components under single axial and biaxial vibration conditions, as shown in Figure 3-15. Ernst et al. assumed that this shift corresponded to fatigue crack growth in the component lead shown in Figure 3-14. Their results also revealed that natural frequency was lower when the CCA was exposed to multiaxial excitation, but they indicated that further investigation is needed to verify this phenomenon. Ernst et al. proposed

using this approach as a possible method for failure prognostics and prediction for the components' remaining life. This approach has been observed in current studies exploring methods for improving accelerated fatigue testing by simultaneously monitoring the modal parameters of critical components [138–142].

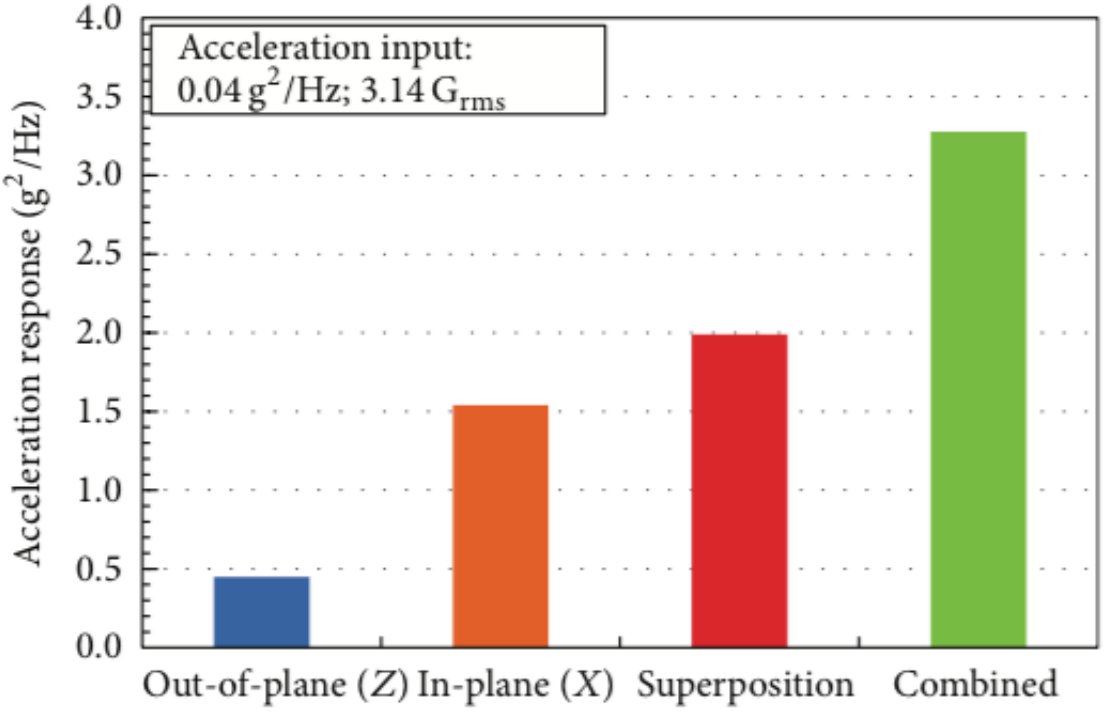

Figure 3-12. Component 2 acceleration response in the *x*-direction at $3.14G_{rms}$

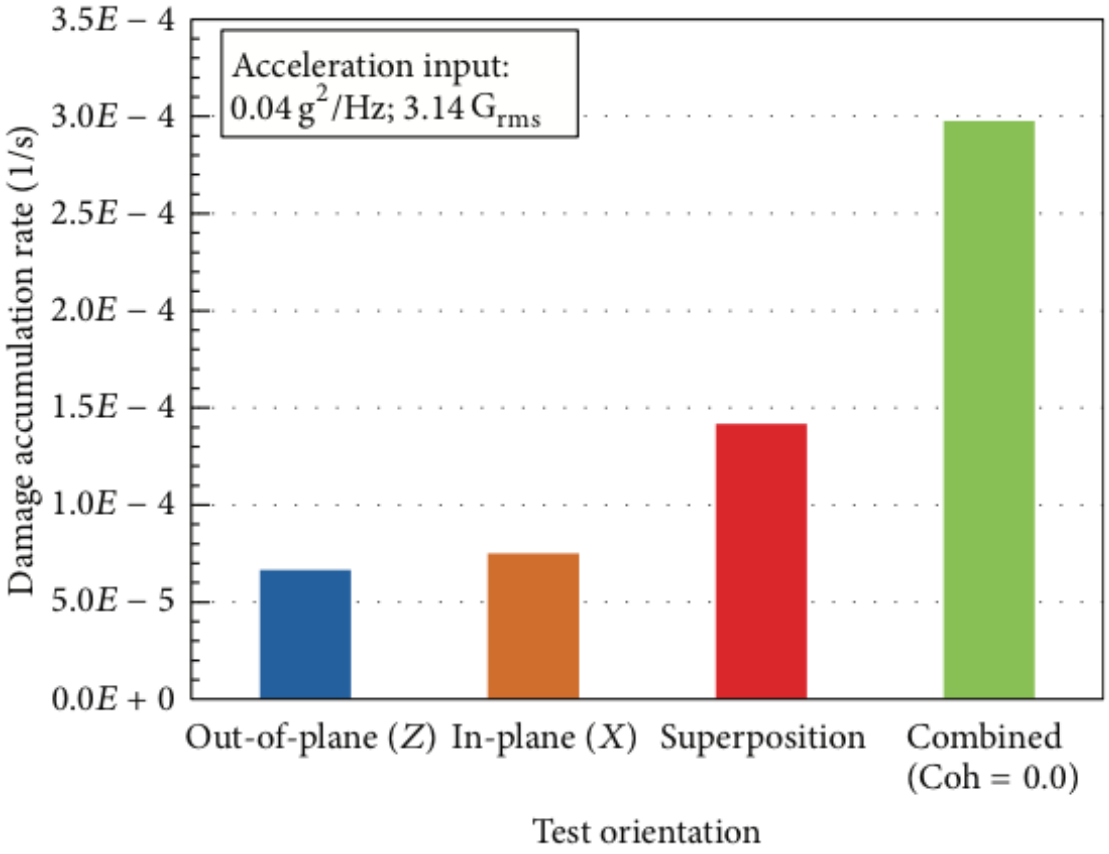

Figure 3-13. Component 2 damage accumulation rate at $3.14G_{rms}$

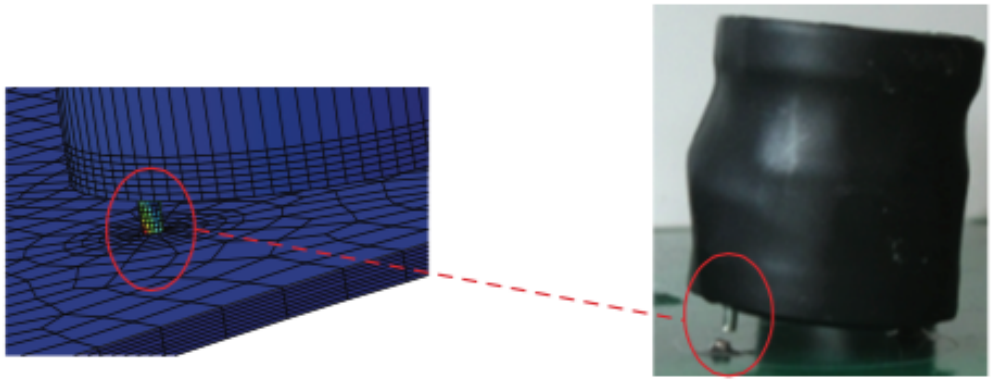

Figure 3-14. Component L2 failure due to in-plane and out-of-plane excitations at 3.14 G_{rms}

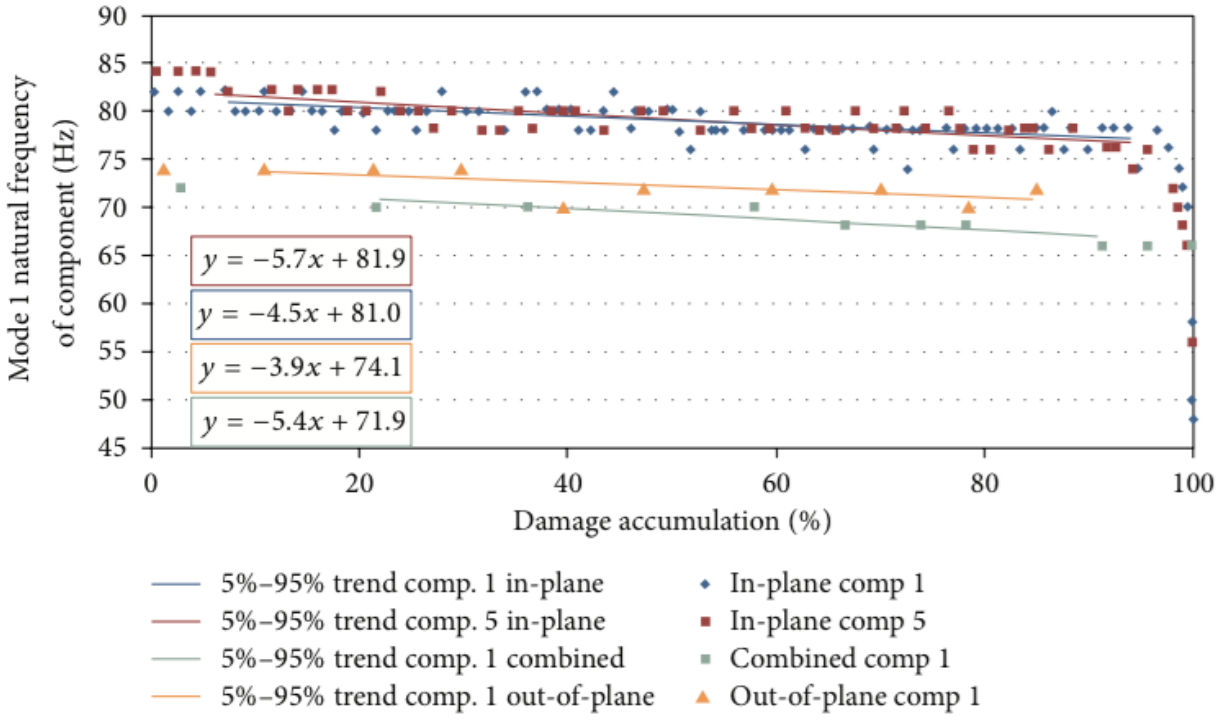

Figure 3-15. Change in the natural frequency as a function of damage accumulation [49]

3.7 Future Directions

Based on the literature review and interaction with government agencies, industries, and academia, the authors recognized three major thrust areas for continued research and deployment: modeling and simulation, experimental and testing, and standards and procedures updating. These thrust areas are summarized in Figure 3-16. As mentioned above, several closed-form solutions and computational models were developed to approximate the response and fatigue life of linear and nonlinear structures exposed to complex vibration loading. Most of these models are based on unique approximations and can only be applied to specific loading and boundary conditions. Some of these loading conditions were not possible to duplicate in a laboratory environment prior to the introduction of the multiaxial electrodynamic shaker capable of producing rotational degrees of freedoms. This capability is opening a plethora of

opportunities to validate and update existing multibodies and flexible-bodies dynamic models and produce new realistic models to adequately approximate the response of structures and subsequently their remaining life. Analysts may be able to move beyond the laborious approach of conducting explicit FEM analysis calibrated with suspect transfer functions obtained from sequential testing, then following it by another explicit analysis based on time history data and comparing the strain results to those from testing. There might be a possibility for developing spectral FEM models to avoid using the cumbersome and expensive explicit FEM.

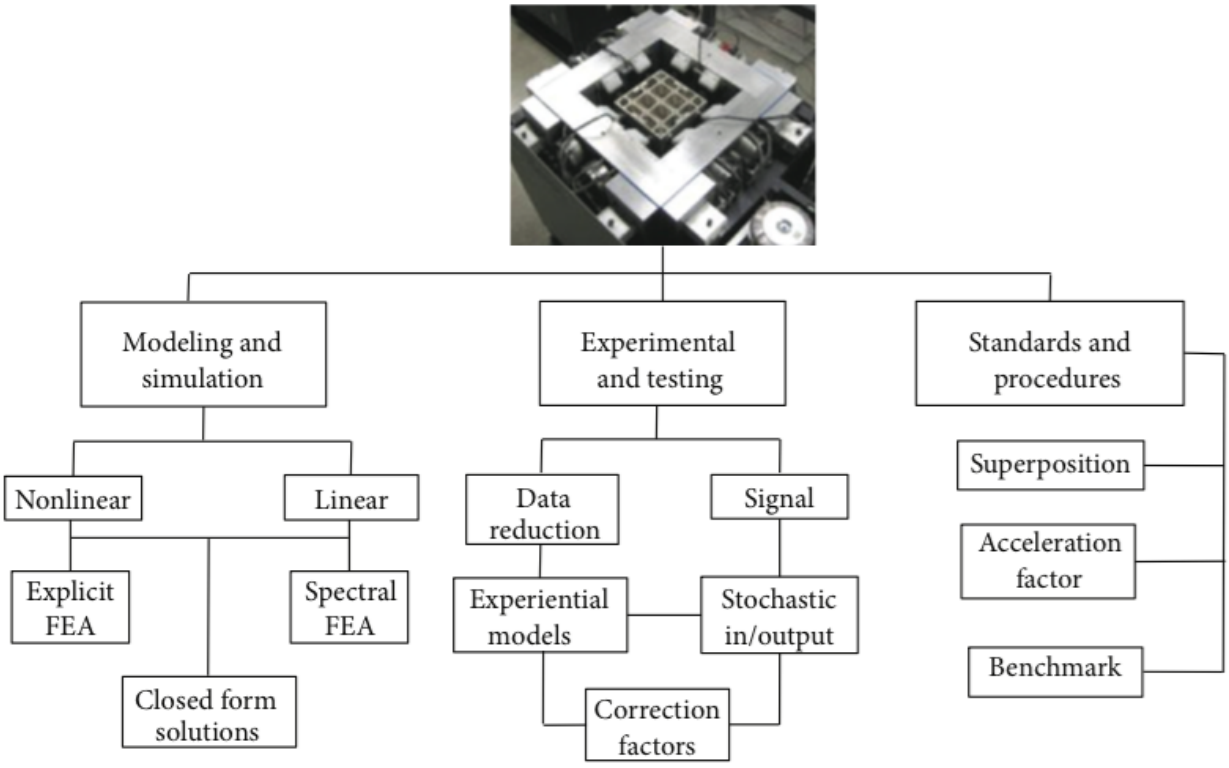

Figure 3-16. Research areas and potential gaps

As shown above, CALCE/ARL has shown that simultaneous multiaxial vibration may have the potential to generate higher stresses through nonlinear cross-axis interactions at the component level. This was possible because of the capabilities that the MDoF electrodynamic shaker was able to provide. However, generating the loads for different complex operational

conditions and tracking the structural response of critical components require significant signal processing, data reduction, and real-time computation of the inputs/outputs. Stochastic models may potentially be updated as a result of the coherent/incoherent multiaxial random vibration excitation that can be achieved with the MDoF electrodynamic technology. Accelerated test factors are currently incorporated in the MIL-STF-810G combined with exaggeration factors to provide conservatism in the uniaxial test schedules. Multiaxial vibration studies may provide insights into whether these factors are reasonable or not and provide new guidelines for accelerated life testing using MDoF technologies. Furthermore, the design for prognostic and diagnostics, structural health management and condition-based maintenance may be enhanced and ruggedized through real-world multiaxial dynamics laboratory simulations.

3.8 Conclusion

It can be concluded from this literature review that it is essential to understand the structural characteristics of devices in order to correlate the defects with the dynamic responses. As mentioned above, the main challenge in structural systems is the prediction of the reliability and lifetime of the critical components. Therefore, it is imperative to identify the failure mechanisms of the components through adequate computational and experimental analyses. How- ever, the experimental and computational approaches must emulate the real-world operational conditions, which include simulating MDoF dynamic loads. This involves estimating and measuring the transient multiaxial displacements, which can be accomplished with the aid of a multiaxial shaker.

Establishing the relationship between different flexible structures formulations is an important issue since there is a need to clearly define the assumptions and approximations underlying each formulation. This may allow for establishing guidelines and criteria that define

the limitations of each approach used in flexible structures dynamics. This task can now be accomplished by utilizing multiaxial vibration capability, which is making it possible to perform the CALCE/ARL joint research efforts to study large deformation of flexible systems exposed to multiaxial excitations.

3.9 References

[1] J. E. Shigley and C. R. Mischke, *Mechanical Engineering Design*, McGraw-Hill, Boston, Ma, USA, 6th edition, 2001.

[2] N. E. Dowling, *Mechanical Behavior of Materials: Engineering Methods for Deformation, Fracture, and Fatigue*, Prentice Hall, Upper Saddle River, NJ, USA, 2nd edition, 1999.

[3] I. Elishakoff, "Generalized Eringen problem: influence of axial force on random vibration response of simply supported beam," *Structural Safety*, vol. 4, no. 4, pp. 255–265, 1987.

[4] C. Leser, L. Juneja, S. Thangjitham, and N. E. Dowling, "On multi-axial random fatigue load modeling," SAE Technical Chapter 980696, Society of Automotive Engineering, 1996.

[5] Y. Liu and S. Mahadevan, "Multiaxial high-cycle fatigue criterion and life prediction for metals," *International Journal of Fatigue*, vol. 27, no. 7, pp. 790–800, 2005.

[6] X. Pitoiset, A. Preumont, and A. Kernilis, "Tools for a multiaxial fatigue analysis of structures submitted to random vibrations," in *Proceedings of the European Conference on Spacecraft Structures Materials and Mechanical Testing*, Braunschweig, Germany, November 1998.

[7] D. J. Segalman, C. W. G. Fulcher, G. M. Reese, and R. V. Field Jr., "Efficient method for calculating rms von Mises stress in a random vibration environment," *Journal of Sound and Vibration*, vol. 230, no. 2, pp. 393–410, 2000.

[8] D. Socie and G. Marquis, *Multiaxial Fatigue*, Society of Automotive Engineers, Warrendale,

Pa, USA, 2000.

[9] K. A. Sweitzer, *Random Vibration Response Statistics for Fatigue Analysis of Nonlinear Structures [Ph.D. thesis]*, University of Southampton, Southampton, UK, 2006.

[10] W. E. Whiteman and M. S. Berman, "Fatigue failure results for multi-axial versus uniaxial stress screen vibration testing," *Shock and Vibration*, vol. 9, no. 6, pp. 319–328, 2002.

[11] M. Paulus, A. Dasgupta, and E. Habtour, "Life estimation model of a cantilevered beam subjected to complex random vibration," *Fatigue and Fracture of Engineering Materials and Structures*, vol. 35, no. 11, pp. 1058–1070, 2012.

[12] R. M. French, R. Handy, and H. L. Cooper, "A comparison of simultaneous and sequential single-axis durability testing," *Experimental Techniques*, vol. 30, no. 5, pp. 32–37, 2006.

[13] W. E. Whiteman and M. Berman, "Inadequacies in uniaxial stress screen vibration testing," *Journal of the Institute of Environmental Sciences and Technology*, vol. 44, no. 4, pp. 20– 23, 2001.

[14] E. Habtour, C. Choi, G. Drake, A. Dasgupta, and M. Al- Bassyiouni, "Improved reliability testing with multiaxial electrodynamics vibration," in *Proceedings of the 56th Annual Reliability and Maintainability Symposium*, San Jose, Ca, USA, 2010.

[15] E. Habtour, C. Choi, M. Osterman, and A. Dasgupta, "Novel approach to improve electronics reliability in the next generation of US army small unmanned ground vehicles under complex vibration conditions," *Journal of Failure Analysis and Prevention*, vol. 12, no. 1, pp. 86–95, 2012.

[16] C. J. Dodds and C. H. Ward, "The ubiquitous four-poster," *Engineering Integrity Society*, vol. 16, no. 1, pp. 17–23, 2005.

[17] C. M. Awate, S. M. Panse, and C. J. Dodds, "Validation of an accelerated test on a four-

post road simulator," Chapter 2007-26- 070, Society of Automotive Engineering, pp. 761–767, 2007.

[18] C. J. Dodds and A. R. Plummer, "Laboratory road simulation for full vehicle testing a review," in *Proceedings of the Symposium on International Automotive Technology*, 2001.

[19] J. C. Delamotte, R. F. Nascimento, and J. R. F. Arruda, "Simple models for the dynamic modeling of rotating tires," *Shock and Vibration*, vol. 15, no. 3-4, pp. 383–393, 2008.

[20] C. Q. Liu, "Combination of an improved FRF-based substructure synthesis and power flow method with application to vehicle axle noise analysis," *Shock and Vibration*, vol. 15, no. 1, pp. 51–60, 2008.

[21] N. W. M. Bishop, "Vibration fatigue analysis in the finite element environment," in *Proceedings of the 16th Encuentro del Grupo Espan˜ol de Fractura*, Torremolinos, Spain, 1999.

[22] M. H. A. Bonte, A. De Boer, and R. Liebregts, "Prediction of mechanical fatigue caused by multiple random excitations," in *Proceedings of the ISMA Conference*, pp. 697–708, September 2004.

[23] M. H. A. Bonte, A. de Boer, and R. Liebregts, "Determining the von Mises stress power spectral density for frequency domain fatigue analysis including out-of-phase stress components," *Journal of Sound and Vibration*, vol. 302, no. 1-2, pp. 379–386, 2007.

[24] P. H. Wirsching, T. L. Paez, and K. Ortiz, *Random Vibrations: Theory and Practice*, John Wiley and Sons, New York, NY, USA, 1995.

[25] T. Dirlik, *Application of Computers in Fatigue Analysis [Ph.D. thesis]*, University of Warwick, Warwick, UK, 1985.

[26] D. A. Thomas, K. Avers, and M. Pecht, "The "troublenotidentified" phenomenon in automotive electronics," *Microelectronics Reliability*, vol. 42, no. 4-5, pp. 641–651, 2002.

[27] D. H. Hodges and G. A. Pierce, *Introduction to Structural Dynamics and Aeroelasticity*, 2nd edition, 2011.

[28] J. M. Sater, C. R. Crowe, R. Antcliff, and A. Das, "An assessment of smart Air and space structures: demonstrations and technology," IDA Report P-3552, Log: H 00-002035, Institute for Defense Analysis, Alexandria, Va, USA, 2000.

[29] M. R. M. C. Da Silva, "Non-linear flexural-flexural-torsional- extensional dynamics of beams-I. Formulation," *International Journal of Solids and Structures*, vol. 24, no. 12, pp. 1225–1234, 1988.

[30] M. R. M. Crespo Da Silva and C. L. Zaretzky, "Nonlinear flexural-flexural-torsional interactions in beams including the effect of torsional dynamics. I: primary resonance," *Nonlinear Dynamics*, vol. 5, no. 1, pp. 3–23, 1994.

[31] E. H. Dowell, "Damping in beams and plates due to slipping at the support boundaries," *Journal of Sound and Vibration*, vol. 105, no. 2, pp. 243–253, 1986.

[32] D. H. Hodges and E. H. Dowell, "Nonlinear equations of motion for the elastic bending and torsion of twisted nonuniform rotor blades," NASA Technical Notes NASA TN D-7818, 1974.

[33] D. S. Whithead, "The analysis of blade vibration due to random excitation," Tech. Rep. 3253, United Kingdom Ministry of Aviation: Aeronautical Research Council Reports and Memoranda, London, UK, 1960.

[34] M. Aykan and M. Celik, "Vibration fatigue analysis and multi- axial effect in testing of aerospace structures," *Mechanical Systems and Signal Processing*, vol. 23, no. 3, pp. 897–907, 2009.

[35] G. V. Chary, E. Habtour, and G. S. Drake, "Improving the reliability in the next generation of US army platforms through physics of failure analysis," *Journal of Failure Analysis and*

Prevention, vol. 12, no. 1, pp. 75–58, 2012.

[36] Y. Zhou, M. Al-Bassyiouni, and A. Dasgupta, "Vibration durability assessment of sn3.0ag0.5cu and sn37pb solders under harmonic excitation," *Journal of Electronic Packaging*, vol. 131, no. 1, 2009.

[37] J. H. Lau, *Solder Joint Reliability, Theory and Applications*, Van Nostrand Reinhold, New York, NY, USA, 1990.

[38] J. Lau, K. Gratalo, E. Schneider, T. Marcotte, and T. Baker, "Solder joint reliability of large plastic ball grid array assemblies under bending, twisting, and vibration conditions," *Circuit World*, vol. 22, no. 1, pp. 27–32, 1995.

[39] J. H. Lau and P. Yi, *Solder Joint Reliability, of BGA, CSP, Flip Chip and Fine Pitch SMT Assemblies*, McGraw-Hill, New York, NY, USA, 1997.

[40] X. Liu, V. K. Sooklal, M. A. Verges, and M. C. Larson, "Experimental study and life prediction on high cycle vibration fatigue in BGA packages," *Microelectronics Reliability*, vol. 46, no. 7, pp. 1128–1138, 2006.

[41] X. Yang, Y. Luo, and Q. Gao, "Constitutive modeling on time-dependent deformation behavior of 96.5Sn-3.5Ag solder alloy under cyclic multiaxial straining," *Journal of Electronic Packaging*, vol. 129, no. 1, pp. 41–47, 2007.

[42] Y. Zhou, M. Al-Bassyiouni, and A. Dasgupta, "Harmonic and random vibration durability of SAC305 and Sn37Pb solder alloys," *IEEE Transactions on Components and Packaging Technologies*, vol. 33, no. 2, pp. 319–328, 2010.

[43] J. Gu, D. Barker, and M. Pecht, "Prognostics implementation of electronics under vibration loading," *Microelectronics Reliability*, vol. 47, no. 12, pp. 1849–1856, 2007.

[44] D. B. Barker, Y. S. Chen, and A. Dasgupta, "Estimating the vibration fatigue life of quad

leaded surface mount components," *Journal of Electronic Packaging*, vol. 115, no. 2, pp. 195–200, 1993.

[45] R. S. Li, "A methodology for fatigue prediction of electronic components under random vibration load," *Journal of Electronic Packaging*, vol. 123, no. 4, pp. 394–400, 2001.

[46] E. Martynenko, W. Zhou, A. Chudnovsky, R. S. Li, and L. Poglitsch, "High cycle fatigue resistance and reliability assessment of flexible printed circuitry," *Journal of Electronic Packaging*, vol. 124, no. 3, pp. 254–259, 2002.

[47] S. Mathew, D. Das, M. Osterman, M. Pecht, R. Ferebee, and J. Clayton, "Virtual remaining life assessment of electronic hardware subjected to shock and random vibration life cycle loads," *Journal of the Institute of Environmental Sciences and Technology*, vol. 50, no. 1, pp. 86–97, 2007.

[48] S. Shetty, V. Lehtinen, A. Dasgupta, V. Halkola, and T. Reinikainen, "Fatigue of chip scale package interconnects due to cyclic bending," *Journal of Electronic Packaging*, vol. 123, no. 3, pp. 302–308, 2001.

[49] M. Ernst, C. Choi, A. Dasgupta, and E. Habtour, "Physics of failure models for multiaxial vibration fatigue in electronics assemblies," in *Proceedings of the Accelerated Stress Testing and Reliability Workshop*, Ontario, Canada, 2012.

[50] A. C. Eringen, "Response of beams and to random loads," *Journal of Applied Mechanics*, vol. 24, pp. 46–52, 1957.

[51] R. E. Herbert, "Random vibrations of a nonlinear elastic beam," *Journal of the Acoustical Society of America*, vol. 36, no. 11, pp. 2090–2094, 1964.

[52] I. Elishakoff and D. Livshits, "Some closed-form solutions in random vibration of Bernoulli-Euler beams," *International Journal of Engineering Science*, vol. 22, no. 11-12, pp.

1291–1301, 1984.

[53] I. Elishakoff, J. Fang, and R. Caimi, “Random vibration of a nonlinearly deformed beam by a new stochastic linearization technique,” *International Journal of Solids and Structures*, vol. 32, no. 11, pp. 1571–1584, 1995.

[54] R. A. I. brahimand, R. J. Somnay, “Nonlinear dynamic analysis of an elastic beam isolator sliding on frictional supports,” *Journal of Sound and Vibration*, vol. 308, no. 3–5, pp. 735–757, 2007.

[55] C.-H. Ho, R. A. Scott, and J. G. Eisley, “Non-planar, non-linear oscillations of a beam-I. Forced motions,” *International Journal of Non-Linear Mechanics*, vol. 10, no. 2, pp. 113–127, 1975.

[56] C.-H. Ho, R. A. Scott, and J. G. Eisley, “Non-planar, non-linear oscillations of a beam II. Free motions,” *Journal of Sound and Vibration*, vol. 47, no. 3, pp. 333–339, 1976.

[57] M. R. M. Crespo da Silva and C. C. Glynn, “Nonlinear flexural-flexural-torsional dynamics of inextensional beams. I: equations of motion,” *Journal of Structural Mechanics*, vol. 6, no. 4, pp. 437–448, 1978.

[58] M. R. M. Crespo de Silva and C. C. Glynn, “Nonlinear flexural- flexural-torsional dynamics of inextensional beams. II: forced motions,” *Journal of Structural Mechanics*, vol. 6, no. 4, pp. 449– 461, 1978.

[59] M. R. M. C. Da Silva, “Non-linear flexural-flexural-torsional- extensional dynamics of beams-II. Response analysis,” *International Journal of Solids and Structures*, vol. 24, no. 12, pp. 1235– 1242, 1988.

[60] A. H. Nayfeh and P. F. Pai, “Non-linear non-planar parametric responses of an inextensional beam,” *International Journal of Non-Linear Mechanics*, vol. 24, no. 2, pp. 139–

158, 1989.

[61] P. F. Pai and A. H. Nayfeh, “Non-linear non-planar oscillations of a cantilever beam under lateral base excitations,” *International Journal of Non-Linear Mechanics*, vol. 25, no. 5, pp. 455–474, 1990.

[62] C. L. Zaretzky and M. R. M. Crespo da Silva, “Nonlinear flexural-flexural-torsional interactions in beams including the effect of torsional dynamics. II: combination resonance,” *Non- linear Dynamics*, vol. 5, no. 2, pp. 161–180, 1994.

[63] H. N. Arafat, A. H. Nayfeh, and C.-M. Chin, “Nonlinear non- planar dynamics of parametrically excited cantilever beams,” *Nonlinear Dynamics*, vol. 15, no. 1, pp. 31–61, 1998.

[64] A. H. Nayfeh and H. N. Arafat, “Investigation of subcombination internal resonances in cantilever beams,” *Shock and Vibration*, vol. 5, pp. 289–296, 1998.

[65] A. H. Nayfeh and H. N. Arafat, “Nonlinear response of cantilever beams to combination and subcombination resonances,” *Shock and Vibration*, vol. 5, no. 5-6, pp. 277–288, 1998.

[66] H. N. Arafat, *Nonlinear Dynamic Analysis of Cantilever Beam [Ph.D. thesis]*, Virginia Polytechnic Institute and State University, Blacksburg, Va, USA, 1999.

[67] J. R. Banerjee, “Explicit analytical expressions for frequency equation and mode shapes of composite beams,” *International Journal of Solids and Structures*, vol. 38, no. 14, pp. 2415–2426, 2001.

[68] P. Malatkar and A. H. Nayfeh, “On the transfer of energy between widely spaced modes in structures,” *Nonlinear Dynamics*, vol. 31, no. 2, pp. 225–242, 2003.

[69] P. Malatkar, and A. H. Nayfeh, “A parametric identification technique for single-degree-of-freedom weakly nonlinear systems with cubic nonlinearities,” *Journal of Vibration and Control*, vol. 9, no. 3-4, pp. 317–336, 2003.

[70] P. Malatkar, *Nonlinear Vibrations of Cantilever Beams and Plates [Ph.D. thesis]*, Virginia Polytechnic Institute and State University, Blacksburg, Va, USA, 2003.

[71] T. J. Anderson, B. Balachandran, and A. H. Nayfeh, "Nonlinear resonances in a flexible cantilever beam," *Journal of Vibration and Acoustics*, vol. 116, no. 4, pp. 480–484, 1994.

[72] J. Dugundji, and V. Mukhopadhyay, "Lateral bending-torsion vibrations of a thin beam under parametric excitation," *Journal of Applied Mechanics*, vol. 40, no. 3, pp. 693–698, 1973.

[73] D. M. Tang and E. H. Dowell, "Damping in beams and plates due to slipping at the support boundaries. Part 2: numerical and experimental study," *Journal of Sound and Vibration*, vol. 108, no. 3, pp. 509–522, 1986.

[74] C. W. S. To, "Vibration of a cantilever beam with a base excitation and tip mass," *Journal of Sound and Vibration*, vol. 83, no. 4, pp. 445–460, 1982.

[75] M. P. Cartmell and J. W. Roberts, "Simultaneous combination resonances in a parametrically excited cantilever beam," *Strain*, vol. 23, no. 3, pp. 117–126, 1987.

[76] B. Balachandran and A. H. Nayfeh, "Nonlinear motions of beam-mass structure," *Nonlinear Dynamics*, vol. 1, no. 1, pp. 39– 61, 1990.

[77] B. Balachandran, and A. H. Nayfeh, "Observations of modal interactions in resonantly forced beam-mass structures," *Nonlinear Dynamics*, vol. 2, no. 2, pp. 77–117, 1991.

[78] J. W. Jaworski, and E. H. Dowell, "Free vibration of a cantilevered beam with multiple steps: comparison of several theoretical methods with experiment," *Journal of Sound and Vibration*, vol. 312, no. 4-5, pp. 713–725, 2008.

[79] M. Ansari, E. Esmailzadeh, and N. Jalili, "Coupled vibration and parameter sensitivity analysis of rocking-mass vibrating gyroscopes," *Journal of Sound and Vibration*, vol. 327, no. 3–5, pp. 564–583, 2009.

[80] A. M. Wickenheiser, “Design optimization of linear and non- linear cantilevered energy harvesters for broadband vibrations,” *Journal of Intelligent Material Systems and Structures*, vol. 22, no. 11, pp. 1213–1225, 2011.

[81] M. Ansari, E. Esmailzadeh, and N. Jalili, “Exact frequency analysis of a rotating cantilever beam with tip mass subjected to torsional-bending vibrations,” *Journal of Vibration and Acoustics*, vol. 133, no. 4, Article ID 041003, 2011.

[82] A. Erturk and D. J. Inman, “Parameter identification and optimization in piezoelectric energy harvesting: analytical relations, asymptotic analyses, and experimental validations,” *Proceedings of the Institution of Mechanical Engineers. Part I: Journal of Systems and Control Engineering*, vol. 225, no. 4, pp. 485–496, 2011.

[83] A. Erturk, “Assumed-modes modeling of piezoelectric energy harvesters: Euler-Bernoulli, Rayleigh, and Timoshenko models with axial deformations,” *Computers and Structures*, vol. 106- 107, pp. 214–227, 2012.

[84] M. Esmaeili, N. Jalili, and M. Durali, “Dynamic modeling and performance evaluation of a vibrating beam microgyroscope under general support motion,” *Journal of Sound and Vibration*, vol. 301, no. 1-2, pp. 146–164, 2007.

[85] S. C. Stanton, C. C. McGehee, and B. P. Mann, “Nonlinear dynamics for broadband energy harvesting: investigation of a bistable piezoelectric inertial generator,” *Physica D: Nonlinear Phenomena*, vol. 239, no. 10, pp. 640–653, 2010.

[86] C. P. Green and J. E. Sader, “Torsional frequency response of cantilever beams immersed in viscous fluids with applications to the atomic force microscope,” *Journal of Applied Physics*, vol. 92, no. 10, pp. 6262–6274, 2002.

[87] S. C. Stanton, A. Erturk, B. P. Mann, E. H. Dowell, and D. J. Inman, “Nonlinear

nonconservative behavior and modeling of piezoelectric energy harvesters including proof mass effects," *Journal of Intelligent Material Systems and Structures*, vol. 23, no. 2, pp. 183–199, 2012.

[88] S. C. Stanton, B. A. M. Owens, and B. P. Mann, "Harmonic balance analysis of the bistable piezoelectric inertial generator," *Journal of Sound and Vibration*, vol. 331, no. 15, pp. 3617–3627, 2012.

[89] H. J. R. Westra, D. M. Karabacak, S. H. Brongersma, M. Crego- Calama, H. S. J. Van Der Zant, and W. J. Venstra, "Interactions between directly- and parametrically-driven vibration modes in a micromechanical resonator," *Physical Review B: Condensed Matter and Materials Physics*, vol. 84, no. 13, Article ID 134305, 2011.

[90] K. Wolf, and O. Gottlieb, "Nonlinear dynamics of a cantilever beam actuated by piezoelectric layers in symmetric and asymmetric configuration," Tech. Rep. ETR-2001-02, Institute of Technology, Haifa, Israel, 2001.

[91] L. G. Villanueva, R. B. Karabalin, M. H. Matheny, D. Chi, J. E. Sader, and M. L. Roukes, "Nonlinearity in nanomechanical cantilevers," *Physical Review B*, vol. 87, Article ID 024304, 2013.

[92] V. Kumar, J. K. Miller, and J. F. Rhoads, "Nonlinear parametric amplification and attenuation in a base-excited cantilever beam," *Journal of Sound and Vibration*, vol. 330, no. 22, pp. 5401– 5409, 2011.

[93] J. F. Rhoads, N. J. Miller, S. W. Shaw, and B. F. Feeny, "Mechanical domain parametric amplification," *Journal of Vibration and Acoustics*, vol. 130, no. 6, Article ID 061006, 2008.

[94] S. F. Ali, S. Adhikari, M. I. Friswell, and S. Narayanan, "The analysis of piezomagnetoelastic energy harvesters under broadband random excitations," *Journal of Applied*

Physics, vol. 109, no. 7, Article ID 074904, 2011.

[95] G. Wu, H. J., K. Hansen et al., "Origin of nanomechanical cantilever motion generated from biomolecular interactions," *Proceedings of the National Academy of Sciences of the United States of America*, vol. 98, no. 4, pp. 1560–1564, 2001.

[96] K. S. Hwang, J. H. Lee, J. Park, D. S. Yoon, J. H. Park, and T. S. Kim, "In-situ quantitative analysis of a prostate-specific antigen (PSA) using a nanomechanical PZT cantilever," *Lab on a Chip: Miniaturisation for Chemistry and Biology*, vol. 4, no. 6, pp. 547– 552, 2004.

[97] J. Dorignac, A. Kalinowski, S. Erramilli, and P. Mohanty, "Dynamical response of nanomechanical oscillators in immiscible viscous fluid for in Vitro biomolecular Recognition," *Physical Review Letters*, vol. 96, no. 18, Article ID 186105, 2006.

[98] A. Salehi-Khojin, S. Bashash, and N. Jalili, "Modeling and experimental vibration analysis of nanomechanical cantilever active probes," *Journal of Micromechanics and Microengineering*, vol. 18, no. 8, Article ID 085008, 2008.

[99] V. Seena, A. Fernandes, P. Pant, S. Mukherji, and V. R. Rao, "Polymer nanocomposite nanomechanical cantilever sensors: material characterization, device development and application in explosive vapour detection," *Nanotechnology*, vol. 22, no. 29, Article ID 295501, 2011.

[100] S. Suresh, *Fatigue of Materials*, Cambridge University Press, Cambridge, UK, 2nd edition, 1998.

[101] D. Segalman, G. Reese, R. Field Jr., and C. Fulcher, "Estimating the probability distribution of von Mises stress for structures undergoing random excitation," *Journal of Vibration and Acoustics*, vol. 122, no. 1, pp. 42–48, 2000.

[102] S. Sarkani, D. P. Kihl, and J. E. Beach, "Fatigue of welded joints under narrowband non-

Gaussian loadings," *Probabilistic Engineering Mechanics*, vol. 9, no. 3, pp. 179–190, 1994.

[103] D. Radaj, C. M. Sonsino, and W. Fricke, *Fatigue Assessment of Welded Joints By Local Approaches*, Woodhead Publishing Limited, Cambridge, UK, 2006.

[104] A.Z. Palmgren,"Die Lebensdauer VonKugellagern," *Zeitschriyt Des Vereines Der Deutschen Ingenioeren*, vol. 68, pp. 339–341, 1924.

[105] M. A. Miner, "Cumulative damage in fatigue," *Journal of Applied Mechanics*, vol. 12, no. 3, pp. 159–164, 1945.

[106] J. W. Miles, "On structural fatigue under random loading," *Journal of the Aeronautical Sciences*, vol. 21, no. 11, pp. 753–762, 1957.

[107] S. H. Crandall, "Zero crossings, peaks, and other statistical measures of random responses," *Journal of the Acoustical Society of America*, vol. 35, no. 11, pp. 1693–1699, 1963.

[108] Y. K. Lin, "Probability distributions of stress peaks in linear and nonlinear structures," *AIAA Journal*, vol. 1, no. 5, pp. 1133–1138, 1963.

[109] J. S. Bendat, "Probability functions for random responses- prediction of peaks, fatigue damage, and catastrophic failures," NASA CR-33, N64-17990, 1964.

[110] S. O. Rice, "Mathematical analysis of random noise," Selected Chapters on Noise and Stochastic Processes, Dover, New York, NY, USA, 1954.

[111] N. W. M. Bishop, *The Use of Frequency Domain Parameters to Predict Structural Fatigue [Ph.D. thesis]*, University of Warwick, 1988.

[112] N. W. M. Bishop and F. Sherratt, "Theoretical solution for the estimation of "rainflow" ranges from power spectral density data," *Fatigue and Fracture of Engineering Materials and Structures*, vol. 13, no. 4, pp. 311–326, 1990.

[113] K. Upadhyayula, and A. Dasgupta, "Physics-of-failure guidelines for accelerated

qualification of electronic systems," *Quality and Reliability Engineering International*, vol. 14, no. 6, pp. 433-447, 1998.

[114] E. Habtour, M. Paulus, and A. Dasgupta, "Modeling approach for predicting the rate of frequency change of notched beam exposed to Gaussian random excitation," *Shock and Vibration*, 2013.

[115] Y. Lu, *Random Vibration Analysis of Higher-Order Nonlinear Beams and Composite Plates with Applications of ARMA Models [Ph.D. thesis]*, Virginia Polytechnic Institute and State University, Blacksburg, Va, USA, 2008.

[116] T. Łagoda, E. Macha, and A. Niesłony, "Fatigue life calculation by means of the cycle counting and spectral methods under multiaxial random loading," *Fatigue and Fracture of Engineering Materials and Structures*, vol. 28, no. 4, pp. 409–420, 2005.

[117] X. Pitoiset and A. Preumont, "Spectral methods for multiaxial random fatigue analysis of metallic structures," *International Journal of Fatigue*, vol. 22, no. 7, pp. 541-550, 2000.

[118] X. Pitoiset, I. Rychlik, and A. Preumont, "Spectral methods to estimate local multiaxial fatigue failure for structures under- going random vibrations," *Fatigue and Fracture of Engineering Materials and Structures*, vol. 24, no. 11, pp. 715–727, 2001.

[119] A. Carpinteri, E. Macha, R. Brighenti, and A. Spagnoli, "Expected principal stress directions under multiaxial random loading. Part I: theoretical aspects of the weight function method," *International Journal of Fatigue*, vol. 21, no. 1, pp. 83– 88, 1999.

[120] A. Carpinteri, R. Brighenti, E. Macha, and A. Spagnoli, "Expected principal stress directions under multiaxial random loading. Part II: numerical simulation and experimental assessment through the weight function method," *International Journal of Fatigue*, vol. 21, no. 1, pp. 89–96, 1999.

[121] Y. Liu and S. Mahadevan, “A unified multiaxial fatigue damage model for isotropic and anisotropic materials,” *International Journal of Fatigue*, vol. 29, no. 2, pp. 347–359, 2007.

[122] Y. Liu, *Stochastic Modeling of Multiaxial Fatigue and Fracture [Ph.D. thesis]*, Vanderbilt University, Nashville, Tn, USA, 2006.

[123] S. Lambert, E. Pagnacco, and L. Khalij, “A probabilistic model for the fatigue reliability of structures under random loadings with phase shift effects,” *International Journal of Fatigue*, vol. 32, no. 2, pp. 463–474, 2010.

[124] C. Braccesi, F. Cianetti, G. Lori, and D. Pioli, “An equivalent uniaxial stress process for fatigue life estimation of mechanical components under multiaxial stress conditions,” *International Journal of Fatigue*, vol. 30, no. 8, pp. 1479–1497, 2008.

[125] C. Braccesi, F. Cianetti, G. Lori, and D. Pioli, “The frequency domain approach in virtual fatigue estimation of non-linear systems: the problem of non-Gaussian states of stress,” *International Journal of Fatigue*, vol. 31, no. 4, pp. 766–775, 2008.

[126] G. Allegri and X. Zhang, “On the inverse power laws for accelerated random fatigue testing,” *International Journal of Fatigue*, vol. 30, no. 6, pp. 967–977, 2008.

[127] Z. Lei and C. Qiu, “A dynamic stochastic finite element method based on dynamic constraint mode,” *Computer Methods in Applied Mechanics and Engineering*, vol. 161, no. 3-4, pp. 245– 255, 1998.

[128] S. I. McNeill, “A method for determining the fatigue critical plane for biaxial random vibration in the frequency domain: technical Note,” *Fatigue and Fracture of Engineering Materials and Structures*, vol. 33, no. 6, pp. 390–394, 2010.

[129] T. Lagoda, E. Macha, and W. Bedkowski, “Critical plane approach based on energy concepts: application to biaxial random tension-compression high-cycle fatigue regime,” *Inter-*

national Journal of Fatigue, vol. 21, no. 5, pp. 431–443, 1999.

[130] P. A. Tibbits, "Application of algorithms for percentiles of von Mises stress from combined random vibration and static loadings," *Journal of Vibration and Acoustics*, vol. 133, no. 4, Article ID 044502, 2011.

[131] H. Guechichi, S. Benkabouche, A. Amrouche, and M. Benkhettab, "A high fatigue life prediction methodology under constant amplitude multiaxial proportional loadings," *Materials Science and Engineering A*, vol. 528, no. 13-14, pp. 4789–4798, 2011.

[132] D. Gregory, F. Bitsy, and D. O. Smallwood, "Comparison of the response of a simple structure to single axis and multiple axis random vibration inputs," in *Proceedings of the 79th Shock and Vibration Symposium*, Orlando, FL, USA, 2008.

[133] U. Fullekrug, "Utilization of multi-axial shaking tables for the modal identification of structures," *Philosophical Transactions of the Royal Society A: Mathematical, Physical and Engineering Sciences*, vol. 359, no. 1786, pp. 1753-1770, 2001.

[134] D. E. Newland, *An Introduction to Random Vibrations, Spectral and Wavelet Analysis*, Dover, Mineola, NY, USA, 2005.

[135] T. Dahlberg, "The effect of modal coupling in random vibration analysis," *Journal of Sound and Vibration*, vol. 228, no. 1, pp. 157-176, 1999.

[136] E. Habtour, M. Pohland, and A. Dasgupta, "Dynamic characterization of circuit card assemblies using multi-degree-of- freedom random vibration," in *Proceedings of the Accelerated Stress Testing and Reliability Workshop*, San Francisco, Ca, USA, 2011.

[137] L. Meirovitch, *Principles and Techniques of Vibrations*, Prentice Hall, Upper Saddel River, NJ, USA, 1997.

[138] M. Cesnik, J. Slavic, and M. Boltezar, "Uninterrupted and accelerated vibrational fatigue

testing with simultaneous monitoring of the natural frequency and damping," *Journal of Sound and Vibration*, vol. 331, pp. 5370-5382, 2012.

[139] A. Perkins, and S. K. Sitaraman, "Analysis and prediction of vibration-induced solder joint failure for a ceramic column grid array package," *Journal of Electronic Packaging*, vol. 130, no. 1, 2008.

[140] C. Rainieri, G. Fabbrocino, and E. Cosenza, "Near real-time tracking of dynamic properties for standalone structural health monitoring systems," *Mechanical Systems and Signal Processing*, vol. 25, no. 8, pp. 3010-3026, 2011.

[141] R.-J. Wang and D.-G. Shang, "Fatigue life prediction based on natural frequency changes for spot welds under random loading," *International Journal of Fatigue*, vol. 31, no. 2, pp. 361-366, 2009.

[142] Y. J. Yan, L. Cheng, Z. Y. Wu, and L. H. Yam, "Development in vibration-based structural damage detection technique," *Mechanical Systems and Signal Processing*, vol. 21, no. 5, pp. 2198-2211, 2007.

Chapter 4 Fatigue Damage Precursor Detection in Structures Vibrating under Nonlinear Harmonic Transverse Base Excitation

Under Review: Structural Control Health Monitoring, 2015

Chapter 4 is an article currently under review in the *Journal of Structural Control and Health Monitoring (SCHM)*. The paper contains a nonlinear vibration-based methodology for exploiting the sensitivity of the nonlinearities in the equation of motion to damage precursor in isotropic cantilever beam, prior to fatigue crack initiation, based on measurement of the structure nonlinear response to transverse base excitation. The experimental results are utilized to update the nonlinear stiffness in the equation of motion. Authors are Mr. Ed Habtour, Dr. Daniel Cole, Dr. Jarret Riddick, Dr. Volker Weiss, Dr. Samuel C. Stanton, Dr. Mark Robeson, and Professor Abhijit Dasgupta. Mr. Ed Habtour (first author) conducted the vibration experiments and developed the analytical model. He also conducted the SEM experiments. Dr. Daniel Cole conducted the nanoindentation measurements. Mr. Roman Sridharan provided assistance with the control software for the multiaxial vibration shaker. Dr. Samuel Stanton at the Army Research Office checked the derivations. Prospective and insights about Army's applications, environmental standards, reliability guidelines, and testing methodologies were provided by Dr. Jarret Riddick, Dr. Mark Robeson and Dr. Volker Weiss. Professor Dasgupta provided technical and academic guidance in this effort.

Abstract:

A nonlinear vibration methodology is developed for detecting and quantifying early precursors to cyclic fatigue damage, prior to fatigue crack initiation, in isotropic metal structures,

prior to fatigue crack initiation, based on measurement of the structure nonlinear response to harmonic base excitation. As an example, a damage precursor feature was extracted for cantilever beams by quantifying the reduction in the nonlinear structural stiffness due to localized microstructural fatigue damage accumulation. A nonlinear dynamic analytical model was developed to parametrically track the changes in the nonlinear structural stiffening term in the equation of motion, as a function of the structural response history. Experimental results are obtained by exciting the base of cantilever beams at various amplitude levels. At high response amplitudes, the beams experience three competing nonlinear dynamic mechanisms simultaneously: 1) structural stiffening due to kinematic nonlinearity caused by high response amplitude at the fundamental mode; 2) structural softening due to inertial forces; and 3) structural softening due to localized microstructural fatigue damage in the material. The third mechanism—a potential precursor to fatigue crack initiation in the structure—resulted in a cumulative structural softening and is the focus of this study. The loading intensity and number of cycles influenced the relative contribution of these dynamic mechanisms. Nanoindentation studies near the clamped boundary of the cantilever beam were conducted to confirm progressive evolution in the local mechanical properties, as a function of loading cycles. In particular, the apparent indentation stiffness measured from the slope of the unloading curve showed a systematic reduction as a function of fatigue damage accumulation.

The proposed detection method of tracking the changes in the nonlinear part of the structural stiffness successfully detects the presence of damage but lacks the resolution to discern the spatial distribution of the damage intensity. Furthermore, this nonlinear dynamic detection method is found to be a sensitive metric as a fatigue damage precursor, making it an effective method for monitoring structural degradation prior to fatigue crack development. Additional

development of the proposed methodology will be essential to implementing it as a cost effective alternative to current complex inspection techniques.

4.1 Introduction

The purpose of preventive maintenance techniques used in high-value mechanical systems—such as those in aerospace, automotive, and military platforms—is to reduce the risks and costs associated with late-lifecycle maintenance and repairs [1]. Current damage predictors are based on strain measurements and crack detection, which makes estimating the remaining useful life of a system extremely difficult and possibly inaccurate. The objective of this study is to develop a fatigue damage precursor detection method for monitoring the early stages of structural fatigue degradation prior to crack initiation. *Fatigue damage precursor* is defined here as any observable early degradation of the material microstructural morphology and resulting changes in or the physical properties of a structure, prior to any detectable fatigue crack initiation. Examples of measurable precursors to fatigue crack development may involve, but are not restricted to, changes in the microstructure, chemical composition, electrical signal, acoustic response, thermal signature or mechanical response of a structure. Recognizing a damage precursor requires classifying and recognizing damage incubators and initiators such as residual or compressive stress, phase changes, microstructural evolution, microvoid nucleation, etc. This study focuses on detecting a fatigue damage precursor by tracking its effect on nonlinear structural response to harmonic vibratory loads.

Research to monitor a structure and detect damage at the earliest possible stage is ubiquitous throughout aerospace, civil, mechanical, and electronics engineering communities [6, 7]. In the present study, early identification of fatigue damage precursor in a vibrating beam was possible through exploiting the sensitivity of the nonlinear terms in the equations of motion to

fatigue degradation of the beam material. One of the potential impacts of this technique is that it may provide an opportunity for assessing the structural durability of mechanical systems when exposed to extreme vibratory loads using conventional sensors such as accelerometers, making it feasible to use the proposed technique in existing health monitoring systems. Physical replacement or addition of sensors to existing systems would not be necessary because the nonlinear terms can simply be included in the detection codes.

According to the literature, vibration-based damage detection techniques are the most common methodologies for assessing the health of engineering structures [2-5]. The popularity of monitoring the fundamental frequencies to detect cracks is due to the fact that the measurements can be obtained easily using an accelerometer, a strain gage, or a piezoelectric sensor at a single point of interest. The core idea behind vibration-based damage detection built on system-identification is that modal parameters (notably fundamental frequencies and modal damping) are functions of the physical properties of the structure (mass, damping, and stiffness). Therefore, changes in the physical properties may cause detectable changes in the modal properties that can be captured and extracted from vibratory data.

Most vibration-based damage identification methods in the literature rely on linear dynamic models [3, 8]. Linear methods are generally inappropriate when the structural response is nonlinear, which is a common occurrence in many mechanical and electro-mechanical systems [9-10]. Furthermore, linear vibration-based procedures do not always provide useful results because of their inherent low sensitivity to defects [4]. This study suggests that nonlinear dynamic system identification methods may hold a better promise for more sensitive damage detection capabilities. Additional information on various vibration-based recognition methods can be found in comprehensive reviews on damage identification and health monitoring of

structural and mechanical systems in the literature [3, 11, 12].

In this study, we provide a new vibration-based methodology that accounts for the effects of nonlinear response of a cantilever beam by combining a model-based approach with measurement of the acceleration response. This is accomplished by modifying the nonlinear Euler-Bernoulli beam model to account for changes in the local stiffness at high-stress sites. The study shows that the nonlinear vibration-based measurement techniques detected the onset of fatigue prior to crack initiation. Furthermore, microstructural evolution observed at the maximum stress site is believed to exacerbate the nonlinear softening response of the beam and is believed to be direct evidence of the damage precursor of fatigue crack initiation. The effectiveness of nonlinear vibration testing for identifying damage precursors is illustrated through the application of global damage detection methods. Further work is required to extend this methodology to complex structures. Prior to discussing the details of the nonlinear dynamic model and the detection techniques, we provide a brief overview of the nonlinear vibration response of damaged structures.

4.1.1 Nonlinear Structural Dynamics

Nonlinearity in the dynamic response of structures can be instigated by material properties such as nonlinear constitutive relations [13, 14], non-ideal boundary conditions [15, 16], complex multiaxial loading [17], damping mechanisms [18], and large-deformation kinematics (geometric nonlinearity) with inertial effects [19]. Geometric nonlinearity arises from nonlinear strain-displacement relations for large deformations, and produces a nonlinear structural stiffening effect that appears in many engineering applications [20-21]. (This effect is called a “hardening effect” in the nonlinear dynamic literature. Since this chapter addresses nonlinear structural sensitivity to microstructural degradation, we will use “stiffening effect”

instead.) The most noticeable nonlinear effect is a restoring force that is proportional to the cube of displacement in the equations of motion [22]. Thus, the total restoring force includes both linear and nonlinear stiffness components. Inertial nonlinearities, on the other hand, augment the effective mass of the structure, thus causing a nonlinear softening response. In general, linear models are applicable only in restrictive conditions such as very low vibration amplitude [10], making them inaccurate when the amplitudes of oscillations are sufficiently high and the natural frequencies become increasingly dependent on these amplitudes [23].

Many structural materials are capable of enduring reasonably large deformations before their intrinsic stress-strain characteristic starts to deviate from the linear regime. Therefore, it is common to encounter geometric and inertial nonlinearities in dynamic mechanical systems long before the intrinsic material behavior reaches the nonlinear regime especially in micro/nano systems [16, 24 and 25]. Consequently, the linear equation of motion with linear restoring force has to be replaced with nonlinear models, which contain additional nonlinear terms such as geometric stiffness, inertial effects, and gyroscopic contributions [24]. The analytical model in this chapter includes these geometric and inertial effects. The nonlinear geometric term can assist the linear restoring force, thus stiffening the structure and increasing its resonant frequency. Unlike the case of a linear system, the maximum value of the amplitude occurs at an excitation frequency higher than the structure's natural frequency [26]. The nonlinear inertial term softens the response of the structure and reduces its natural frequency [27]. Inertial nonlinearities often appear in damping mechanisms. The nonlinear inertial term becomes increasingly sensitive to the amplitude displacements at resonances higher than the first mode [19]. Potentially, additional sources of nonlinearity may appear during the experimental study of cantilever isotropic slender beams due to practical reasons such as the manner in which the beam is clamped to the

surrounding material at its boundaries [17]. The clamping nonlinearities are assumed to be negligible in this study since the beams are clamped to a rigid fixture, which is a reasonable idealization.

4.1.2 Dynamics of Damaged Structures

Crack detection and monitoring methods were developed by the power industry in the early 1970s [2]. The presence of cracks in a structure is usually detected by adopting a linear approach through the monitoring of changes in the structure's dynamic response features, such as natural frequencies and mode shapes [28, 29]. Several studies have reported analytical and experimental results for vibration of cracked Euler-Bernoulli beams and the effects of surface cracks on fundamental frequencies and vibration modes of beams [30-32]. Ismail et al. investigated the effect of crack closure on the resonance frequency changes of cracked cantilever beams and claimed that vibration testing is a reliable method for detecting the presence of cracks [28]. Shen and Chu used a Galerkin procedure to develop the equation of motion of a uniform simply supported beam containing one single-edge breathing crack [33]. Nonlinear behavior was uncovered in the time history and frequency spectrum. Changes in the dynamic response of cracked structures were utilized to infer the size of the crack. Using closing crack Finite Element Model (FEM) model (fully open or fully closed crack) to represent a damaged element, Ruotolo et al. studied the response of a cracked cantilevered beam due to harmonic excitation [34]. They employed first and higher order harmonics to characterize the nonlinear behavior of the cracked beam, which was a computationally expensive approach. Tsyfansky and Beresnevich presented computational results of flexural vibrations encountered in a cracked aircraft wing under harmonic excitation, where they included an initial static deformation in the stiffness term of the equations of motion [35].

Several authors presented sophisticated techniques, which accounted for the change in the stiffness at the crack site, in order to correctly estimate the dynamic response of the cantilever beam with breathing cracks exposed to harmonic excitation [30, 36-38]. Pugno et al. used a crack function to account for the variation in local stiffness at the crack [36]. Chondros et al. used continuous cracked beam vibration theory to predict changes in transverse vibration of a simply supported beam with a breathing crack [30]. Saavedra and Cuitino presented an FEM model to estimate the dynamic behavior of beams containing a transverse crack [37]. The change in the local stiffness in the vicinity of the crack was accounted for by continuously updating the finite element stiffness matrix. Loutridis et al. implemented a similar approach, where a simple single-degree-of-freedom (SDoF) system with time varying stiffness was used to simulate the dynamic behavior of a cracked beam [38]. The time-varying stiffness was modeled using a simple empirical function based on the experimental results. Paulus et al. provided a semi-analytical model to estimate the evolution in the dynamic behavior of a cantilever beam due to the presence and propagation of a crack, which was then validated with an experimental approach coupled with an FEM analysis utilizing linear fracture mechanics theory [31-32].

Acoustics and Lamb-wave diagnostic techniques have been developed in recent years to monitor fatigue crack detection growth in metallic and composite structures exposed to a vibratory environment. These techniques rely on diagnostic signal generation, signal processing, and damage interpretation that can be fairly complex [29, 39, 40]. The drawbacks of these powerful techniques are that they require significant signal processing, on-board computations, and recalibration during the service life of the system; they additionally assume that the structure is linear. Sun et al provided an excellent review on the latest acoustic wave generation and detection techniques for structural health monitoring [12].

4.1.3 Proposed Approach

The observation that changes in microstructural properties and damage precursor instigate changes in the nonlinear dynamic response is the impetus for using nonlinear vibration-based methods for damage identification and health monitoring. The nonlinear vibration-based method is an attractive and simple global approach for monitoring the changes in the structural dynamic characteristics due to damage. Specifically, the present study shows that linear vibration approaches are inherently less sensitive than nonlinear vibration approaches to fatigue degradation features prior to crack initiation. The nonlinear vibration approach can detect very early stiffness changes, even prior to crack development. The experimental results confirmed that there was microstructural evolution at high stress sites, even though the beam stress-strain characteristic is intrinsically linear. The nonlinear equation of motion is updated accordingly to capture the local microstructural evolution by adjusting the nonlinear stiffness term. The global nonlinear vibration-based method uses the nonlinear structural updates from the experiments to estimate the beam tip response and number of fatigue cycles. Unlike linear dynamic model, the nonlinear stiffness term in the nonlinear dynamic model provided more useful sensitivity to the evolution in the material due to fatigue-induced damage. The method appears to be a promising health mentoring metric and may potentially provide reasonable estimate for structural damage precursors. This study provides a detailed description of the analytical model and the experimental approach.

4.2 Modeling Development

As discussed, studies in the literature predict a stiffening effect in the response of a linear-elastic, isotropic, cantilever beam under harmonic excitation at the first fundamental frequency, due to geometric nonlinearity. In contrast, a softening effect is predicted for higher-

order modes [19]. However, in the present study, experiments on steel cantilever beams revealed a softening effect during extended harmonic base excitation near the resonance frequency. This softening phenomenon at the fundamental mode has been reported in several investigations of harvester piezoceramics [41-43]. In these investigations, parameters that yielded stiffening responses were based on the nonlinear Euler-Bernoulli beam model, while their experimental response produced softening curves. The studies' common hypotheses—none of which were verified—were that these devices experienced material nonlinearity, residual stresses due to fabrications, and/or nonlinear boundary conditions. Villanueva et al observed similar softening effects at the fundamental mode in a nonlinear nanomechanical cantilever beam exposed to transverse harmonic base excitations [16]. They showed that the nonlinear Euler-Bernoulli beam theory predictions differ significantly from their measurements for the nonlinearity of the first fundamental mode. They speculated that the deviation from nonlinear Euler-Bernoulli beam theory was due to the beam's short aspect ratio (AR=Length/width=8) and potential material nonlinearity, but did not provide conclusive evidence of the cause of the nonlinearity.

The focus of this study is the nonlinear response of a slender isotropic cantilever beam exposed to harmonic transverse base excitation near its fundamental frequency. An analytical model is developed using nonlinear Euler-Bernoulli beam theory, with modified nonlinear stiffness to account for possible changes in the local material stiffness near the beam root (at the fixed end). A beam with AR=8 is analyzed and tested, similar to the study of Villanueva et al [16]. The experimental results demonstrated a softening effect due to long dwells at specific frequencies, over a range of frequencies. A global method utilizing nonlinear dynamic theory is used to capture a global structural softening response as a function of the excitation level and number of fatigue cycles, due to local degradation in the material stiffness. An investigation of

the local micromechanical properties near the fixed boundary condition showed that there is significant reduction in the local elastic modulus, where the maximum stress amplitudes occur.

The geometric and inertial nonlinearities in a cantilever beam with symmetric cross-section and tip mass are included in the equations of motion according to nonlinear Euler-Bernoulli beam theory. This section describes the nonlinear dynamics of a uniform cantilever beam carrying a tip mass exposed to a transverse base excitation (Figure 4-1). The beam is idealized as an inextensional beam (that is, stretching of the neutral axis is insignificant). Beams with one end clamped and the other end free can be assumed to be inextensional [44]. Therefore, nonlinear Euler-Bernoulli theory is employed to model the beam response; the effects of warping and shear deformation are ignored. The consequence of large peak response amplitude is that the nonlinear terms in the equations of motion become comparable to the linear ones. Since the beam length to width ratio is kept short (AR<30), it can be assumed that the beam undergoes purely planar flexural vibrations as long as the tip mass and cross-section geometry are symmetric with respect to the beam's centerline [45]. The assumed first mode deflection is the exact linear mode shape generated from solving the linear problem with attached lumped mass that includes the rotary inertia effect [19].

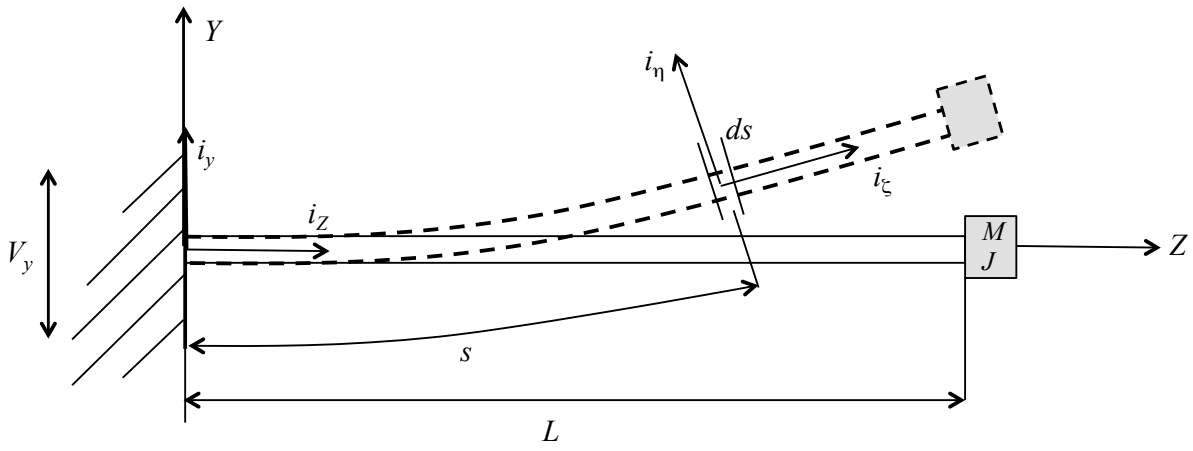

Figure 4-1 Slender beam with tip mass under base excitation

The beam is considered to be a uniform and straight isotropic cantilever beam of length L and volumetric density ϱ, clamped at the base with tip mass M and rotary inertia J (Figure 4-1). The Z-axis is taken as the neutral axis associated with pure bending. It is assumed the loci of both shear centers and mass centers of the undeformed beam are coincident with the Z-axis. The base motion causes each cross section of the beam to experience an elastic displacement of its centroid. The dynamics of the beam with respect to the Y and Z axes at the undeformed length from the root of the beam to the reference point, s, and time, t, can be described in terms of: the axial displacement $w(s,t)$, the transverse displacement $v(s,t)$ along the inertial coordinate system YZ, and the rotational angle ψ. The orthogonal unit vectors for the inertial coordinate system are (i_Y, i_Z). The local curvilinear coordinate system at s, in the deformed position, has the orthogonal unit vectors (i_η, i_ζ).

The kinetic energy can be expressed as follows [43]:

$$T = \frac{1}{2}\int_0^L \int_{A_1}^{A_2} \varrho\,(\dot{w}^2 + \dot{v}^2 + V_y^2 + 2\mathrm{V}_y\dot{v} + 2\eta\dot{w}\dot{\psi}\cos\psi + \eta^2\dot{\psi}^2 - 2\eta\dot{v}\dot{\psi}sin\psi$$

$$- 2\mathrm{V}_y\eta\dot{\psi}sin(\psi))dAds + \frac{1}{2}M(\dot{w}^2 + \dot{v}^2 + V_y^2 + 2\mathrm{V}_y\dot{v})\Big|_{s=L} \qquad \text{Eq. 4-1}$$

$$+ \frac{1}{2}J\dot{\psi}^2\Big|_{s=L}$$

where the dots denote derivatives with respect to time. Set:

$$\rho = \int_{A_1}^{A_2} \varrho\, dA\, J_1 = \int_{A_1}^{A_2} \varrho\,\eta dA\, J_2 = \int_{A_1}^{A_2} \varrho\,\eta^2 dA$$

Since the reference point coincides with the mass centroid and η is a principal axis of the differential beam element, J_1 is set equal to zero. For a uniform slender beam the rotational inertia, J_2, is very small and can be ignored [19]. Therefore, the kinetic energy becomes:

$$T = \frac{1}{2}\int_0^L [\rho(\dot{w}^2 + \dot{v}^2 + V_y^2 + 2\mathrm{V}_y\dot{v})]ds + \frac{1}{2}M\left(\dot{w}^2 + [\dot{v} + V_y]^2\right)\Big|_{s=L}$$

$$+ \frac{1}{2}J\dot{\psi}^2\Big|_{s=L} \qquad \text{Eq. 4-2}$$

Performing Taylor's expansion up to cubic nonlinearities and assuming w and v are small but finite, the kinetic and potential energies can be expressed as follows [46]:

$$T = \frac{1}{2}\int_0^L \left[\rho\left(\frac{1}{4}\left(\frac{\partial}{\partial t}\int_0^\zeta v'^2 ds\right)^2 + \dot{v}^2 + V_y^2 + 2\mathrm{V}_y\dot{v}\right)\right] ds$$

$$+ \frac{1}{2}M\left(\frac{1}{4}\left(\frac{\partial}{\partial t}\int_0^\zeta v'^2 ds\right)^2 + [\dot{v} + V_y]^2\right)\Big|_{s=L} \qquad \text{Eq. 4-3}$$

$$+ \frac{1}{2}J(\dot{v}'^2 + \dot{v}'^2 v'^2)\Big|_{s=L}$$

$$\Pi = \frac{EI}{2}\int_0^L (v''^2 + v''^2 v'^2) ds \qquad \text{Eq. 4-4}$$

where the primes denote derivatives with respect to distance. Approximate series solutions are now assumed of the form:

$$v(t,z) = \sum_{j=1}^{N} q_j(t) Y_j(z)$$

where the trial functions, Y_j, are known linearly-independent comparison functions from a complete, orthogonal, sufficiently differentiable function set that satisfies the kinematic boundary conditions of this cantilever beam problem. The undamped linear mode shapes offer a convenient set of trial functions. The term q_j denotes the generalized modal coordinates and describes the modal participation. For unimodal response the assumed solution becomes [47]:

$$v(t,z) = q(t)Y(s)$$

Substituting the assumed solution into the kinetic energy, Eq. 4-4, and the potential energy, Eq. 4-3, and simplifying yields the following:

$$T = \frac{1}{2}\left[\rho \int_0^L Y^2\, ds + MY^2|_{s=L} + JY'^2|_{s=L}\right]\dot{q}^2$$

$$+\frac{1}{2}\left[\rho \int_0^L \left(\int_0^\zeta Y'^2 ds\right)^2 ds + M\left(\int_0^\zeta Y'^2 ds\right)^2\right|_{s=L}$$

$$+ JY'^4|_{s=L}\Big]q^2\dot{q}^2 + \left[\rho \int_0^L Y ds + MY|_{s=L}\right]\mathrm{V}_y\dot{q} \qquad \text{Eq. 4-5}$$

$$+\frac{1}{2}[\rho L + M|_{s=L}]V_y^2$$

$$\Pi = \frac{EI}{2}\int_0^L (q^2 Y''^2 + q^4 Y''^2 Y'^2\,) ds \qquad \text{Eq. 4-6}$$

The Euler-Lagrangian equation is then applied to the Lagrangian, $L = T - \Pi$ as follows:

$$\frac{\partial}{\partial t}\left(\frac{\partial L}{\partial \dot{q}}\right) - \frac{\partial L}{\partial q} = 0$$

The nonlinear equation of motion becomes:

$$\alpha_1\ddot{q} + \alpha_2(q^2\ddot{q} + q\dot{q}^2) + K_1 q + K_2 q^3 = \alpha_3\dot{\mathrm{V}}_y \qquad \text{Eq. 4-7}$$

where the inertial coefficient including the rotary inertia (or effective mass) is:

$$\alpha_1 = \rho\int_0^L Y^2 ds + MY^2|_{s=L} + J(Y'^2)|_{s=L}$$

The nonlinear inertial coefficient including tip rotary inertia is:

$$\alpha_2 = \rho\int_0^L \left(\int_0^\zeta Y'^2 ds\right)^2 ds + M\left(\int_0^\zeta Y'^2 ds\right)^2\Big|_{s=L} + JY'^4|_{s=L}$$

The linear stiffness coefficient (or effective elastic stiffness) is:

$$K_1 = EI \int_0^L Y''^2 ds$$

The nonlinear geometric stiffness coefficient is:

$$K_2 = 2EI \int_0^L (Y'Y'')^2 ds$$

and the base excitation inertial coefficient is:

$$\alpha_3 = -\rho \left(\int_0^L Y ds \right) - MY|_{s=L}$$

Adding a viscous damping term to the equation of motion leads to the final form of the governing equation for a transversely excited beam:

$$\alpha_1 \ddot{q} + \alpha_2 (q^2 \ddot{q} + q\dot{q}^2) + c\dot{q} + K_1 q + K_2 q^3 = \alpha_3 \dot{\mathrm{V}}_y \qquad \text{Eq. 4-8}$$

The mass normalized eigenfunction of the n[th] free undamped vibration mode is expressed as follows [47]:

$$Y(x) = A_n[\cos \beta_n x - \cosh \beta_n x + C_n(\sin \beta_n x - \sinh \beta_n x)]$$

where,

$$C_n = \frac{\sin \beta_n L - \sinh \beta_n L + \beta_n L \bar{M}(\cos \beta_n L - \cosh \beta_n L)}{\cos \beta_n L + \cosh \beta_n L - \beta_n L \bar{M}(\sin \beta_n L - \sinh \beta_n L)}$$

Thus, the first mode is:

$$Y(x) = A[\cos \beta x - \cosh \beta x + C(\sin \beta x - \sinh \beta x)]$$

where,

$$C = \frac{\sin \beta L - \sinh \beta L + \beta L \bar{M}(\cos \beta L - \cosh \beta L)}{\cos \beta L + \cosh \beta L - \beta L \bar{M}(\sin \beta L - \sinh \beta L)}$$

A is a modal amplitude constant which is obtained by normalizing the eigenfunction.

4.3 Experimental Development

The slender cantilever beams used in the experimental study were made of blue-finished, polished, spring-tempered AISI 1095 high-carbon steel. This type of steel is typically fabricated using cold rolling, which can cause a temper to form in the material, increasing the yield strength. The cold rolling process may cause some degree of material orthotropy. Therefore, the isotropy assumption is an approximation in this study. The principal alloying elements are 0.95wt% C, 0.4wt% Mn, and 0.2wt% Si. The density and the elastic modulus of the material are 7.85g/cm^3 and 205GPa, respectively. The hardness is Rockwell C48 with AR= 8. The beam length and cross-section area are 127mm and 15.88mm × 1.08mm, respectively.

4.3.1 Beam Characterizations

The overall surface profile of the beam was assessed to ensure that potential initial curvature did not cause any anomalous geometric softening effect. Therefore, a topological surface profile of the slender beam was measured using a Keyence LK-G5001 laser displacement sensor. The beam was mounted on a motion platform that is capable of precise motion, down to ±1μm. The beam's three-dimensional surface profile is shown in Figure 4-2. The curvature of the beam along its length was insignificant (Figure 4-3). The maximum beam height at the center of its width was less than 0.1mm. Since the product of the initial curvature and the beam width is much smaller than unity, it is reasonable to assume the initial curvature did not contribute to nonlinear effects [48].

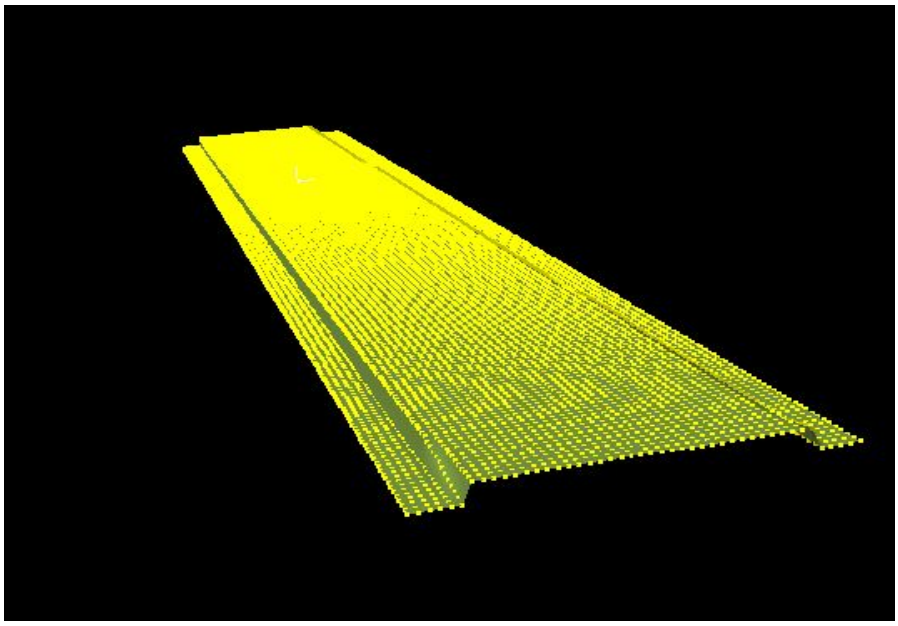

Figure 4-2. Three-dimensional surface profile of beam

A static defection experiment was performed to determine the initial nonlinear stiffness of the beam. The tip displacement of the cantilever beam was measured for different levels of transverse static force applied at its tip. The applied force versus displacement is shown in Figure 4-4. At low external force, the beam deflection was small and the bending resistance took the role of opposing the external force. Thus, the beam experienced linear behavior; i.e., the slope of the straight line is the linear stiffness. As the forces increases, the beam deflection increased and its curvature was noticeable, resulting in a foreshortening of the horizontal span of the beam. Thus, the axial strain created a membrane force, which caused an additional resistance, which dominated the behavior of the beam (Figure 4-4). At that point, the beam behaved nonlinearly, resulting in nonlinear stiffening; i.e., the stiffness curve was no longer a straight line. The test results suggest that the initial material nonlinearity, warpage, or residual stresses due to fabrication were not significant enough to overcome the geometric nonlinear stiffening and therefore could not be responsible for the nonlinear dynamic softening reported later in the vibration experiments.

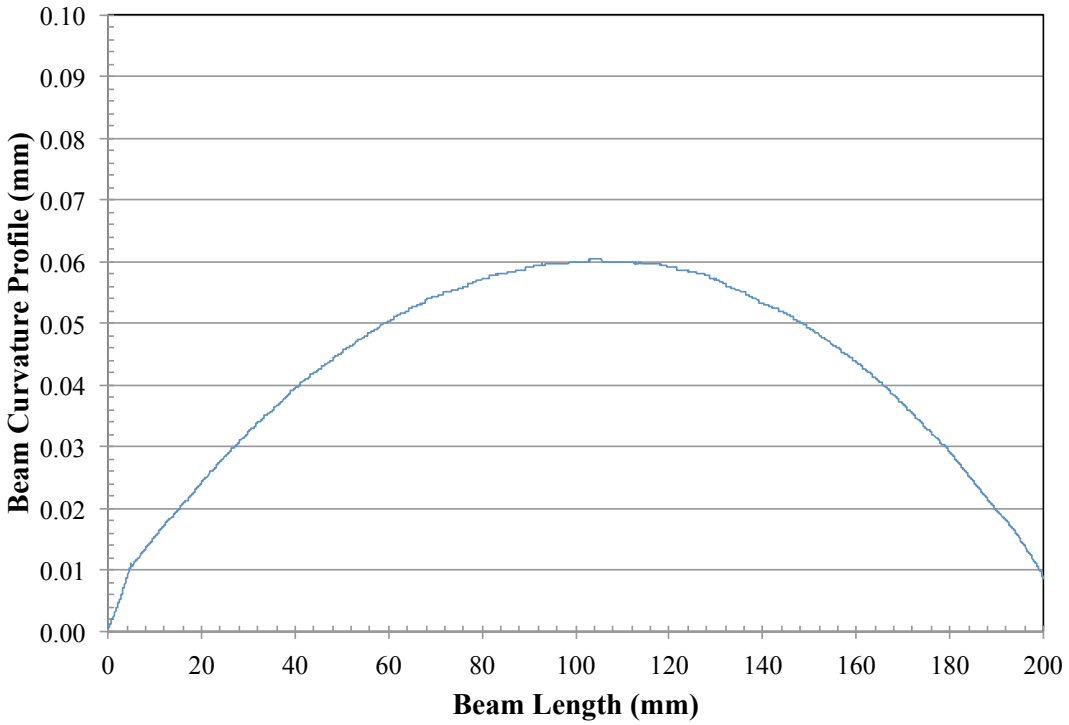

Figure 4-3. Beam curvature along its length

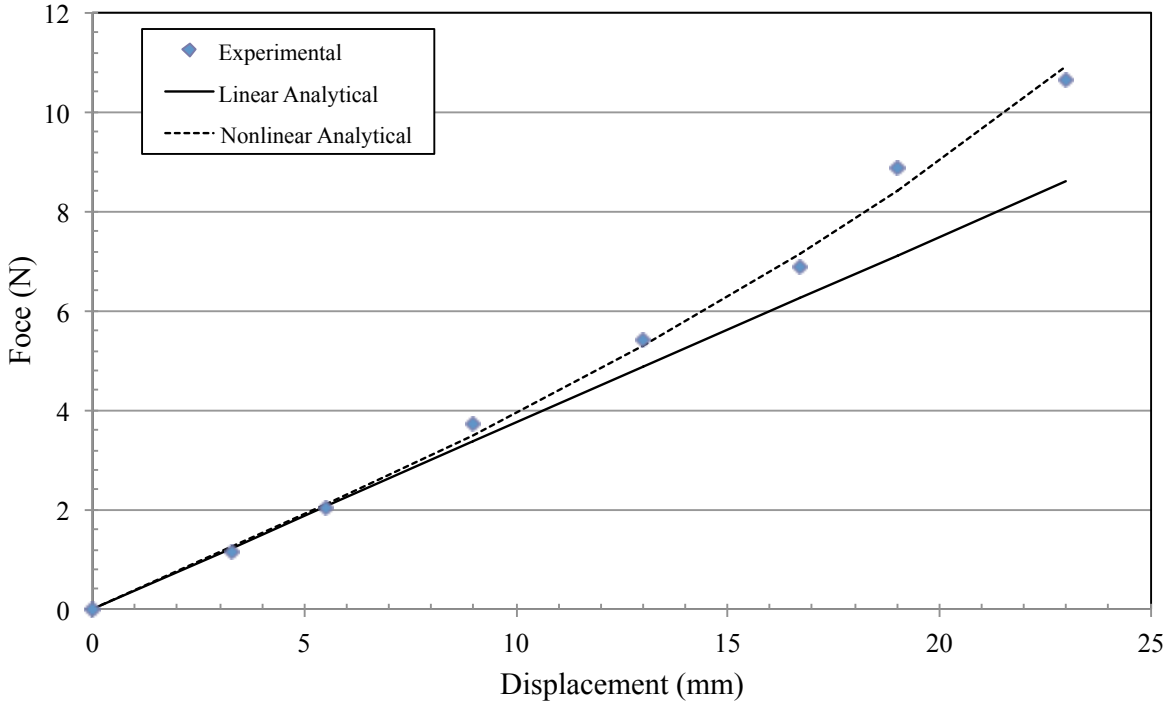

Figure 4-4. Nonlinear stiffening due to large static deflection

4.3.2 Experimental Dynamic Approach

The vibration experiment setup and instrumentation schematics are shown in Figure 4-5. Each beam was mounted horizontally on a rigid fixture where the bolts were torqued to 22.6 N-m. The system was then attached to an electrodynamic single-axis shaker table controlled by a triaxial accelerometer, which was mounted on the base fixture (Figure 4-5). The beam tip displacement was measured using accelerometer. The tip accelerometer mass was approximately 1.5g.

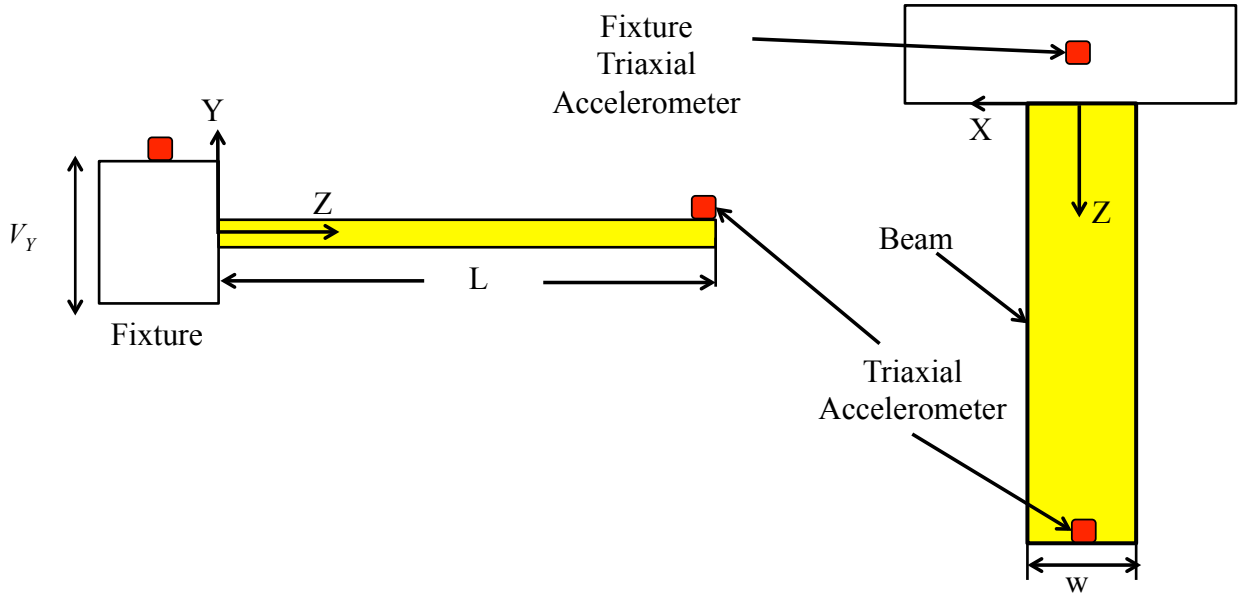

Figure 4-5. Experimental setup for vibration test

Table 4-1 Nonlinear experimental cases

Case			Test	Total Cycles (10^3)
I	Base Excitation (g)	0.1	1	0-97
			2	97-173
	Linear Resonance (Hz)	47.41	3	173-248

			4	248-324
	Max. Strain (10^{-3})	0.1	5	324-400
			6	400-475
II	Base Excitation (g)	0.2	1	0-71
	Linear Resonance (Hz)	46.64	2	71-130
	Max. Strain (10^{-3})	0.3	3	130-183
			4	183-244
III	Base Excitation (g)	0.3	1	0-97
	Linear Resonance (Hz)	47.52	2	97-182
			3	182-279
	Max. Strain (10^{-3})	0.6	4	279-362
			5	362-454

Three sets of experiments—Cases I, II, and III—were conducted. Table 4-1 lists the detail of each case. Once the linear fundamental frequency for each beam was identified using sine-sweep excitation, the beams were exposed to the transverse harmonic base excitation amplitudes stated above at discrete forward dwell frequencies near the fundamental frequencies. The ramp-up time and dwell time for each frequency were 30s and 20s, respectively. An example of time history data for the base excitation and tip response is shown in Figure 4-6. The dwell time at each excitation frequency ensured that steady state response conditions were reached. Figure 4-6 is an example of a close-up dwell period for the base excitation and the beam tip response. The constant response amplitudes in Figure 4-7 are clear indications that steady state conditions were reached during the dwells at each frequency. The frequency step for each dwell was 0.05 Hz. Therefore, the excitation frequency was increased 0.05 Hz every 50s (30s

ramp-up plus 20s dwell).

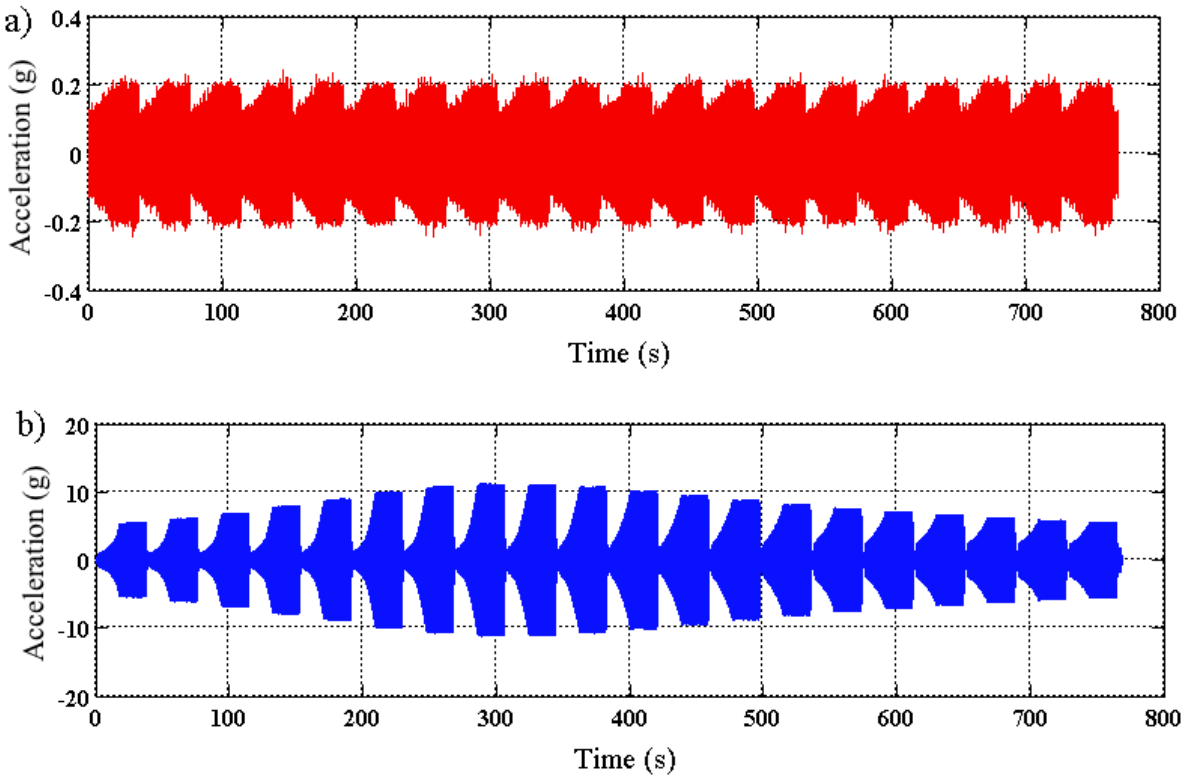

Figure 4-6. Ramp up and dwells of a) base excitation and b) corresponding tip response

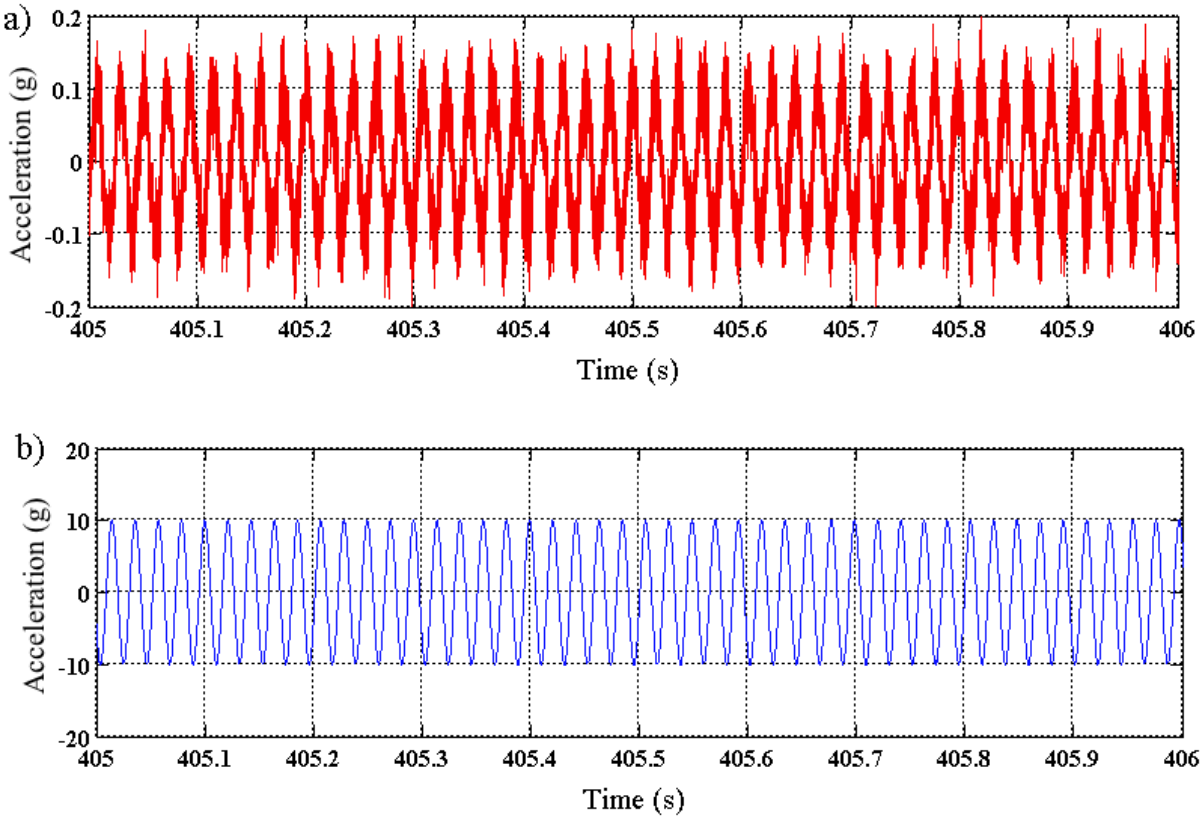

Figure 4-7. Example of 1.0s dwell period of a) base excitation and b) corresponding tip response

4.3.3 Local Mechanical Characterization

Instrumented nanoindentation is a method used for examining local mechanical properties of materials [49]. The technique has been used to characterize the elastic modulus, elastic-plastic stress-strain curves, creep properties, and hardness of a wide range of materials and structures, including traditional steels [50], film-substrate systems [51], functionally graded structures [52, 53], polymers and polymer composites [54-56], and individual microfibers [57].

In the current study, the local mechanical properties of the beam samples near the fixed boundary were examined using nanoindentation (Figure 4-8). Each sample was carefully cut to minimize mechanical damage to the edges to prevent unintended alterations to the overall mechanical properties. The surface of each sample was then polished up to 0.1 microns to

minimize the effect of surface roughness on the indentation response. The indentation experiments were performed using a diamond Berkovich tip (radius of curvature approximately 100 nm). Positions along the center of the beam surface were located using the optical microscope in the indentation system. For each targeted location, 100 indentations were performed in a 10×10 grid, spaced 5 μm apart. The edge of the initial indent array was positioned 10 μm from the clamped portion of the beam; subsequent arrays were positioned in approximately 2 mm increments stepping away from the fixed boundary position and moving toward the beam-free end. Measurements were performed in load control mode, with a maximum applied force, P, of approximately 5000 μN. A drift correction was performed prior to indentation using a preload of 1 μN for 20s. A triangular force profile was used with a quasi-static loading rate of 625 μN s^{-1}.

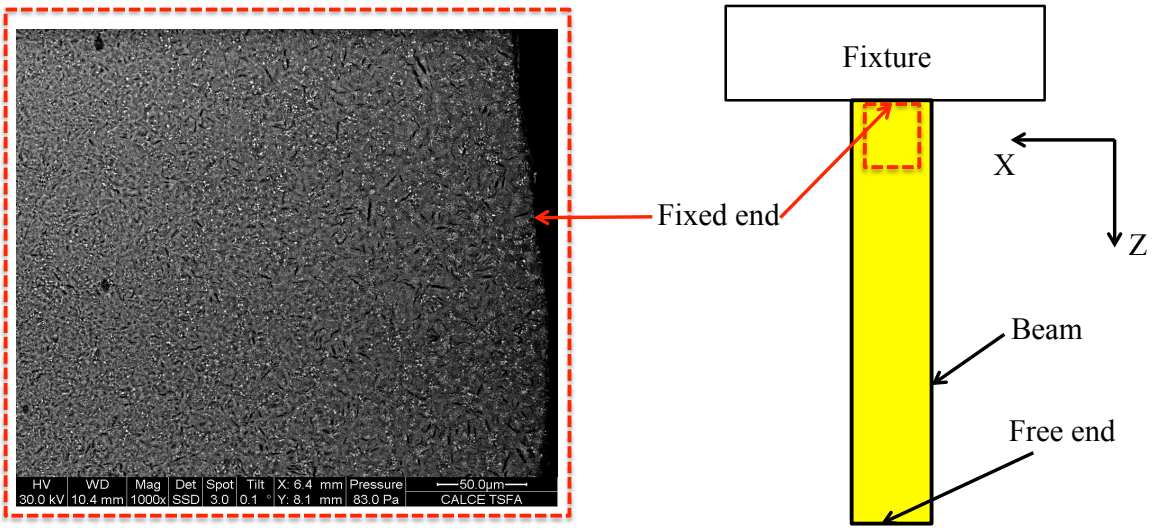

Figure 4-8. Surface microstructure near beam root after 0.3g vibration test, 1000X magnification

Indentation results provided a reduced indentation stiffness E_r, which can be related to the sample indentation modulus E_s through: $1/E_r = (1-\nu_i^2)/E_i + (1-\nu_s^2)/E_s$, where E_i is the elastic modulus of the tip and ν_i and ν_s are the Poisson's ratios of the tip and sample, respectively. The

indentation stiffness is obtained from the initial slope of the unloading part of the indentation load-displacement curve. Some studies relate the indentation stiffness to the material stiffness. To obtain sample properties in this study, E_i, ν_i and ν_s were assumed to be 1140 GPa, 0.17, and 0.30, respectively.

4.4 Results and Discussion

Detailed discussion of the experimental results is provided in this section. The utilization of the nonlinearities in the dynamic model provided good agreement between the model predictions and the experimental results. The sensitivity of the nonlinear geometric stiffness to fatigue damage precursor is discussed as well. This section also exploits the sensitive link between micromechanics and global nonlinear dynamics, which was a powerful tool in detecting the local fatigue damage precursor.

4.4.1 Experimental Results of Nonlinear Vibration Tests

Each dynamic experimental set contained four to six step-dwell tests, as shown in Figure 4-9 through Figure 4-11. The objective was to capture the shift in the fundamental frequency and the softening phenomenon due to repeated dwells. Figure 4-9 through Figure 4-11 reveal that the resonance frequency continued to decrease every time the test was repeated due to continuing accumulation of cyclic fatigue damage. The nonlinear softening effect on the fundamental modes was apparent in the beam tip responses. The frequency-response curves were skewed to the left, indicating a softening nonlinearity and a dominance of material softening over the structural nonlinear kinematic stiffening.

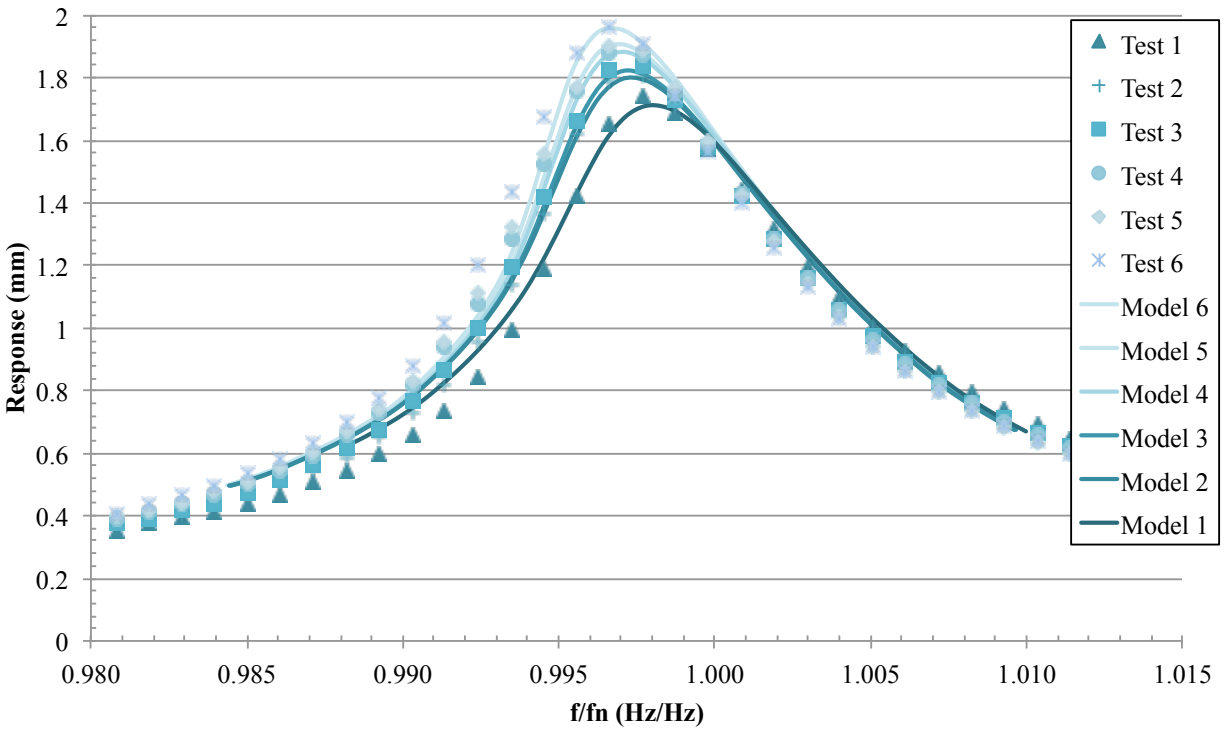

Figure 4-9. Experimental and analytical nonlinear softening response for Case I

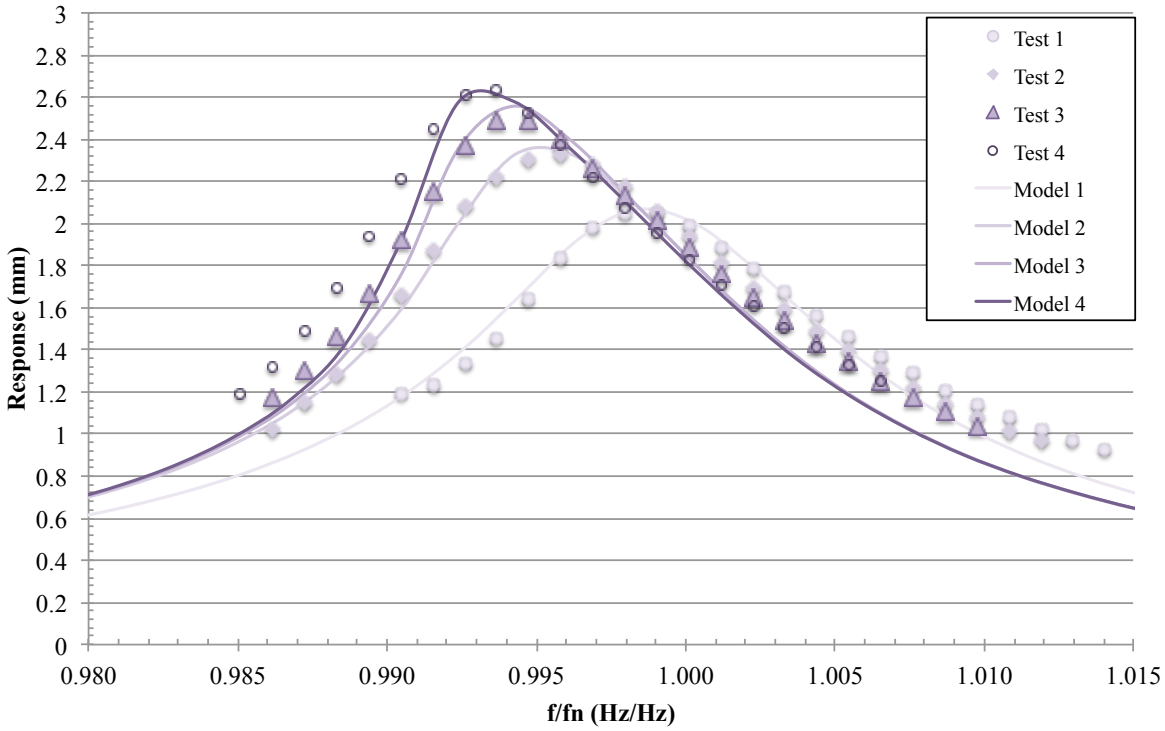

Figure 4-10. Experimental and analytical nonlinear softening response for Case II

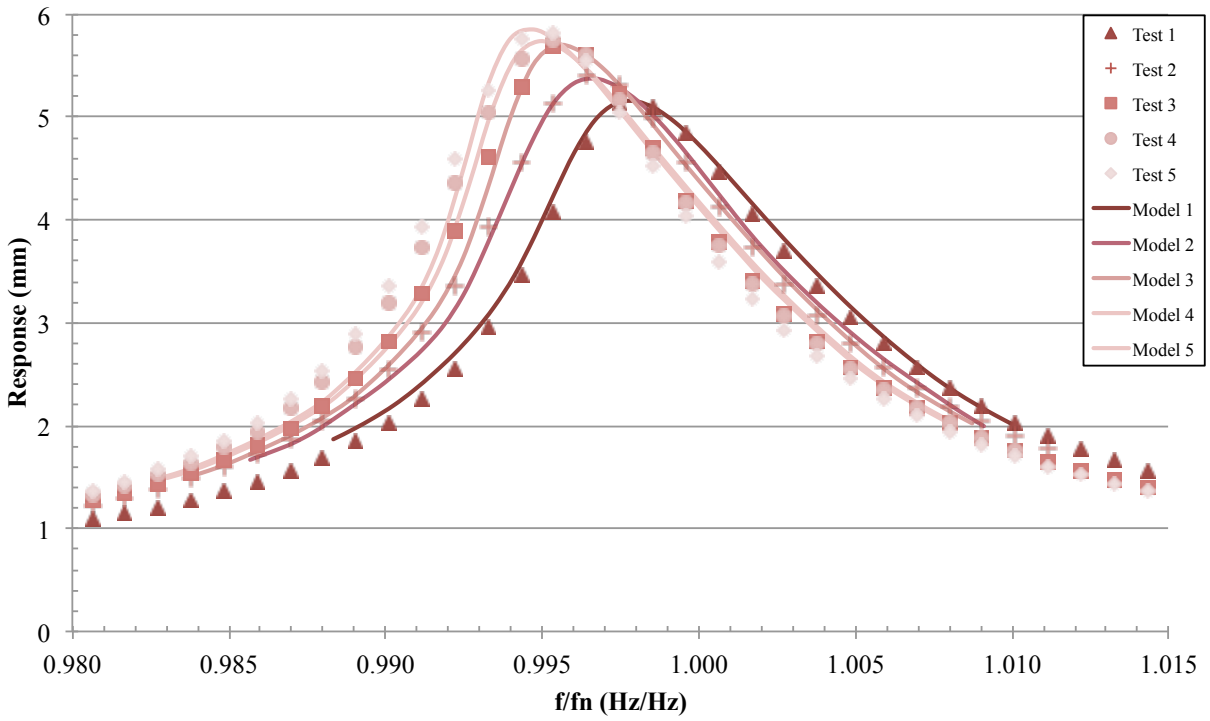

Figure 4-11. Experimental and analytical nonlinear softening response for Case III

The beams continued to experience softening due to an increase in the number of vibration cycles and in the level of the base excitation. The accumulation of loading cycles led to continuing fatigue damage buildup, resulting in a corresponding reduction in the local stiffness, with the reduction in magnitude being proportional to the stress level. These experimental results diverged from several theoretical models that predicted nonlinear stiffening at the fundamental mode [14, 44]. This discrepancy can be explained by the fact that there were three competing mechanisms occurring simultaneously in the experiments: 1) structural stiffening due to nonlinear kinematic effects at high amplitude response; 2) nonlinear structural softening due to inertial effects; and 3) progressive structural softening due to localized material degradation caused by high-cycle fatigue. The theoretical models that predict nonlinear stiffening are based only on the first two mechanisms. The structural softening experimentally observed in this study

is attributed to the fact that the third effect (material fatigue degradation) is stronger than the first two.

Malatkar encountered similar material degradation phenomena, but avoided potential fatigue from the high-amplitude and high-cyclical loading by reducing the number of dwells and repeating each experiment only twice [46]. Interestingly, experimental results to illustrate the effect of material degradation on the fundamental vibration mode have been limited [16]. Priya et al. and Yu et al. observed similar softening phenomena at the fundamental frequency when studying harvester piezoceramics, but did not provide any explanation for the softening [41, 42]. Stanton et al. assumed that the nonlinear softening was due to material nonlinearities in their piezoceramic device or instrumentation errors [43]. Saavedra and Cuitino also witnessed softening trends on a cracked mild steel beam exposed to harmonic vibratory loads [37]. The present experimental results displayed similar trends to the studies mentioned above, which deviated from nonlinear Euler-Bernoulli beam theory.

4.4.2 Microstructural Analysis

To investigate the local change in the beam material and the associated stiffness, the beam root microstructure of Case III was examined using Scanning Electron Microscopy (SEM), as discussed in Section 4.3.3. Figure 4-12a shows the microstructure of the fatigued beam; the edge seen in the right side of the image is the clamped position of the beam. The beam surface near the fixed boundary displayed coarsening of features and a relatively high density of long dark, slender elliptical regions (Figure 4-12c). The concentration of these dark regions lessened as distance from the clamped boundary increased (Figure 4-12b). The literature has presented some evidence that this type of microstructural variation near these highly stressed regions is likely due to localized dislocation motion resulting in the formation of persistent slip bands

(PSBs) [58-60]. Dislocation motion is the primary mechanism of plastic deformation in metals and has been shown to result in slip within the grains in similar polycrystalline materials [60, 61]. The authors provide no evidence that PSBs are forming in the material used in this study. Further investigation is required and it is beyond the scope of this study. A pristine beam surface was also examined and compared to the fatigued beam microstructure (Figure 4-13). The microstructure of the unfatigued beam appeared uniformly more fine-featured throughout (Figure 4-13b).

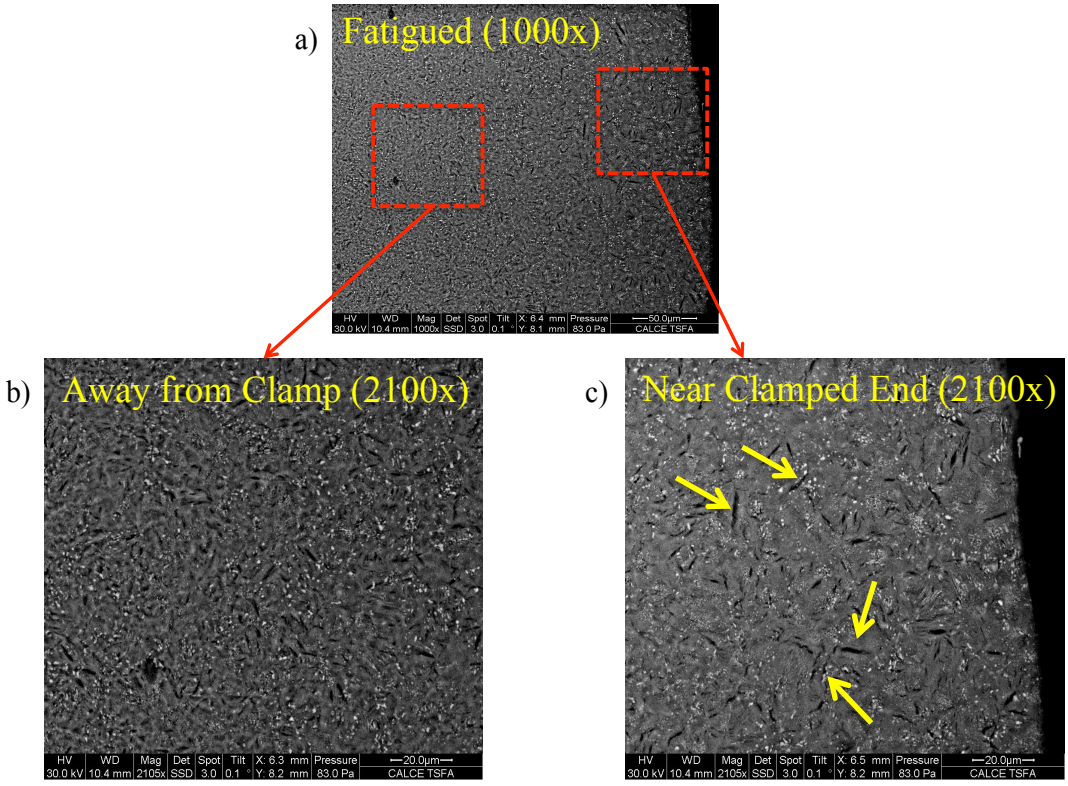

Figure 4-12. Surface microstructure near beam root for case III after $454x10^3$ cycles, a)1000X magnification b) 2100X magnification away from beam fixed end c) 2100X magnification at fixed end

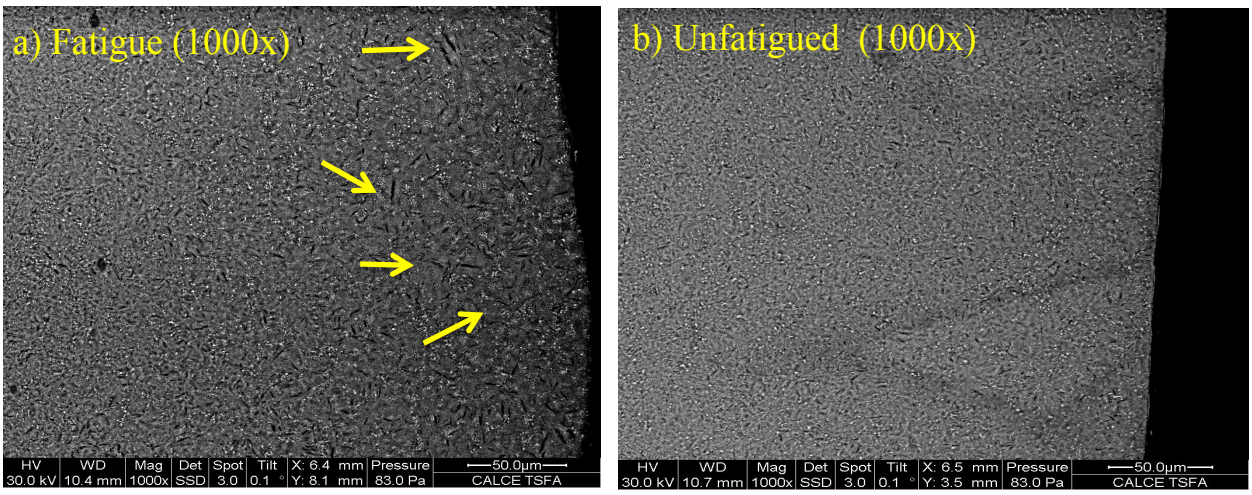

Figure 4-13. Surface microstructure shows a) higher concentrations of dark bands near the fixed end for case III after 454×10^3 cycles and b) uniform microstructure of unfatigued beam

4.4.3 Local Degradation Characterization

As discussed earlier in Section 4.3.3, nanoindentation tests were organized in 10×10 arrays and positioned at various points along the central axis of the beam (Figure 4-14). The location x=0 indicates the clamped edge during cantilever excitation (and the expected position of maximum stress according to beam theory). The indentation stiffness is shown as a function of position x, from the clamped end of the beam. The dotted lines in Figure 4-14 show the upper and lower bounds of indentation tests performed on a control sample, while the inset shows scanning probe imaging of a typical indent array on beam surface. Tests were performed in load control mode using a peak force of 5000µN; these applied forces resulted in indentation depths of approximately 150–200 nm (approximately 1.5–2.0% of the cross-sectional depth). For comparison, an unfatigued control sample was tested at three separate locations near the center of the specimen, for a total of 300 indents (shown with dotted interval lines in Figure 4-14).

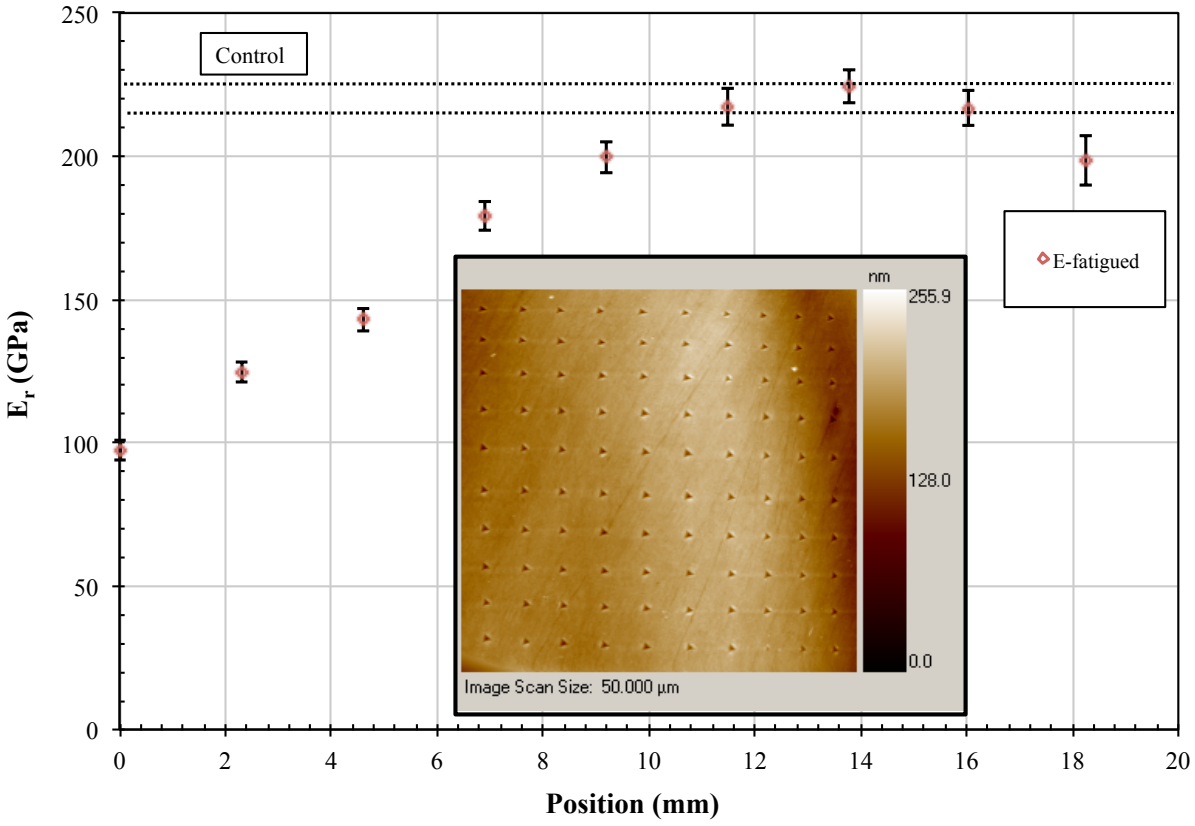

Figure 4-14. Local mechanical characterization of fatigued beam as determined by nanoindentation

Indentation results on the fatigued sample showed a clear localized reduction in the indentation stiffness of the material near the clamped position of the beam. As indicated earlier, this apparent stiffness is obtained from the initial slope of the unloading part of the load-displacement curve in the indentation test. The defined zero position, which includes tests as close as 10 µm from the fixed boundary location, showed an average indentation stiffness of approximately 100 GPa. Stepping away from the clamped position, the average apparent indentation stiffness eventually approached 220 GPa, which was the approximate baseline elastic modulus of the unfatigued control sample (Figure 4-14). The results suggest that the average indentation stiffness over the first few hundred nanometers near the sample surface was reducing

as a result of the high number of tension-compression cycles. The literature suggests that such loading may be expected to result in PSB formation [60]. This reduction in the indentation stiffness appeared more pronounced in areas adjacent to the clamped beam positions, which was not surprising considering the high-cycle fatigue damage expected in these locations due to the flexural stress concentration expected near the root of a cantilever beam. To be clear, these initial indentation tests cannot fully describe variations in the dynamic behavior of the beam, but are an important first step in explaining how cyclic fatigue damage accumulation may affect surface microstructure and thus local mechanical properties in areas of interest. It is important to point out that the approximate maximum strain near the root is 0.6×10^{-3} strain, which is still in the linear region of the stress-strain curve for 1095 steel.

4.4.4 Model Results

Excitations that produced a nonlinear response led to localized damage, which caused local softening near the fixed boundary (Figure 4-15). Attempts were made to tune the linear stiffness term in the equation of motion to track the fatigue degradation; however, minute modifications to the linear stiffness term caused drastically unrealistic shifts in resonance frequency. Thus, nonlinear dynamics analysis was implemented where the nonlinear geometric stiffness was modified to account for the fatigue-induced material evolution near the fixed end. This modification to the nonlinear stiffness provided a better curve fit to the experimental results. Unlike linear dynamic model, the nonlinear stiffness term in the nonlinear dynamic model provided more useful sensitivity to the evolution in the material due to fatigue-induced damage. The nonlinear equation of motion was solved numerically using the Runge-Kutta method, where the integration time step was 10^{-5} s and the initial conditions were zero displacement and velocity. The integration time limits were set from 0s to 30s to ensure that steady state condition

was reached. A selection of the numerical response curves over a frequency range near the first mode is provided in Figure 4-16. As expected, the model results indicate that increasing the base excitation stiffens the beam, i.e. the fundamental flexural frequency increases (Figure 4-16). The accelerometer mass was included in the model, but its contribution was relatively minor. Subsequently, the geometric nonlinear stiffening effect dominated over inertial nonlinear softening.

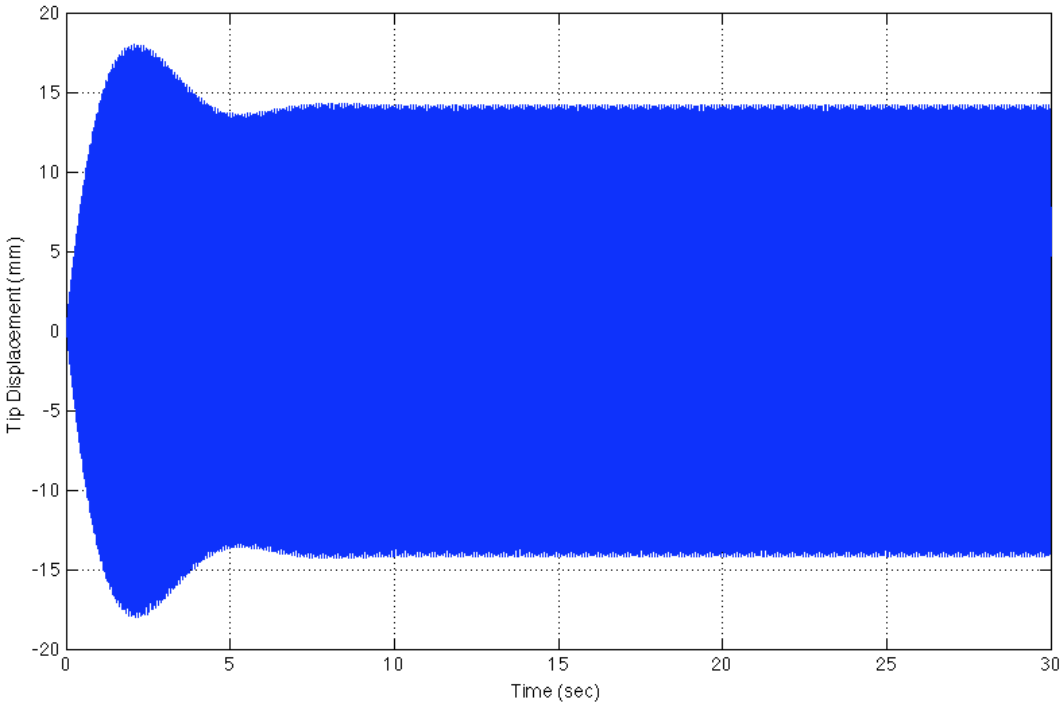

Figure 4-15. Example of analytical beam tip response after 30 s

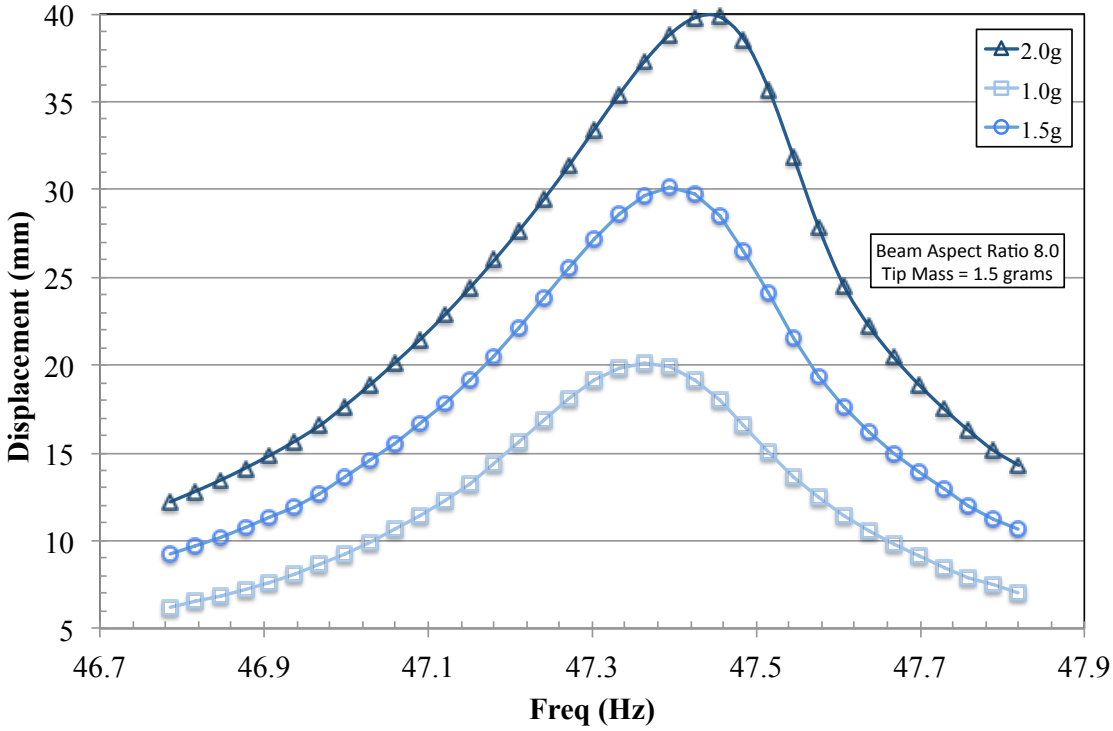

Figure 4-16. Selection of numerical nonlinear response curves

The experimental results provided in Figure 4-9 through Figure 4-11 show that increasing the excitation amplitudes enhances the softening effects (resonant frequency decreases), which contradicts the nonlinear Euler-Bernoulli model. This contradiction is because the nonlinear dynamic model (Eq. 4-8 and other similar models in the literature [19-22]) does not incorporate material property evolution due to fatigue. When examining the data closely, it is clear that cyclic fatigue played an important role in altering the results. Damage accumulated near the beam root due to ramp-up and dwell cycles, causing the beam to soften locally, thus increasing the beam tip response amplitude, and reducing the resonant frequency. Figure 4-17 shows the maximum amplitudes for Cases I, II, and III (base excitations 0.1, 0.2, and 0.3g, respectively). The cycles of each case is provided in Table 4-1. The maximum response amplitudes from Figure 4-9 through Figure 4-11 are plotted as a function of loading cycles. Not surprisingly, the

beam tip maximum response amplitudes increased as a result of increasing the excitation amplitudes [62]. However, for each excitation level, the maximum response amplitudes increased logarithmically as a function of the loading cycles due to the local material degradation caused by the cyclic fatigue damage accumulation (Figure 4-17).

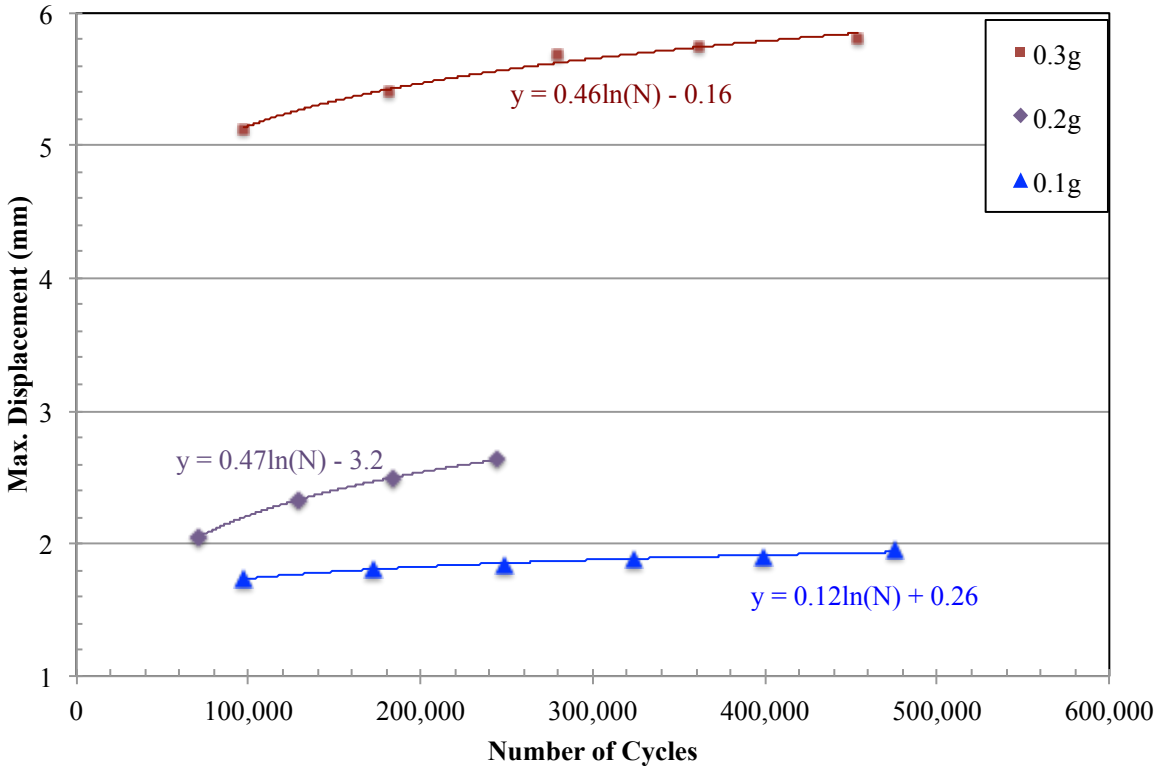

Figure 4-17. Maximum tip displacement response for each test, as a function of number of fatigue cycles

The softening in the dynamic beam structural response, observed in the nonlinear dynamic experiments as a results of fatigue damage precursor, is captured in the analytical model by adjusting the nonlinear geometric stiffness term, K^* in the equation of motion, Eq. 4-9. This types of parametric adjustments were also utilized by Carrella and Ewins [63], and Zwink [4] to model the response of lump mechanical systems. The governing equation was modified as follows:

$$\alpha_1\ddot{q} + \alpha_2(q^2\ddot{q} + q\dot{q}^2) + c\dot{q} + K_1 q + K^* q^3 = \alpha_3 \dot{V}_y \qquad \text{Eq. 4-9}$$

where parameter K^* was modified as follows:

$$K^* = \delta K_2$$

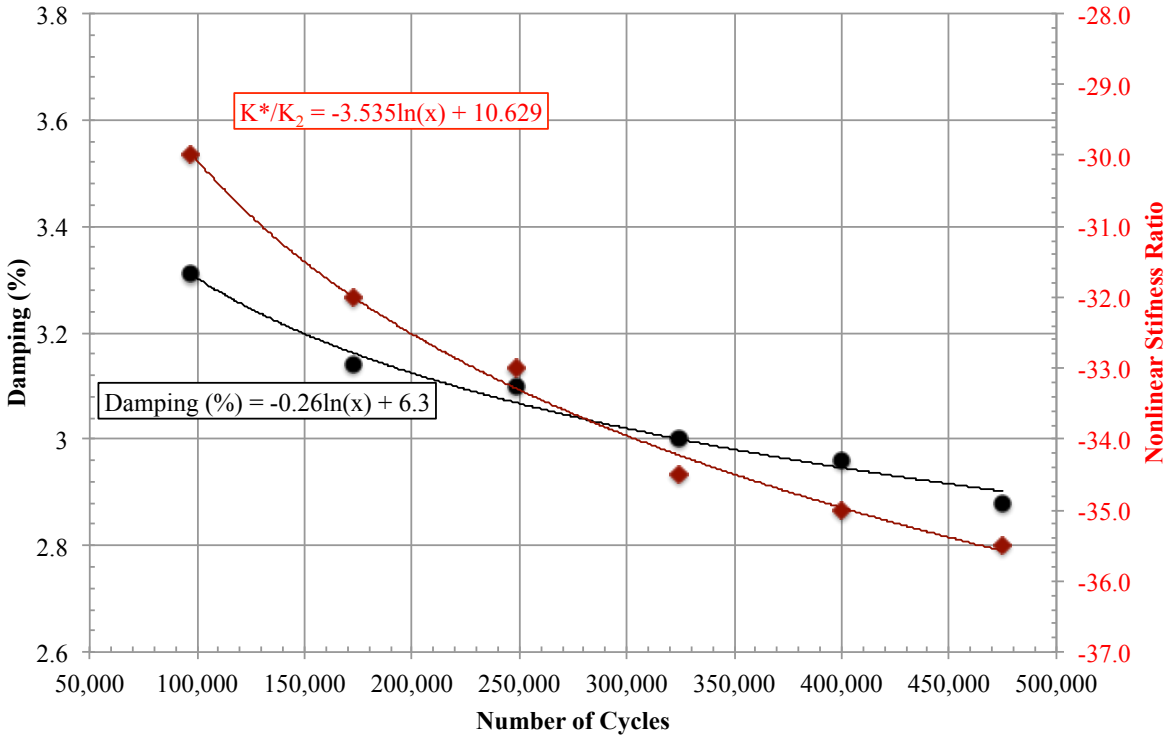

Figure 4-18. Nonlinear stiffness and damping changes due to fatigue cycles for Case I

where the modified nonlinear stiffness, K^*, is the geometric stiffness, K_2, multiplied by the nonlinear adjustment factor, δ. The model results for the response amplitude superimposed on top of the experimental data in Figure 4-9 through Figure 4-11 illustrate that calibration of the nonlinear stiffness term in the model can provide good agreement between the experiment and model results. The nonlinear adjustment factor for each run is plotted as a function of the total number of cycles in Figure 4-18 through Figure 4-20. The experimental and numerical results show that the nonlinear adjustment factor logarithmically decreases as the number of loading cycles increases. Furthermore, the adjustment factor has a negative sign, which is clear indication

of a softening phenomenon due to fatigue, even though the stresses in the beams were still in the elastic region. The logarithmic decay in the material stiffness was consistent with fatigue behavior [61]. For completeness, the damping ratio was plotted as a function of fatigue cycles. Figure 4-18-20 show that the beams displayed slight logarithmic decay in damping. The beams may exhibit nonlinear damping behavior, which is worthy of further future investigation. Nonetheless, δ had significantly more influence on the nonlinear geometric stiffness term than on the damping term.

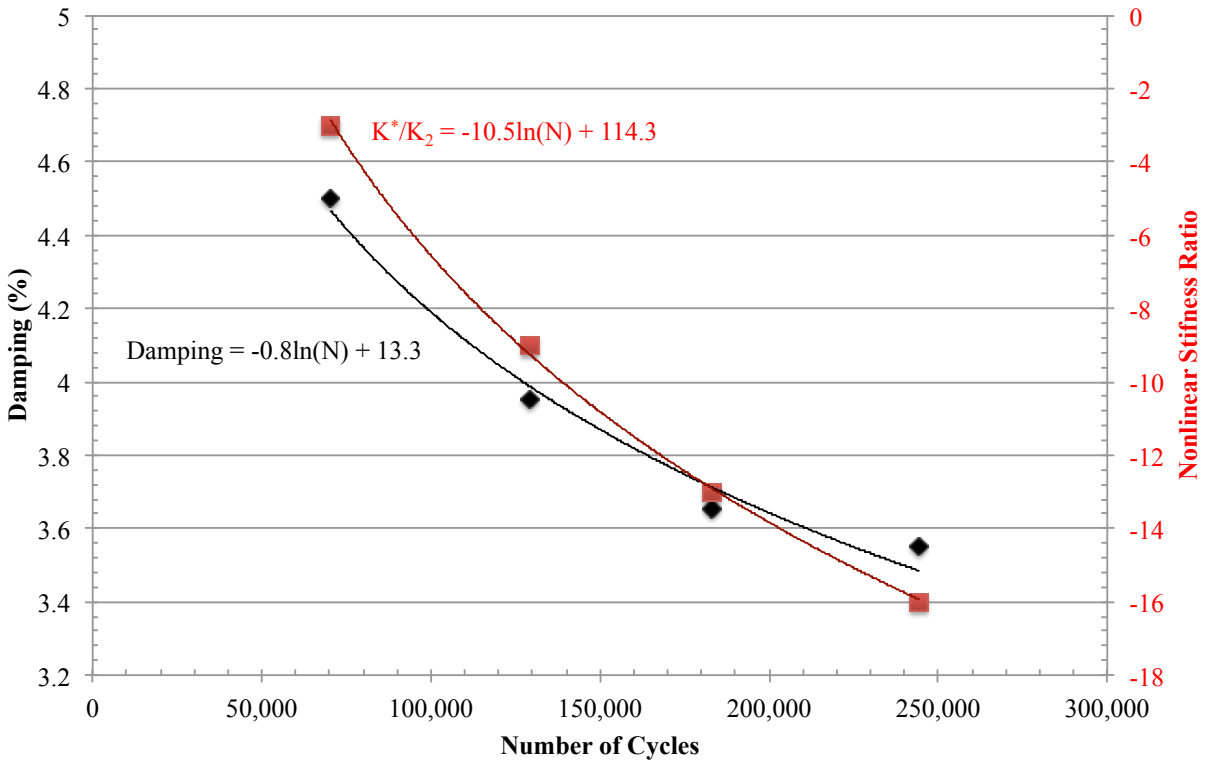

Figure 4-19. Nonlinear stiffness and damping changes due to fatigue cycles for Case II

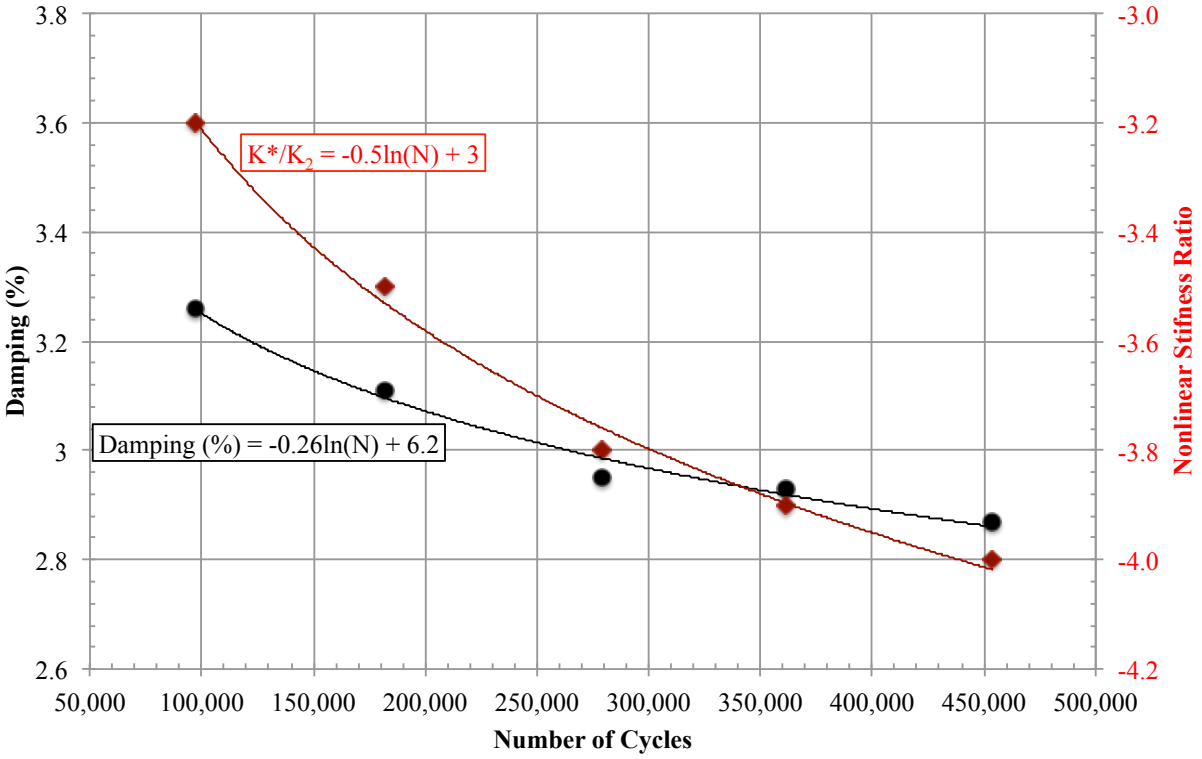

Figure 4-20. Nonlinear stiffness and damping changes due to fatigue cycles for Case III

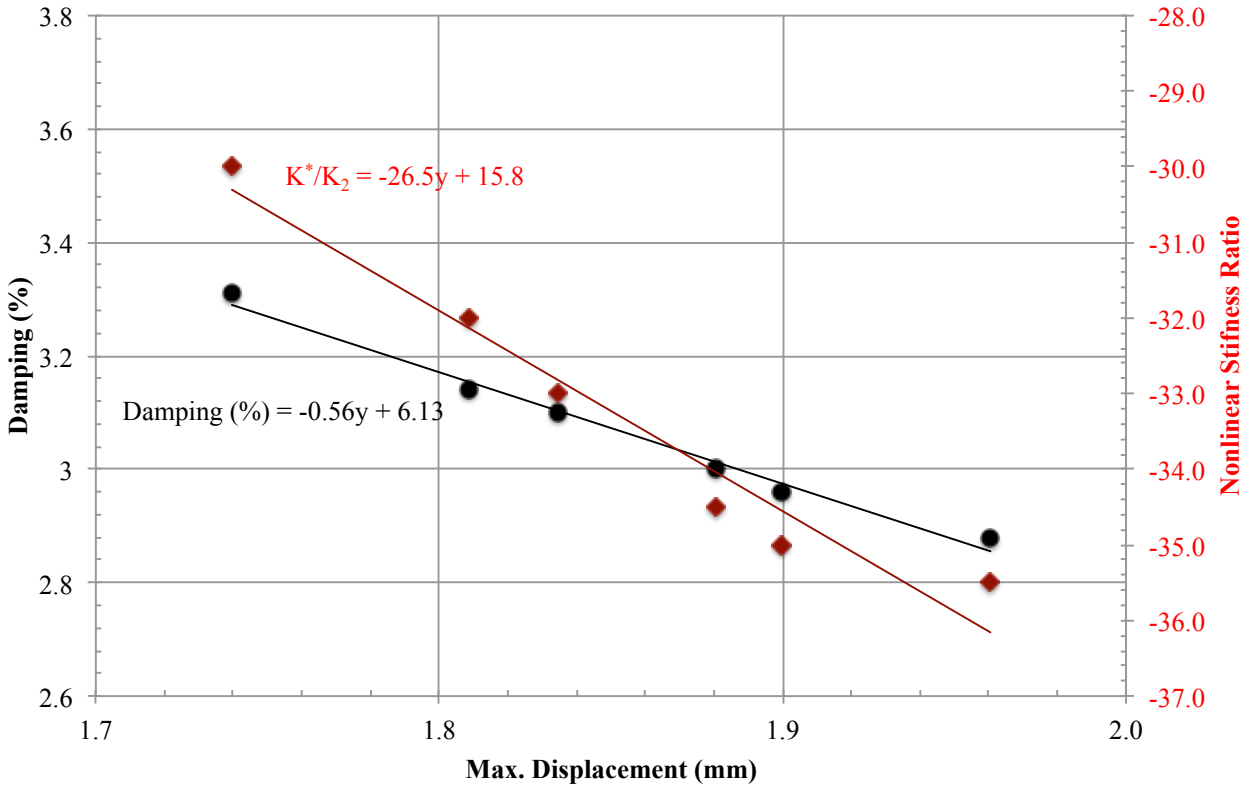

Figure 4-21. Nonlinear stiffness and damping changes as a function of displacement for Case I

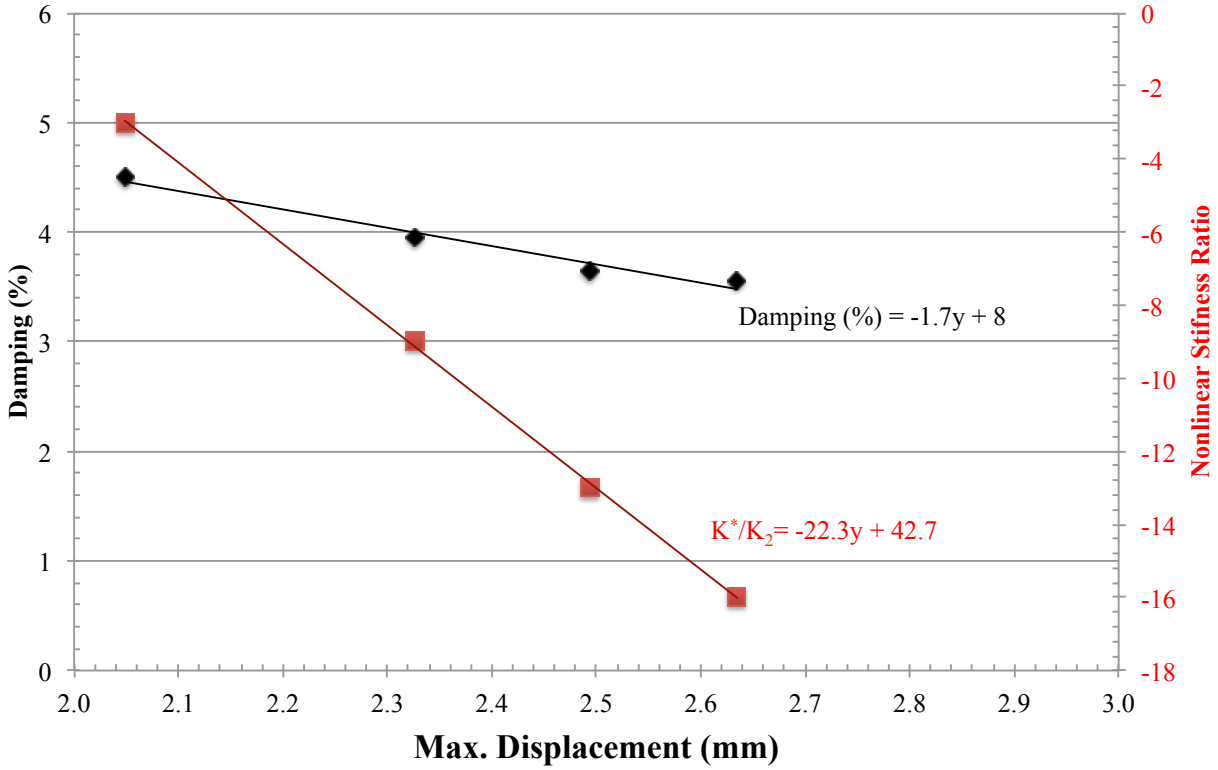

Figure 4-22. Nonlinear stiffness and damping changes as a function of displacement for Case II

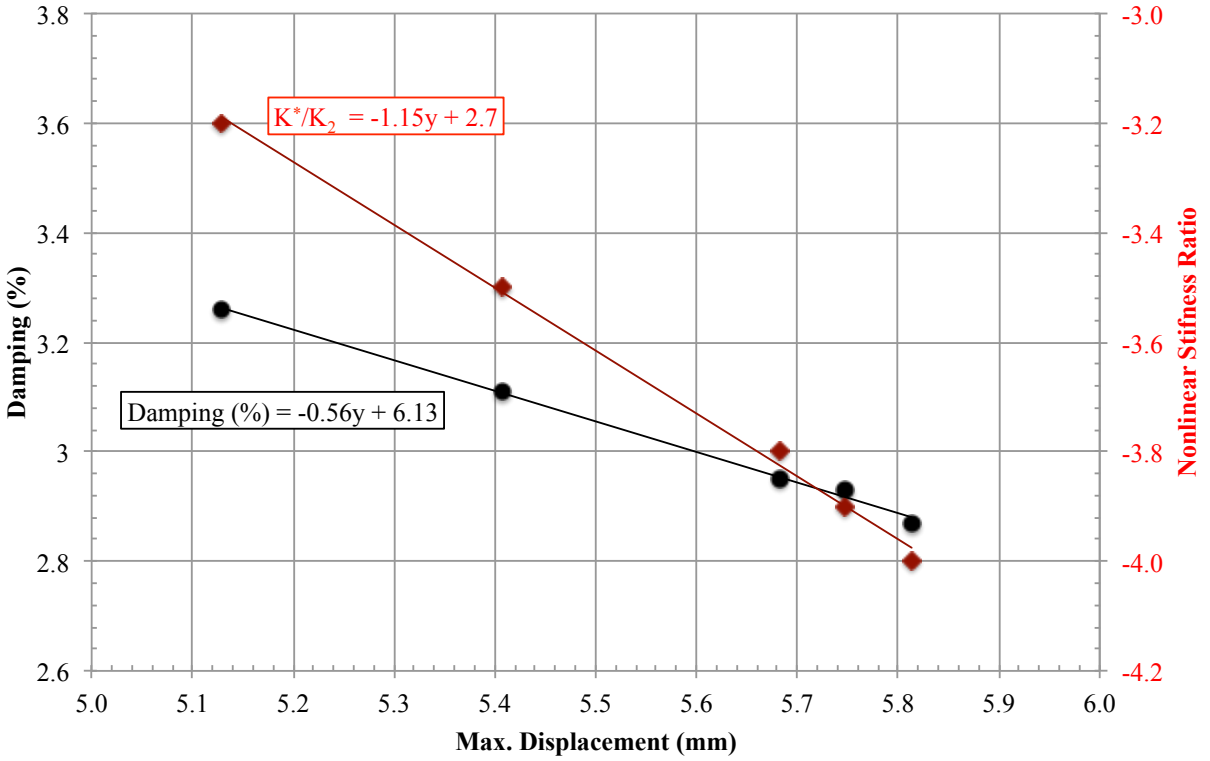

Figure 4-23. Nonlinear stiffness and damping changes as a function of displacement for Case III

It was reasonable to conclude that the local material degradation decreased the resonance frequency when it was appreciable, i.e. when the base excitation amplitude was large. It resulted in an effective nonlinear stiffness reduction for oscillations with large amplitude and high cycle loading, making it necessary to include the stiffness reduction in the model as a function of the beam response history for each excitation. The modified nonlinear stiffness of the beam decreased linearly with an increase in the response amplitude (Figure 4-21 through Figure 4-23). It is important to point out that the sensitivity of the nonlinear stiffness decreased with increase in the base excitation amplitude. This is because the beams experienced three opposing mechanisms simultaneously: 1) structural kinematic stiffening due to high tip displacement; 2) structural softening due to inertial forces; and 3) structural softening due to local material damage accumulation as a precursor to fatigue damage. All three mechanisms increased with increase in the base excitation and beam response. To illustrate the importance of the nonlinear stiffness term as a potential health monitoring metric, the changes in the nonlinear stiffness ratio are compared to for the change in the maximum dip deflection form from 100,000 to 245,000 loading cycles Cases I, II and III, as shown Figure 4-24. The nonlinear stiffness sensitivity is more sensitive than the nonlinear deflection. For Cases I and III, the sensitivity of the nonlinear stiffness ratio is approximately double the nonlinear deflection sensitivity. However, for Case II, the stiffness sensitivity is three times the deflection sensitivity. The cause of higher stiffness sensitivity in Case II is not clear. Nonetheless, exploiting the nonlinear stiffness term as a potential health monitoring metric appears to be a promising and deserve further investigation and development.

The changes in the damping ratio as a function of displacement are illustrated in Figure 4-21 through Figure 4-23. The linear decline in the damping with an increase in the beam tip displacement was minor.

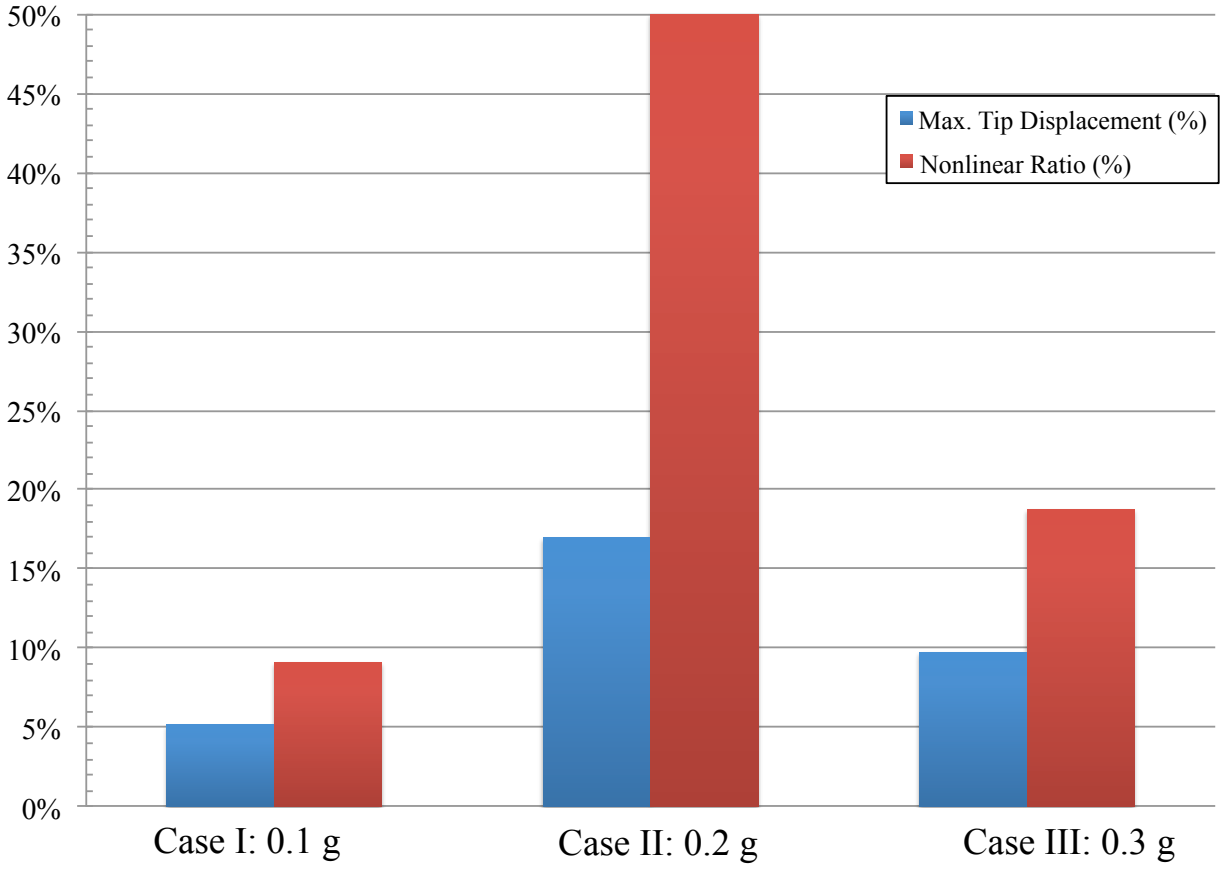

Figure 4-24. Changes in nonlinear stiffness ratio and maximum tip displacement from100,000 to 245,000 cycles for Cases I, II, and III

4.5 Summary and Conclusions

This study presents clear evidence of the sensitivity of nonlinear vibration response of slender metallic structures to fatigue damage precursor, which occurs prior to any fatigue crack initiation in toughened steel structures. The sensitivity of the nonlinear geometric stiffness in an analytic model of the equation of motion enabled the detection of this fatigue damage precursor. As an example, steel cantilever beams were fatigued using nonlinear vibration loading. The

nonlinear dynamic model provided a methodology for estimating the changes in the nonlinear dynamic response due to local material degradation prior to crack initiation. This is accomplished by adjusting the nonlinear geometric stiffness term in the equation of motion. The effect of viscous damping on the nonlinear structural response is also studied and found to be relatively small when compared to the effect of the nonlinear geometric stiffness term. The experimental results also the effects of three competing mechanisms that influenced the beam response: 1) structural stiffening due to kinematic nonlinearity in high response amplitude; 2) structural softening due to inertial forces; and 3) structural softening due to localized microstructural material damage precursor. Linear vibration-based detection would have not captured the damage precursor making the sensitivity of the nonlinear vibration approach a viable method in monitoring the state and health of the structure materials.

Higher order nonlinearities beyond the cubic terms and the beam rotational inertia are investigated as well and found to be insignificant. However, it is possible to include an additional cubic damping term of the form $\dot{q}^3$. Combining the nonlinear geometric stiffness and cubic damping terms may provide designers and structural health monitoring systems with additional sensitivities to predict, detect, and monitor the longevity of complex system, which can be the subject of future studies.

The simplicity of the proposed nonlinear dynamic methodology for detecting damage precursor makes it a powerful alternative to current inspection methods. The attraction of the nonlinear approach is that it provides a sensitive method that utilizes conventional sensors such as accelerometers and can be implemented in many platforms without the replacement of existing sensors.

4.6 References

[1] Dixon, M. C. The Maintenance Costs of Aging Aircraft: Insights from Commercial Aviation, Rand Publishing, Arlington, VA, 2006.

[2] Dimarogonas, Andrew D. "Vibration of Cracked Structures: A State of the Art Review." *Engineering Fracture Mechanics* 55.5 (1996): 831-57.

[3] Doebling, S. W., Farrar, C. R., Prime, M. B., and Shevitz, D. W., "Damage Identification and Health Monitoring of Structural and Mechanical Systems from Changes in their Vibration Characteristics: A Literature Review, Los Alamos National Laboratory report LA-13070-MS, 1996.

[4] Zwink, B. R. "Nondestructive Evaluation of Composite Material Damage Using Vibration Reciprocity Measurements." *Journal of Vibration and Acoustics* 134.4 (2012): 041013-1-41013-8.

[5] Wang, D., Q. Maio, Q. Zhou, and G. Zhou. "An Intelligent Prognostic System for Gear Performance Degradation Assessment and Remaining Useful Life Estimation." *Journal of Vibration and Acoustics* 137.2 (2015): 021004-1-21004-12.

[6] Staszewski, W. J., C. Boller, and Geoffrey R. Tomlinson. *Health Monitoring of Aerospace Structures: Smart Sensor Technologies and Signal Processing*. West Sussex, England: Hoboken, NJ, 2004.

[7] Farrar, C. R., and K. Worden. *Structural Health Monitoring: A Machine Learning Perspective*. Chichester, West Sussex, U.K.: Wiley, 2013.

[8] Worden, K., and Geoffrey R. Tomlinson. *Nonlinearity in Structural Dynamics: Detection, Identification, and Modelling*. Bristol: Institute of Physics, 2001.

[9] Habtour, E., C. Choi, M. Osterman, and A. Dasgupta. "Novel Approach to Improve

Electronics Reliability in the Next Generation of US Army Small Unmanned Ground Vehicles Under Complex Vibration Conditions." *Journal of Failure Analysis and Prevention* 12.1 (2012): 86-95.

[10] Ernst, M., E. Habtour, A. Dasgupta, M. Pohland, M. Robeson, and M. Paulus. "Comparison of Electronic Component Durability Under Uniaxial and Multiaxial Random Vibrations." *Journal of Electronics Packaging* 137.1, 2015.

[11] Salawu, O. S., 1997a, "Detection of Structural Damage Through Changes in Frequency: A Review," *Engineering Structures*, Vol. 19, No. 9, pp. 718-723.

[12] Sun, Z., B. Rocha, K. Wu, and N. Mrad. "A Methodological Review of Piezoelectric Based Acoustic Wave Generation and Detection Techniques for Structural Health Monitoring." *International Journal of Aerospace Engineering* 2013 (2013): 1-22.

[13] Venstra, W. J., H. J. R. Westra, and H. S. J. Van Der Zan. "Mechanical Stiffening, Bistability, and Bit Operations in a Microcantilever." *Applied Physics Letters* 97.12 (2010): 193107.

[14] Kacem, N., J. Arcamone, F. Perez-Murano, and S. Hentz. "Dynamic Range Enhancement of Nonlinear Nanomechanical Resonant Cantilevers for Highly Sensitive NEMS Gas/mass Sensor Applications." *Journal of Micromechanics and Microengineering* 20.4 (2010): 045023.

[15] Dowell, E. "Damping in Beams and Plates Due to Slipping at the Support Boundaries." *Journal of Sound and Vibration* 105.2 (1986): 243-53.

[16] Villanueva, L. G., R. B. Karabalin, M. H. Matheny, D. Chi, J. E. Sader, and M. L. Roukes. "Nonlinearity in Nanomechanical Cantilevers." *Physical Review B* 87 (2013).

[17] Habtour, E., W. Connon, M. F. Pohland, S. C. Stanton, and M. Paulus. "Review of Response and Damage of Linear and Nonlinear Systems under Multiaxial Vibration." *Shock and Vibration*, vol. 2014, Article ID 294271, 2014-a. doi:10.1155/2014/294271.

[18] Zaitsev, S., A. K. Pandey, O. Shtempluck, and E. Buks. "Forced and Self-excited Oscillations of an Optomechanical Cavity." *Physical Review E* 84 (2011): 046605.

[19] Hamdan, M. N., and M. H. F. Dado. "Large Amplitude Free Vibrations Of A Uniform Cantilever Beam Carrying An Intermediate Lumped Mass And Rotary Inertia." *Journal of Sound and Vibration* 206.2 (1997): 151-168.

[20] Pai, P. F., and A. H. Nayfeh. "Non-linear Non-planar Oscillations of a Cantilever Beam under Lateral Base Excitations." *International Journal of Non-Linear Mechanics* 25.5 (1990): 455-474.

[21] Crespo Da Silva, M. R. M. and C. L. Zaretzky. "Nonlinear Flexural-Flexural-Torsional Interactions in Beams Including the Effect of Torsional Dynamics. I: Primary Resonance." *Nonlinear Dynamics* 5.1 (1994): 3-23.

[22] Balachandran, B., and E. B. Magrab. *Vibrations*. 2nd ed. Toronto, Canada: Cengage Learning, 2009.

[23] Glaz, B., Friedmann, P. P., and Liu, L., "Vibration Reduction and Performance Enhancement of Helicopter Rotors Using an Active/Passive Approach," AIAA Chapter 2008-2178, Proceedings of the 49thAIAA/ASME/ ASCHE/AHS/ASC Structures, Structural Dynamics & Materials Conference, Schaumburg, IL, April 2008.

[24] Lifshitz, R., M. C. Cross. “Nonlinear Dynamics of Nanomechanical and Micromechanical Resonators.” edited by: Schuster, H. G. *Reviews of Nonlinear Dynamics and Complexity.* Vol. I. Weinheim: Wiley-VCH, 2008.

[25] Lifshitz, R., E. Kenig, and M. C. Cross. "Collective Dynamics in Arrays of Coupled Nonlinear Resonators." edited by: Dykman, M. I. *Fluctuating Nonlinear Oscillators: From Nanomechanics to Quantum Superconducting Circuits*. Oxford: Oxford UP, 2012.

[26] Glaz, B., Friedmann, P. P., Liu, L., Kumar, D., and Cesnik, C. E. S., "The AVINOR Aeroelastic Simulation Code and its Application to Reduced Vibration Composite Rotor Blade Design," AIAA Chapter 2009-2601, Proceedings of the 50th AIAA/ASME/ASCHE/AHS/ASC Structures, Structural Dynamics & Materials Conference, Palm Springs, CA, May 2009.

[27] Jordan, D. W., and P. Smith. *Nonlinear Ordinary Differential Equations: An Introduction for Scientists and Engineers*. 4th ed. Oxford England: Oxford UP, 2007.

[28] Ismail, F., A. Ibrahim, and H.R. Martin. "Identification of Fatigue Cracks from Vibration Testing." *Journal of Sound and Vibration* 140.2 (1990): 305-17.

[29] Hollkamp, J. J., R. W. Gordon, and S. M. Spottswood. "Nonlinear Modal Models for Sonic Fatigue Response Prediction: A Comparison of Methods." *Journal of Sound and Vibration* 284.3-5 (2005): 1145-163.

[30] Chondros, T. G., A. D. Dimarogonas, and J. Yao. "Vibration Of A Beam With A Breathing Crack." *Journal of Sound and Vibration* 239.1 (2001): 57-67.

[31] Paulus, M., A. Dasgupta, and E. Habtour. "Life Estimation Model of a Cantilevered Beam Subjected to Complex Random Vibration." *Fatigue & Fracture of Engineering Materials & Structures* 35.11 (2012): 1058-70.

[32] Habtour, E., M. Paulus, and A. Dasgupta. "Modeling Approach for Predicting the Rate of Frequency Change of Notched Beam Exposed to Gaussian Random Excitation." *Shock and Vibration*, vol. 2014, Article ID 164039, 2014-b. doi: 10.1155/2014/164039.

[33] Shen, M. H., and Y. C. Chu. "Vibrations of Beams with a Fatigue Crack." *Computers &*

Structures 45.1 (1992): 79-93.

[34] Ruotolo, R., C. Surace, P. Crespo, and D. Storer. "Harmonic Analysis of the Vibrations of a Cantilevered Beam with a Closing Crack." *Computers & Structures* 61.6 (1996): 1057-074.

[35] Tsyfansky, S.l., and V.I. Beresnevich. "Non-Linear Vibration Method For Detection Of Fatigue Cracks In Aircraft Wings." *Journal of Sound and Vibration* 236.1 (2000): 49-60.

[36] Pugno, N., C. Surace, and R. Ruotolo. "Evaluation Of The Non-Linear Dynamic Response To Harmonic Excitation Of A Beam With Several Breathing Cracks." *Journal of Sound and Vibration* 235.5 (2000): 749-62.

[37] Saavedra, P. N., and L. A. Cuitino. "Crack Detection and Vibration Behavior of Cracked Beams." *Computers & Structures* 79.16 (2001): 1451-459.

[38] Loutridis, S., E. Douka, and L. J. Hadjileontiadis. "Forced Vibration Behaviour and Crack Detection of Cracked Beams Using Instantaneous Frequency." *NDT & E International* 38.5 (2005): 411-19.

[39] Ihn, J. B., and F. Chang. "Detection and Monitoring of Hidden Fatigue Crack Growth Using a Built-in Piezoelectric Sensor/actuator Network: I. Diagnostics." *Smart Materials and Structures* 13.3 (2004): 609-20.

[40] Ryles, M., F. H. Ngau, I. Mcdonald, and W. J. Staszewski. "Comparative Study of Nonlinear Acoustic and Lamb Wave Techniques for Fatigue Crack Detection in Metallic Structures." *Fatigue & Fracture of Engineering Materials & Structures* 31.8 (2008): 674-83.

[41] Priya S, Viehland D, Carazo A. High-power reso- nant measurements of piezoelectric materials: importance of elastic nonlinearities. Journal of Applied Physics 90.3 (2001): 1469–1479.

[42] Yu S, He S and Li W. Theoretical and experimental studies of beam bimorph piezoelectric

power harvesters. Journal of Mechanics and Materials of Structures 5.3 (2010): 427–445.

[43] Stanton, S. C., A. Erturk, B. P. Mann, E. H. Dowell, and D. J. Inman, "Nonlinear nonconservative behavior and modeling of piezoelectric energy harvesters including proof mass effects," *Journal of Intelligent Material Systems and Structures*, vol. 23, no. 2, pp. 183–199, 2012.

[44] Nayfeh, A. H., and P. F. Pai. *Linear and Nonlinear Structural Mechanics*. Hoboken, NJ: Wiley-Interscience, 2004.

[45] Zavodney, L. D., and A. H. Nayfeh. "The Non-linear Response of a Slender Beam Carrying a Lumped Mass to a Principal Parametric Excitation: Theory and Experiment." *International Journal of Non-Linear Mechanics* 24.2 (1989): 105-25.

[46] Malatkar, P., *Nonlinear Vibrations of Cantilever Beams and Plates, Ph.D. thesis*, Virginia Polytechnic Institute and State University, Blacksburg, Va, USA, 2003.

[47] Meirovitch, L. *Fundamentals of Vibrations*. Boston: McGraw-Hill, 2001.

[48] Hsiao, K.m., and R.t. Yang. "Effect Of Member Initial Curvature On A Flexible Mechanism Response." *Journal of Sound and Vibration* 190.2 (1996): 177-94.

[49] Oliver, W. C., and G. M. Pharr. "An improved technique for determining hardness and elastic modulus using load and displacement sensing indentation experiments." *Journal of Materials Research*, Vol. 7, No. 6 (1992): 1564-83.

[50] Taylor, M. D., K. S. Choi, X. Sun, D. K. Matlock, C. E. Packard, L. Xu, F. Barlat. "Correlations between nanoindentation hardness and macroscopic mechanical properties in DP980 steels." *Materials Science & Engineering A*. Vol. 597 (2014): 431-39.

[51] Saha, R., and W. D. Nix. "Effects of the substrate on the determination of thin film mechanical properties by nanoindentation." *Acta Materialia* 50 (2002): 23-38.

[52] Cole, D. P., H. A. Bruck, and A. L. Roytburd. “Nanoindentation studies of graded shape memory alloy thin films processed using diffusion modification.” *Journal of Applied Physics* 103 (2008): 064315.

[53] Cole, D. P., H. Jin, W. Lu, A. L. Roytburd, and H. A. Bruck. “Reversible nanoscale deformation in compositionally graded shape memory alloy films.” *Applied Physics Letters* 94 (2009): 193114.

[54] Gregory, J. R., and S. M. Spearing. “Nanoindentation of neat and *in situ* polymers in polymer-matrix composites.” *Composites Science and Technology 65.3-4* (2005): 595-607.

[55] Gershon, A. L., D. P. Cole, A. K. Kota, and H. A. Bruck. “Nanomechanical characterization of dispersion and its effects in nano-enhanced polymers and polymer composites.” *Journal of Materials Science* 45 (2010): 6353-6364.

[56] Cole, D. P. and K. S. Strawhecker. “An improved instrumented indentation technique for single microfibers.” *Journal of Materials Research* 29.9 (2014): 1104-1112.

[57] Cole, D. P., A. L. M. Reddy, M. G. Hahm, R. McCotter, A. H. C. Hart, R. Vajtai, P. M. Ajayan, S. P. Karna, and M. L. Bundy. “Electromechanical properties of polymer electrolyte-based stretchable supercapacitors.” *Advanced Energy Materials* 4 (2014): 1300844.

[58] Klesnil, M., and P. Lukáš. *Fatigue of Metallic Materials*. Amsterdam: Elsevier, 1992.

[59] Kang, S.K., Y-S. Jung, B-G. Yoo, J-I. Jang, and Y-K. Lee. "Orientation-dependent Indentation Modulus and Yielding in a High Mn Twinning-induced Plasticity Steel." *Materials Science and Engineering: A* 532 (2012): 500-04.

[60] Sangid, M. D. "The Physics of Fatigue Crack Initiation." *International Journal of Fatigue* 57 (2013): 58-72.

[61] Dowling, N. E., *Mechanical Behavior of Materials: Engineering Methods for Deformation,*

Fracture, and Fatigue, Prentice Hall, Upper Saddle River, NJ, USA, 2nd edition, 1999.

[62] Cartmell, M. *Introduction to Linear, Parametric, and Nonlinear Vibrations*. London: Chapman and Hall, 1990.

[63] Carrella, A., and D.J. Ewins. "Identifying and Quantifying Structural Nonlinearities in Engineering Applications from Measured Frequency Response Functions." *Mechanical Systems and Signal Processing* 25.3 (2011): 1011-027.

.

Chapter 5 Fatigue Damage Precursor Detection in Structures Vibrating under Nonlinear Harmonic Rotational Base Excitation

Under Review: International Journal of Mechanical Sciences, 2015

Chapter 5 is an article currently under review in the *International Journal of nonlinear Mechanics (IJNM)*, which provides a promising analytical approach to model and predict the response of cantilever beam exposed to a varying rotation base excitation. The model takes into account the evolution of the material due to damage accumulation. Authors are Mr. Ed Habtour, Dr. Daniel Cole, Dr. Samuel C. Stanton, Mr. Roman Sridharan and Professor Abhijit Dasgupta. Mr. Ed Habtour (first author) conducted the vibration experiments and developed the analytical model. He also conducted the SEM experiments. Dr. Daniel Cole conducted the nanoindentation measurements. Mr. Roman Sridharan provided assistance with the control software for the multiaxial vibration shaker. Dr. Samuel Stanton at the Army Research Office checked the derivations. Professor Dasgupta provided technical and academic guidance in this effort.

Abstract:

This chapter presents a nonlinear dynamic methodology for monitoring early precursors of fatigue damage in a slender metallic cantilever beam structure under time varying rotational base excitation. The methodology accounts for important dynamic nonlinearities due to the complex loading generated by rotational loading. These nonlinearities include: structural kinematic stiffening due to gyroscopic motion and high-response amplitude at the fundamental mode, structural softening due to inertial forces and gyroscopic loads, and due to localized microstructural material evolution due to cyclic fatigue degradation. The loading intensity and

number of vibration cycles intensify these nonlinearities. The change in the dynamic response due to fatigue damage accumulation is experimentally investigated by exciting a cantilever beam at variable rotational base motions. Nanoindentation studies near the beam clamped boundary are conducted to confirm gradual progression in the local mechanical properties, as a function of loading cycles, and microstructural studies are conducted to obtain qualitative preliminary insights into the microstructure evolution.

The observed fatigue evolution in the material microstructure at regions of large stresses (and the resulting progressive structural softening) is tracked by quantifying the growth in the tip response, the change in the natural frequency of the beam and the skewedness of the stepped-sine response curve. The systematic reduction in the measured apparent indentation stiffness near high stress concentration region confirmed the existence of localized fatigue damage accumulation. A nonlinear analytical model is presented to track the degradation in the structural stiffness as a function of the nonlinear dynamic response, by tracking the progressive reduction in the nonlinear part of the beam stiffness in the equation of motion.

5.1 Introduction

There are many engineering systems that experience varying rotational base excitations, such as flexible robotics components, heavy electronics components, and unmanned ground and aerial systems [1, 2]. Many of these systems may experience harsh dynamic loads during their life cycles [3, 4]. Mechanical structures under varying rotational base excitations may experience complex dynamic effects such as gyroscopic stiffening and softening, nonlinear geometric stiffening, and nonlinear inertial softening [1, 2]. Modeling and measuring the dynamic response can be complicated when the material properties evolve due to fatigue damage evolution. In this study we are interested in the growth of early precursors to such fatigue degradation. *Fatigue*

damage precursor is defined here as any observable early degradation of the material microstructural morphology and resulting changes in or the physical properties of a structure, prior to any detectable fatigue crack initiation. Examples of measurable precursors to fatigue crack development may involve, but are not restricted to, changes in the microstructure, chemical composition, electrical signal, acoustic response, thermal signature or mechanical response of a structure.

This study demonstrates that the nonlinear dynamic response to rotational vibration excitation can serve as a particularly sensitive precursor for fatigue degradation evolution. To facilitate this demonstration, this study provides an analytical nonlinear dynamic model that includes nonlinearities due to high amplitude response coupled with nonlinearities generated by harmonic rotational base excitation. The presented methodology shows that it is possible to capture fatigue damage precursor by tracking the nonlinear stiffness term in the equations of motion. The nonlinear equation of motion is updated accordingly to capture the local microstructural evolution by adjusting the nonlinear structural stiffness term. The global nonlinear vibration-based method uses the nonlinear structural updates from the experiments to estimate the beam tip response and number of fatigue cycles. Unlike linear dynamic model, the nonlinear stiffness term in the nonlinear dynamic model provided more useful sensitivity to the evolution in the material due to fatigue-induced damage.

Multiple studies have been devoted to nonlinear dynamics and vibrations of beams because of their importance in many engineering applications. One of the most cited studies in nonlinear dynamics is the effort presented by Hodges and Dowell [6], where they developed the equations of motion for a rotor blade–idealized as a beam–using Hamilton's principle. They maintained the cubic nonlinear terms and included the effect of warping. Partial-differential

equations for the motion of nonlinear inextensional and extensional beams were developed for planar and nonplanar base excitation, where the geometric and inertial nonlinearities were included [7-12].

Beam models were improved to idealize more complex structures such as antenna and radar structures and aircraft wings. Tip mass was utilized to enhance the dynamic performance of wind turbines and to modify the vibration frequency of components such as rotor blades. Modeling the above cases was achieved with cantilever beam, stepped beam, or L-shape beam models with tip mass under a base excitation [13-17].

Several researchers have investigated the dynamics of rotating linear and nonlinear flexible beams and flexible hub-beams (rotor-blades) with tip mass [18-20]. These dynamic models were developed in a consistent manner through the formulation of energy expressions and application of Hamilton's principle. The models included dynamic stiffening and inertial softening [21]. Hodges [22] developed nonlinear dynamic models for composite beams and blades exposed to base rotation excitation. Radially rotating uniform linear beams under constant and non-constant angular velocity has also been investigated [23-25]. However, most of the research performed in studying the vibrational behavior of radially rotating beams was focused on constant spin velocity with various combinations of free, clamped, and simply-supported boundaries [17, 20, 26].

What is absent in the structural dynamics and structural health monitoring literature is a comprehensive theoretical and experimental study of the nonlinear response of structures exposed to vibrational rotational base excitation that includes all of the following nonlinearities: 1) geometric stiffening, 2) inertial effect, 3) gyroscopic stiffening and softening, 4) higher order nonlinear gyroscopic stiffening, and 5) coupling between the rotational excitation (primary

motion) and local displacement (secondary motion). These five nonlinearities become important when modeling fast and flexible robot manipulators, robotic arms, and adaptive structures. High cycle vibrations in these structures may lead to fatigue, instability, and loss of position accuracy. The problem is exacerbated in structures where the system dynamic response progressively changes as the material continues to degrade due to accumulation of cyclic fatigue damage. Thus, monitoring structural health of the system is important in aiding the vibration control to correct the system's operations and prolong the life cycle.

In the current research study, we exploit the sensitivity of the nonlinear geometric stiffness to fatigue damage, by modifying the nonlinear stiffness terms in the equation of motion to account for degradation in the local stiffness at high-stress sites. This approach appears to be a promising metric for providing sensitive and robust structural health monitoring predictions of structures with fatigue damage precursor. The study shows nonlinear vibration-based measurement techniques that can sense the development of fatigue damage precursor prior to crack initiation. The fatigue-induced structural softening of the beam vibration response was evident even at excitation level where the deformations remained in the elastic domain. SEM observations reveal that the localized material microstructure is progressively evolves at high stress concentration regions, with accumulation of fatigue cycles. Nanoindentation measurements at the regions of high stress concentration reveal an accompanying reduction in the apparent stiffness (nanoindentation stiffness) of the material. This study demonstrates the effectiveness of nonlinear vibration response to identify fatigue damage precursors in slender structures through the application of global damage detection methods..

5.2 Model Development

The focus of this chapter is to examine the nonlinear vibration response of a slender

isotropic cantilever beam exposed to harmonic rotational base excitation near its fundamental frequency in order to observe the influence of fatigue cycles. As discussed later in this paper (in Section 5.3), the authors studied a cantilever beam with an aspect ratio of 8 (AR=length/width). The experimental results with forward stepped harmonic rotational vibration of the base demonstrated progressive structural softening. An analytical model is developed in this section, using nonlinear Euler-Bernoulli beam theory with a tunable nonlinear structural stiffness term to account for the observed changes in the global structural response due to possible local changes in the material 'stiffness' near the beam root (at the fixed end). In other words, the model uses a global structural parameter to capture the global structural softening response; due to local changes in the material microstructure. In addition, the model accounts for other nonlinear structural stiffening and structural softening phenomena due to large deformation as a function of the rotational vibration level, such as: the gyroscopic stiffening and softening effects, the inertial softening effects and the geometric stiffening effect.

5.2.1 Kinematics Development

Figure 5-1 illustrates the nonlinear dynamics of a cantilever beam with a uniform cross-section, carrying a tip mass exposed to a varying rotational base excitation. The beam is idealized to be inextensional; that is, stretching of the neutral axis is insignificant [27]. The beam is fixed rigidly at one end and free at the other end (Figure 5-1). Nonlinear Euler-Bernoulli theory is employed to estimate the beam tip displacement, where the effects of warping and transverse shear deformation are neglected [14].

At the large peak response amplitudes encountered in this study, the nonlinear terms in the equations of motion become as important as the linear ones. The beam length-to-width ratio is long enough to cause significant nonlinear flexural deformation but is short enough to assume

that the beam undergoes purely planar flexural vibrations as long as the tip mass and cross-section geometry are symmetric with respect to the beam's centerline [1]. The first flexural mode is approximated to be same as the mode shape generated from solving the linear problem with tip mass that contains the rotary inertia effect.

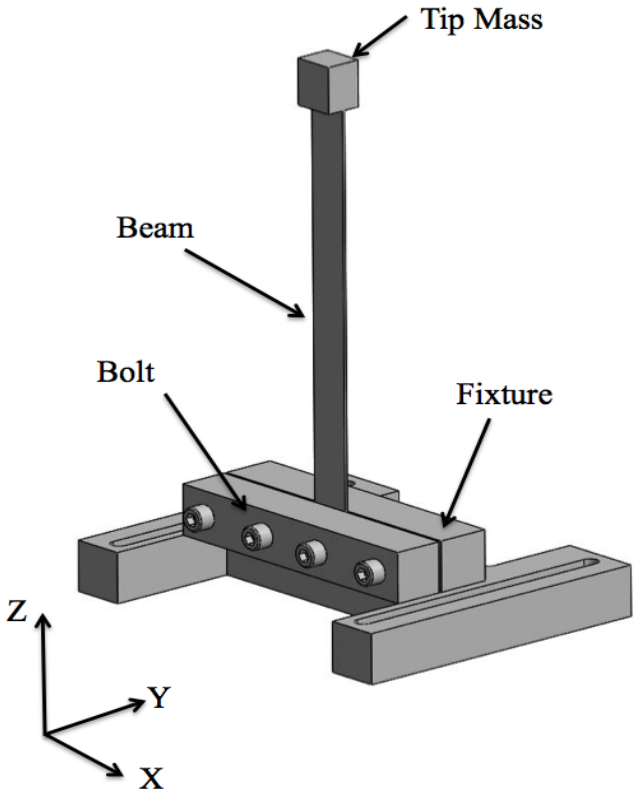

Figure 5-1. Slender beam with tip mass attached to a rigid fixture

The cantilever beam is considered to be a uniform and straight isotropic structure of length L and volumetric density ϱ, clamped at the base with tip mass M and rotary inertia J, as shown in Figure 5-2. The Z-axis is taken as the neutral axis associated with pure bending. It is assumed the loci of both shear centers and mass centers of the undeformed beam are coincident with the Z-axis. The base motion causes each cross section of the beam to experience an elastic displacement of its centroid. The dynamics of the beam with respect to Y and Z axes at the

undeformed length from the root of the beam to the reference point, *s,* and time, *t,* is described in terms of: the axial displacement $w(s,t)$, the transverse displacement $v(s,t)$ along the inertial coordinate system *YZ*, and the rotational angle ψ. The orthogonal unit vectors for the inertial coordinate system are (i_Y, i_Z). The local curvilinear coordinate system at *s*, in the deformed position, has the orthogonal unit vectors (i_η, i_ζ). The rotating reference frame approach is used, where the reference frame is attached to the undeformed position of the beam (at the base of the beam). The position vector of a point is expressed as follows:

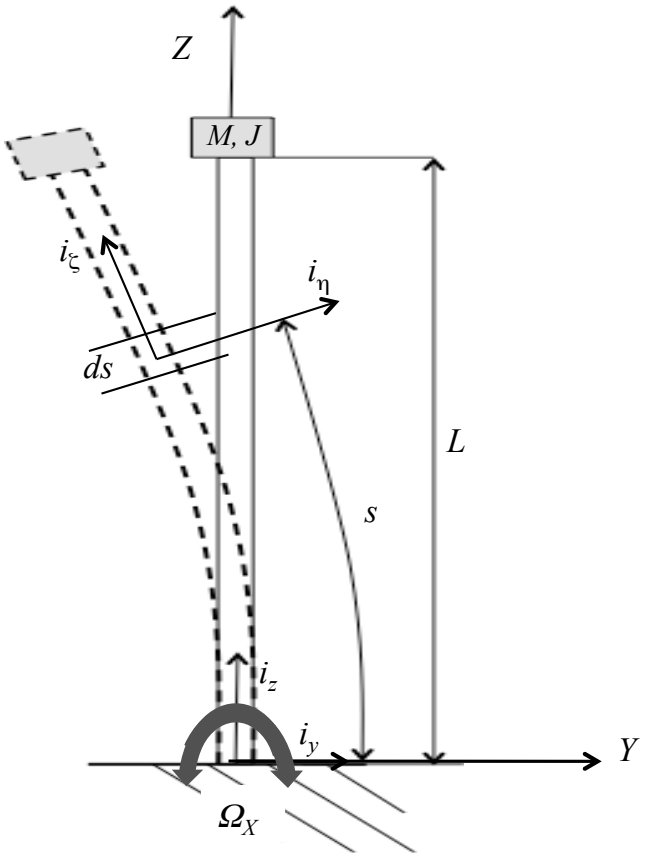

Figure 5-2. Slender beam with tip mass under rotation base excitation

$$\boldsymbol{R} = v\boldsymbol{i_Y} + (s + w)\boldsymbol{i_Z} + \eta\boldsymbol{i}_\eta \qquad \text{Eq. 5-1}$$

The variable s denotes the arc-length along $\boldsymbol{R}$, and the local deformation is ηi_η. Differentiating $\boldsymbol{R}$ with respect to t:

$$\dot{\boldsymbol{R}} = \left(\dot{v} - \eta\dot{\psi}sin(\psi)\right)\boldsymbol{i}_Y + \left(\dot{w} + \eta\dot{\psi}\cos\psi\right)\boldsymbol{i_Z} + \boldsymbol{\Omega_{Base}}\times\boldsymbol{R} \qquad \text{Eq. 5-2}$$

where:

$$\boldsymbol{\Omega_{Base}} = \Omega_x(t)\boldsymbol{i_x}$$

The tracking frame primary motion is $\Omega_x(t)$. Since the reference frame is selected *a priori*, $\Omega_x(t)$ becomes a known quantity, instead of a variable [28]. Substituting $\boldsymbol{\Omega_{Base}}\times\boldsymbol{R}$ and combining terms yields the following:

$$\begin{aligned}\dot{\boldsymbol{R}} = &\left(\dot{v} - \eta\dot{\psi}sin(\psi) - s\Omega_X - w\Omega_X - \eta\Omega_X sin(\psi)\right)\boldsymbol{i}_Y \\ &+ \left(\dot{w} + \eta\dot{\psi}\cos\psi + v\Omega_X + \eta\Omega_X cos(\psi)\right)\boldsymbol{i_Z}\end{aligned} \qquad \text{Eq. 5-3}$$

5.2.2 Equation of Motion Development

Kinetic energy can be expressed as follows:

$$T = \frac{1}{2}\int_0^L \int_{A_1}^{A_2} \varrho\, \dot{\boldsymbol{R}}\cdot\dot{\boldsymbol{R}}\, dAds + \frac{1}{2}M\left(\dot{\boldsymbol{R}}\cdot\dot{\boldsymbol{R}}\right)\Big|_{s=L} \qquad \text{Eq. 5-4}$$

Substituting $\dot{\boldsymbol{R}}$ into the kinetic energy expression and set:

$$\rho = \int_{A_1}^{A_2} \varrho\, dA\, J_1 = \int_{A_1}^{A_2} \varrho\, \eta dA\, J_2 = \int_{A_1}^{A_2} \varrho\, \eta^2 dA$$

Since the reference point coincides with the mass centroid and η is a principal axis of the differential beam element, J_1 is set equal to zero. However, the beam rotary inertia is maintained in the kinetic energy. Therefore,

$$T = \frac{1}{2}\int_0^L \Big[\rho(\dot{v}^2 + \dot{w}^2 + v^2\Omega_X^2 + (w+s)^2\Omega_X^2 - 2(s+w)\dot{v}\Omega_X + 2v\dot{w}\Omega_X) + J_2\big(\Omega_X + \dot{\psi}\big)^2\Big]ds + \frac{1}{2}M[\dot{v}^2 + \dot{w}^2 + v^2\Omega_X^2 + (w+s)^2\Omega_X^2 - 2(s+w)\dot{v}\Omega_X + 2v\dot{w}\Omega_X]\Big|_{s=L} + \frac{1}{2}J\big(\Omega_X + \dot{\psi}\big)^2\Big|_{s=L} \quad \text{Eq. 5-5}$$

Performing Taylor's expansion up to cubic nonlinearities and assuming that w and v are small but finite, the potential energy and the kinetic energy can be expressed as follows [11]:

$$\Pi = \frac{EI}{2}\int_0^L (v''^2 + v''^2 v'^2)ds - \frac{1}{2}\rho g\int_0^L (L-s)v'^2 ds - \frac{1}{2}Mg\int_0^L v'^2 ds \quad \text{Eq. 5-6}$$

$$T = \frac{1}{2}\int_0^L \Bigg[\rho\Bigg(\dot{v}^2 + \frac{1}{4}\Bigg(\frac{\partial}{\partial t}\int_0^\zeta v'^2 ds\Bigg)^2 + v^2\Omega_X^2 + \Bigg(-\frac{1}{4}\Bigg(\int_0^\zeta v'^2 ds\Bigg)^2 + s\int_0^\zeta v'^2 ds + s^2\Bigg)\Omega_X^2 - \Bigg(2s - \int_0^\zeta v'^2 ds\Bigg)\dot{v}\Omega_X - v\Omega_X\frac{\partial}{\partial t}\Bigg(\int_0^\zeta v'^2 ds\Bigg)\Bigg) + J_2(\Omega_X^2 + 2\Omega_X\dot{v}' + \Omega_X\dot{v}'v'^2 + \dot{v}'^2 + \dot{v}'^2 v'^2)\Bigg]ds + \frac{1}{2}M\Bigg(\dot{v}^2 + \frac{1}{4}\Bigg(\frac{\partial}{\partial t}\int_0^\zeta v'^2 ds\Bigg)^2\Bigg)\Bigg|_{s=L} + \frac{1}{2}J(\dot{v}'^2 + \dot{v}'^2 v'^2)\Big|_{s=L} \quad \text{Eq. 5-7}$$

where the dots and the primes denote the temporal and spatial derivatives, respectively.

The approximate solutions are assumed in series form, as follows:

$$v(t,z) = \sum_{j=1}^{N} q_j(t) Y_j(z) \qquad \text{Eq. 5-8}$$

where Y_j are known comparison functions from a complete orthogonal function set and denote the undamped linear mode shapes; while q_j denote the generalized modal coordinates [29]. For a single response mode, the assumed solution becomes:

$$v(t,z) = q(t)Y(z) \qquad \text{Eq. 5-9}$$

Eq. 5-9 is substituted into the kinetic energy and potential energy equations. The Euler-Lagrangian equation is then applied to the Lagrangian, $L = T - \Pi$ as follows:

$$\frac{\partial}{\partial t}\left(\frac{\partial L}{\partial \dot{q}}\right) - \frac{\partial L}{\partial q} = 0$$

The equation of motion with the appropriate nonlinear terms for the system understudy is:

$$a_1\ddot{q} + a_2(q^2\ddot{q} + q\dot{q}^2) + a_3\dot{\Omega}_X q^2 + (k_1 - h_1\Omega_X^2)q + (k_2 - h_2\Omega_X^2)q^3 = a_4\dot{\Omega}_X \qquad \text{Eq. 5-10}$$

Adding a viscous damping term to the equation of motion leads to the final form of the governing equation for a cantilever beam with varying rotational base excitation:

$$a_1\ddot{q} + a_2(q^2\ddot{q} + q\dot{q}^2) + c\dot{q} + a_3\dot{\Omega}_X q^2 + (k_1 - h_1\Omega_X^2)q + (k_2 - h_2\Omega_X^2)q^3 = a_4\dot{\Omega}_X \qquad \text{Eq. 5-11}$$

The inertial coefficient including the rotary inertia (or effective mass) is:

$$a_1 = \rho\int_0^L Y^2 ds + J_2\int_0^L Y'^2 ds + MY^2|_{s=L} + JY'^2|_{s=L}$$

The nonlinear inertial coefficient including tip rotary inertia is:

$$a_2 = \rho \int_0^L \left(\int_0^\zeta Y'^2 ds \right)^2 ds + J_2 \int_0^L Y'^4 ds + M \left(\int_0^\zeta Y'^2 ds \right)^2 \Big|_{s=L} + JY'^4|_{s=L}$$

$$a_3 = \frac{1}{2}\left(-\rho \int_0^L Y \int_0^\zeta Y'^2 ds\, ds + J_2 \int_0^L Y'^3 ds - MY \int_0^\zeta Y'^2 ds \Big|_{s=L} + JY'^3 \big|_{s=L} \right)$$

The linear stiffness coefficient is:

$$k_1 = EI \int_0^L Y''^2 ds - \rho g \left(\int_0^L (L-s) Y'^2 ds \right) - Mg \left(\int_0^L Y'^2 ds \right) \Big|_{s=L}$$

The gyroscopic stiffening and softening coefficient is [26, 28]:

$$h_1 = \rho \int_0^L Y^2 ds - \frac{1}{2}\rho \int_0^L (L^2 - s^2) Y'^2 ds + MY^2|_{s=L} - \frac{1}{2} M (L^2 - s^2) Y'^2|_{s=L}$$

The nonlinear geometric stiffness coefficient:

$$k_2 = 2EI \int_0^L Y''^2 Y'^2 ds$$

The nonlinear gyroscopic stiffness coefficient:

$$h_2 = \frac{1}{2}\left[\rho \int_0^L \left(\int_0^\zeta Y'^2 ds \right)^2 ds + M \left(\int_0^\zeta Y'^2 ds \right)^2 \Big|_{s=L} \right]$$

The base excitation inertial coefficient is:

$$a_4 = \rho \int_0^L sY ds - J_2 \int_0^L Y' ds + MLY|_{s=L} - JY'|_{s=L}$$

If the rotational base motion is dropped, we recover the classical free vibration nonlinear equation of motion with the nonlinear inertial effect (terms two and three) and the nonlinear geometric stiffness [30]:

$$a_1\ddot{q} + a_2(q^2\ddot{q} + q\dot{q}^2) + k_1 q + k_2 q^3 = 0$$

As seen above, the rotational motion introduces additional nonlinearities and coupling between base motion and local motion. Accordingly, coefficients h_1 and h_2 are included in the equation of motion. The contribution of positive terms in h_1 increases the gyroscopic stiffness while the negative terms augment the gyroscopic softening. The equation of motion produced in this study is an expansion of the model provided by Smith and Baruh [26], which did not include the nonlinear geometric stiffness and nonlinear inertial terms:

$$a_1\ddot{q} + (k_1 - h_1\Omega_X^2)q = a_4\dot{\Omega}_X$$

For flexible structures such as compliant robotic arms and legs, the nonlinear inertial and geometric stiffness effects become important. Furthermore, high displacement vibratory load may intensify the structural softening effect due to localized fatigue damage precursor at high-stress concentration sites. This structural softening effect due to fatigue can be globally accounted for by introducing the nonlinear structural adjustment factor, which is discussed in the following section. The contribution of the rotational motion is also included in the nonlinear stiffness calculation (coefficient h_2).

5.3 Experimental Approach

5.3.1 Test Specimen

The slender Blue-finished and polished spring-tempered AISI 1095 high carbon steel cantilever beams were used in this study. This type of steel is typically fabricated using cold rolling, which may produce some level of material orthotropy. Accordingly, the isotropy assumption is an approximation in this study. The density and the elastic modulus of the material are 7.85 g/cm^3 and 205 GPa, respectively. The hardness is Rockwell C48 with AR= 8. The beam

length and cross-section area are 127 mm and 15.88x1.08 mm^2, respectively.

5.3.2 Test Setup

To produce varying rotational base excitations, it was necessary to utilize a multiaxial electrodynamic shaker. The multiaxial shaker was used in this study; it consists of eight plane actuators and four out-of-plane actuators underneath the shaker table (Figure 5-3), which are mechanically coupled to the table. This architecture allows the shaker to produce a true six degrees-of-freedom (DoF) vibration environment (three translations and three rotations). The four out-of-plane actuators underneath the shaker table are employed to drive the base rotation about the x-axis. The other eight actuators are used to ensure a pure rotational excitation by reducing potential noise and misalignments. For additional details related to the multiaxial shaker, refer to Ernst et al. [2].

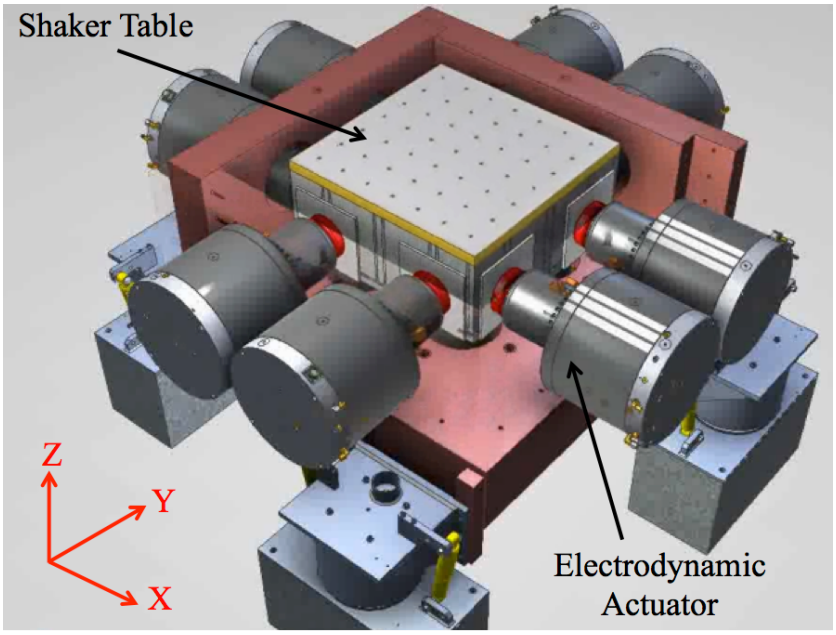

Figure 5-3. Multiaxial shaker (Team Corporation)

The vibration experiment setup and instrumentation are shown in Figure 5-4. Each beam

was mounted vertically on a rigid fixture and its bolts were torqued to 22.6 N-m. The system was then attached to multiaxial shaker table controlled by four triaxial accelerometers. Each corner on the shaker table was assigned one accelerometer. Two additional accelerometers were mounted on the fixture as shown in Figure 5-4; these two accelerometers were used as a backup to ensure that the base excitation was purely rotational. The beam tip displacement was measured using two accelerometers, which were mounted on each side of the beam. The mass of each accelerometer was approximately 1.5g.

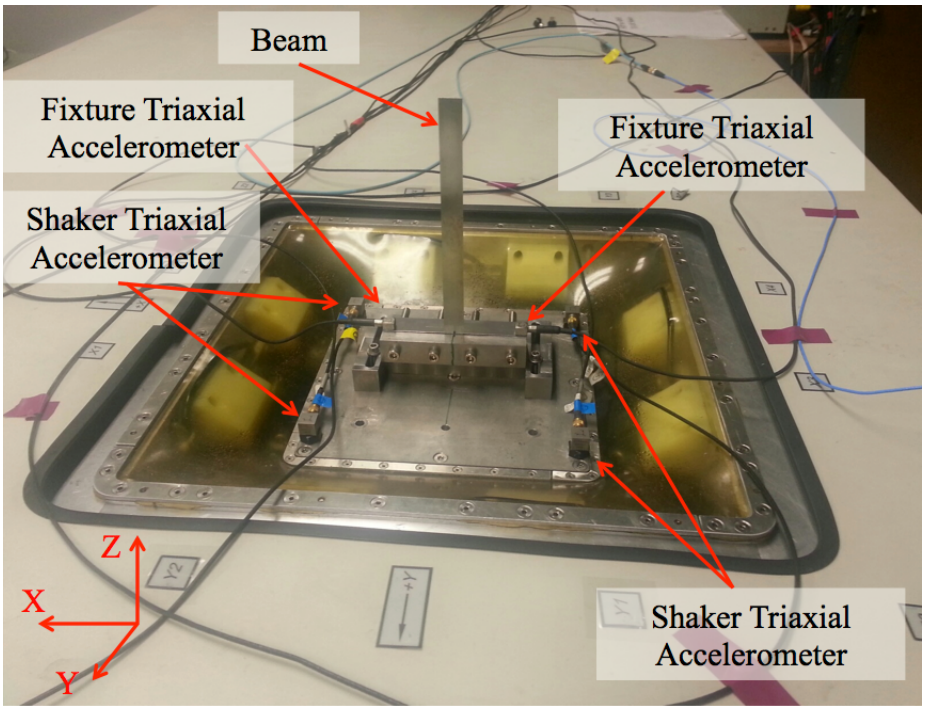

Figure 5-4. Experimental setup for vibration test

Three sets of experiments (Cases I, II, and III) were conducted. The details of each case are listed in Table 5-1. The beam in each case was exposed to a constant amplitude rotational harmonic base excitation. The loading cycles depended on the shift in the resonance frequency due to material softening, meaning the tests were repeated until significant change in the resonance was observed. Furthermore, the continual move in the resonance made it challenging

to control the loading cycles. Once the linear fundamental frequency for each beam was identified using sine-sweep excitation, the beams were exposed to the rotational harmonic base excitation at discrete forward dwell frequencies near the fundamental frequencies. The ramp-up time and dwell time for each frequency were 30s and 25s, respectively. The ramp-up time and dwell time at each excitation frequency ensured that steady state response conditions were met. The frequency step for each dwell was 0.05Hz. Therefore, the excitation frequency was increased 0.05Hz every 55s (30s ramp-up plus 25s dwell).

Table 5-1. Nonlinear experimental cases

Case			**Test**	**Total Cycles (10^3)**
I	Base Excitation (rad/s^2)	30	1	0-67
			2	67-135
	Linear Resonance (Hz)	42.35	3	135-202
			4	202-269
	Max. Strain (10^{-3})	0.3		
II	Base Excitation (rad/s^2)	50	1	0-81
	Linear Resonance (Hz)	42.35	2	81-151
	Max. Strain (10^{-3})	0.4	3	151-220
			4	220-290
			5	290-359
III	Base Excitation (rad/s^2)	70	1	0-81
	Linear Resonance (Hz)	42.33	2	81-151
			3	151-224

	Max. Strain (10^{-3})	0.8	4	224-294

Instrumented nanoindentation is a method used for examining local mechanical properties of materials [31]. The technique has been frequently used to characterize a wide range of complex materials and structures, including film-substrate systems [32], functionally graded structures [33-35], single microfibers [36], and polymer nanocomposites [37-38]. In the current study, local mechanical properties of similarly-fatigued beams were probed via instrumented nanoindentation. Samples were polished to 0.1 μm and indentation experiments were performed using a diamond Berkovich tip (radius of curvature approximately 100 nm). Positions along the beam surface were located using the optical microscope in the indenter machine. For each targeted location, 25 indentations were performed in a 5×5 grid, spaced 5 μm apart. The edge of the initial indent array was positioned approximately 10 μm from the clamped portion of the beam; subsequent arrays were positioned in approximately 2 mm increments, stepping away from the fixed boundary position and moving toward the beam-free end. Measurements were performed in load control mode, with a maximum applied force, P, of approximately 5000 μN. The applied forces resulted in indentation depths of approximately 150–200 nm (approximately 1-2% of the cross-sectional depth). A drift correction was performed prior to indentation using a preload of 1 μN for 20s. A triangular force profile was used with a quasi-static loading rate of 625 μN s^{-1}.

5.4 Results and Discussion

The results of the dynamic model showed good agreement with the experimental results due to the utilization of nonlinearities in the equation of motion. The sensitivity of the nonlinear

geometric stiffness to fatigue damage precursor is discussed as well. This section also illustrates the link between micromechanics and global nonlinear dynamics, which is a powerful approach for detecting fatigue damage precursors.

5.4.1 Experimental Results of Nonlinear Vibration Tests

Each experimental set (Cases I, II, and III) contained four to five step-dwell tests (Table 5-1; Figure 5-5 and

Figure 5-7). The objective of conducting multiple tests for each case was to capture the shift in the fundamental frequency and the increase in the response amplitude due to repeated dwells, which are symptomatic of localized material softening. Figure 5-5 to

Figure 5-7 show that the resonance frequency continued to drop every time the test was repeated due to ongoing accumulation of fatigue damage. The nonlinear softening effect on the resonance frequency was apparent in the increase in the beam tip response amplitude, as shown in Figure 5-5, 5-6 and 6-7. The frequency-response curves were skewed to the left, indicating a softening nonlinearity due to material change that eventually surpassed the structural nonlinear geometric stiffening. It can be said for all cases that the accumulation of loading cycles led to continuing fatigue damage accumulation, resulting in a corresponding increase in the maximum beam tip deflection reduction in the local stiffness, with the reduction magnitude being proportional to the stress level.

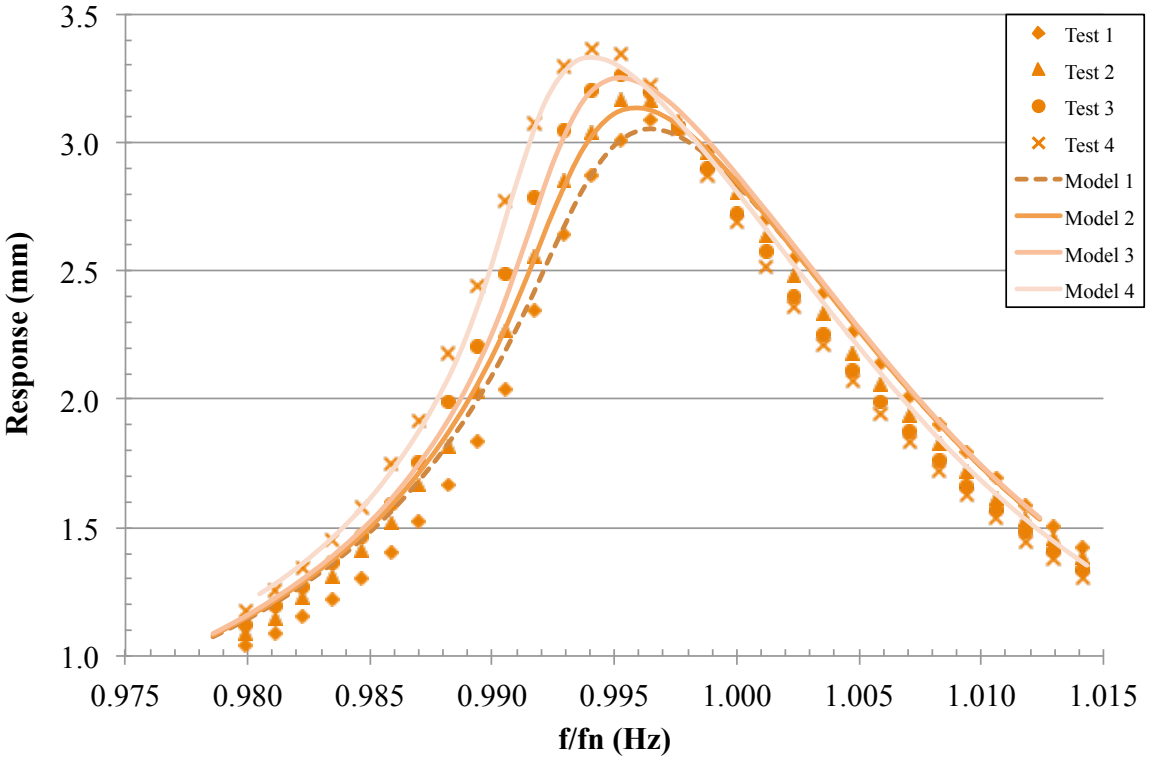

Figure 5-5. Experimental and analytical nonlinear softening response for Case I

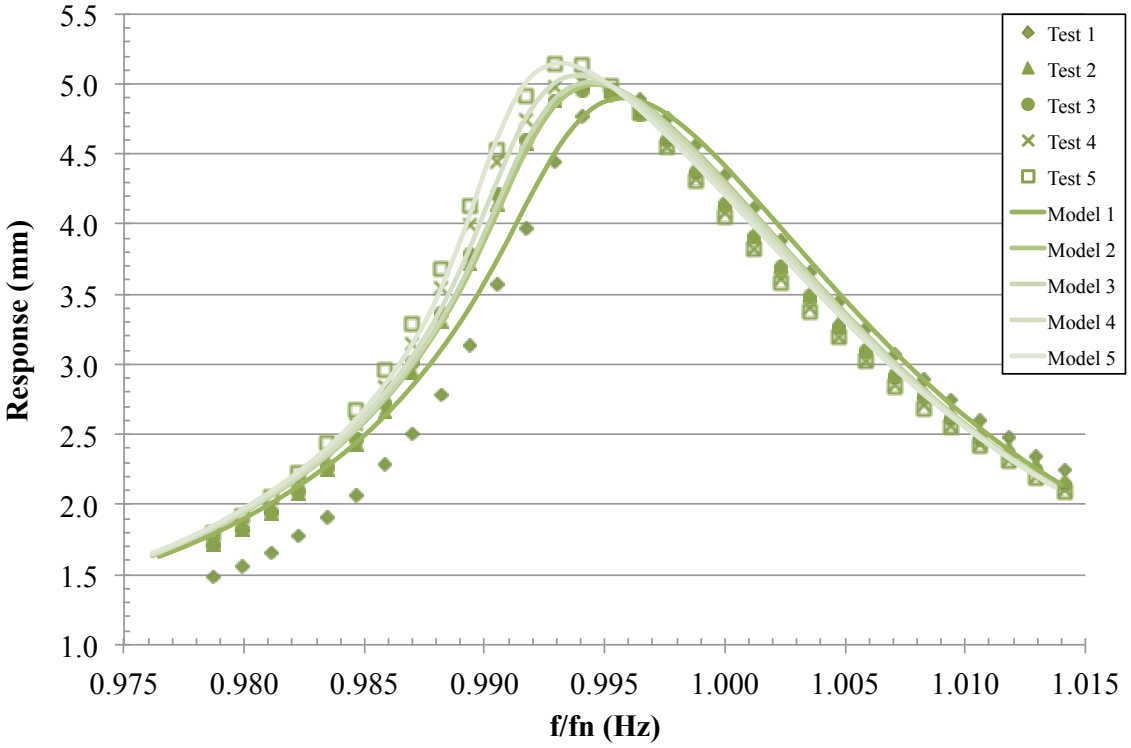

Figure 5-6. Experimental and analytical nonlinear softening response for Case II

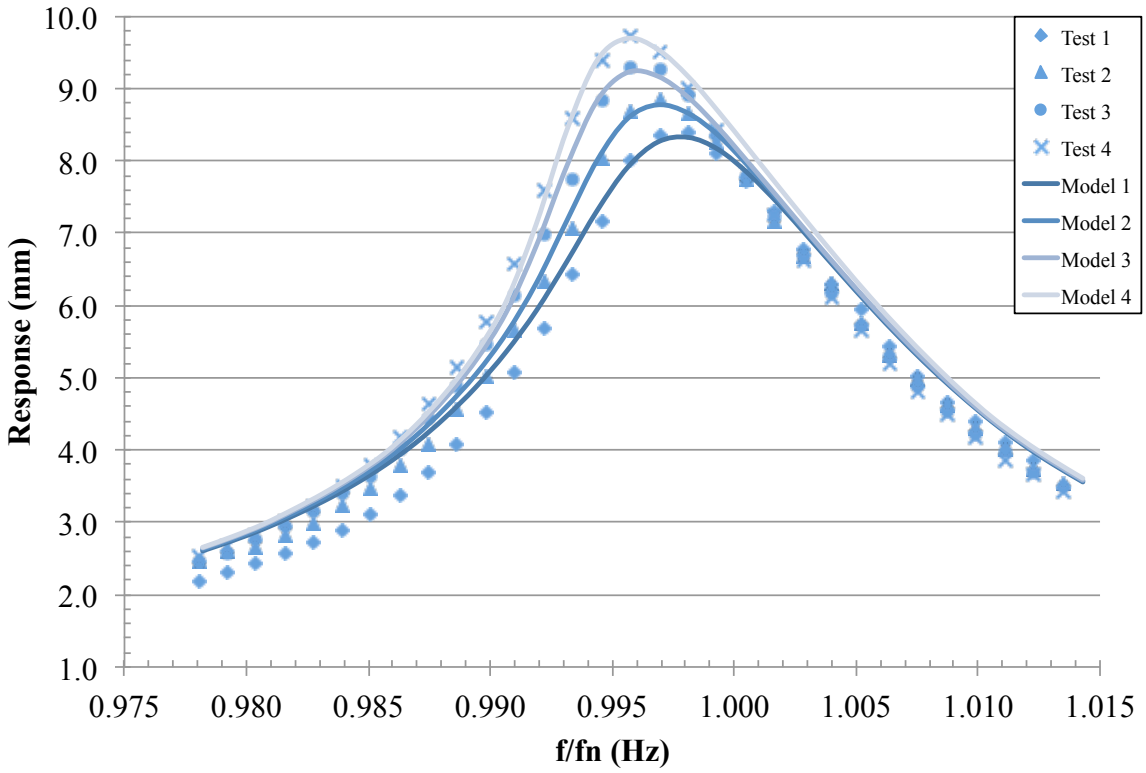

Figure 5-7. Experimental and analytical nonlinear softening response for Case III

Malatkar [11] encountered similar softening phenomena in a cantilever beam exposed to transverse nonlinear base excitations. Malatkar avoided fatigue damage due to high amplitude loading by reducing the number of dwells and repeating each experiment only twice. The authors' observation of the softening behavior at the fundamental mode is similar to the softening response seen in harvester piezoceramics investigations [39-41]; however, these studies did not explain the cause of the softening. Stanton et al. [42] assumed that the nonlinear softening was due to material nonlinearities in their piezoceramic device. Softening trends were also witnessed by Saavedra and Cuitino in their study on a cracked mild steel beam exposed to harmonic vibratory loads [43]. Villanueva et al. encountered the softening response for the first mode of a nano-cantilever beam, where they assumed residual stresses due to the fabrication process as a possible instigator [44].

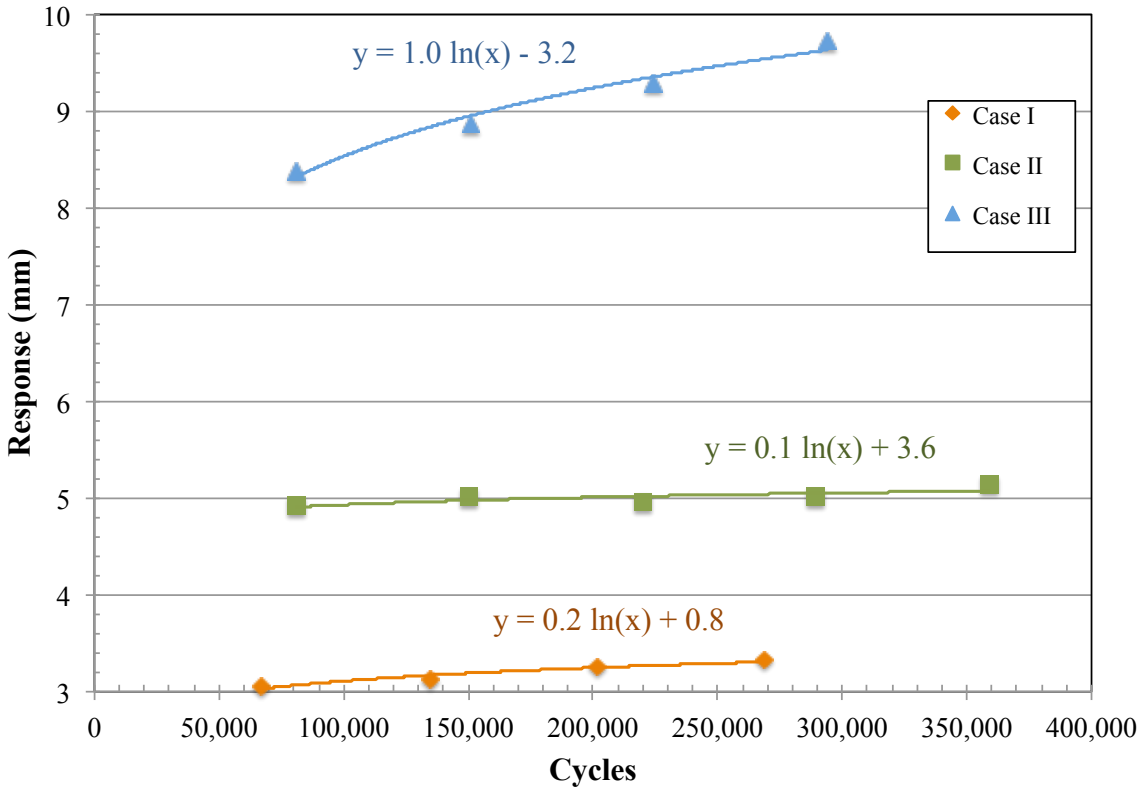

Figure 5-8. Maximum tip displacement response for each test, as a function of number of fatigue cycles

To verify the potential damage accumulation in the current study, nano-indentation tests were performed on a similarly-fatigued beam near the fixed boundary, which was an area of relatively high stress. The local elastic modulus of a sample exposed to approximately 150,000 cycles was compared to an unfatigued control sample. Figure 5-9 displays the results of the indentation experiments. The location x=0 indicates the clamped edge during cantilever base excitation, which was the expected position of maximum stress. The apparent indentation stiffness, as measured by the unloading curve of the nano-indentation test, is shown as a function of x. The horizontal dotted line in Figure 5-9 shows the average value of the indentation stiffness for the unfatigued sample (0 cycle). Indentation results for the fatigued specimen showed a clear reduction in the local apparent elastic modulus near the clamped position of the beam. The defined zero position, which includes tests as close as 10 μm from the fixed boundary location,

showed an average indentation stiffness of approximately 120 GPa for the fatigued sample. Stepping away from the clamped position, the average apparent stiffness eventually approached 183 GPa. The results suggest that the first few hundred nanometers of the sample surface were becoming apparently more compliant as a result of the high number of tension-compression cycles. The average indentation stiffness of an unfatigued (control) sample obtained from the nanoindentation measurement was approximately 225 GPa (Figure 5-9).

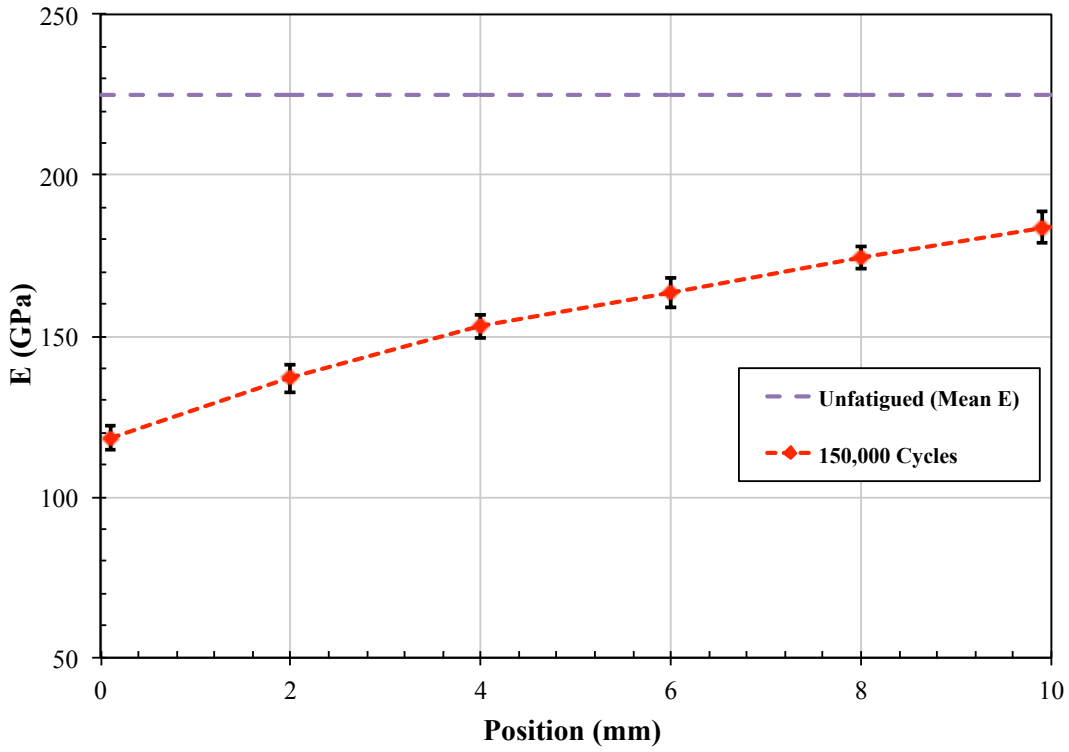

Figure 5-9. Local mechanical characterization of fatigued beams as determined by nano-indentation

To further investigate the local change in the beam material, and in the associated stiffness, the microstructure of the material near the root of the beam of a similarly-fatigued test specimen was examined via Scanning Electron Microscopy (SEM). Figure 5-10A shows the microstructure of an unfatigued control sample, while Figure 5-10B shows the microstructure of the fatigued beam. For the fatigued sample, the area investigated was within 100 μm of the

clamped position of the beam. The control sample showed a uniform microstructure throughout, while the surface of the fatigued beam near the fixed boundary displayed a relatively high density of long dark slender elliptical regions. The concentration of these long dark ellipses decreased with respect to distance from the beam clamped boundary. According to the literature, microstructural variation near these highly stressed regions could be due to localized dislocation motion resulting in the formation of persistent slip bands (PSBs) [45-50]. Dislocation motion is the primary mechanism of plastic deformation in metals and has been shown to result in slip within the grains in similar polycrystalline materials [46-47]. The PSB band is often believed to be a preferential precursor mechanism under strain cycling, accompanied by extrusion and intrusion regions [48]. The formation of the extrusion or intrusion regions is due to the dislocation motion under cyclical loading (compression-tension), which intensifies micro-plastic deformation.

The indentation tests cannot fully describe variations in the dynamic behavior of the beam, but are an important first step in elucidating how cyclic fatigue damage accumulation may affect surface microstructure and thus local mechanical properties in areas of high stress concentrations. It is important to point out that the approximate maximum strain near the root is $0.8x10^{-3}$ strain, which is still in the linear region of the stress-strain curve for 1095 steel. The combination of (1) the increase in the nonlinear response of the beam and (2) the change in localized apparent material stiffness through instrumented indentation is able to identify early strain localization through potential PSB formation, which is a known precursor to crack formation [48-50].

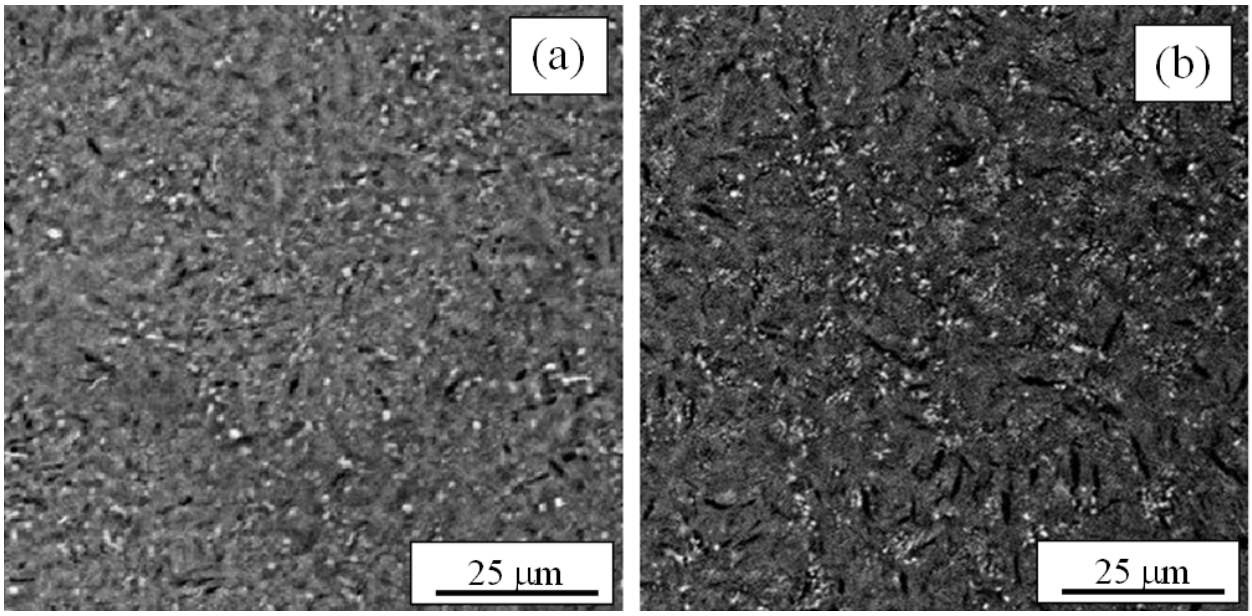

Figure 5-10 Microstructure of (a) unfatigued control sample with uniform microstructure and (b) fatigued specimen near clamped position (high density of long dark ellipses)

5.4.2 Model Results

The dynamic base excitations in Case I, II, and III produced nonlinear responses, which led to localized damage caused by local evolution in the material micromechanical properties near the clamped boundary. The application of linear dynamic theory does not account for the structural degradation, thus, it limits the accuracy of the dynamic response and the structural health. Attempts were made to tune the linear stiffness term in the equation of motion to track the fatigue degradation; however, minute modifications to the linear stiffness term caused drastically unrealistic shifts in resonance frequency. Thus, nonlinear dynamics analysis was implemented where the nonlinear geometric stiffness was modified to account for the fatigue-induced material evolution near the fixed end. This modification to the nonlinear stiffness provided a better curve fit to the experimental results. Consequently, the nonlinear dynamics analytical approach was implemented and modified to incorporate the material evolution near the clamped end. The

nonlinear equation of motion was solved numerically using the Runge-Kutta method, where the integration time step was 10^{-4}s. The integration time limits were set from 0s to 30s to ensure that steady state condition was reached. The accelerometer mass was included in the model, but its contribution was relatively minute.

It is clear that cyclic fatigue played an important role in altering the results. Damage accumulated near the beam root due to ramp-up and dwell cycles, causing the beam to soften locally (hence the reduction in resonant frequency and increase the beam tip response amplitude). The maximum response amplitudes in Figure 5-5 through

Figure 5-7 for Cases I, II, and III (base excitations: 30, 50, and 70 rad/s^2, respectively) are plotted as a function of loading cycles in Figure 5-8. The number of loading cycles for each case is reported in Table 5-1. The beam tip maximum response amplitudes increased as a result of increasing the excitation amplitudes; however, for each excitation level, the maximum response amplitudes increased logarithmically as a function of the loading cycles (Figure 5-8) due to the structural softening caused by the cyclic fatigue damage accumulation.

The structural softening response in the beam, observed in the nonlinear dynamic experiments as a damage-precursor for cyclic fatigue damage, is captured in the analytic model by adjusting the nonlinear geometric stiffness term, k^* in the structural equation of motion (Eq. 5-12). The governing equation was modified as follows:

$$a_1\ddot{q} + a_2(q^2\ddot{q} + q\dot{q}^2) + c\dot{q} + a_3\dot{\Omega}_X q^2 + (k_1 - h_1\Omega_X^2)q + (k^* - h_2\Omega_X^2)q^3 = a_4\dot{\Omega}_X \quad \text{Eq. 5-12}$$

where, parameter k^* was modified as follows:

$$k^* = \delta k_2$$

where the modified nonlinear stiffness, k^*, is the geometric stiffness, k_2, multiplied by the nonlinear adjustment factor, δ. The model results for the response amplitude superimposed on top of the experimental data in Figure 5-5-7 illustrate that calibrating the geometric stiffness term in the model can provide reasonable agreement between the experiment and model results. The nonlinear adjustment factor for each run is plotted as a function of the total number of cycles in Figure 5-11, Figure 5-13, and Figure 5-15. The experimental and numerical results show that the nonlinear adjustment factor logarithmically declines as the number of loading cycles increases. Furthermore, the adjustment factor has a negative sign, which is an indication of structural softening due to fatigue, even though the stresses in the beams were still in the elastic region. The logarithmic decay in the structural stiffness was consistent with fatigue behavior [51].

For completeness, the damping ratio was plotted as a function of fatigue cycles as shown in Figure 5-11, Figure 5-13, and Figure 5-15. It can be seen that the beams displayed slight logarithmic decay in damping as a function of cycles. The beams may exhibit nonlinear damping behavior, which is beyond the scope of this chapter and is worthy of further future investigation. Nonetheless, δ had significantly more influence on the nonlinear geometric stiffness term than on the damping term.

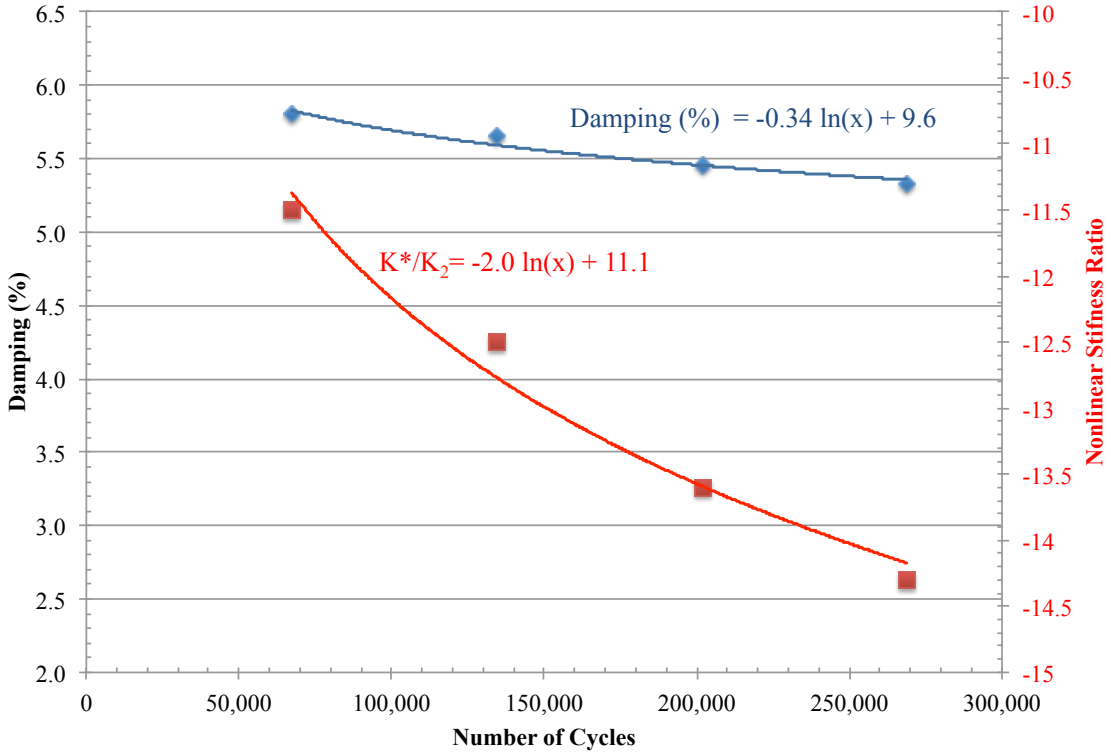

Figure 5-11. Case I: Nonlinear stiffness and damping changes due to fatigue cycles

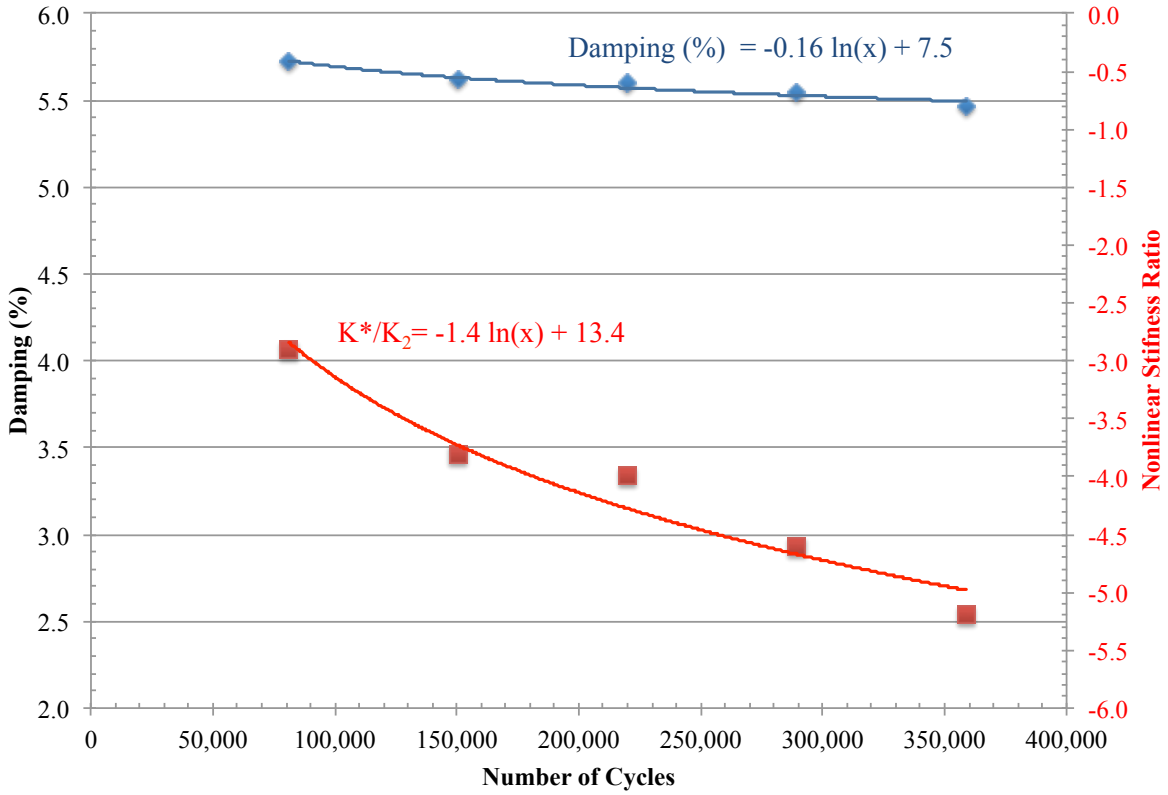

Figure 5-12. Case II: Nonlinear stiffness and damping changes due to fatigue cycles

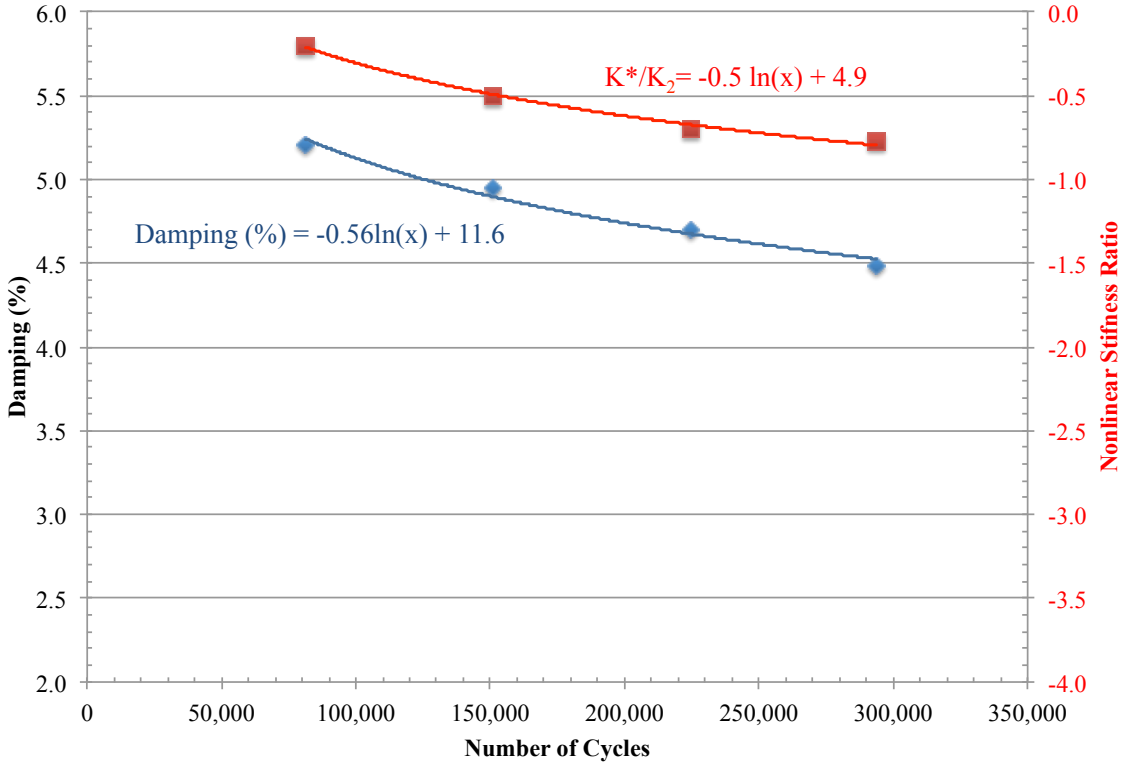

Figure 5-13. Case III: Nonlinear stiffness and damping changes due to fatigue cycles

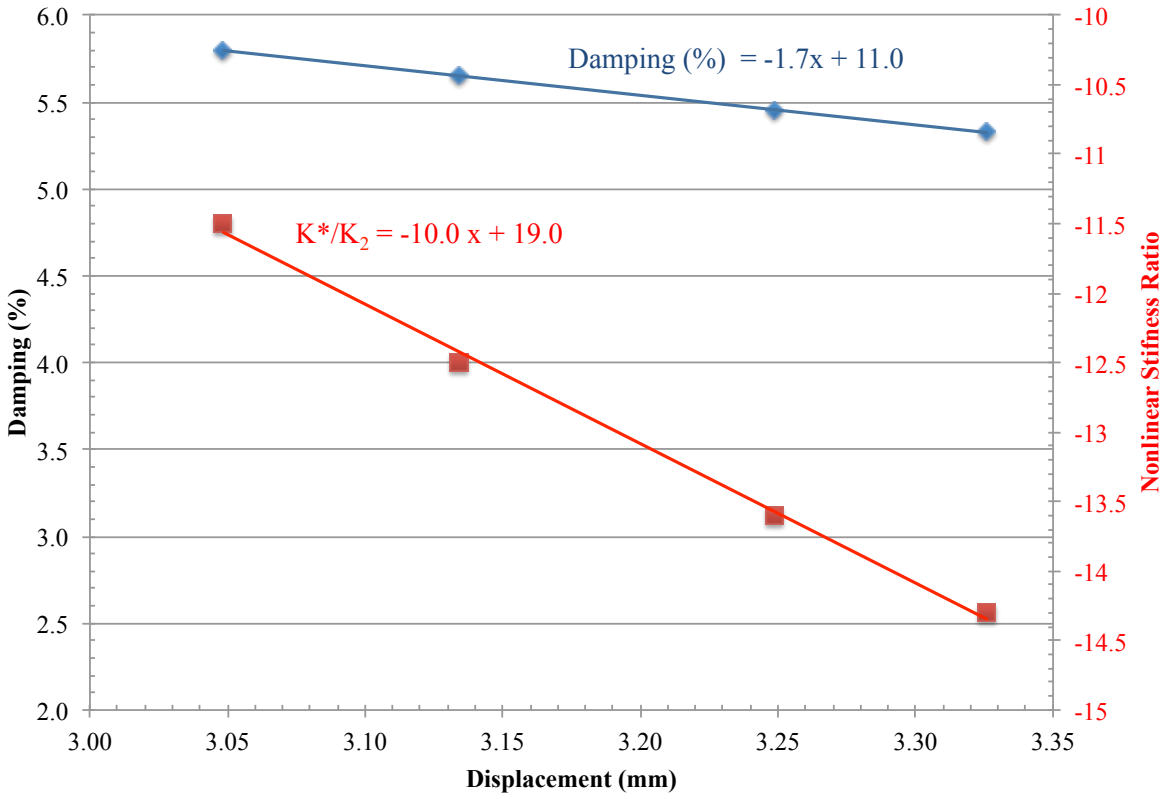

Figure 5-14. Case I: Nonlinear stiffness and damping changes as a function of displacement

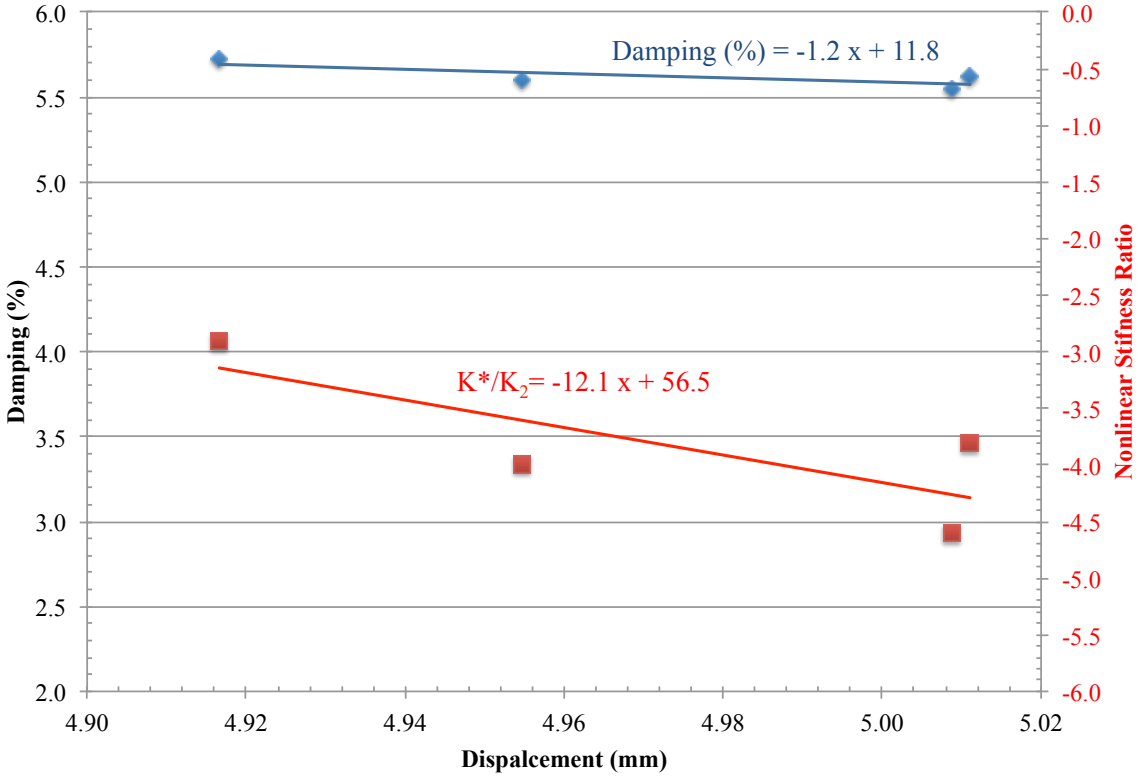

Figure 5-15. Case II: nonlinear stiffness and damping changes as a function of displacement

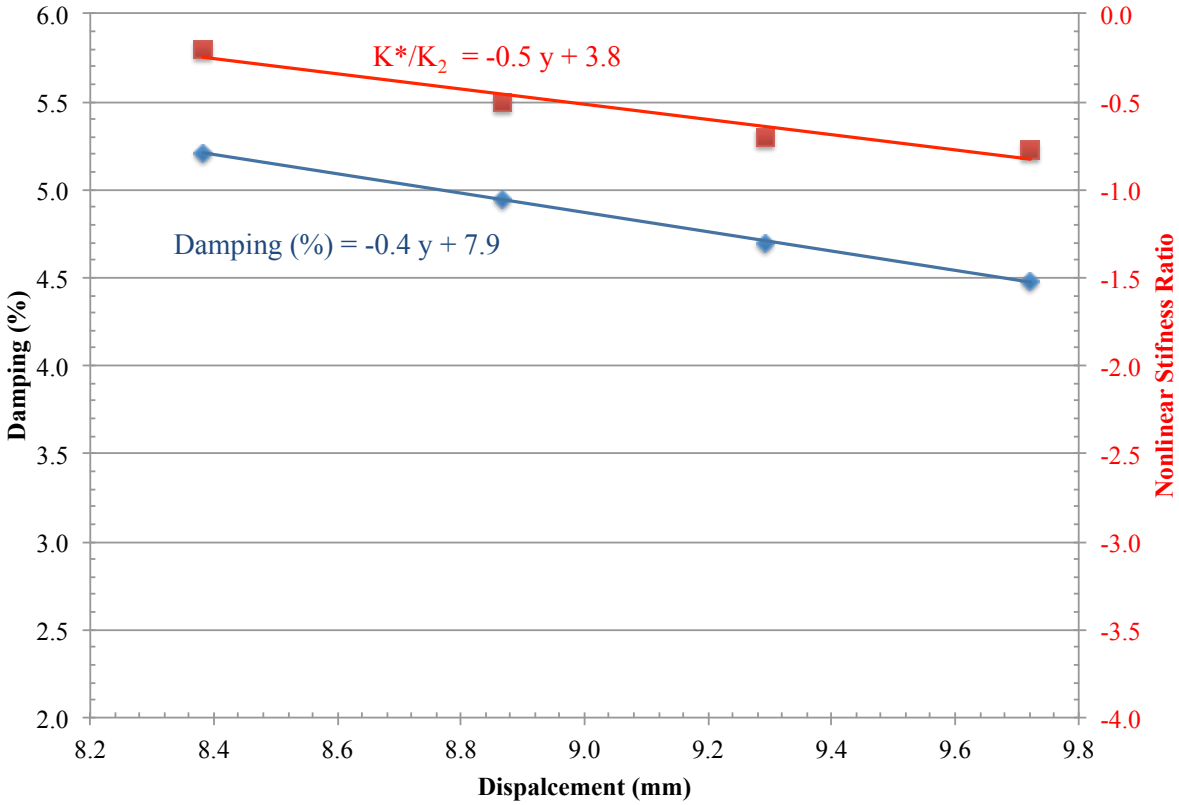

Figure 5-16. Case III: Nonlinear stiffness and damping changes as a function of displacement

It is reasonable to conclude that the local material microstructural evolution decreased the resonance frequency when it was appreciable, that is, when the base excitation amplitude was large. The local material evolution caused an increase in the tip deflection. Therefore, it was necessary to include the evolution in the nonlinear stiffness as a function of the beam response amplitude for each excitation. Indeed, the drop in the nonlinear stiffness of the beam grew linearly with an increase in the response amplitude and base excitation amplitude, as shown in Figure 5-12, Figure 5-14, and Figure 5-16. This is because the beams experienced three competing mechanisms simultaneously: 1) structural stiffening effect due to nonlinear geometric and kinematics effects at high amplitude response, 2) nonlinear structural softening due to inertial, and 3) structural softening effect caused by material microstructural evolution due to fatigue damage precursor. These three mechanisms all amplified with the increase in the base excitations, beam dynamic response, and fatigue cycles. The change in the damping ratio as a function of displacement is illustrated in Figure 5-12, Figure 5-14, and Figure 5-16.

The dynamic trends were consistent in all cases with the exception of Case II, where the resonance frequency in Tests 2, 3 and 4 remained unchanged at approximately 42.10Hz; the resonance frequency decreased in Test 5. It is believed that the competing mechanisms between the stiffening effect (due to high response amplitude influence on geometric and gyroscopic stiffness) and the softening effect (due to nonlinear inertia term and gyroscopic softening) caused this deviation. Eventually, the material evolution (increase in the apparent stiffness) overcomes the nonlinear dynamic stiffening effect due to the continual damage induced by the high cycle fatigue and the beam tip response continued to increase while the resonance frequency decreased.

5.5 Summary and Conclusion

This chapter reports a unique nonlinear approach to detect vibration fatigue damage precursor when a structure is subjected to rotational excitation. The damage precursor occurred prior to any crack initiation in toughened steel structures. Nonlinear terms due to the coupling effect of the primary and secondary motions are included in the equation of motion. Exploiting the sensitivity of the nonlinear geometric stiffness enabled the detection of fatigue damage precursor. A damage precursor detection approach, based on nonlinear varying rotational vibration testing and modeling, is presented for an elastic isotropic cantilever beam. The nonlinear dynamic model provided a methodology for estimating the nonlinear dynamic response due to local material degradation prior to crack initiation. This was accomplished by adjusting the nonlinear geometric stiffness term in the equation of motion. The effect of viscous damping was also studied and found to be insignificant when compared to the geometric stiffness term. It was also found that there are three opposing mechanisms that influenced the beam response: 1) stiffening due to high beam tip response amplitude and gyroscopic motion, 2) softening due to inertial forces and gyroscopic load, and 3) softening due to localized microscopic materials damage precursor (surface material compliance).

5.5 References

[1] Habtour, E., W. Connon, M. F. Pohland, S. C. Stanton, M. Paulus, and A. Dasgupta. "Review of Multiaxial Vibration in Linear and Nonlinear Structures." *Shock and Vibration* 2014 (2014): *DOI: 10.1155/2014/294271*.

[2] Ernst, M., E. Habtour, A. Dasgupta, M. Pohland, M. Robeson, and M. Paulus. "Comparison of Electronic Component Durability under Uniaxial and Multiaxial Random Vibrations." *Journal of Electronics Packaging* 137.1 (2015): n. pag. *DOI: 10.1115/1.4028516*.

[3] Chary, G. V., E. Habtour, and G. S. Drake. "Improving the Reliability in the Next Generation of US Army Platforms through Physics of Failure Analysis." *Journal of Failure Analysis and Prevention* 12.1 (2012): 74-85.

[4] Habtour, E., C. Choi, M. Osterman, and A. Dasgupta. "Novel Approach to Improve Electronics Reliability in the Next Generation of US Army Small Unmanned Ground Vehicles Under Complex Vibration Conditions." *Journal of Failure Analysis and Prevention* 12.1 (2012): 86-95.

[5] E. Habtour, C. Choi, G. Drake, A. Dasgupta, and M. Al-Bassyiouni, "Improved reliability testing with multiaxial electrodynamics vibration," in *Proceedings of the 56th Annual Reliability and Maintainability Symposium* (2010), San Jose, CA.

2010.

[6] Hodges, D. H., and E. H. Dowell. *Nonlinear Equations of Motion for the Elastic Bending and Torsion of Twisted Nonuniform Rotor Blades*. Rep. no. NASA TN D-7818: NASA Technical Notes, 1974.

[7] Crespo Da Silva, M. R. M., and C. C. Glynn. "Nonlinear Flexural-Flexural-Torsional Dynamics of Inextensional Beams. I. Equations of Motion." *Journal of Structural Mechanic* 6.4 (1978): 437-448.

[8] Dowell, E. "Damping in Beams and Plates Due to Slipping at the Support Boundaries." *Journal of Sound and Vibration* 105.2 (1986): 243-53.

[9] Pai, P. F., and A. H. Nayfeh. "Non-linear Non-planar Oscillations of a Cantilever Beam under Lateral Base Excitations." *International Journal of Non-Linear Mechanics* 25.5 (1990): 455-474.

[10] Crespo Da Silva, M. R. M. and C. L. Zaretzky. "Nonlinear Flexural-Flexural-Torsional Interactions in Beams Including the Effect of Torsional Dynamics. I: Primary Resonance." *Nonlinear Dynamics* 5.1 (1994): 3-23.

[11] Malatkar, P. *Nonlinear Vibrations of Cantilever Beams and Plates*. Diss. Virginia Polytechnic Institute and State University, 2003. Blacksburg, VA.

[12] Glaz, B., Friedmann, P. P., and Liu, L., "Vibration Reduction and Performance Enhancement of Helicopter Rotors Using an Active/Passive Approach," AIAA Paper 2008-2178, Proceedings of the 49thAIAA/ASME/ ASCHE/AHS/ASC Structures, Structural Dynamics & Materials Conference, Schaumburg, IL, April 2008.

[13] Cartmell, M. P., and J. W. Roberts. "Simultaneous Combination Resonances in a Parametrically Excited Cantilever Beam." *Strain* 23.3 (1987): 117-26.

[14] Balachandran, B., and A. H. Nayfeh. "Nonlinear Motions of Beam-mass Structure." *Nonlinear Dynamics* 1.1 (1990): 39-61.

[15] Balachandran, B., and A. H. Nayfeh. "Observations of Modal Interactions in Resonantly Forced Beam-mass Structures." *Nonlinear Dynamics* 2.2 (1991): 77-117.

[16] Jaworski, J. W., and E. H. Dowell. "Free Vibration of a Cantilevered Beam with Multiple Steps: Comparison of Several Theoretical Methods with Experiment." *Journal of Sound and Vibration* 312.4-5 (2008): 713-725.

[17] Ansari, M., E. Esmailzadeh, and N. Jalili. "Exact Frequency Analysis of a Rotating Cantilever Beam With Tip Mass Subjected to Torsional-Bending Vibrations." *Journal of Vibration and Acoustics* 133.4 (2011).

[18] Hodges,D. H., "Nonlinear Equations for Dynamics of Pre-twisted Beams Undergoing Small Strains and Large Rotations," NASA TP 2470, May 1985.

[19] Chung, J., and H. H. Yoo. "Dynamic Analysis Of A Rotating Cantilever Beam By Using The Finite Element Method." *Journal of Sound and Vibration* 249.1 (2002): 147-64.

[20] Glaz, B., Friedmann, P. P., Liu, L., Kumar, D., and Cesnik, C. E. S., "The AVINOR Aeroelastic Simulation Code and its Application to Reduced Vibration Composite Rotor Blade Design," AIAA Paper 2009-2601, Proceedings of the 50th AIAA/ASME/ASCHE/AHS/ASC Structures, Structural Dynamics & Materials Conference, Palm Springs, CA, May 2009.

[21] Bauchau, O. A., and Hong, C. H., "Finite Element Approach to Rotor Blade Modeling," *Journal of the American Helicopter Society,* Vol. 32, No. 1, 1987, pp. 60-67.

[22] Hodges, D. H., "Review of Composite Rotor Blade Modeling," *AIAA Journal,* Vol.3, No. 82, 1990, p.561-565.

[23] Yigit, A., R. Scott, and A. Galipulsoy. "Flexural Motion of a Radially Rotating Beam Attached to a Rigid Body." *Journal of Sound and Vibration* 121.2 (1988): 201-10.

[24] Liao, C., and Y. Y. Dang. "Structural Characteristics of Spinning Pretwisted Orthotropic Beams." *Computers & Structures* 45.4 (1992): 715-31.

[25] Chen, W. R. "On the Vibration and Stability of Spinning Axially Loaded Pre-twisted Timoshenko Beams." *Finite Elements in Analysis and Design* 46.11 (2010): 1037-047.

[26] Smith, C., and H. Baruh. "Dominance of Stiffening Effects for Rotating Flexible Beams." *Journal of Guidance, Control, and Dynamics* 14.5 (1991): 1072-074.

[27] Anderson, T.J., B. Balachandran and A. H. Nayfeh, Nonlinear Resonances in a Flexible Cantilever Beam, *Journal of Vibration and Acoustics* 116 (4) (1994), 480-484.

[28] Baruh, H. *Analytical Dynamics*. Boston, MA: WCB/McGraw-Hill, 1999.

[29] Meirovitch, L. *Fundamentals of Vibrations*. Boston: McGraw-Hill, 2001.

[30] Nayfeh, A. H. and D. T. Mook, *Nonlinear Oscillations,* Wiley-VCH, New York, 1995.

[31] Oliver, W. C., and G. M. Pharr. "An improved technique for determining hardness and elastic modulus using load and displacement sensing indentation experiments." *Journal of Materials Research*, Vol. 7, No. 6 (1992): 1564-83.

[32] Saha, R., and W. D. Nix. "Effects of the substrate on the determination of thin film mechanical properties by nanoindentation." *Acta Materialia* 50 (2002): 23-38.

[33] Cole, D. P., H. A. Bruck, and A. L. Roytburd. "Nanoindentation studies of graded shape memory alloy thin films processed using diffusion modification." *Journal of Applied Physics* 103 (2008): 064315.

[34] Cole, D. P., H. Jin, W. Lu, A. L. Roytburd, and H. A. Bruck. "Reversible nanoscale deformation in compositionally graded shape memory alloy films." *Applied Physics Letters* 94 (2009): 193114.

[35] Cole, D. P., Bruck, H. A., Roytburd, A. L., "Nanomechanical characterisation of graded NiTi films fabricated through diffusion modification," *Strain* 45 (2009): 232-237.

[36] Cole, D. P. and K. S. Strawhecker. "An improved instrumented indentation technique for single microfibers." *Journal of Materials Research* 29.9 (2014): 1104-1112.

[37] Cole, D. P., A. L. M. Reddy, M. G. Hahm, R. McCotter, A. H. C. Hart, R. Vajtai, P. M. Ajayan, S. P. Karna, and M. L. Bundy. "Electromechanical properties of polymer electrolyte-based stretchable supercapacitors." *Advanced Energy Materials* 4 (2014): 1300844.

[38] Gershon, A. L., D. P. Cole, A. K. Kota, and H. A. Bruck. "Nanomechanical characterization of dispersion and its effects in nano-enhanced polymers and polymer composites." *Journal of Materials Science* 45 (2010): 6353-6364.

[39] Kacem, N., J. Arcamone, F. Perez-Murano, and S. Hentz. "Dynamic Range Enhancement of Nonlinear Nanomechanical Resonant Cantilevers for Highly Sensitive NEMS Gas/mass Sensor Applications." *Journal of Micromechanics and Microengineering* 20.4 (2010): 045023.

[40] Priya S, Viehland D, Carazo A, et al. (2001) High-power resonant measurements of piezoelectric materials: importance of elastic nonlinearities. Journal of Applied Physics 90(3): 1469–1479.

[41] Yu, S., He S., and Li W. Theoretical and Experimental Studies of Beam Bimorph Piezoelectric Power Harvesters." *Journal of Mechanics and Materials of Structures* 5.3 (2010): 427-445.

[42] Stanton, S. C., A. Erturk, B. P. Mann, E. H. Dowell, and D. J. Inman, "Nonlinear nonconservative behavior and modeling of piezoelectric energy harvesters including proof mass effects," *Journal of Intelligent Material Systems and Structures*, vol. 23, no. 2, pp. 183–199, 2012.

[43] Saavedra, P. N., and L. A. Cuitino. "Crack Detection and Vibration Behavior of Cracked Beams." *Computers & Structures* 79.16 (2001): 1451-459.

[44] Villanueva, L. G., R. B. Karabalin, M. H. Matheny, D. Chi, J. E. Sader, and M. L. Roukes. "Nonlinearity in Nanomechanical Cantilevers." *Physical Review B* 87 (2013).

[45] Villarino de Castro, D. B., J. M. Ventura, C. O. F. T. Ruckert, D. Spinelli, W. W. B. Filho. "Influence of phosphorus content and quenching/tempering temperature on fracture toughness and fatigue life of SAE 5160 Steel." *Materials Research* 13(4) (2010): 445-455.

[46] Kang, S.K., Y-S. Jung, B-G. Yoo, J-I. Jang, and Y-K. Lee. "Orientation-dependent Indentation Modulus and Yielding in a High Mn Twinning-induced Plasticity Steel." *Materials Science and Engineering: A* 532 (2012): 500-04.

[47] Sangid, M. D. "The Physics of Fatigue Crack Initiation." *International Journal of Fatigue* 57 (2013): 58-72.

[48] Mura, T. *Micromechanics of Defects in Solids*. The Hague: Nijhoff, 1982.

[49] Charsley, P., and M.P.E. Desvaux. "The Behaviour of Copper-12% Aluminium under Simple Reversed Stresses." *Materials Science and Engineering* 4.4 (1969): 211-20.

[50] Tanaka, K., and T. Mura. "A Theory of Fatigue Crack Initiation at Inclusions." *Metallurgical Transactions A* 13.1 (1982): 117-23

[51] Dowling, N. E., *Mechanical Behavior of Materials: Engineering Methods for Deformation, Fracture, and Fatigue*, Prentice Hall, Upper Saddle River, NJ, USA, 2nd edition, 1999.

Chapter 6 Nonlinear Structural Dynamic Response under Multiaxial Vibrations: Rotational and Transverse Base Excitations

To be submitted to Shock and Vibration (2015)

Chapter 6 is an article being prepared for publication in *Shock and Vibration* Journal. The article presents analytical and experimental results that show structural dependency on the phase difference between different axes of excitation, when a structure is exposed to multiaxial vibration. Results show that cross-axis coupling between rotation and simultaneous transverse excitations promoted nonlinear amplification/attenuation in the response of the structure, depending on the phase relationship between the rotational and the translational excitations. Authors are Mr. Ed Habtour, Dr. Samuel C. Stanton, and Professor Abhijit Dasgupta. Mr. Ed Habtour (first author) conducted the vibration experiments and developed the analytical model. Dr. Samuel Stanton at the Army Research Office checked the derivations. Professor Dasgupta provided technical and academic guidance in this effort.

Abstract:

This chapter presents a nonlinear dynamic analytical model and experimental results to investigate the dynamic response of a cantilever metallic beam structure under varying combinations of rotational and translational harmonic base excitation in the transverse direction. The study demonstrates the importance of cross-axis coupling between the rotational and translational harmonic base excitations, especially as a function of the relative phase angle between the two excitations. The experiments are performed using a unique six degree-of-freedom electrodynamic shaker with high degree of controllability over the excitation frequency spectrum of each axis, the relative phase between different axes for harmonic excitation, and cross-axis coherence for random vibration.

The analytic and the experimental results show that increasing the phase angle between the rotational and translational excitations from 0^o-180^o increased the beam tip response and the beam nonlinear stiffening effect. The beam response decreased as the phase increased from 180^o-360^o, where 360^o is equivalent to 0^o. However, the beam tip displacement predictions obtained from the model do not agree with the experimental results. The discrepancy is due to the buildup of fatigue damage during the experiments, which is manifested by a shift in the resonance frequency and an increase in the response amplitude as a function of the accumulated number of vibration cycles. The current nonlinear analytical model does not take into account this reduction in the structural stiffness due to accumulation of cyclic fatigue damage. Exploiting the sensitivity of the phase angle between the rotation and transverse base excitation enabled structural control without changing the loading amplitudes.

6.1 Introduction

The reliability of mechanical systems exposed to vibration environment depends primarily on the vibration response of their internal components. Designers rely on the use of vibration isolators, stiffeners and dampers in mechanical systems, without full understanding of the dynamic loads being transmitted though the system, Uninformed use of vibration isolators, stiffeners, and dampers is inadequate for sustaining the desired life-cycle of mechanical systems operating, which are often inadequate for sustaining the desired life-cycle in vibratory environments. There are two major reasons for these conventional strategies. The first reason is that cost and time limitations often drive designers to employ linear modeling tools to predict the response of structures. Linear models are inaccurate in slender mechanical structures when the amplitudes of oscillations are sufficiently high and

the natural frequencies become increasingly dependent on these amplitudes [1]. Realistically, many slender mechanical systems have to operate beyond the regime of linear dynamic response and consequently, linear response models of such systems have severe limitations.

Second, designers often have an inadequate understanding of how the nonlinear responses of mechanical components are aggravated when exposed to complex vibrational environments containing multiaxial excitations. Many mechanical systems such as aircraft, rotorcraft, and automotive and military platforms are exposed to complex dynamic environments that tend to be multiaxial. It is essential to characterize how the dynamic excitations in those systems are transmitted through the structure and into critical components. Systems exposed to such multiaxial vibration experience synergistic dynamic nonlinearities due to cross-axes coupling [2–4]. One of the key challenges in recreating vibration conditions during design and qualification testing in the laboratory is reproducing simultaneous multiaxial vibratory environments that structures experience during their operational cycle. Dynamic response predictions under multiaxial dynamic loading have been shown to be extremely complex and less tractable than uniaxial models [5, 6]. Furthermore, multiaxial shakers are extremely complex to develop and use. The traditional vibration testing practice therefore has been to sequentially apply uniaxial excitation to test articles along three orthogonal axes then superimpose the responses. Such sequential testing is well suited to traditional uniaxial shakers and has been used to test products even though most field data indicate that these products are exposed to multiaxial dynamic loading environments [2–4, 7, 8]. In fact, military and commercial standards have also traditionally adopted this practice of sequential uniaxial excitation as a compromise for simultaneous multiaxial excitation. The vibration profiles used for such uniaxial tests are provided in

standards such as MIL-STD-810G [7].

Thus, serious compromises must be made in the experimental design to perform meaningful sequential tests on uniaxial electrodynamic shakers [3]. One of those compromises is the application of the principle of linear superposition, which in some cases generates misleading results. Furthermore, increasing the oscillation amplitude (as in accelerated stress testing) increases the nonlinear cross-axis coupling and exacerbates the inaccuracy of the linear superposition approach. To accurately estimate the dynamic response of a structure under multiaxial base excitations, it is important to include the nonlinearities in the analysis.

It was apparent during the literature review that research related to multiaxial vibrations is limited. One of the common approaches in industry to simulate multiaxial environments is termed 'High Accelerated Life Testing' (HALT©), which is widely used in industry during prototyping, and product qualification [2]. The basic idea of HALT is to induce random repetitive shock response of the shaker table, using multiple pneumatic impact actuators located at different locations of the table along different orientations (relative to the table axis system). The actuators are fired in some pre-selected sequence to generate a sequence of 'bursts' of quasi-random shock response spectra, based on the table dynamics. The typical excitation frequency spectrum for most commercially available HALT shakers ranges from 10-10 kHz. The shape of this spectrum cannot be controlled and is a function of the table design, fixture design and test specimen dynamics. The average RMS (Root Mean Square) amplitude of the excitation is usually controlled only along one axis (usually in the direction orthogonal to the plane of the shaker table). The response along the other axes therefore varies in some proportional manner but is not independently

controllable. In summary, the shaker table and the structure under test are exposed to inadequately controlled multiaxial random excitation, which makes it difficult to accurately predict dynamic response of the structure [2, 7].

Studies evaluating the merits of multiaxial vibration testing using multiaxial electrodynamic shakers are limited [2–4, 9–11]. These studies have pointed out the shortcomings of the sequential uniaxial vibration method. These studies also reported evidence of different failure modes and fatigue durability between uniaxial and multiaxial vibration loading generated by multiaxial shakers. Whiteman and Berman performed a uniaxial translational random vibration experiment in the transverse direction then repeated the same test for sequential excitation in the axial direction followed by the transverse direction and compared the results to simultaneous triaxial translational excitation [9]. Their study reports that the excitation in the axial direction did not weaken the specimens; on the contrary, it increased the samples' fatigue life. Whiteman and Berman did not provide a theoretical explanation or approach to predict structural response or life-cycle of the specimens under multiaxial excitation [9]. French et al. performed durability experiments on notched beam specimens using both sequential uniaxial and simultaneous biaxial testing on a hydraulic triaxial shaker [10]. The base excitation signal was a sine chirp from 10–35 Hz over 30 s. The peak-to-peak acceleration amplitude was held constant at 4G. The sequential uniaxial and simultaneous biaxial experiments produced different damage accumulation rates and different failure modes. Gregory et al. utilized a six degrees-of-freedom (DoF) multiaxial electrodynamic shaker to perform a dynamic characterization for a short cantilever beam with large tip mass [11]. The beams were subjected to uniaxial and multiaxial broadband random excitations with a bandwidth of 20–2000Hz at low acceleration power spectrum

density (PSD) input level of 0.0032 G^2/Hz. The experimental results showed significant differences in the beam response for uniaxial and multiaxial excitations. Ernst et al. experimentally investigated the synergy between axial and transverse translational excitation of an electronic circuit card containing tall, heavy electronic components [4]. The study uncovered nonlinear dynamic coupling between different response modes, in response to simultaneous transverse and axial random vibration base excitation. The combination of inertial nonlinearity (due to component heavy mass) and fatigue damage accumulation in the system produced a softening dynamic response and a drop in the components' resonance frequencies [4].

Limited analytical studies are found in the literature that dealt with structures under multiaxial base excitations [12, 13]. Esmaeili et al. developed equations of motion for a micro-gyroscope, which was modeled as a linear cantilever beam with a tip mass exposed to excitation at the base [12]. The governing equations were derived from Hamilton's principle with six DoF base motion where torsion and nonlinear effects were neglected. Kumar et al. studied the effects of structural and inertial nonlinearities in near-resonant response for a flexible inextensional slender cantilever beam exposed to base excitation combined with simultaneously parametric excitation [13]. The parametric excitation of a system transpired when the resonance frequency to the excitation frequency ratio is close to $n/2$ (n = 1, 2, 3…) To simulate simultaneous biaxial base excitation the beam was oriented at 80^o, which induce both direct and parametric excitations using a uniaxial shaker. The energy method was utilized to derive the governing equations, where rotational inertia and the torsion were assumed to be negligible.

The motivation for the multiaxial vibration research effort in this study is prompted by the serious need to understand "real-world" complex dynamic systems operating in multiaxial vibratory environments such as helicopter blades, aircraft wings, accelerometers, sensors, MEMS, energy harvesters and electronics. The need to understand the nonlinear response of structures exposed to complex dynamic loads requires the use of a fully controllable multiaxial excitation shaker. The objectives of this research effort are to understand the nonlinear dynamic response of a cantilever beam exposed to combined rotational and translational base excitation and to provide an analytical approach to include the cross-axis coupling effects experienced under multiaxial excitations due to geometric and inertial nonlinearities. A slender cantilever beam is selected in this research effort because it is one of the fundamental elements of an engineering structure. The dynamics of a beam can provide important insights into the nonlinear response of many complex flexible structures such as helicopter rotor blades, spacecraft antennae, flexible satellite structures, airplane wings, robotic arms, and electronics interconnects. In this research effort, an isotropic metallic slender cantilever beam is exposed to combined base rotation and base translation in the transverse direction, using a unique multiaxial electrodynamic shaker capable of simultaneously producing three translational and three rotational excitations. The time-varying flexural base rotation and transverse excitations are chosen to be harmonic functions with constant amplitudes and the same constant frequency for both axes, for all experiments. The phase angle between the rotation and transverse base excitations was varied from 0^{o}-360^{o}. The analytical and experimental results revealed the important of the phase relationship between the rotation and transverse base motions, which can amplify or mitigate the nonlinear structural response. Manipulating the phase relation between the base excitations

can be a useful parameter in controlling the structural response without applying any changes to the loads at the base. The analytical model shows (and experimental measurements confirm) that increasing the phase angle from 0^o-180^o increases the beam tip response and the beam shows structural stiffening, due to an overall increase in the combined base excitation. The results also reveal that increasing the phase angle from 180^o-360^o creates the opposite effect, where the beam tip response decreases. However, the analytical model does not predict the absolute beam tip response accurately. This is due to possible localized micro-plasticity at the high stress concentration site near the fixed end of the beam, caused by high-cycle fatigue [14]. The analytical model provides an option to include materials nonlinearities, as discussed in previous chapters of this dissertation, but is not considered here since it is beyond the scope of this chapter.

6.2 Model Development

This section describes the nonlinear dynamics of a cantilever beam with uniform cross-section carrying a tip mass exposed to a selected harmonic combination of rotational and translational base excitation in the flexural direction, as shown in Figure 6-1. The beam is idealized to be inextensional; that is, stretching of the neutral axis is insignificant [15]. The beam is rigidly fixed at one end and free at the other end, as shown in Figure 6-1. Nonlinear Euler-Bernoulli theory is employed to estimate the beam tip displacement, where the effects of warping and shear deformation are neglected [16].

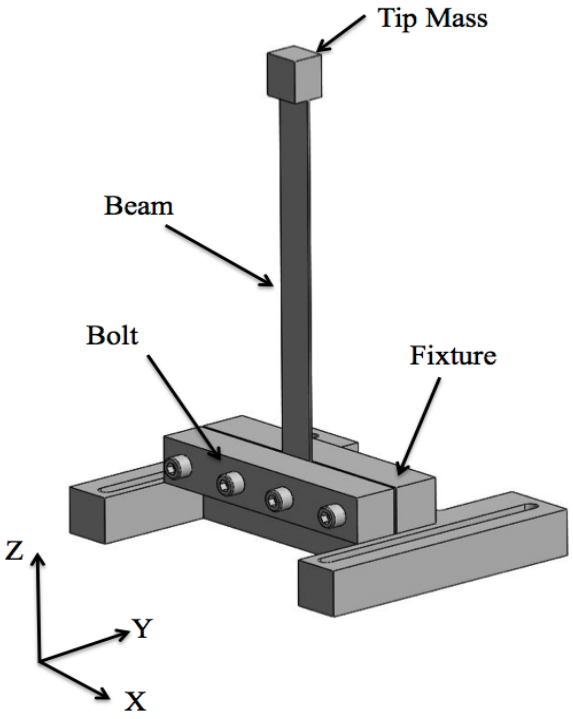

Figure 6-1. Slender beam with tip mass attached to a rigid fixture

The significance of large peak response amplitude is that the nonlinear terms in the equations of motion become as important as the linear ones. Since the beam length to width ratio is kept short (AR<30), it can be assumed that the beam undergoes purely planar flexural vibrations as long as the tip mass and cross-section geometry are symmetric with respect to the beam's centerline [14]. The first flexural mode is assumed to be the exact linear mode shape generated from solving the linear problem with tip mass that contains the rotary inertia effect [17].

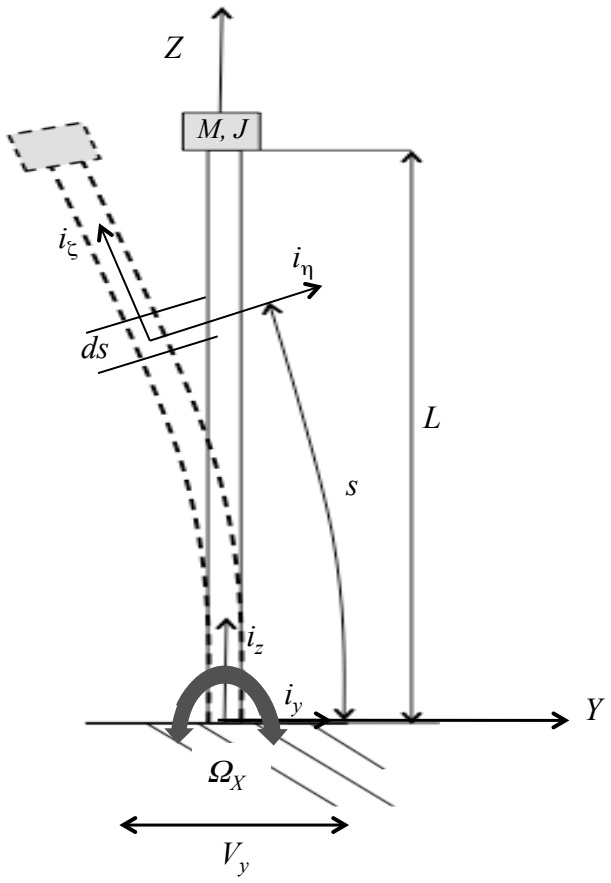

Figure 6-2. Slender beam with tip mass under combined rotational and translational base excitation in the flexural direction

The cantilever beam is considered to be a uniform and straight isotropic structure of length L, clamped at the base, with volumetric density ϱ, tip mass M and rotary inertia J, as shown in Figure 6-2. The Z-axis is taken as the neutral axis associated with pure bending. It is assumed the loci of both shear centers and mass centers of the undeformed beam are coincident with the Z-axis. The base motion causes each cross section of the beam to experience an elastic displacement of its centroid. The dynamics of the beam with respect to Y and Z axes at the undeformed length from the root of the beam to the reference point, s, and time, t, is described in terms of the axial displacement $w(s,t)$, the transverse displacement

$v(s,t)$ along the inertial coordinate system *YZ*, and the rotational angle ψ. The orthogonal unit vectors for the inertial coordinate system are (i_Y, i_Z). The local curvilinear coordinate system at *s*, in the deformed position, has the orthogonal unit vectors (i_η, i_ζ). The rotating reference frame approach is used, where the reference frame is attached to the undeform position of the beam (at the base of the beam). The position vector of a point is expressed as follows:

$$\boldsymbol{R} = v\boldsymbol{i_Y} + (s+w)\boldsymbol{i_Z} + \boldsymbol{R_{local}} \qquad \text{Eq. 6-1}$$

The variable s denotes the arc-length along $\boldsymbol{R}$.

$$\boldsymbol{R_{local}} = \eta \boldsymbol{i}_\eta$$

Therefore,

$$\boldsymbol{R} = v\boldsymbol{i_Y} + (s+w)\boldsymbol{i_Z} + \eta \boldsymbol{i}_\eta \qquad \text{Eq. 6-2}$$

where,

$$\boldsymbol{i}_\eta = cos(\psi)\boldsymbol{i}_Y + sin(\psi)\boldsymbol{i}_Z$$

Substituting $\boldsymbol{i}_\eta$ into Eq. 6-2 yields:

$$\boldsymbol{R} = (v + \eta cos(\psi))\boldsymbol{i}_Y + \big(s + w + \eta sin(\psi)\big)\boldsymbol{i_Z} \qquad \text{Eq. 6-3}$$

Differentiating $\boldsymbol{R}$ with respect to t:

$$\dot{\boldsymbol{R}} = \big(V_y + \dot{v} - \eta\dot{\psi} sin(\psi)\big)\boldsymbol{i}_Y + \big(\dot{w} + \eta\dot{\psi}\cos\psi\big)\boldsymbol{i_Z} + \boldsymbol{\Omega_{Base}}\times\boldsymbol{R} \qquad \text{Eq. 6-4}$$

Where the dots denote the time derivatives, and

$$\boldsymbol{\Omega_{Base}} = \Omega_x(t)\boldsymbol{i_X}$$

The tracking frame primary motion is $\Omega_x(t)$. Since the reference frame is selected *a priori*, $\Omega_x(t)$ becomes a known quantity, instead of a variable [18]. Substituting Eq. 6-3 into Eq. 6-4 and combining terms yields the following:

$$\dot{\boldsymbol{R}} = \left(V_y + \dot{v} - \eta\dot{\psi}sin(\psi) - s\Omega_X - w\Omega_X - \eta\Omega_X sin(\psi)\right)\boldsymbol{i}_Y + \left(\dot{w} + \eta\dot{\psi}\cos\psi + v\Omega_X + \eta\Omega_X cos(\psi)\right)\boldsymbol{i}_Z \quad \text{Eq. 6-5}$$

The kinetic energy can be expressed as follows:

$$T = \frac{1}{2}\int_0^L \int_{A_1}^{A_2} \varrho\, \dot{\boldsymbol{R}} \cdot \dot{\boldsymbol{R}}\, dAds + \frac{1}{2}M\left(\dot{\boldsymbol{R}} \cdot \dot{\boldsymbol{R}}\right)\Big|_{s=L} \quad \text{Eq. 6-6}$$

Set:

$$\rho = \int_{A_1}^{A_2} \varrho\, dA \qquad J_1 = \int_{A_1}^{A_2} \varrho\, \eta dA \qquad J_2 = \int_{A_1}^{A_2} \varrho\, \eta^2 dA$$

Since the reference point coincides with the mass centroid and η is a principal axis of the differential beam element, J_1 is set equal to zero. However, the beam rotary inertia is maintained in the kinetic energy. Substituting Eq. 6-5 into the kinetic energy expression, Eq. 6-6 yields the following:

$$T = \frac{1}{2}\int_0^L \Big[\rho\big(\dot{v}^2 + 2\dot{v}V_Y + {V_Y}^2 + \dot{w}^2 - 2s\dot{v}\Omega_X - 2(s+w)V_Y\Omega_X - 2\dot{v}w\Omega_X$$

$$+ 2v\dot{w}\Omega_X + v^2{\Omega_X}^2 + (w+s)^2{\Omega_X}^2\big) + J_2\big(\Omega_X + \dot{\psi}\big)^2\Big]\,ds$$

$$+ \frac{1}{2}M\big[\dot{v}^2 + 2\dot{v}V_Y + {V_Y}^2 + \dot{w}^2 - 2s\dot{v}\Omega_X - 2(s+w)V_Y\Omega_X \qquad \text{Eq. 6-7}$$

$$- 2\dot{v}w\Omega_X + 2v\dot{w}\Omega_X + v^2{\Omega_X}^2 + (w+s)^2{\Omega_X}^2\big]\Big|_{s=L}$$

$$+ \frac{1}{2}J\big(\Omega_X + \dot{\psi}\big)^2\Big|_{s=L}$$

Performing Taylor's expansion up to cubic nonlinearities and assuming that w and v are small but finite, applying inextensionality and neglecting torsion, the potential energy and the kinetic energy can be expressed as follows:

$$\Pi = \frac{EI}{2}\int_0^L (v''^2 + v''^2 v'^2)ds - \frac{1}{2}\rho g\int_0^L (L-s)v'^2 ds - \frac{1}{2}Mg\int_0^L v'^2 ds \qquad \text{Eq. 6-8}$$

$$T = \frac{1}{2}\int_0^L \Bigg[\rho\Bigg(\dot{v}^2 + 2\dot{v}V_Y + {V_Y}^2 + \frac{1}{4}\left(\frac{\partial}{\partial t}\int_0^\zeta v'^2 ds\right)^2 + \left(\int_0^\zeta v'^2 ds - 2s\right)V_Y\Omega_X$$
$$+ \left(\int_0^\zeta v'^2 ds - 2s\right)\dot{v}\Omega_X - \frac{\partial}{\partial t}\left(\int_0^\zeta v'^2 ds\right)v\Omega_X + v^2{\Omega_X}^2$$
$$+ \left(s - \frac{1}{2}\int_0^\zeta v'^2 ds\right)^2 {\Omega_X}^2\Bigg)$$
$$+ J_2(\Omega_X^2 + 2\Omega_X\dot{v}' + \Omega_X\dot{v}'v'^2 + \dot{v}'^2 + \dot{v}'^2v'^2)\Bigg] ds \qquad \text{Eq. 6-9}$$
$$+ \frac{1}{2}M\Bigg[\dot{v}^2 + 2\dot{v}V_Y + {V_Y}^2 + \frac{1}{4}\left(\frac{\partial}{\partial t}\int_0^\zeta v'^2 ds\right)^2$$
$$+ \left(\int_0^\zeta v'^2 ds - 2s\right)V_Y\Omega_X + \left(\int_0^\zeta v'^2 ds - 2s\right)\dot{v}\Omega_X$$
$$- \frac{\partial}{\partial t}\left(\int_0^\zeta v'^2 ds\right)v\Omega_X + v^2{\Omega_X}^2 + \left(s - \frac{1}{2}\int_0^\zeta v'^2 ds\right)^2 {\Omega_X}^2\Bigg]\Bigg|_{s=L}$$
$$+ \frac{1}{2}J(\Omega_X^2 + 2\Omega_X\dot{v}' + \Omega_X\dot{v}'v'^2 + \dot{v}'^2 + \dot{v}'^2v'^2)\Big|_{s=L}$$

where, the primes denote the spatial derivatives. The approximate solutions are assumed in the form:

$$v(t,z) = \sum_{j=1}^{N} q_j(t)Y_j(z) \qquad \text{Eq. 6-10}$$

where, the trial functions, Y_j, are known independent comparison functions from a complete orthogonal function set and denote the undamped linear mode shapes, while q_j denotes the generalized modal coordinates [19]. For a single mode, the assumed solution becomes:

$$v(t,z) = q(t)Y(z) \qquad \text{Eq. 6-11}$$

Eq. 6-11 is substituted into the kinetic energy and potential energy equations (Eq. 6-8, and Eq. 6-9). The Euler-Lagrange equation is then obtained for the Lagrangian functional, $L = T - \Pi$, as follows:

$$\frac{\partial}{\partial t}\left(\frac{\partial L}{\partial \dot{q}}\right) - \frac{\partial L}{\partial q} = 0 \qquad \text{Eq. 6-12}$$

The equation of motion with the appropriate nonlinear terms for the system under study is:

$$\begin{aligned} a_1\ddot{q} + a_2(q^2\ddot{q} + q\dot{q}^2) + a_3\dot{\Omega}_X q^2 + (k_1 - n_1 V_Y \Omega_X - h_1\Omega_X^2)q \\ + (k_2 - h_2\Omega_X^2)q^3 = a_3\dot{V}_Y + a_4\dot{\Omega}_X \end{aligned} \qquad \text{Eq. 6-13}$$

The inertial coefficient including the rotary inertia (or effective mass) is:

$$a_1 = \rho\int_0^L Y^2 ds + J_2\int_0^L Y'^2 ds + MY^2|_{x=L} + JY'^2|_{s=L} \qquad \text{Eq. 6-14}$$

The nonlinear inertial coefficients including tip rotary inertias are:

$$a_2 = \rho\int_0^L \left(\int_0^\zeta Y'^2 ds\right)^2 ds + J_2\int_0^L Y'^4 ds + M\left(\int_0^\zeta Y'^2 ds\right)^2\Bigg|_{s=L} + JY'^4|_{s=L} \qquad \text{Eq. 6-15}$$

$$a_3 = \frac{1}{2}\left(-\rho\int_0^L Y\int_0^\zeta Y'^2 ds\, ds - MY\int_0^\zeta Y'^2 ds\Big|_{s=L} + J_2\int_0^L Y'^3 ds + JY'^3|_{s=L}\right) \qquad \text{Eq. 6-16}$$

The first order structural stiffness coefficients (or effective elastic structural stiffness coefficients) are:

$$k_1 = EI\int_0^L Y''^2 ds - \rho g\left(\int_0^L (L-s)Y'^2 ds\right) - Mg\left(\int_0^L Y'^2 ds\right) \qquad \text{Eq. 6-17}$$

$$n_1 = 2\rho \int_0^L \int_0^\zeta Y'^2 ds\, ds + 2\,M \int_0^\zeta Y'^2 ds\Big|_{s=L} \quad \text{Eq. 6-18}$$

$$h_1 = \rho \int_0^L Y^2 ds - \frac{1}{2}\rho \int_0^L (L^2 - s^2) Y'^2 ds + MY^2|_{s=L} - \frac{1}{2} M (L^2 - s^2) Y'^2\Big|_{s=L} \quad \text{Eq. 6-19}$$

The third order nonlinear geometric elastic stiffness coefficients are:

$$k_2 = 2EI \int_0^L Y''^4 ds \quad \text{Eq. 6-20}$$

$$h_2 = \frac{1}{2}\left(\rho \int_0^L \left(\int_0^\zeta Y'^2 ds\right)^2 ds + \frac{1}{2} M \left(\int_0^\zeta Y'^2 ds\right)^2\Big|_{s=L}\right) \quad \text{Eq. 6-21}$$

The base excitation inertial coefficients are:

$$a_4 = \rho \int_0^L Y ds + MY|_{s=L} \quad \text{Eq. 6-22}$$

$$a_5 = -\rho \int_0^L sY ds - MsY|_{s=L} + J_2 \int_0^L Y' ds + JY'|_{s=L} \quad \text{Eq. 6-23}$$

Adding a viscous damping term to the equation of motion leads to the final form of the governing equation for this cantilever beam whose base is undergoing simultaneous flexural rotation and transverse translational excitation:

$$\begin{aligned} a_1\ddot{q} + a_2(q^2\ddot{q} + q\dot{q}^2) + c\dot{q} + a_3\dot{\Omega}_X q^2 + (k_1 - n_1 V_Y \Omega_X - h_1 \Omega_X^2) q \\ + (k_2 - h_2 \Omega_X^2) q^3 = a_4 \dot{V}_Y + a_5 \dot{\Omega}_X \end{aligned} \quad \text{Eq. 6-24}$$

The equation of motion contains distinctive nonlinearities in additional to the traditional inertial (second and third terms) and geometric nonlinearities (ninth term) due to this combined multiaxial vibration loading. The fifth term is the nonlinear inertial contribution due to the variable rotational base excitation. The seventh term is the nonlinear

coupling effect between the rotation and transverse base excitation. This coupling term has a negative sign, which reduces the overall structural stiffness of the beam. The eighth term also reduces the beam structural stiffness due to time varying rotational base excitation. Finally, time varying rotation in the tenth term lowers the nonlinear geometric stiffness.

6.3 Experimental Approach

This section describes the test specimen's properties. Detailed explanation of the experimental setup and procedure are also provided.

6.3.1 Test Specimens:

The cantilever beams for this study were constructed from blue-finished and polished spring-tempered AISI 1095 high carbon steel. The beams were fabricated using cold rolling method, which may generate some level of material orthotropy. Accordingly, the isotropy assumption is an approximation in this study. The density and the elastic modulus of the material are 7.85 g/cm^3 and 205 GPa, respectively. The hardness is Rockwell C48 with AR= 8. The beam length and cross-section area are 127 mm and 15.88×1.08 mm^2, respectively.

6.3.2 Test Setup

To produce combined transverse translation and flexural rotation of the base, it was necessary to utilize a multiaxial electrodynamic shaker. A commercially produced prototype multiaxial shaker was used in this study. This 6 DOF electrodynamic shaker consists of eight actuators in the plane of the shaker table (two pairs along each X and Y directions) and two more pairs of out-of-plane actuators underneath the shaker table in the Z direction, as shown in Figure 6-3. These twelve electrodynamic actuators were mechanically coupled to the table through self-aligning hemispherical hydrodynamic bearings. This architecture allowed the

shaker to produce a true six degrees-of-freedom (DoF) vibration environment (three translations and three rotations).

In this study, the four out-of-plane actuators underneath the shaker table were employed to produce base rotation about the x-axis. This produced flexural vibration because the beam was vertically oriented (along the z direction), as shown in Figure 6-4. The four horizontal actuators in the Y-direction, shown in Figure 6-3, were utilized to produce the simultaneous translational excitation in the transverse (Y) direction. The other four actuators were used to reduce potential noise along other axes due to misalignments, thus ensuring a pure rotational excitation about the X-direction and pure translation in Y-direction. Additional details related to the capabilities of the multiaxial shaker are provided elsewhere in the literature [3].

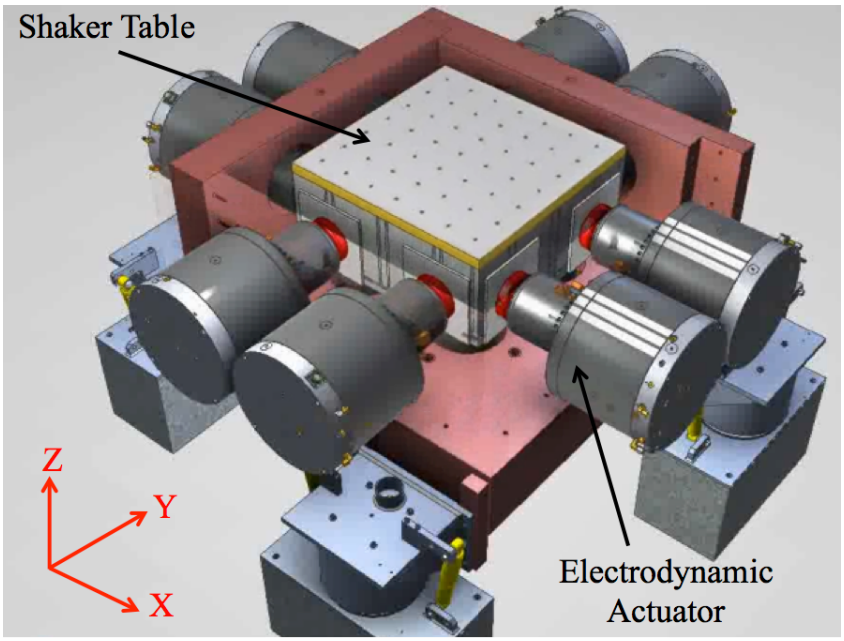

Figure 6-3. Multiaxial shaker (TEAM Corp.)

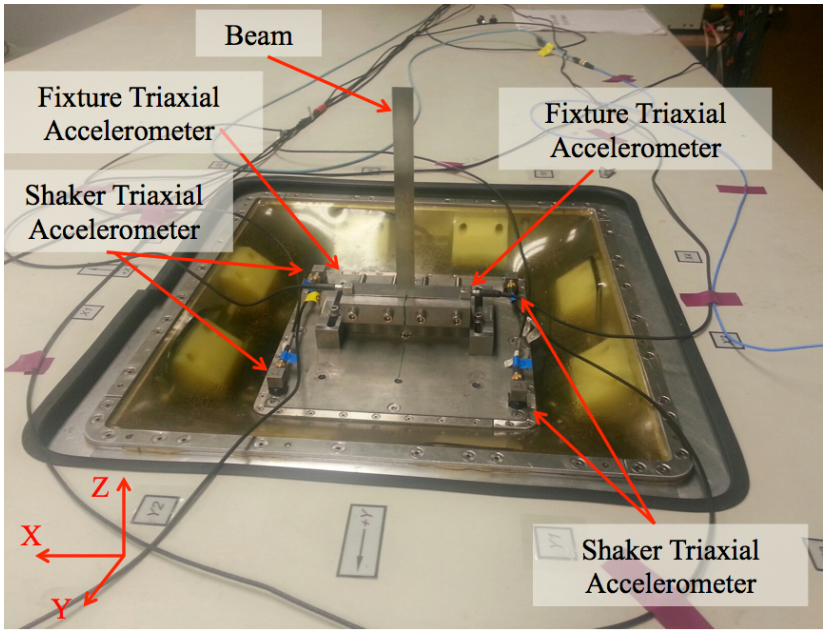

Figure 6-4. Experimental setup for vibration test

The vibration experiment setup and instrumentation are shown in Figure 6-4. Each beam was mounted vertically (pointed along the Z direction, as shown in Figure 6-4) on a rigid fixture and the four clamping bolts were torqued to 22.6 N-m. As shown in Figure 6-3,

the fixture was mounted to the multiaxial shaker table using four clamping bolts. The shaker table was controlled using four commercial triaxial accelerometers. One accelerometer was attached to each corner on the shaker, as shown Figure 5-4. The beam tip displacement was measured using two accelerometers; one accelerometer for each side of the beam. The mass of each accelerometer was approximately 1.5 g. Two additional accelerometers were mounted on the fixture (Figure 5-4) to ensure that that the base excitation was pure rotation about the X-axis and pure translation along the Y-direction.

6.3.3 Test Procedure:

Four sets of experiments (Cases: I, II, III, and IV in Table 6-1) were conducted. The details of each case are listed in Table 6-1. The beam in each case was exposed to constant amplitude rotational and transverse harmonic base excitation, 70 rad/s^2 and 0.3 g, respectively. The phase angle, θ, between the rotation and transverse harmonic excitations was varied for each case, as stated in Table 6-1. The number of loading cycles applied in this study depended on the observed irreversible shift in the resonance frequency and the irreversible change in the beam tip displacement response due to material 'softening' caused by early fatigue degradation. In other words, the tests were repeated until significant changes in the resonant frequency or tip displacement were observed. Furthermore, the continual shift in the resonance made it challenging to control the multiaxial loading. After the linear fundamental frequency for each beam was identified using sine-sweep excitation, the beams were exposed to the specified base excitations at discrete number of forward-stepping dwell frequencies near the fundamental frequency. The ramp-up time and dwell time for each frequency were 35s and 25s, respectively. The ramp-up time and dwell time at each excitation frequency was selected to be long enough to ensure that steady state response

conditions were met. The frequency step for each dwell was 0.05Hz. Thus, the excitation frequency was increased by 0.05 Hz every 60s (35 s ramp up plus 25s dwell). It is important to point out that this study we do not address the effect of backward stepping dwell. Thus, the conclusions provided in this chapter are applicable to forward-stepping excitations only.

Table 6-1 Nonlinear experimental cases

Case	Test	Total Cycles ($x10^3$)	Phase (^{o})	Linear Resonance (Hz)	Strain Amplitude ($x10^{-3}$)
I	1	0-41	0	40.77	1.4
	2	41-117			
	3	117-188			
	4	188-247			
II	1	0-68	45	40.28	1.7
	2	68-135			
	3	135-202			
III	1	0-68	90	40.65	2.3
	2	68-137			
	3	137-205			
IV	1	0-70	135	40.30	3.0
	2	70-140			
	3	140-210			

6.4 Results and Discussion

6.4.1 Experimental Results

Detailed discussion of the experimental results is provided in this section. Each experimental set contained three stepped-dwell tests with the exception of case I, as shown in Table 6-1, Figure 6-5 and Figure 6-8, for Cases I, II, III, and IV, respectively. The base excitation frequency and resonance frequencies are ω and ω_r, respectively. In Case I, the first stepped-dwell test (Test 1) was terminated at $\omega/\omega_r = 1.002$ due to unexpected power loss with one of the shaker's actuators (Figure 6-5). Thus, unlike Cases II, III and VI, Case I contains four tests instead of three tests, as shown in Table 1.

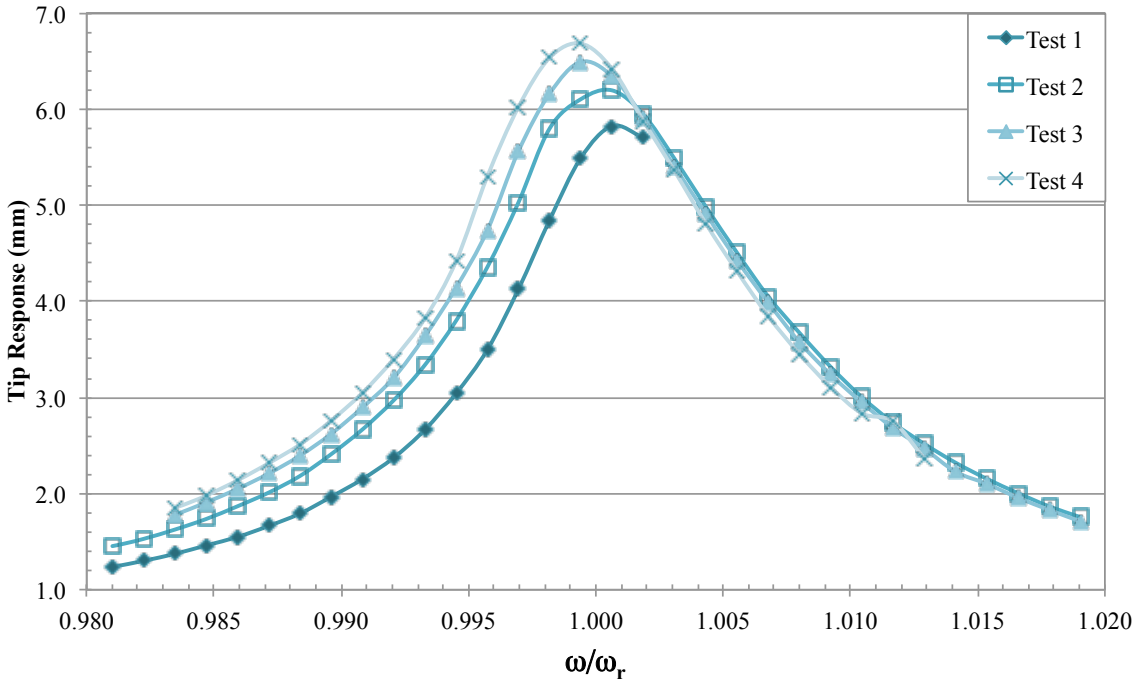

Figure 6-5. Tip response due to 70 rad/s^2 and 0.3g base rotation and transverse excitations, θ=0^o

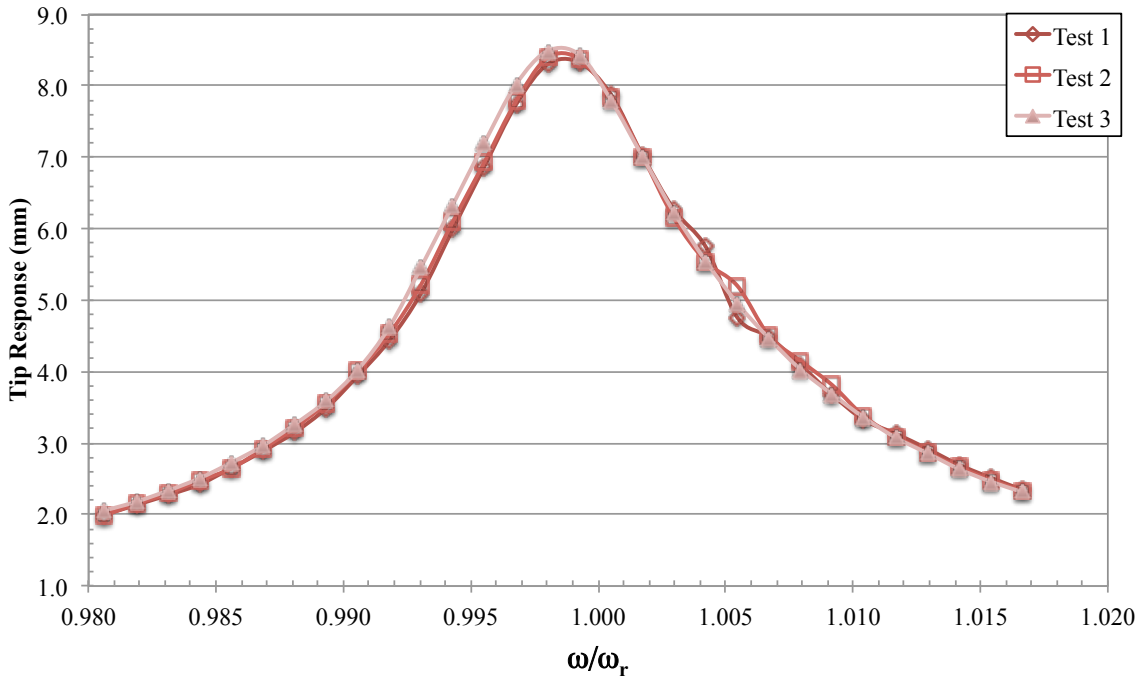

Figure 6-6.Tip response due to 70 rad/s^2 and 0.3g base rotation and transverse excitations, θ =45^o

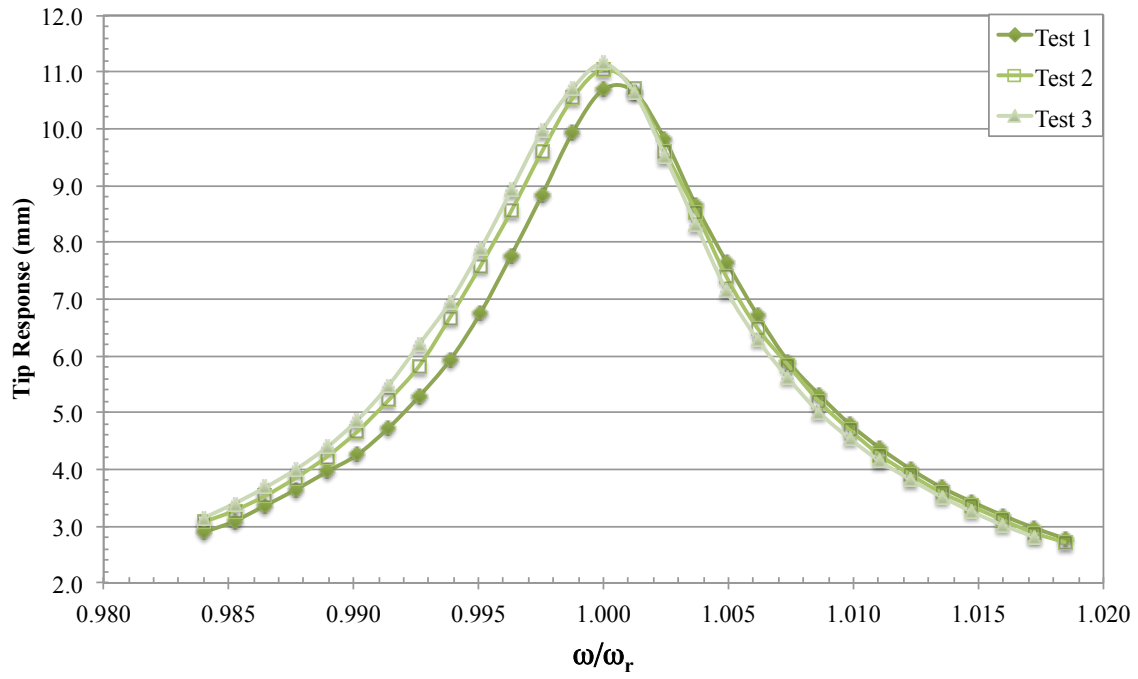

Figure 6-7. Tip response due to 70 rad/s^2 and 0.3g base rotation and transverse excitations, θ =90^o

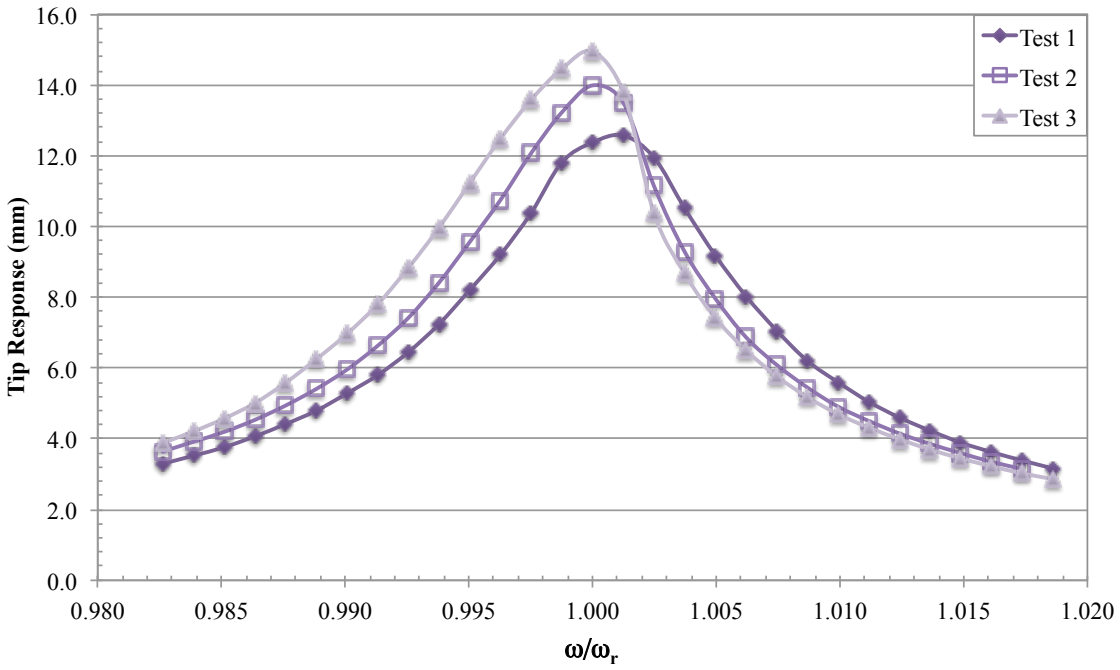

Figure 6-8. Tip response due to 70 rad/s^2 and 0.3g base rotation and transverse excitations, θ =135^o

The experimental objectives were to monitor the shift in the resonance frequency and changes in the beam tip response due to changes in the phase angle between the rotation and transverse nonlinear base excitations. The shift in the fundamental frequency and the increase in the response amplitude due to repeated dwells were indicative of four possible mechanisms: 1) localized material 'softening' effect (due to possible micro-plasticity) caused by high-cycle fatigue [14], 2) softening due to nonlinear inertial forces [4], 3) kinematic (geometric) stiffening due to high amplitude displacement [20], and 4) phase variation between the rotational and transverse base excitations. Figure 6-5–Figure 6-8 show that the resonance frequency decreased every time the test was repeated, due to continuous accumulation of fatigue damage. In each individual case where the phase was held constant, nonlinear material 'softening' amplified the beam tip response each time the test was

repeated, as shown in Figure 6-9. In other words, the increase in the number of cycles increased the beam tip response amplitude.

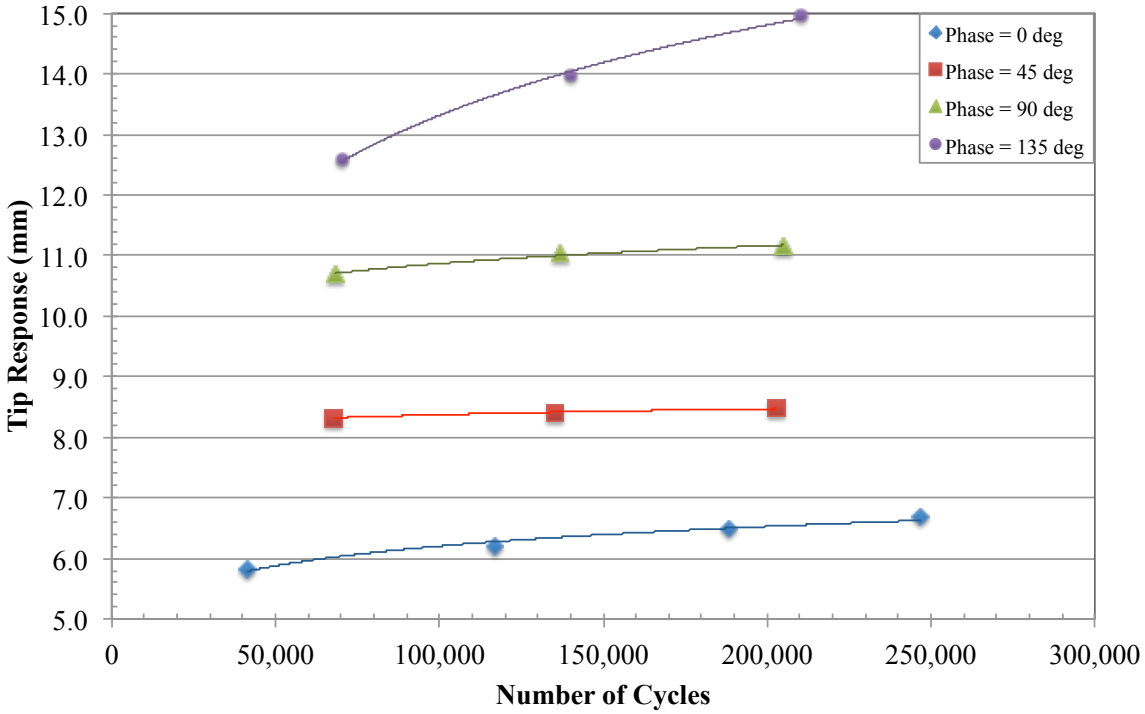

Figure 6-9. Tip response as function of cycles, at four different relative phases, due to 70 rad/s^2 and 0.3 g base rotation and transverse excitations, respectively

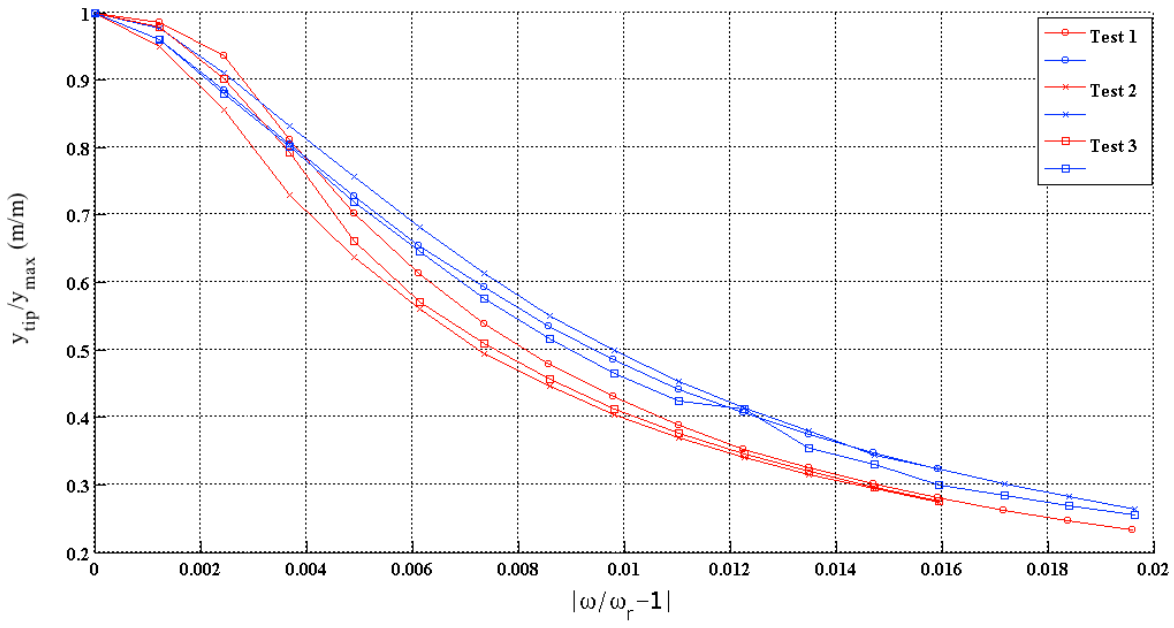

Figure 6-10. Phase $\theta = 0^o$ curves skewedness indicates slight softening effect

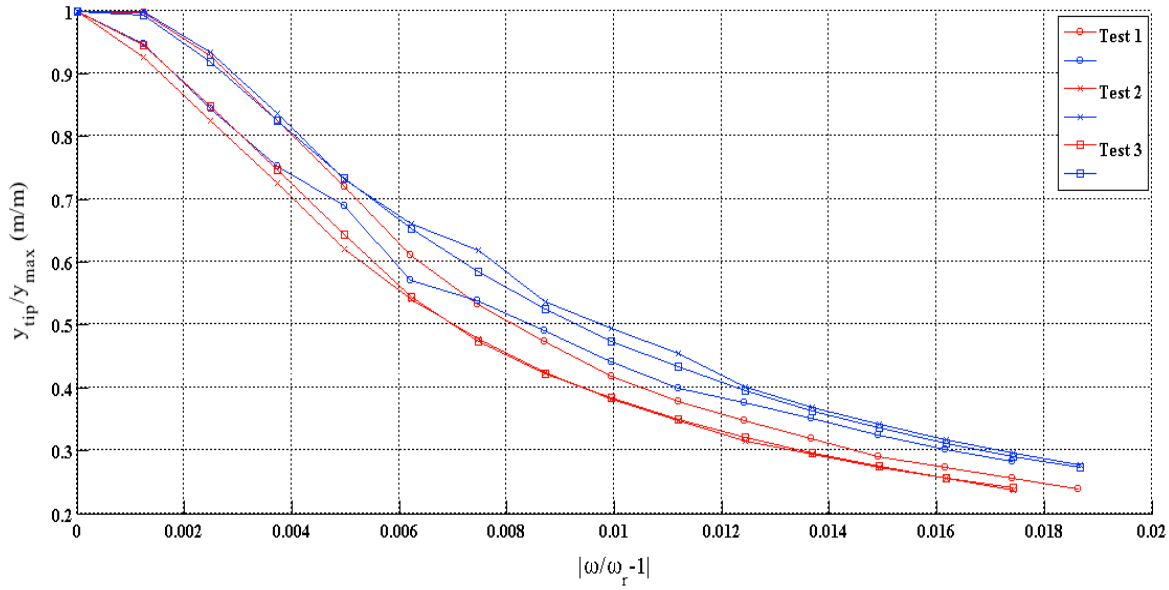

Figure 6-11. Phase $\theta = 45^o$ curves skewedness indicates softening effect

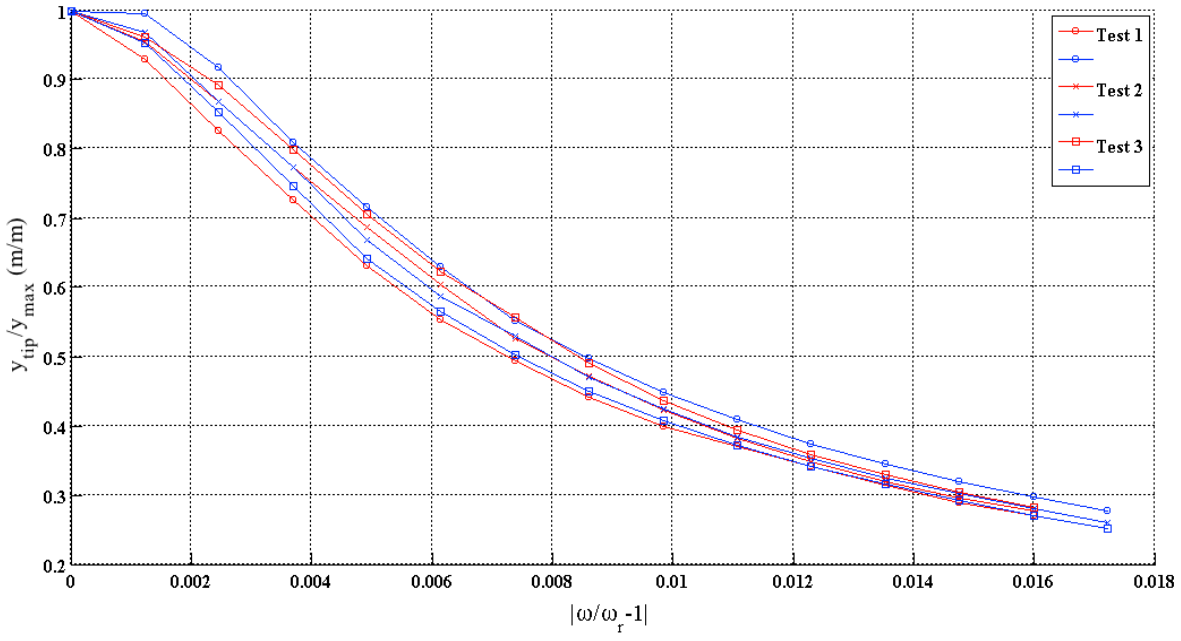

Figure 6-12. Phase θ = 90^o curves skewedness indicates no softening effect

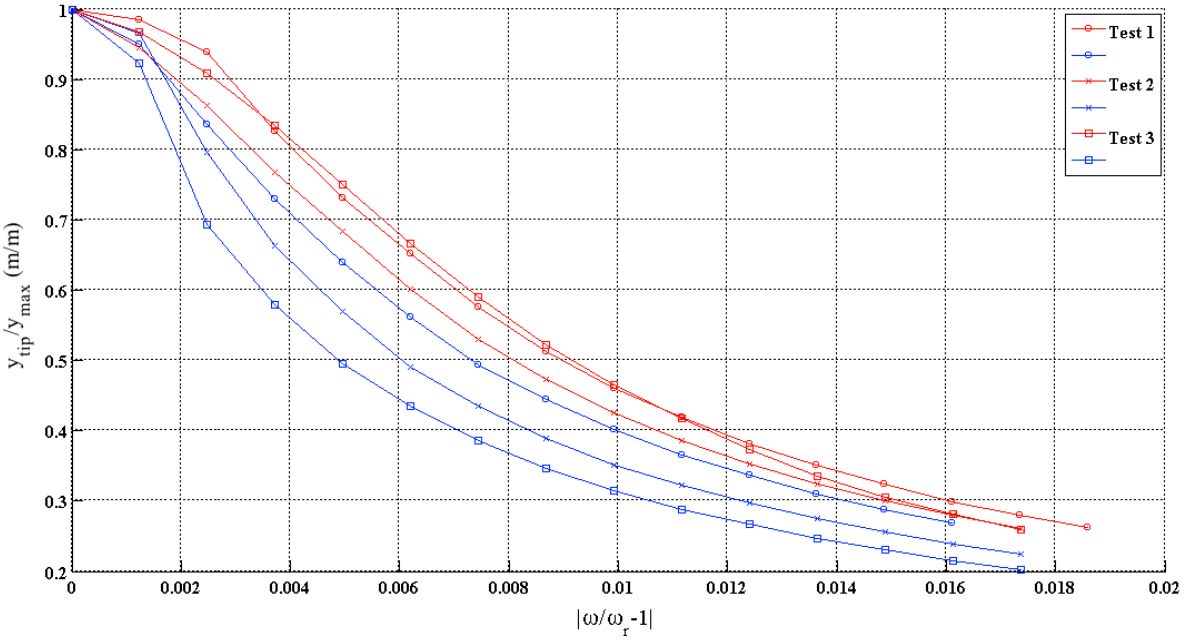

Figure 6-13. Phase θ = 135^o curves skewedness indicates stiffening effect

The frequency-response curves in Cases I, and II (θ = 0^o and 45^o) were skewed to the left, indicating that nonlinear softening surpassed the nonlinear geometric stiffening, and the

gyroscopic stiffening with time, as shown in Figure 6-5 and Figure 6-6, respectively. The appearance of no stiffening effect in Case III (θ = 90^o) is believed to be due to material 'softening' and the nonlinear geometric countered each other (Figure 6-12). The beams dynamic showed a simultaneous increase in the amplitude response and decrease in the resonance frequencies for Case IV (θ = 135^o, Figure 6-8). The shift from softening to stiffening was illustrated by normalizing the tip displacement and the excitation frequency for each test, as shown in Figure 6-10–Figure 6-13. Dividing by the maximum displacement for each curve provided a normalized tip displacement with a maximum value of 1.0 for all the tests in each case. The excitation frequency was normalized as follows:

$$\omega_{norm} = \frac{\omega}{\omega_r} - 1 \qquad \text{Eq. 6-25}$$

The subtraction of 1.0 forced the data points for each curve before and after the resonance to line-up on top of each other, thus, the effects of the phase increase on the curve skewedness can be visualized. The red and blue curves in Figure 6-10-Figure 6-13 are the beam response prior to reaching the peak amplitude and after reaching the maximum amplitude, respectively. When θ equal to 0^o and 45^o (case I and II), it can be seen from Figure 6-10, and Figure 6-11 the beam response exhibited softening behavior where the blue curves were above the red curves. In Cases I, and II, the localized material 'softening' influence was stronger than the geometric stiffening effect. The blue and red curves were nearly coincident when θ increased to 90^o in Case III (Figure 6-12). In Case III, it is likely that the increase in the tip displacement reached a sufficient level to equally counter the structural softening effect, which generated frequency responses that appeared to be linear, as shown in Figure 6-7, and Figure 6-12. The lack of skewedness was apparent in Figure 6-12.

In reality, the dynamic response for Case III was not linear due to the high amplitude displacement, where the maximum displacement reached approximately 11 mm. The structural stiffening response became more apparent in Case IV, when θ increased to 135^{o}, as shown in Figure 6-8. The skewedness of the response curves for Case IV was shown in Figure 6-13, where the red curves moved above the blue curves. It is also important to point out that the gaps between the beam tip response prior to reaching the maximum displacement amplitude (blue curves) and post the maximum displacement (red curves) were wider for Case I, II and IV when the softening or stiffening effects dominated. However, the gaps were much narrower for the Case III when the phase and tip displacement were 90^{o} and 11mm, respectively. Thus, the frequency response curves in Case III may appear linear (Figure 6-7 and Figure 6-12), but in reality stiffening and softening nonlinearities counteracted each other. This observation was found in the forward-stepping dynamic experiments and may not be applicable to backward-stepping. The backward-stepping effect may have different and important consequences in nonlinear excitation, which will be the subject of future studies.

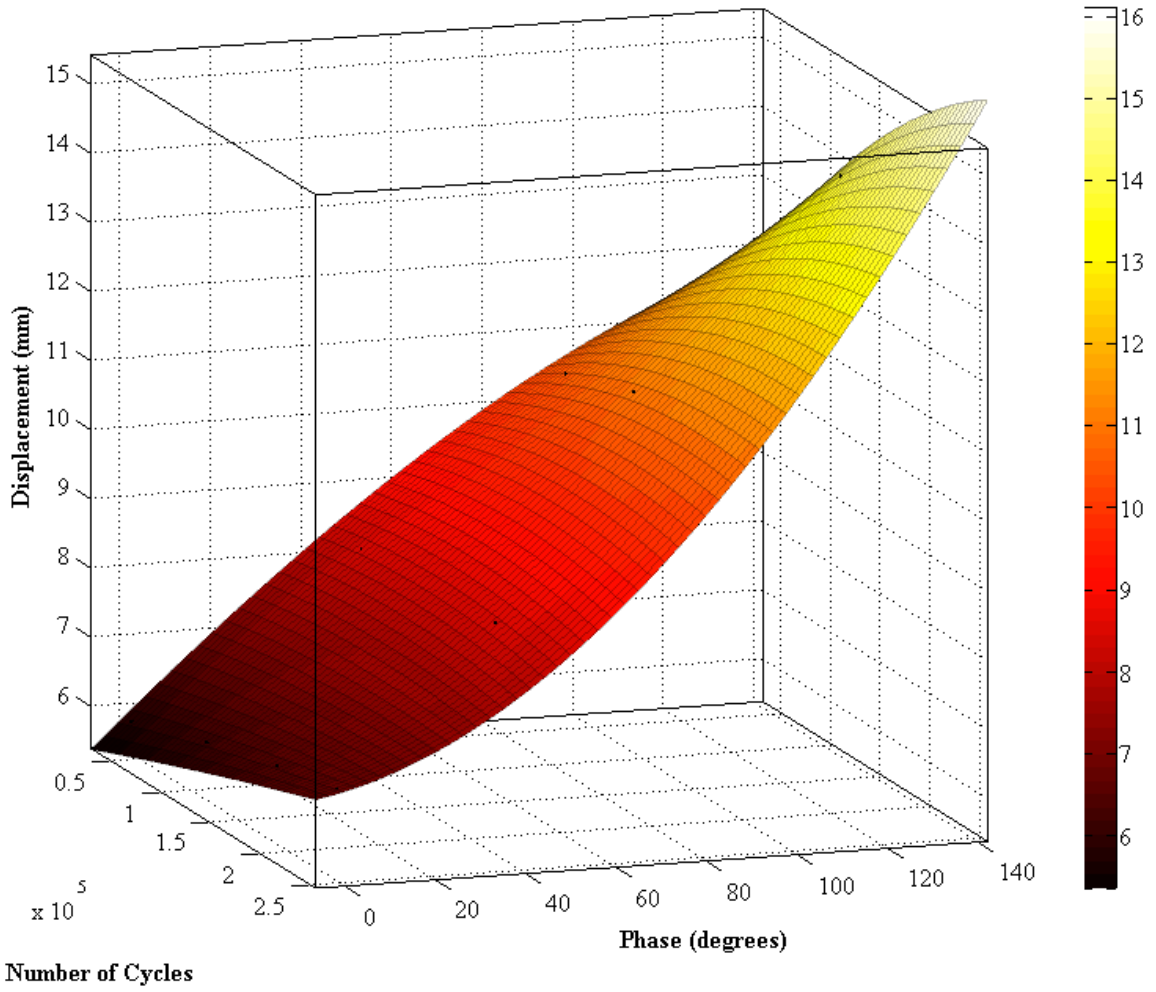

Figure 6-14. Beam tip response as a function of cycles and phase

The accumulation of loading cycles led to continual fatigue damage accumulation, resulting in a corresponding reduction in the local stiffness, when the excitation phase was less than 90^{o}. Beyond 90^{o} the beam frequency response curves are skewed to the right indicating that the beam was stiffening, but the resonance frequency shifted to the left and the maximum displacement amplitude increased for each test, as shown in Figure 6-8. The decrease in the resonance and increase in the amplitude response as a result of loading cycles accumulation of are clear evidence of fatigue damage precursor build up. The experimental results also demonstrated that the simultaneous increase in the loading cycles and phase

angle between the rotation and transverse excitation increased the beam tip response, as shown in Figure 6-14. The contour in Figure 6-14 is produced by preforming a curve fit on the frequency response data obtained from the experiments. The sum of squares due to error (SSE) and the adjusted R^2 statistics are 0.02585 and 0.9998, respectively. The SSE and R^2 values suggest the model fits the data well. A SSE statistic value closer to zero is an indication of a better fit. The adjusted R^2 statistics is generally an indicator of the fit quality. The polynomial fit is:

$$v(\theta, N) = p_{0,0} + p_{1,0}\theta + p_{0,1}N + p_{2,0}\theta^2 + p_{1,1}\theta N + p_{0,2}N^2 + p_{3,0}\theta^3 + p_{2,1}\theta^2 N$$

where, *N* is the number of cycles and polynomial coefficients (with 95% confidence bounds) are: $p_{0,0}$ = 5.592 , $p_{1,0}$ =0.06369, $p_{0,1}$ = 5.527E-06, $p_{2,0}$ = -0.0001469, $p_{1,1}$ = -1.17E-07, $p_{0,2}$ =-4.16E-12, $p_{3,0}$ =-2.667E-07, and $p_{2,1}$ = 2.081E-09.

It is important to point out that Figure 6-14 curve fit are applicably only to the structural configuration tested in this study using forward-stepping excitations. The displacement response as a function of the number of loading cycles and the phase angle between the base excitation can be use as a fatigue damage precursor indicator. Response contour plots of representative mechanical component similar to Figure 6-14 can be generated experimentally and stored in a structural health monitoring system to track the health of the component and provide dynamic control laws to adapt to health of the structure. Ideally, the structural health monitoring system can determine the number of loading cycles based on the displacement and loading conditions.

6.4.2 Model Results and Discussion

The combined rotational and transverse base excitations investigated in this study produced a nonlinear displacement response, which caused localized damage manifested by changes in the material compliance near the clamped boundary. The linear dynamic theory is not adequate in assessing the structural degradation or the effects of the high amplitude excitations and phase variation between the base excitations. Hence linear dynamic theory limits the accuracy of the structural response and endurance. Nonlinear structural dynamic analysis, which takes into account the effects of the nonlinear coefficients due to multiaxial excitations, was implemented. The nonlinear equation of motion, Eq. 6-24, was solved numerically using the Runge-Kutta method, where the integration time step was 10^{-5} s. The initial displacement and velocity were set equal to zero. The integration time limits were set from 0 to 30 s to ensure that steady state condition was reached. The accelerometer's mass was included in the model. The experimental rotational and transverse base excitations amplitudes were used as vibration load inputs in the models, which were 70 rad/s^2 and 0.3g, respectively. The equation of motion was solved for four phase angles: 0^o, 45^o, 90^o, and 135^o (Figure 6-15). The rotation and transverse excitations frequencies were maintained identical in both analytical and experimental studies. The rotation and transverse excitations frequencies ω/ω_r ranged from approximately 0.985 to 1.015 Hz/Hz.

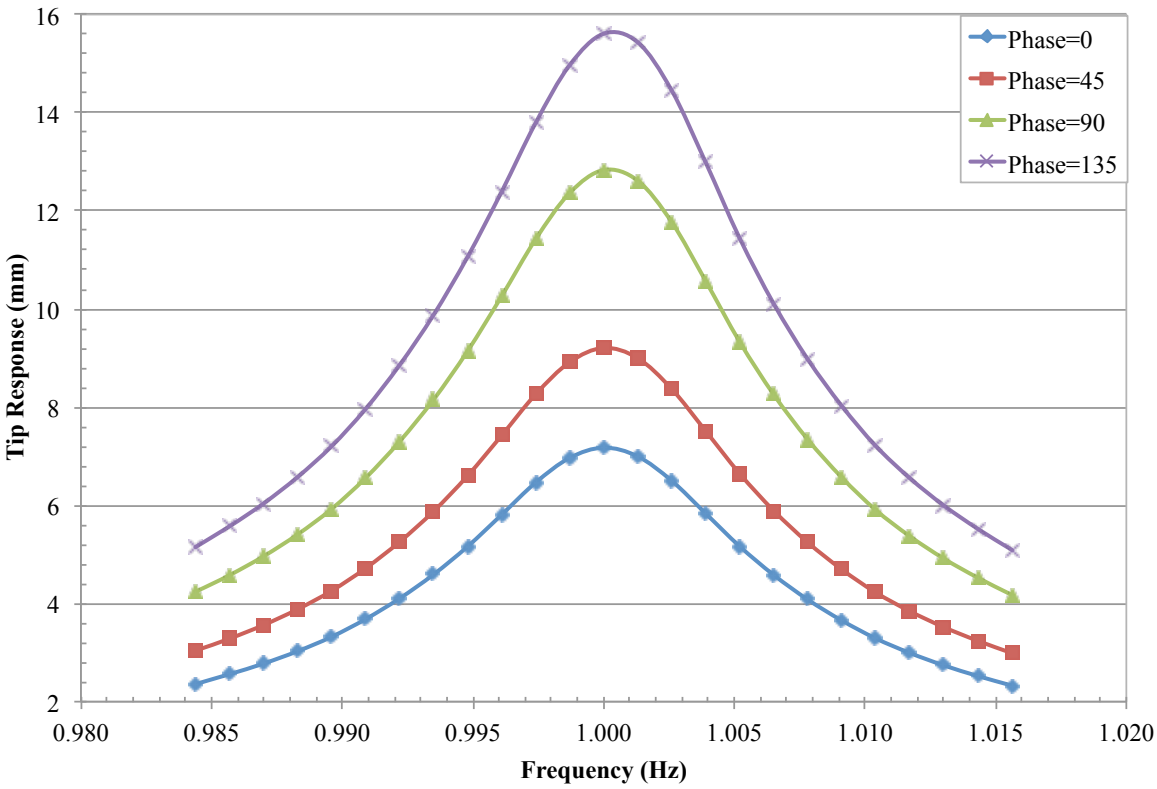

Figure 6-15. Tip response due to 70 rad/s^2 and 0.3g base rotation and transverse excitations,

The absolute values of the beam tip response obtained from the model (Figure 6-15) for various phase angles did not agree with the experimental results. However, there were common trends between the experimental and modeling results; e.g. the beam tip displacement amplitude increased with an increase in the phase angle between excitations, while holding the rotation and transverse excitations frequencies identical. Additional dynamic analysis was conducted to capture the maximum tip displacement amplitude for phase angles from 0^o-360^o (Figure 6-16). The tip maximum amplitude increased as a function of phase until reaching 180^o angle (Figure 6-16). The response amplitude decreased after increasing the phase angle beyond 180^o. Figure 6-16 provides clear evidence that the effect of the phase angle is periodic. Increasing the phase angle from 0^o-180^o increased the tip

response from 7.17 to 16.65 mm, respectively, without any increase to the excitation amplitudes. Increasing the phase angle from 180^{o}-360^{o} brought back the tip displacement from 16.65 to 7.17 mm, respectively. Thus, the dynamic response of a structure can be tuned by manipulating the phase angle between axes of excitations to achieve an optimal performance, while maintaining a stable structure. This type of structural control can be achieved without changing the base excitation magnitude or frequency.

The calculated maximum strain values are listed in Table 6-1. These strain values show that the beam response is still nominally within the elastic limit of the material. However, the shift in the natural frequency is a clear indication that fatigue damage is occurring. The analytical model did not take into account the effect of vibration fatigue cycles in this study, but it will be the subject of future multiaxial vibration research.

The fatigue damage accumulation is the primary cause of the model deviation from the experimental results. Malatkar [21] encountered similar softening phenomena in a cantilever beam exposed to transverse nonlinear base excitations. Malatkar avoided fatigue damage due to the high amplitude loading by reducing the duration and number of dwells and repeating each experiment only twice [21]. Limited experimental results have substantiated the rationale of our softening assumption for the fundamental mode [22, 23], where they observed softening phenomena at the fundamental frequency when studying harvester piezoceramics, but did not provide any explanation. Stanton et al. [24] assumed that the nonlinear softening was due to material nonlinearities in their piezoceramic device. Villanueva et al. [25] encountered the softening response for the first mode of a nano-cantilever beam, where they assumed residual stresses due to the fabrication process as a possible instigator.

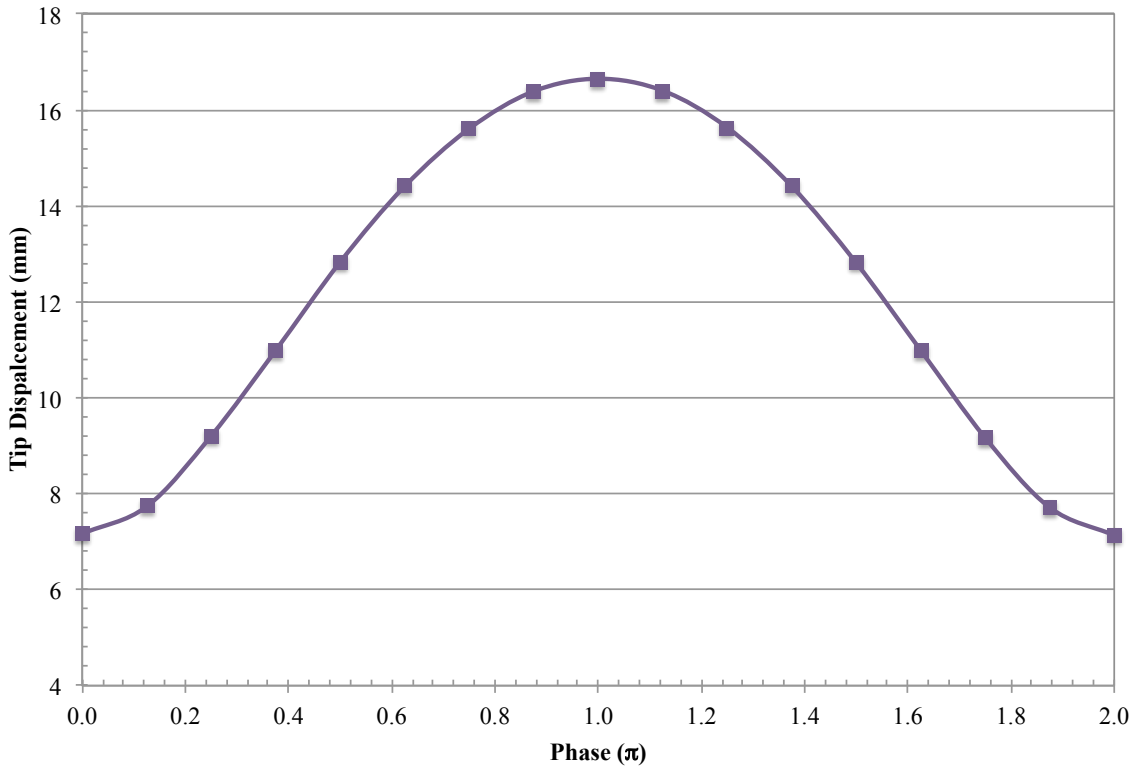

Figure 6-16. Tip response, as a function of phase due to 70 rad/s^2 and 0.3g base rotation and transverse excitations

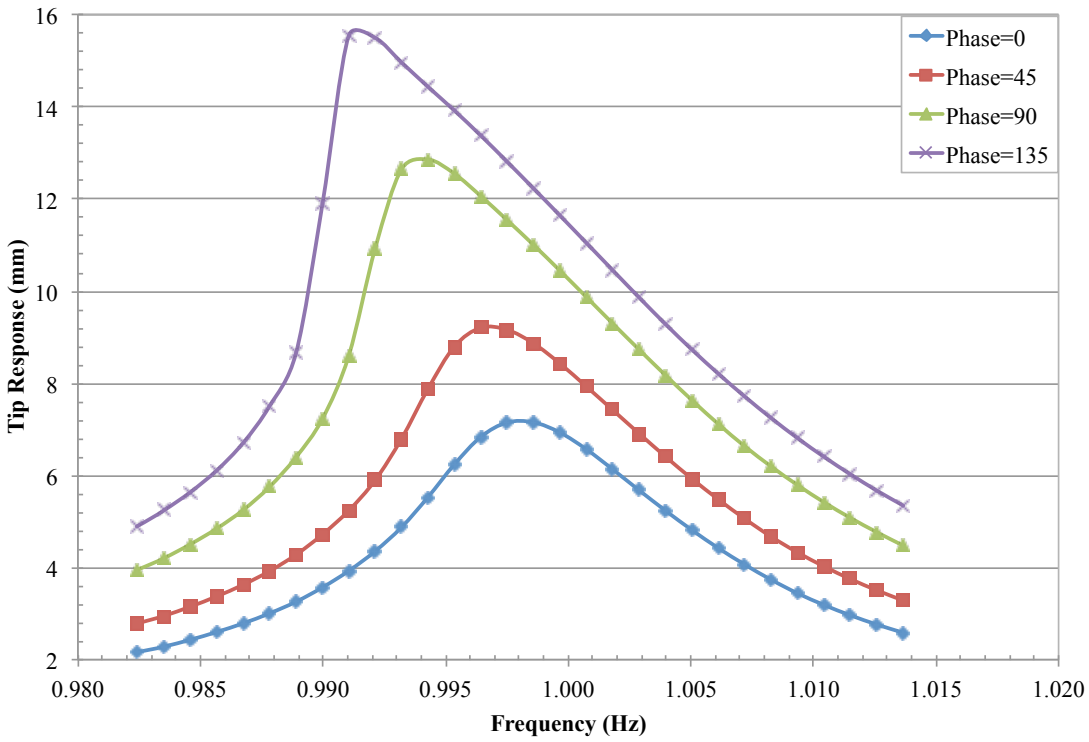

Figure 6-17. Tip response due to 70 rad/s^2 and 0.3g base rotation and transverse excitations, δ=-0.5 (nonlinear adjustment factor)

In a previous uniaxial transverse vibration study, Habtour et al. [14] introduced a modified nonlinear stiffness, K^*, which was the geometric stiffness, k_2, multiplied by the nonlinear adjustment factor, δ. Habtour et al. approach provided good agreement between the experiment and model results for uniaxial transverse harmonic translation of the base. Their experimental and numerical results showed that the nonlinear adjustment factor decreased as the number of loading cycles increased [14]. Furthermore, δ was negative value in the present of material microplasticity and positive in the existence of structural stiffening. Adjusting the nonlinear stiffness approach was examined for δ= -0.5 and -1.0, as shown in Figure 6-17, and Figure 6-18, respectively. Adjusting δ captured the softening and stiffening trends seen in the experiments not, but was not sufficient enough to match the experimental

values. This is due to potential micro-plasticity in structures under complexity of multiaxial dynamic loading influences additional nonlinearities besides k_2 that must be considered. Habtour et al. confirmed the reduction in the local stiffness of the beam surface near the clamed boundary by applying nano-indentations at high stress concentration sites within 0-10 mm distance from the clamped boundary [14]. They also witnessed changes in the microstructure near the clamped boundary using Scanning Electron Microscope (SEM). Thus, micromechanics models must be coupled with dynamic models to improve the structural response prediction. A quantitative investigation of fatigue contribution under combined multiaxial loading is the subject of future studies and is beyond the scope of this chapter.

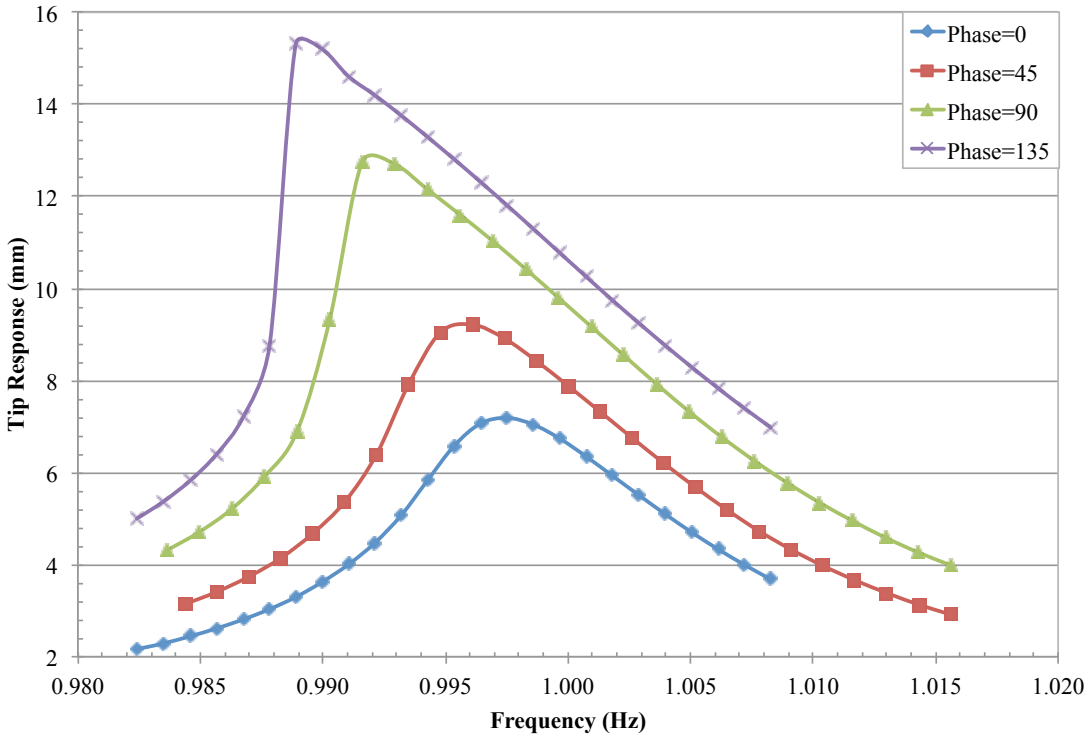

Figure 6-18. Tip response due to 70 rad/s^2 and 0.3g base rotation and transverse excitations, δ=-1.0 (structural softening)

The application of the principle of linear superposition was investigated in this study. For single axis transverse excitation, the rotation base excitation was set equal to zero. Thus, the equation of motion becomes:

$$a_1\ddot{q} + a_2(q^2\ddot{q} + q\dot{q}^2) + c\dot{q} + k_1 q + k_2 q^3 = a_4\dot{V}_Y \qquad \text{Eq. 6-26}$$

For single rotation base excitation, the transverse base excitation was set equal to zero. Thus, the equation of motion becomes:

$$a_1\ddot{q} + a_2(q^2\ddot{q} + q\dot{q}^2) + c\dot{q} + a_3\dot{\Omega}_X q^2 + (k_1 - h_1\Omega_X^2)q + (k_2 - h_2\Omega_X^2)q^3 = a_5\dot{\Omega}_X \qquad \text{Eq. 6-27}$$

The response of the cantilever beam due to transverse, rotation and combined base excitations was calculated and compared to the superposition approach, as shown in Figure 6-19. The tip beam response for both 0.3g transverse and 70rad/s^2 rotation excitation base excitations were plotted separately in Figure 6-19. The results were compared to the nonlinear combined excitation, where the relative phase, θ, was set equal to zero. The beam response due to the combined excitation can be seen to be lower than the response due to the rotation base excitation by approximately 38%. The reason for the reduction in the beam response is due to combined transverse and rotation base excitations at θ=0, which were expressed by the terms $a_4\dot{V}_Y$, and $a_5\dot{\Omega}_X$ in the full equation of motion (Eq. 6-24). When examining the velocity vector in Eq. 6-5, one can notice that the base velocity, V_y, and rotation velocity, Ω_X, have opposing signs in the unit direction $\boldsymbol{i}_Y$. On the other hand at θ=180, the sings for V_y, and Ω_X are the same, thus higher excitation energy is transited into the system. The cross-axis coupling has also an interesting effect on the structural stiffness. In the full equation of motion (Eq. 6-24), the system structural stiffness is expressed as:

$k_1 - n_1 V_Y \Omega_X - h_1 \Omega_X^2$. Thus, cross-axis coupling, $n_1 V_Y \Omega_X$, reduces the overall structural stiffness, which would increase the beam tip amplitude. However, the opposing effect of V_y, and Ω_X excitations is stronger than the cross-axis coupling, $n_1 V_Y \Omega_X$. Nonetheless, for systems with significant tip mass and beam inertia the effect of the cross-axis coupling, $n_1 V_Y \Omega_X$, since n_1 is a function of ρ and M. It is worth noting that the structural stiffness term becomes a nonlinear variable parameter that changes as a function of the structural inertia. The beam response due to uniaxial transverse excitation and uniaxial rotation excitation were linearly added (superposition principle). The principle of superposition response predicted a larger tip response than the nonlinear combined excitation response by approximately 57%, as shown in Figure 6-19. The beam response prediction using the superposition principle generated overly conservative results. The high oscillation amplitude augmented the nonlinearity and exacerbated the inaccuracy of the superposition approach. To accurately estimate the dynamic response of a structure under multiaxial base excitations, it is important to include the nonlinearities in the analysis.

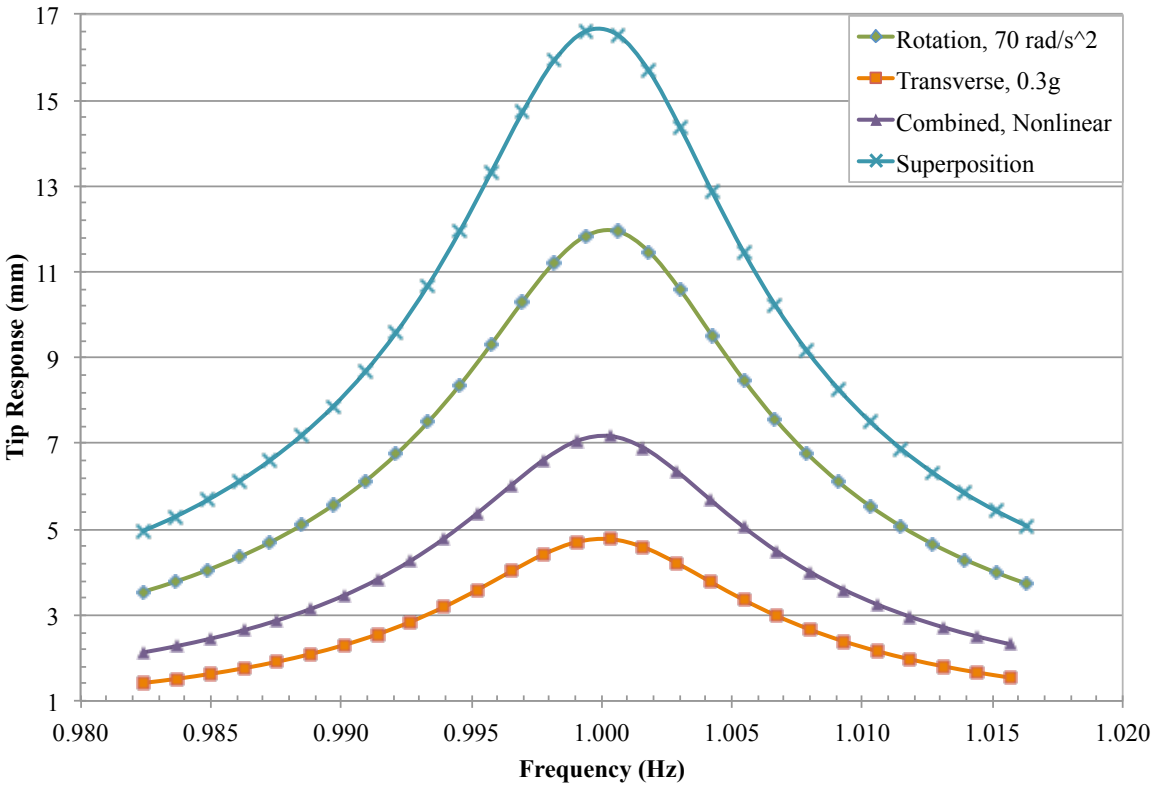

Figure 6-19. Comparison between combined (phase θ =0) multiaxial and superposition at 0.3g transverse and 70rad/s^2 rotation

6.5 Summary and Conclusion

This chapter provides a nonlinear dynamic model for cantilever beam with tip mass exposed to simultaneous nonlinear rotational and transverse base excitations. The coupling due to the multiaxial interactions is shown to contribute to the overall structural stiffness. Exploiting the sensitivity of the phase angle between the rotation and transverse base excitation enables control of the beam response without changing the loading amplitudes. The model captures only the dynamic stiffening effects due to the nonlinear time-varying rotational excitation coupled with harmonic transverse vibration. The model and the experimental results show that increasing the phase angle between the harmonic rotation and transverse signals from 0^o-180^o increases the beam tip response. Furthermore, due to the rotational excitation and the cross-axis coupling, the structural stiffness in the equation of

motion became time varying and nonlinear. For zero phase angle, cross-axis coupling cause small reduction in the structural stiffness. Increasing the angle up to 180^o would increase the structural stiffness. The beam response decreases as the phase increases from 180^o-360^o, where 360^o is equivalent to 0^o. Although the model is successful in capturing the increase in the tip displacement amplitudes with the increase in the phase angle from 0^o-180^o, the model does not agree the absolute values witnessed in the experiments. The cause of the deviation for the experiments is because the model does not include material nonlinearity due to fatigue damage buildup. Based on extrapolation from the nonlinear dynamic studies reported in Chapters 4 and 5, the nonlinear dynamic model provided in this chapter needs further development to include potential localized change in the materials properties, even though the strain measurements in the experiments show that the beam is still in the elastic region.

It can be concluded that it is essential to understand the dynamic characteristics of mechanical structures in order to correlate damage with the nonlinear dynamic response. Studies of multiaxial excitation of nonlinear structures are lacking. In addition, comparison between uniaxial and multiaxial excitations and their impact on the structure's response are not well understood. Experimental and analytical studies are also limited for nonlinear structures under variable multiaxial rotational base excitation. Additional studies are required to understand the nonlinear effects of cross-axis coupling. Utilization of multiaxial electrodynamic vibration technologies with high controllability may enable the development of nonlinear dynamic models that incorporate material damage precursors due to distributed microstructural damage prior to crack initiation. Understanding the coupling effects due to multiaxial base excitation is an important step in predicting the structural response and life-cycle of complex systems, which will be the subject of future studies.

6.6 References

[1] Nayfeh, A. H. and D. T. Mook, *Nonlinear Oscillations,* Wiley-VCH, New York, 1995.

[2] Habtour, E., C. Choi, M. Osterman, and A. Dasgupta. "Novel Approach to Improve Electronics Reliability in the Next Generation of US Army Small Unmanned Ground Vehicles Under Complex Vibration Conditions." *Journal of Failure Analysis and Prevention* 12.1 (2012): 86-95.

[3] Habtour, E., W. Connon, M. F. Pohland, S. C. Stanton, M. Paulus, and A. Dasgupta. "Review of Multiaxial Vibration in Linear and Nonlinear Structures." *Shock and Vibration* 2014 (2014): *DOI: 10.1155/2014/294271*.

[4] Ernst, M., E. Habtour, A. Dasgupta, M. Pohland, M. Robeson, and M. Paulus. "Comparison of Electronic Component Durability under Uniaxial and Multiaxial Random Vibrations." *Journal of Electronics Packaging* 137.1 (2015): n. pag. *DOI: 10.1115/1.4028516*.

[5] Paulus, M., A. Dasgupta, and E. Habtour. "Life Estimation Model of a Cantilevered Beam Subjected to Complex Random Vibration." *Fatigue & Fracture of Engineering Materials & Structures* 35.11 (2012): 1058-70.

[6] Habtour, E., M. Paulus, and A. Dasgupta. "Modeling Approach for Predicting the Rate of Frequency Change of Notched Beam Exposed to Gaussian Random Excitation." *Shock and Vibration*, vol. 2014, Article ID 164039, 2014-b. doi: 10.1155/2014/164039.

[7] E. Habtour, C. Choi, G. Drake, A. Dasgupta, and M. Al- Bassyiouni, “Improved reliability testing with multiaxial electrodynamics vibration,” in *Proceedings of the 56th Annual Reliability and Maintainability Symposium*, San Jose, Ca, USA, 2010.

[8] G. V. Chary, E. Habtour, and G. S. Drake, "Improving the reliability in the next generation of US army platforms through physics of failure analysis," *Journal of Failure Analysis and Prevention*, vol. 12, no. 1, pp. 75–58, 2012.

[9] W. E. Whiteman and M. S. Berman, "Fatigue failure results for multi-axial versus uniaxial stress screen vibration testing," *Shock and Vibration*, vol. 9, no. 6, pp. 319–328, 2002.

[10] R. M. French, R. Handy, and H. L. Cooper, "A comparison of simultaneous and sequential single-axis durability testing," *Experimental Techniques*, vol. 30, no. 5, pp. 32–37, 2006.

[11] D. Gregory, F. Bitsy, and D. O. Smallwood, "Comparison of the response of a simple structure to single axis and multiple axis random vibration inputs," in *Proceedings of the 79th Shock and Vibration Symposium*, Orlando, FL, USA, 2008.

[12] M. Esmaeili, N. Jalili, and M. Durali, "Dynamic modeling and performance evaluation of a vibrating beam microgyroscope under general support motion," *Journal of Sound and Vibration*, vol. 301, no. 1-2, pp. 146–164, 2007.

[13] V. Kumar, J. K. Miller, and J. F. Rhoads, "Nonlinear parametric amplification and attenuation in a base-excited cantilever beam," *Journal of Sound and Vibration*, vol. 330, no. 22, pp. 5401– 5409, 2011.

[14] Habtour, E., Cole, D. P., Riddick, J. C., Weiss, V., Robeson, Sridharan, R., and Dasgupta, A., "Detection of Fatigue Damage Precursor Using a Nonlinear Vibration Approach", *Journal of Structural Health Monitoring*, (under review).

[15] Anderson, T.J., B. Balachandran and A. H. Nayfeh, Nonlinear Resonances in a Flexible Cantilever Beam, *Journal of Vibration and Acoustics* 116 (4) (1994), 480-484.

[16] Balachandran, B., and A. H. Nayfeh. "Nonlinear Motions of Beam-mass Structure." *Nonlinear Dynamics* 1.1 (1990): 39-61.

[17] Hamdan, M. N., and M. H. F. Dado. "Large Amplitude Free Vibrations Of A Uniform Cantilever Beam Carrying An Intermediate Lumped Mass And Rotary Inertia." *Journal of Sound and Vibration* 206.2 (1997): 151-168.

[18] Baruh, H. *Analytical Dynamics*. Boston, MA: WCB/McGraw-Hill, 1999.

[19] Meirovitch, L. *Fundamentals of Vibrations*. Boston: McGraw-Hill, 2001.

[20] Glaz, B., Friedmann, P. P., and Liu, L., "Vibration Reduction and Performance Enhancement of Helicopter Rotors Using an Active/Passive Approach," AIAA Paper 2008-2178, Proceedings of the 49thAIAA/ASME/ ASCHE/AHS/ASC Structures, Structural Dynamics & Materials Conference, Schaumburg, IL, April 2008.

[21] Malatkar, P. *Nonlinear Vibrations of Cantilever Beams and Plates*. Diss. Virginia Polytechnic Institute and State University, 2003. Blacksburg, VA.

[22] Priya S, Viehland D, Carazo A, et al. “High-power resonant measurements of piezoelectric materials: importance of elastic nonlinearities.” *Journal of Applied Physics* 90(3): 1469–1479. (2001)

[23] Yu, S., He S., and Li W. Theoretical and Experimental Studies of Beam Bimorph Piezoelectric Power Harvesters.” *Journal of Mechanics and Materials of Structures* 5.3 (2010): 427-445.

[24] Stanton, S. C., A. Erturk, B. P. Mann, E. H. Dowell, and D. J. Inman, “Nonlinear

nonconservative behavior and modeling of piezoelectric energy harvesters including proof mass effects," *Journal of Intelligent Material Systems and Structures*, vol. 23, no. 2, pp. 183–199, 2012.

[25] Villanueva, L. G., R. B. Karabalin, M. H. Matheny, D. Chi, J. E. Sader, and M. L. Roukes. "Nonlinearity in Nanomechanical Cantilevers." *Physical Review B* 87 (2013).

Chapter 7 : Summary

This chapter contains a summary of the results contained in previous chapters, the major contributions of this dissertation, discussion of the limitations of this study and recommendations for relevant future work.

7.1 Major Conclusions

Experimental results from nonlinear vibrations of a cantilevered metallic beam showed there are three competing mechanisms that influenced the nonlinear structural response: 1) kinematic structural stiffening due to high displacement amplitude, 2) structural softening due to inertial forces and gyroscopic load, and 3) structural softening due to localized microscale evolution in the material microstructure and mechanical properties. This microstructural evolution is an early precursor to embryonic fatigue crack initiation, which can be best detected using methods of nonlinear dynamic oscillations. The hypothesis is that this fatigue damage evolution is caused by cyclic localized micro-plasticity although the macro-scale strains are well below the elastic limit. Confirming the precise nature of this fatigue-induced microstructural evolution is beyond the scope of this dissertation. Instead, the focus is on the effect of this microstructural evolution on the nonlinear dynamic response of the tested beam structure for SHM purposes.

This study found that this microstructural evolution resulted in an effective structural softening of the tested beam and a sensitive way to quantify this change was to estimate the change in the nonlinear part of the vibration response. This notional partitioning between the linear and nonlinear contributions to the total dynamic deformation of the beam was conducted with the help of an analytic nonlinear beam model. During nonlinear forward stepped-sine-dwells vibration, damage accumulation was found to decrease the structure's natural

frequency while increasing the structural response amplitude. This evolution is tracked in the dynamic model by adjusting the nonlinear geometric stiffness term in the equation of motion. The evolution of this nonlinear stiffness term was found to serve as a convenient and sensitive metric to monitor the early precursor to cyclic fatigue damage in slender structures exposed to nonlinear oscillation. It is important to note that linear vibration-based detection would have not captured the damage precursor.

This nonlinear modeling and testing exercise was conducted as SHM proof of concept for both transverse nonlinear excitation as well as rotational flexural excitation of the base. The SHM metric (nonlinear stiffness degradation) had slightly different mathematical forms in these two cases because of the different structure of their equation of motion. It is important to point out that this concept was demonstrated for a simple isotropic cantilever beam only. Therefore, additional studies are required to investigate the applicability of this concept to more complex structures.

The research outcomes also provide insights into the dynamic and structural behavior of slender cantilever beam exposed to combined harmonic nonlinear rotation and transverse base excitations. The effect of the nonlinear multiaxial coupling on the dynamic response of the cantilever beam is experimentally investigated and analytically modeled. The sensitivity of the phase angle between the rotation and transverse base excitation is an important enabler in controlling the beam response without changing the dynamic loading amplitudes. The nonlinear dynamic model captures only the dynamic stiffening effects due to the nonlinear time varying rotational excitation coupled with harmonic transverse vibration. The effect of fatigue degradation of the material is not included in the combined response model.

The experimental and analytical results show that increasing the phase angle between

the rotation and transverse from 0^o-180^o increases the beam tip response and the beam nonlinear stiffening effect. The beam response decreases as the phase increases from 180^o-360^o. Although the model is successful in capturing these general trends, it does not agree in absolute terms with the experimentally measured response. The cause of the deviation from the experiments is because the model does not include material microstructural degradation due to fatigue damage accumulation. The analytical model requires further development to include the localized plastic strain, number of dislocations, associated energy, and the stress filed caused by the location motion for each loading cycle. The enhancement of the model to include the localized material damage evolution is the subject of future studies.

It is important to point out that linear vibration-based detection would have not captured the damage precursor making the sensitivity of the nonlinear vibration approach extremely critical in monitoring the state and health of the structure materials. The simplicity of the proposed nonlinear dynamic methodology for detecting damage precursor appears to be a promising alternative to current structural health monitoring methods. The attraction of the nonlinear approach is that it utilizes conventional sensors such as accelerometers and can be implemented in many platforms without the replacement of existing sensors.

It can be concluded that it is important to understand the structural characteristics of mechanical systems to correlate the fatigue damage accumulation with the dynamic responses. The main challenge in structural systems is the prediction of the reliability and lifetime of critical components. The approach demonstrated in this study can be useful in SHM for fatigue failure modes of dynamic structures through adequate inclusion of nonlinear parameters in the analysis. The study also demonstrated the importance of experimental and analytical approaches capable of emulating real-world operational conditions, which must

include MDoF dynamic loads. This study is a first step in establishing guidelines and criteria that define multiaxial vibration testing for structural and mechanical applications dynamics.

7.2 Contributions of this Research

The contributions of this dissertation are as follows:

Although there are reports in the literature showing the effectiveness of monitoring the decrease in the natural frequency of cracked structures using health monitoring methods based on changes in linear vibration response frequency, precursor detection methods are still lacking to detect damage accumulation before any cracks are initiated [1-7]. This work expands structural health monitoring beyond crack detection and detects very early fatigue precursors by utilizing nonlinear vibration methods. Exploiting the sensitivity of the nonlinear stiffness coefficient in the equation of motion can be a viable SHM metric to sense the evolution in the material due to damage accumulation.

The experimental work is also the first to present qualitative and quantitative differences between three types of nonlinear harmonic excitations of a cantilever beam structure: transverse base excitation, rotational flexural base excitation, and combined rotation and transverse with varying phase differences. This novel set of experimentation has been possible because of a unique 6-DOF shaker facility that was available for this study. The differences in the structural response due to these three types of vibration and the effect of damage precursor are provided. The analytical model illustrates the contribution of cross-axis coupling to structural nonlinearities under simultaneous rotation and transverse vibratory loads.

The analytic models developed in this research effort allow the quantification of the

damage precursor accumulation due to complex nonlinear uniaxial and multiaxial vibration environments. These models are a substantial improvement over existing models because they allow explicit ability to exploit the sensitivity of the nonlinear equation of motion to quantify fatigue damage precursors. The decrease in the natural frequency and the structural response amplitude can be used and detection parameters to track the criticality of damage precursors. This work is the first step towards developing a more general nonlinear multiaxial vibration models for structural health monitoring. The power of the nonlinear dynamic methodology for detecting damage precursor makes it a viable alternative to current structural health monitoring systems. The attraction of the nonlinear approach is the fact that it utilizes conventional sensors such as accelerometers.

The important of connecting nonlinear dynamic to materials and solid mechanics is illustrated in this investigation. Surprisingly, the physics connecting nonlinear dynamics and fatigue mechanics are lacking. Relating the material mechanics at the micro-level to the structural nonlinear dynamics provided insights into the structural softening effect seen in the structural response as a function of the loading history. Linking nonlinear dynamics to materials and solid mechanics is a first step in guiding the health assessment of current engineering systems as well as developments of future innovative self-reporting engineering material and structures about their health. The holistic nonlinear dynamic methodology provided in this study is a fundamentally new innovation in structural health monitoring that needs further development.

7.3 Limitations and future work

The analytic models are currently restricted to one-dimensional response at the first fundamental mode of a simple cantilever beam under harmonic transverse, rotational, and

combined transverse and rotation base vibration. In general, using a cantilevered beam subject to uniaxial transverse vibration or uniaxial varying rotational base excitation, the analytical model provided good agreement with experimental results, when the geometric stiffness is adjusted. However, under combined rotation and transverse loading the analytical model captures, in general, the change in the nonlinear structural response seen in the experiments as a function of the phase angle, but does not provide adequate fit with the experimental results. The analytical model should be improved to encompass 1) higher modes, 2) three-dimensional structural response, 3) additional DOFs for more complex multiaxial vibration environments, and 4) stochastic vibratory loading.

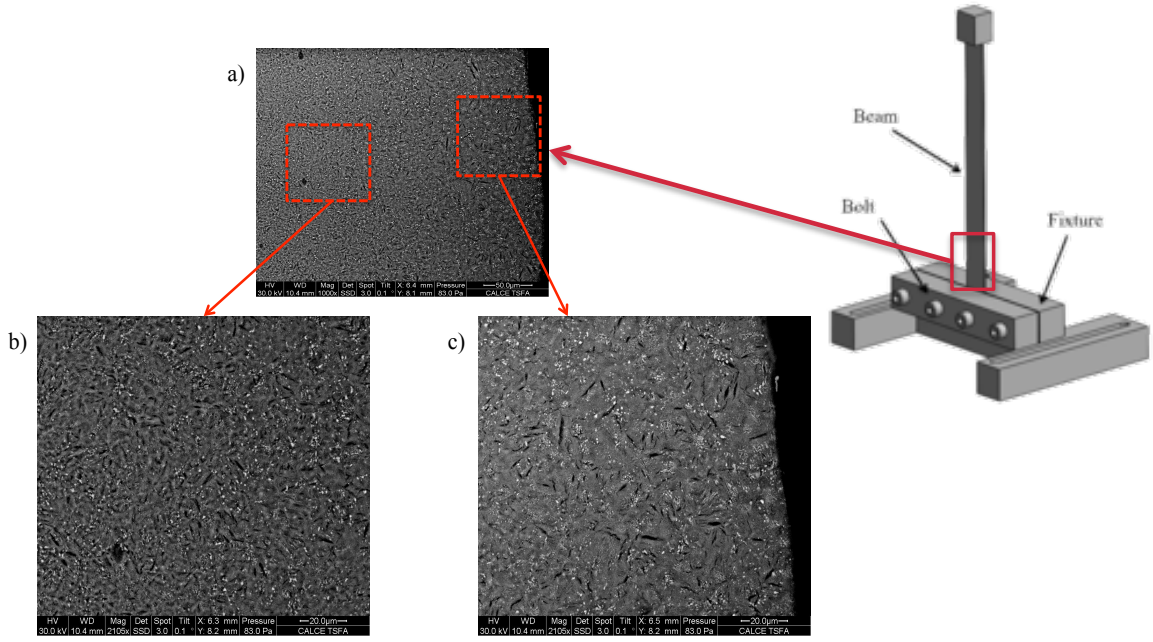

Figure 7-1. Microstructural evolution in material at high stress concentration sites at magnification: a) 1000×, b) 2100× away from boundary c) 2100× near boundary

This study demonstrated that the nonlinear dynamic model worked reasonably well for elastic response for uniaxial excitation when the nonlinear structural stiffness is parametrically calibrated based on the experimental results. The calibration is an attempt to address the localized effect of material degradation and microstructural evolution with increasing loading cycles (Figure 7-1). For engineering application, this approach can be a practical and cost effective

method for structural health monitoring. A structure can be tested in a laboratory environment to extract nonlinear engineering model or a library of models to obtain the nonlinear parameters for the appropriate loading cycles. However, future detailed investigation is necessary to develop possible nonlinear factors that could be introduced in the analytic model.

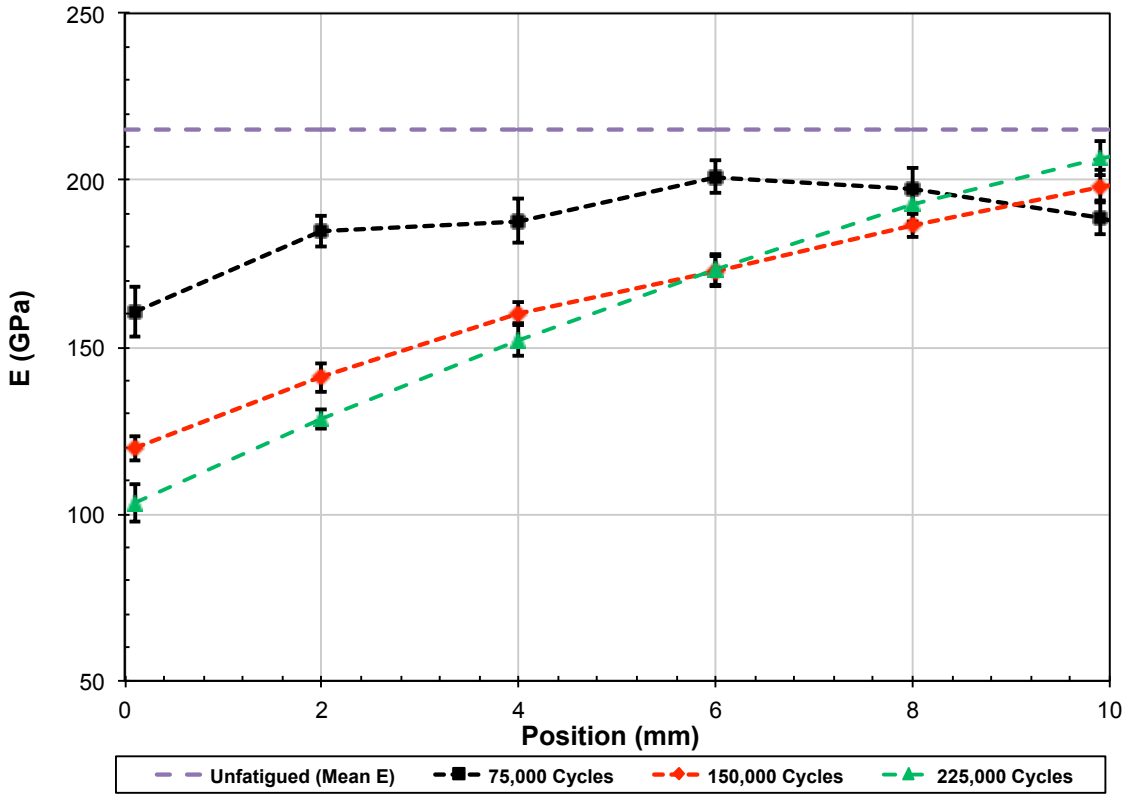

Figure 7-2. Local mechanical characterization of fatigued beams as determined by nano-indentation

A preliminary investigation was conducted during this study to verify the progression of material micromechanical properties as a function of loading cycles. Nano-indentation testing was utilized to measure the local apparent stiffness of the beam samples near the fixed boundary, which was the high stress concentration site (Figure 7-1). The vertical cantilever beams (Figure 7-1) were exposed to 0.3g harmonic excitation at their fundamental frequencies. Four samples are selected after 0 (unfatigued), 75,000, 150,000, and 225,000

loading cycles. For each targeted location, 25 indentations are performed in a 5×5 grid, spaced 5 μm apart along the central axis of the top surface of the beams. The indentation measurements were positioned approximately 2 mm apart, starting from the fixed boundary position and moving toward the beam-free end, as shown in Figure 7-2. Measurements were performed in load control mode, with a maximum applied force, *P*, of approximately 5000 μN. The applied forces resulted in indentation depths of approximately 150–200 nm. The indentation results are shown in Figure 7-2. x=0 indicates the clamped edge of the cantilever beam, which was the expected position of maximum stress. The apparent elastic modulus, as measured by the nanoindentor is shown as a function of position from the clamped beam end; x=0. The horizontal dotted line in Figure 7-2 shows the average apparent elastic modulus for an unfatigued sample (0 cycles). Indentation results for the fatigued specimens showed a clear reduction in the apparent local elastic modulus near the clamped position of the beam. The defined zero position showed average apparent elastic modulus values of approximately 160, 120, and 100 GPa for the samples with 75,000, 150,000, and 225,000 cycles, respectively. Moving away from the clamped position, the average apparent elastic modulus eventually approached 200 GPa, which was both the approximate baseline response of the unfatigued pristine sample and the theoretical elastic modulus of steel 1095. Quantifying the change in the micromechanical properties and integrating them into the dynamic nonlinear model to update the linear and nonlinear structural stiffness terms may improve the ability of the analytic model to predict the structural response and damage accumulation history.

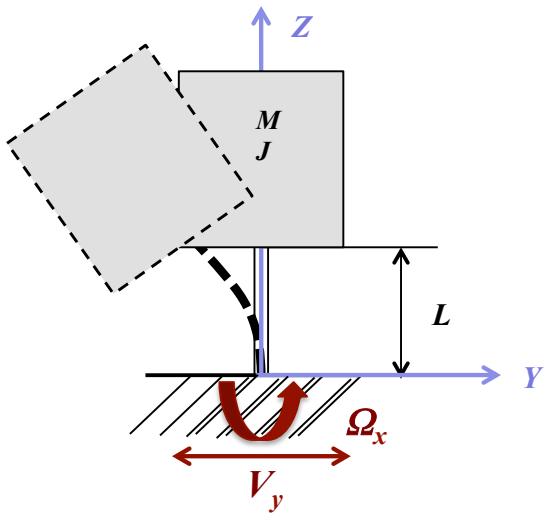

Figure 7-3. Structural component with large tip mass under complex loading

The nonlinear analytical model was verified for simple beams with small tip mass. The next step is to extend the nonlinear detection methodology for complex structures such as: electronic assemblies or complex mechanical systems. In particular, use of the model for vibration durability of solder interconnects in electronic components, where appreciable amount of viscoplasticity is present, may prove to be difficult. Furthermore, application of the model to complex structures with multiple stress concentration sites adds more difficultly. It is essential to understand the structural characteristics of large/heavy structural components in electronic devices in order to correlate the defects with the dynamic responses. The inertial and rotational effects due to the mass contribution must be investigated in future research efforts.

Higher order nonlinearities beyond the cubic terms and the beam rotational inertia were investigated as well and found to be insignificant. However, it is possible to include an additional cubic damping term of the form $\dot{q}^3$. Combining the nonlinear geometric stiffness and cubic damping terms may provide designers and structural health monitoring systems

with additional sensitivities to predict, detect, and monitor the longevity of complex system, which can be the subject of future studies.

Studies of multiaxial excitation of linear and nonlinear structures are lacking. Comparison between uniaxial and multiaxial excitations and their impact on the structure's response are not well understood. Experimental and analytical studies are also limited for nonlinear structures under variable multiaxial rotational base excitation. Additional studies are required to understand the nonlinear effects of cross-axis coupling and modal participation. Utilization of multiaxial electrodynamic vibration technologies with high controllability may enable the development of nonlinear dynamic models that incorporate materials damage precursors prior to crack initiation. Understanding multiaxial base excitation coupling is an important step in predicting the structural response and life-cycle of complex systems, which will be the subject of future studies. Acceleration factors should be explored in future to examine the range of validity of the model over larger ranges of time to failure.

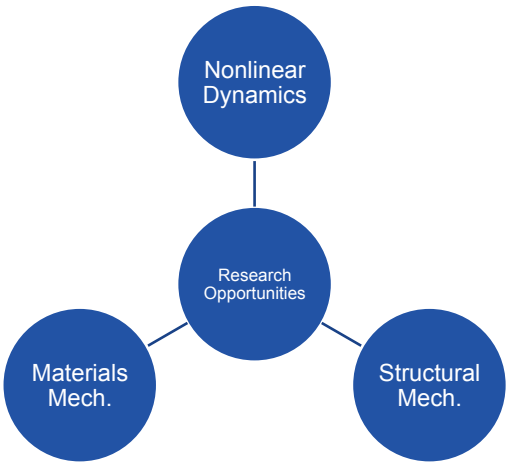

Figure 7-4. Research opportunities to bridge disparate disciplines

Finally, an interdisciplinary spectrum of research is needed develop a broader understanding of structural reliability and health monitoring by linking the nonlinear

dynamic behavior to the evolution of materials as a function of life cycle (Figure 7-4). Thus, within this interdisciplinary spectrum the following must be developed: 1) theoretical, experimental methods connecting global dynamics behavior to micromechanics, 2) contemporary techniques to address modern materials and multifunctional structures, 3) self-aware structures capable of reporting their own health, and 4) models to predict and identify damage precursors in more complex materials systems. Clearly, an interdisciplinary spectrum is needed to bridge seemingly disparate disciplines.

7.4 References

[1] E. Habtour, M. Paulus, and A. Dasgupta, "Modeling approach for predicting the rate of frequency change of notched beam exposed to Gaussian random excitation," *Shock and Vibration*, 2013.

[2] M. Paulus, A. Dasgupta, and E. Habtour, "Life estimation model of a cantilevered beam subjected to complex random vibration," *Fatigue and Fracture of Engineering Materials and Structures*, vol. 35, no. 11, pp. 1058–1070, 2012.

[3] Dimarogonas, Andrew D. "Vibration of Cracked Structures: A State of the Art Review." *Engineering Fracture Mechanics* 55.5 (1996): 831-57.

[4] Saavedra, P. N., and L. A. Cuitino. "Crack Detection and Vibration Behavior of Cracked Beams." *Computers & Structures* 79.16 (2001): 1451-459.

[5] Loutridis, S., E. Douka, and L. J. Hadjileontiadis. "Forced Vibration Behaviour and Crack Detection of Cracked Beams Using Instantaneous Frequency." *NDT & E International* 38.5 (2005): 411-19.

[6] Ryles, M., F. H. Ngau, I. Mcdonald, and W. J. Staszewski. "Comparative Study of Nonlinear Acoustic and Lamb Wave Techniques for Fatigue Crack Detection in Metallic

Structures." *Fatigue & Fracture of Engineering Materials & Structures* 31.8 (2008): 674-83.

[7] Dasgupta, A., C. Choi, and E. Habtour. "Keynote: Simulation and Test Vibration - Nonlinear Dynamic Effects in Vibration Durability of Electronic Systems." *IEEE Proc. of 8th International Conference on Integrated Power Systems (CIPS)*, Nuremberg, Germany (2014): 1-10.

Chapter 8 Appendices

Appendix A: *Modeling Approach for Predicting the Rate of Frequency Change of Notched Beam Exposed to Gaussian Random Excitation*

Published in Shock and Vibration (2014)

During fatigue damage accumulation, cracks propagate through the material leading to catastrophic failure. As the cracks propagate, the natural frequency lowers, leading to a changing stress state. A new method has been developed where the damage accumulation rate is computed in the frequency domain using Linear Elastic Fracture Mechanics (LEFM), stress intensity and the natural frequency. A finite element model was developed to predict the stress intensity and natural frequency during damage accumulation. Validation of the LEFM technique was done through comparison to experimental data. Reasonably good correlation between the FEM and the analytic model were achieved for the stress intensity and natural frequency.

Introduction

It is common knowledge that when a structure experiences vibration, a fatigue crack may eventually develop. When the crack becomes appreciably large, the natural frequency and mode shapes of the system will change [1]. Extensive health assessment work has been performed by utilizing the change in natural frequency as a damage indicator, prior to catastrophic failure. In order to make a meaningful life prediction of failure during random vibration, the change in natural frequency must be accounted for. It is possible to account for the change in the natural frequency using the virtual crack technique within the Finite Element Method (FEM).

The growing role of virtual crack simulation during the design process of mechanical components induces engineers to improve the progress of life prediction using this technique. Industries that wish to improve the reliability of products by simulation of the dynamic response often use the FEM. This approach provides a mathematically stable environment and allows for modeling structures with complex geometries, both of which are essential for industrial application.

One may simulate the level of structural weakness using the virtual crack technique to predict the remaining useful life. For example, despite the presence of cracks in the wings of a typical aircraft, the aircraft may continue to be flight-worthy as long as the cracks do not exceed the damage tolerance. Nonetheless, calculating the remaining life of structures continues to be a challenge, especially when the vibration loading is random. Many methods have been developed for fatigue life evaluation based on a representation of the stress state, both in the time and the frequency domains [2-8]. Approaches using the Power Spectral Density (PSD) and the root-mean-square acceleration, G_{rms}, were developed to obtain an equivalent maximum uni-axial stress or von Mises stress value to estimate the life of critical structures [4, 9]. Reference [3] contains an excellent survey of various equivalent fatigue damage models. Unfortunately, many of these models may not be fully suitable for a general use of the virtual approach to fatigue, especially when the frequency shifting or random dynamic loading is present.

The solution to the problem can be determined using the Rate of Frequency Change (RFC) model [10]. This model characterizes multi-axial dynamic behavior of the mechanical system in the frequency domain. The stress intensity and natural frequency for each crack extension increment are required to fully predict time to failure. The RFC model and FEM

are used to predict the life of structures experiencing random vibration. This method utilizes the frequency domain to model the crack growth. This approach incorporates the change in natural frequency and may offer reasonable predictions of the time to failure. Regardless of the structure complexity, the FEM feeds the RFC model with an updated natural frequency, f_n, and a stress intensity factor, K_I, for each virtual crack extension [10]. The model employs Linear Elastic Fracture Mechanics (LEFM) for fatigue crack propagation and accounts for the frequency shifting. The FEM development and its implementation into the RFC model are discussed in this paper. The full details of the RFC and experimental results are presented in reference [10].

The major advantage of the RFC approach is the ability to estimate time to failure in the frequency domain, where only the input power spectral density and damping factor are required. Monitoring the changes in the natural frequency and the stress intensity factor, regardless of the complexity of the geometry, may lead to a reasonable estimate of the remaining life of weakened structures. Experiments are conducted in parallel to validate the FEM models. Correlation between the analytical model and both FEA and experimental results are achieved.

Finite lelemtn Method Development

In this study, single-edge V-notched cantilever beam specimens were tested and modeled to validate the RFC-FEM coupled model, as shown in Fig 1 and 2. The beam specimens were fabricated from cold rolled 1018 steel. The cantilevered beam was 2.50in long with a cross-sectional area of 1.250x0.1875in^2, as shown in Fig. 2. The V-notch detailed dimensions are depicted in Fig. 3. The test sample was designed such that the first and second modes were closely spaced. The first bending mode in the vertical direction was

330 Hz. In the transverse direction, the first bending mode was also 330 Hz. Detailed explanation of this design is provided in reference [10]. The beam specimen was clamped by a four bolt fixture, as shown in Fig. 1. Each bolt was torqued to 30ft-lb. Final failure was defined to occur when the beam tip made contact with a limit-bar located approximately 2.5 cm below the tip of the beam, as shown in Fig.1.

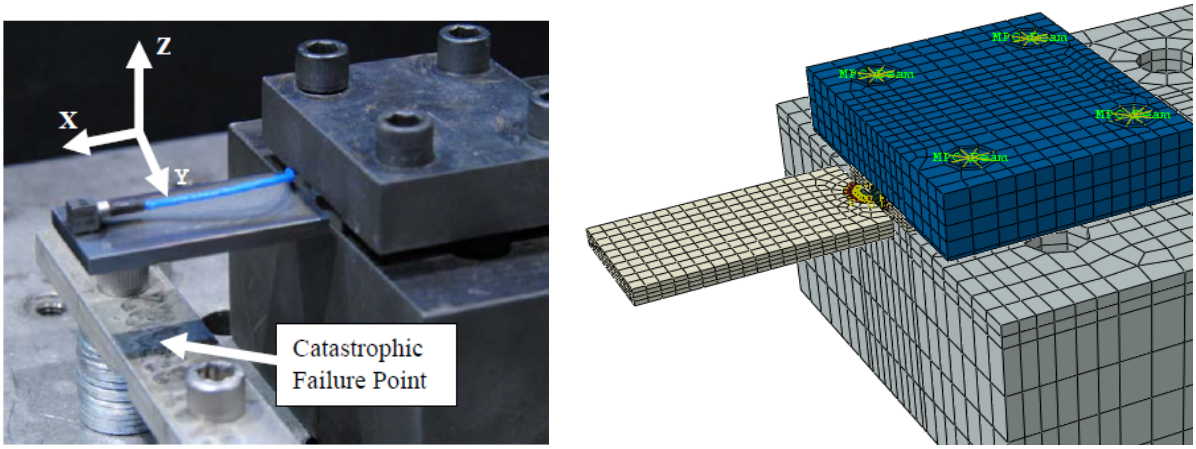

Fig. 1 Single-edge cracked cantilever beam experimental and modeling setups

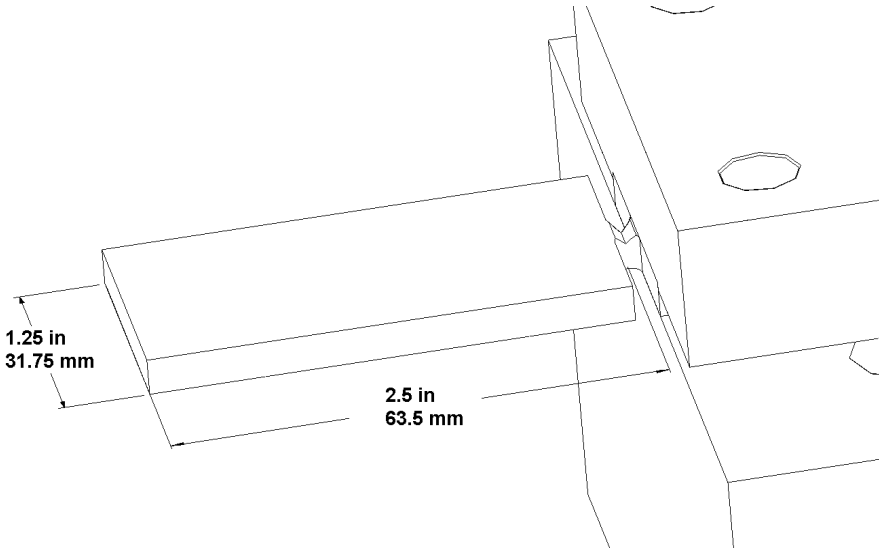

Fig. 2 Test Beam

Notches in structures increase the localized stress concentration, which decreases the maximum load the structures can sustain. Hence, a criterion to evaluate the maximum load that a notched component can sustain is vitally important. The simplest and most frequent geometries are V-notches. They are commonly observed in test samples and in notched structural components [11-13]. Studies show that the critical notch intensity factor as a function of notch angle can be used as a fracture criterion, provided that the V-notches are sharp and plasticity is contained [11, 12].

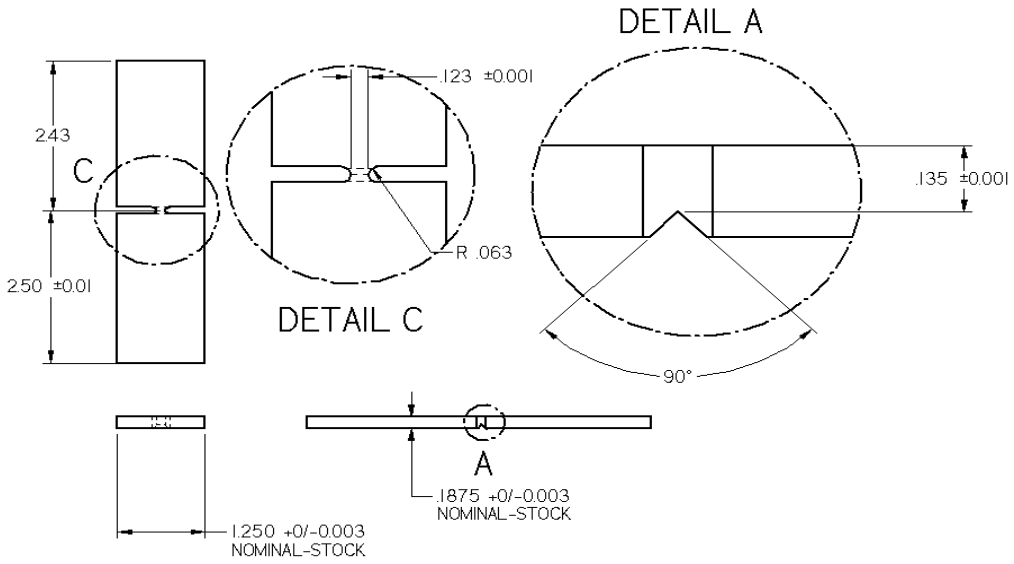

Fig. 3 Test Beam

In order to assess the validity of the RFC-FEM model, stress intensity factors and change in the frequency data were recorded for beams exposed to stationary, Gaussian, random vibration inputs. The input level was 0.0349 G^2/Hz from 20 to 2000Hz. The FEM was utilized to predict the beam modal response, track the natural frequency shift and predict the stress intensity factor for mode I, K_I. Details of the particular vibration environments are discussed in reference [10].

The K_I characterizes the local mode of the crack tip stress field in linear elastic material for mode I loading condition where the principle load is applied normal to the crack plane. Mode I of the crack surface displacement is considered to be the opening of the crack. Modes II and III are the sliding and tearing of the crack respectively. Based on the FEM modal response analysis, the beam bending is the dominating mode. Therefore, only mode I was considered in this study. The K_I depends on the applied remote stress, the geometries of the structure and the crack size as follows:

$$K_I = \sigma_r \sqrt{\pi a} Y \qquad \text{Eq. (1)}$$

where, s_r is the remote stress, a is the crack size and Y is the structure geometric factor. For simple structures, Y can be obtained from handbooks [14]. For complex structures, it is difficult to calculate Y analytically. Numerical methods such as FEM can be utilized to predict Y. Therefore, K_I was determined from FEM using the J-contour integral approach and updated as the virtual crack increased. This approach provided accurate results with surprisingly coarse mesh [13].

In designing the FEM mesh for fracture mechanics problems, the common focus is on the tip of the crack. The crack tip is a singularity point where the stress field becomes mathematically infinite. If the cracked region is modeled with conventional polynomial-based FEM, the mesh must be exceptionally dense around the crack tip. This approach may not be feasible and, depending on the problem complexity, may be costly and time consuming.

In FEM fracture mechanics, it is recommended to use 9-node bi-quadratic Lagrangian elements for two-dimensional problems and 27-node tri-quadratic Lagrangian elements in three-dimensional problems [13, 15]. The 8-node two dimensional and 20-node three-

dimensional elements are also common in crack problems. In this study, conventional 8-node fully elastics elements were used for the beam (away from the crack) and the fixture. For the area near the crack tip, 20-node elements were used and will be discussed in detail later. Multi Point Constraints beam elements were utilized to model the torqued bolts used to clamp the cantilever beam, as shown in Fig. 1. The preload value was applied to each bolt in the FEM model to produce accurate results.

The stresses near the crack tip are characterized by K_I and expressed as follows [15]:

$$\begin{bmatrix}\sigma_{xx}\\ \sigma_{xy}\\ \sigma_{yy}\end{bmatrix} = \frac{K_I}{\sqrt{2\pi r}}\cos\frac{\theta}{2}\begin{bmatrix}1-\sin\frac{\theta}{2}\sin\frac{3\theta}{2}\\ \sin\frac{\theta}{2}\cos\frac{3\theta}{2}\\ 1+\sin\frac{\theta}{2}\sin\frac{3\theta}{2}\end{bmatrix} \qquad \text{Eq. (2)}$$

For plane stress σ_{zz} is zero and for plane strain is equal to $\nu(\sigma_{xx}+\sigma_{yy})$. The displacement near the crack tip is calculated as follows [15]:

$$\begin{bmatrix}u\\ \upsilon\end{bmatrix} = \frac{K_I\sqrt{r}}{2G\sqrt{2\pi}}\begin{bmatrix}\cos\frac{\theta}{2}\left(\kappa-1+2\sin^2\frac{\theta}{2}\right)\\ \sin\frac{\theta}{2}\left(\kappa+1-2\cos^2\frac{\theta}{2}\right)\end{bmatrix} \quad \begin{matrix}\text{For plane strain } \kappa = 3-4\nu\\ \text{For plane stress } \kappa = \dfrac{3-4\nu}{(1+\nu)}\end{matrix} \qquad \text{Eq. (3)}$$

where G is the shear modulus. r and q are shown in Fig 4. It can be seen from the relationships above that the stress varies inversely with $r^{1/2}$ and the displacement varies proportionally with $r^{1/2}$. The present of a singularity of the stress at the tip was attained when r approached zero.

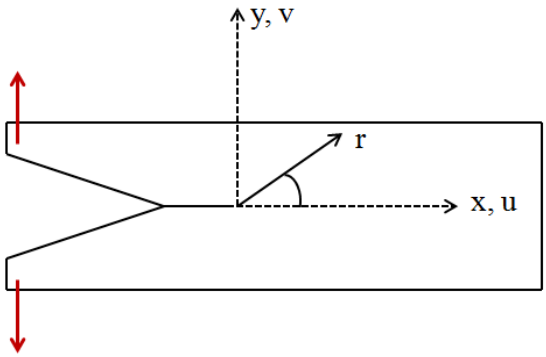

Fig. 4 Crack opening deformation

During fatigue crack growth, both plane strain and plane stress will be present along the crack front [16]. However, the conditions ahead of a crack are neither plane stress or plane strain, but require treatment in three-dimensional case [13]. The material near the crack tip is at higher stresses than the surrounding material. Since there is no stress normal to the free surface, the material on the surface is in a state of plane stress. At the mid-plane of the crack, plane strain conditions exist and σ_{zz} is $\nu(\sigma_{xx}+\sigma_{yy})$.

In this investigation, the behavior of the stress and displacement near the crack tip were modeled using 20-node hexahedral fully elastic elements degenerated down to wedges. The wedge element was identical to the 20-node quadratic hexahedral element, except the nodes facing the crack site collapsed to form a wedge, as shown in Fig. 5. Each of the red three-node edges were collapsed to one corner location, as shown in Fig. 5, while the two middle nodes collapsed into one center location. The collapsed nodes were not merged into one node, but tied together and became coincident. Subsequently, the collapsed nodes formed one line, which was the crack front. The middle nodes located at the faces orthogonal to the crack front were shifted by a quarter of the edge length closer to the crack tip. This modification enhanced the numerical accuracy without requiring significant mesh refinement to capture the crack tip stress field [13]. The final result was a "spider web" meshing

configuration at the crack tip region, as shown in Fig. 6, which is also called the "spider web" meshing technique.

As mentioned above, the stress state at the crack tip in a linear elastic material exhibits a mathematical singularity:

$$\sigma \propto \frac{1}{\sqrt{r}}$$

where, for plane stress:

$$r = \frac{1}{2\pi}\left(\frac{K}{\sigma_y}\right)^2 \qquad \text{Eq. (4)}$$

and for plane strain:

$$r = \frac{1}{6\pi}\left(\frac{K}{\sigma_y}\right)^2$$

where, s_y is the yield stress. The variable r in this case is a first order correction of the plastic zone size. In reality, the crack tip is surrounded by a zone where plastic deformation and material damage may occur. As can be seen from the FEM stress contour in Fig. 7, the crack tip caused stress concentrations, where the stress gradient became larger as the crack tip was approached. The mesh was refined in the vicinity of the crack tip to extract accurate stresses. It is important to point out that LEFM is not accurate inside the plastic zone. However, LEFM may provide accurate results provided the plastic zone is small enough. It was necessary to take advantage of Paris law to predict the crack growth as a function of time. The crack growth rate can be calculated as follows [3]:

$$\frac{da}{dN} = C\left(\Delta K_I\right)^m \qquad \text{Eq. (5)}$$

and

$$\Delta K_I = K_{I,\max} - K_{I,\min} = \Delta\sigma_r \sqrt{\pi a} Y \qquad \text{Eq. (6)}$$

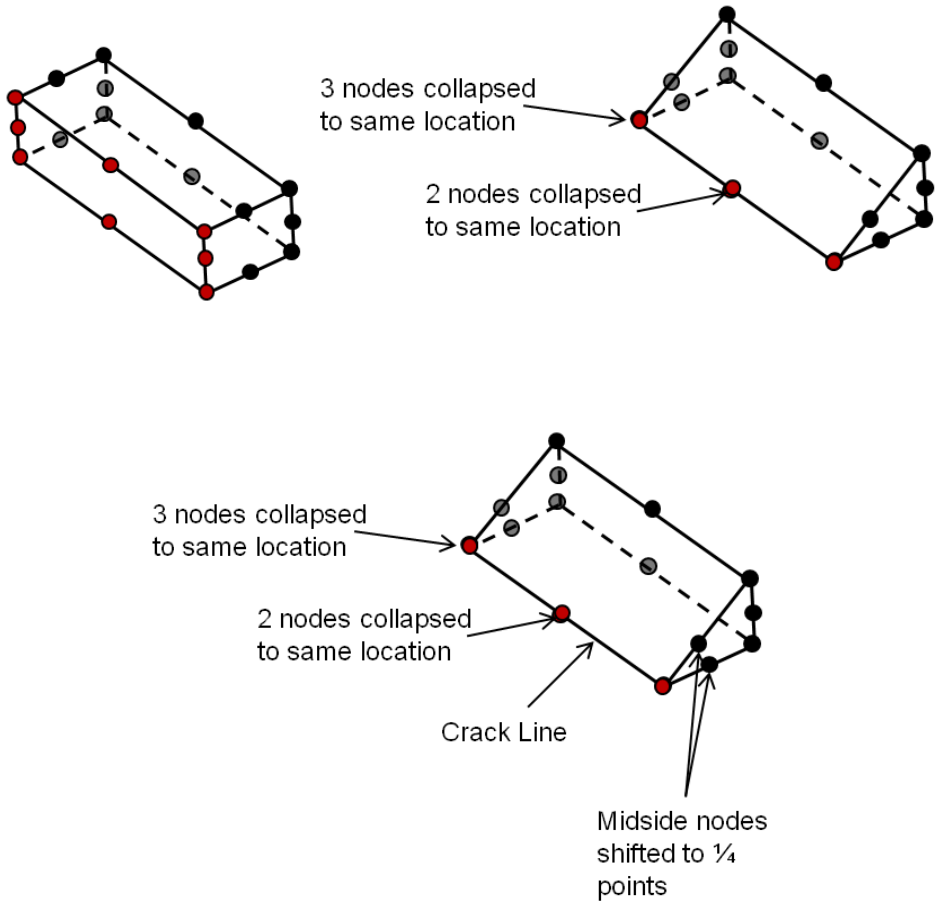

Fig. 5 20-node crack tip element (wedge)

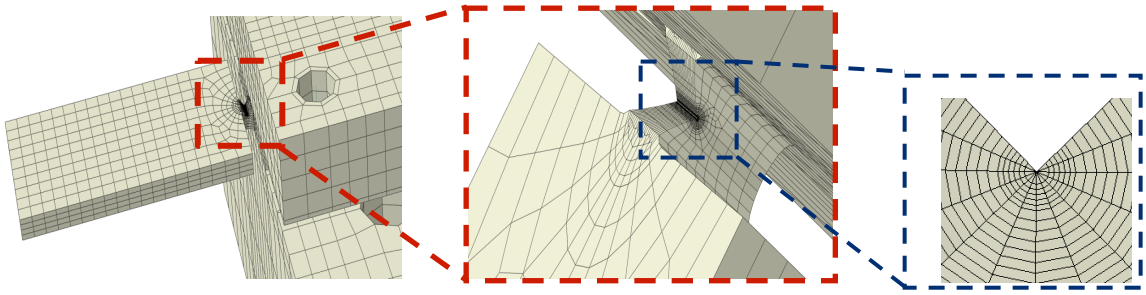

Fig. 6 Spider-web configuration mesh at the crack region

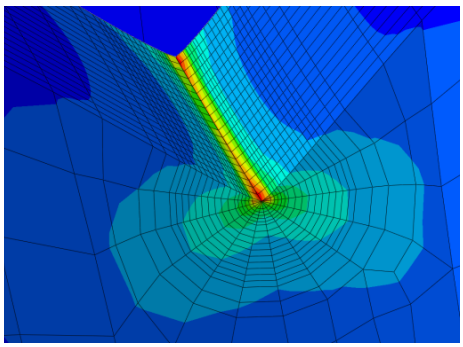

Fig. 7 Stress concentration at crack tip

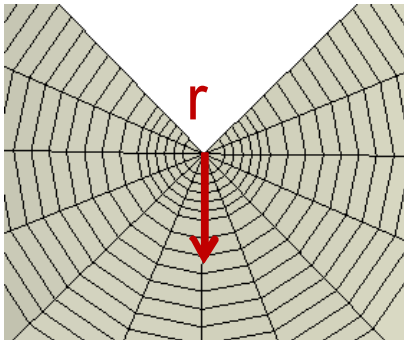

Fig. 8 Assumed virtual crack extension

where, N is the number of cycles, C and m are constant fatigue material properties, $K_{I,max}$ and $K_{I,min}$ are the maximum and minimum stress intensity factors, respectively. To apply the Paris law, the stress intensity factor was calculated by means of the J-contour integral first introduced by Rice [17]. The J-contour integral is usually used in rate-independent quasi-static fracture analysis to characterize the energy release associated with crack growth. It can be related to the stress intensity factor if the material response is linear. The J-contour integral is formulated as a path-independent line integral with a value equal to the decrease in potential energy per increment of crack extension in the material. The path independent implies that J can be seen as a measure of the intensity of stresses and strains at the tip of the notch and crack [18]. Through the J-contour integral, it is possible to calculate accurate K_I values with coarse meshes without maintaining precise local stress values. It is important to point out that the J-contour integral should be independent of the domain used; however, the J-contour integral approximations from different rings in the web-mesh may vary due to the approximate nature of the finite element solution [14]. The strong variation in these estimates is commonly called domain or contour dependence. Therefore, the spider-web mesh was refined in the crack region with 18 contours, as shown in Fig 7 and 8. Although 18 contours

might be excessive for this analysis, computing resources and the simplicity of the problem allowed this excess. Further study into the sensitivity of the results to the number of contours would be warranted. The crack front-line consisted of 21 nodes, which produced a 20-element-thick spider-web mesh, as shown in Fig. 7.

The crack front was defined on the collapsed plane of the wedge elements, which is called the "edge plane". The edge plane is orthogonal to the crack direction. Fig. 7 is a magnified image of the V-notch spider-web meshed region, where the center of the spider-web mesh is the crack front. Although not precisely true, the crack front is assumed to be a straight line. In the FEM model, the direction of the virtual crack extension was assumed to be in the downward vertical direction, which is denoted as the vector r in Fig. 8. The latter assumption is consistent with the experimental results obtained by Paulus *et al.* [10]. The virtual crack extension was updated in the FEM model manually based on Paulus *et al.* experimental results. Four virtual cracks extensions (a=0.000, 0.0206, 0.0311 and 0.0516 in) were analyzed, as shown in Fig. 9. The refined spider-web mesh at the crack tip was maintained for every crack extension.

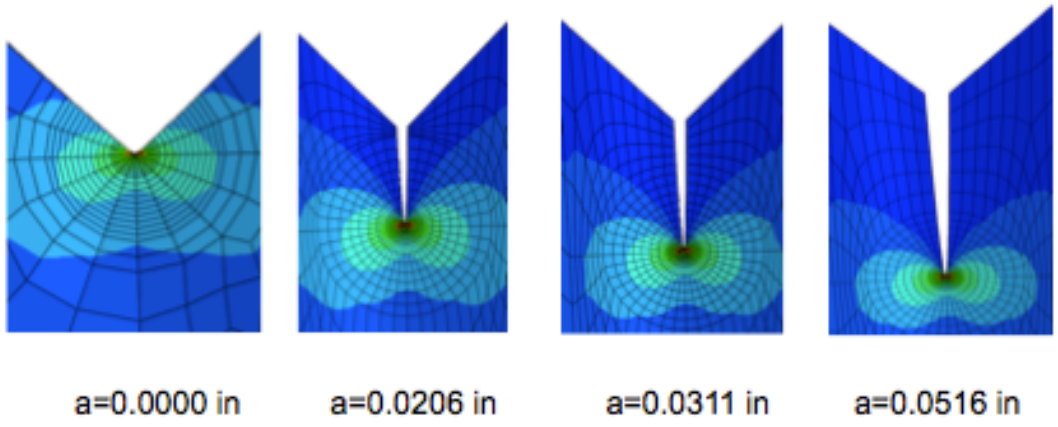

Fig. 9 Virtual crack extension

Rate of Frequency Change Model

This section describes the implementation of the RFC model. Paulus *et al.* provided the derivation of the RFC model in a separate paper [10]. The model implementation is summarized in flowchart in Fig. 10. The first step was to obtain the base excitation PSD $\ddot{w}_{PSD}$. For an equivalent single degree of freedom system, the root-mean-square relative displacement can be calculated as follows [20]:

$$y_{rms}(f_{nc}) = \sqrt{\int_0^\infty \ddot{w}_{PSD}(f)\left[\frac{1}{(2\pi)^4\left(\left(f_{nc}{}^2 - f^2\right)^2 + (2\xi_n f\, f_{nc})^2\right)}\right]df} \qquad \text{Eq. (7)}$$

where, f is the frequency and f_{nc} is the natural frequency for each crack extension. The z_n is the equivalent viscous damping coefficient. Once the relative displacement is known for a given natural frequency, the root-mean-square far-field stress range can be calculated using equivalent strain energy as follows:

$$\Delta\sigma_{rms} = E\frac{f_{nc}y_{rms}}{f_n}\beta^2 c \qquad \text{Eq. (8)}$$

where, f_n is the natural frequency for an uncracked uniform cantilever beam and E is the Young Elastic Modulus. In this study, c is the beam half height of the rectangular cross-section and b is a simplified parameter that can be obtained from the first mode Eigenvalue solution of a uniform uncracked cantilevered beam [10].

During failure, the natural frequency will change as the crack grows. Paulus *et al.* provided a general model for calculating the rate of natural frequency change, *RFC*, as follows [10]:

$$RFC(f_{nc}) = \frac{\Delta f_T f_{nc}}{a_f} C(C_{ray} \Delta \sigma_{rms} (\pi a)^{1/2} Y)^m \qquad \text{Eq. (9)}$$

where, Df_T, total change in natural frequency and C_{ray} is an equivalent damage constant based on Rayleigh's approximation. The constant C_{ray} represents a correction factor for the statistical distribution of the random vibration response, which is assumed to be narrowband, stationary and Gaussian. Determination of C_{ray} can be accomplished statistically as discussed in detail by Paulus et al. [10]. The Rayleigh's approximation can be applied when the response is narrow band, as was the case for this analysis. The *RFC* model relates the crack growth rate to the change in the natural frequency of the structure. The major advantage of this model is that time-to-failure (TTF) estimation can be conducted in the frequency domain. However, the focus of this paper is on the rate of change in the natural frequency and not TTF prediction. The FEM allows the model to be extended to structures with complex geometry, where it may not be possible to compute the equivalent strain energy or the shift in the natural frequency. Fig. 11 illustrates how the FEM can be combined with the RFC model to provide an approximate result instead of a closed form solution.

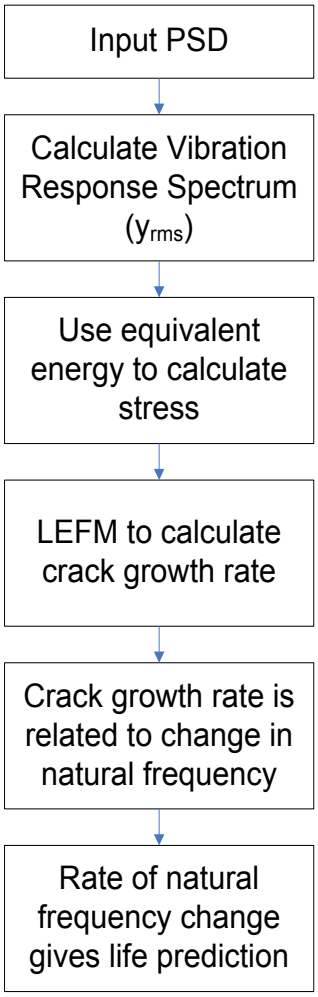

Fig. 10 Implementation of the RFC Model

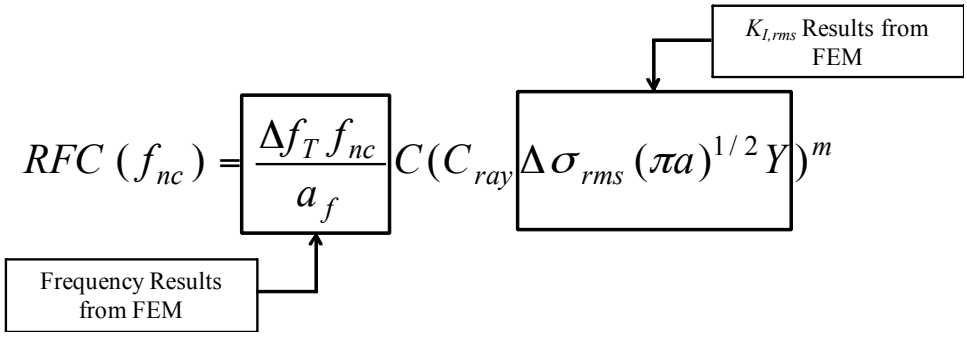

Fig. 11 FEM results feed into the RFC model

Finally, the cracked structure TTF is obtained by integrating the inverse of the RFC with respect to the change in the natural frequency as follows:

$$TTF = \int_{f_{nc\_fail}}^{f_{nc\_start}} \frac{1}{RFC} df_{nc} \qquad \text{Eq. (10)}$$

where, f_{nc_start} and f_{nc_fail} are the natural frequencies of the cracked structure at the initial life (when the crack is discovered) and end of life (when failure is reached), respectively.

Resutls

Computation of natural frequencies and the stress intensity factors as a function of the crack length were performed experimentally and numerically. In the first computation, the modal response analysis was performed for zero crack extension, a=0.000. The experimental and numerical first bending mode values in the vertical direction were 330 and 351Hz, respectively, as shown in Fig. 12. In the transverse direction, the experimental and numerical first bending mode results were also 330 and 351Hz, respectively. This analysis was repeated at varying crack depths from 0.010 to 0.114 in, as shown in Fig. 13. Although a slight bias is apparent, the FEM modal analysis shows a linear relationship between the natural frequency and the crack depth, as shown in Fig. 13. These results are in agreement with Paulus *et al.* assumption that the natural frequency varies linearly as a function of the crack depth [10]. The modal analysis also confirmed that the FEM model is correlated with Paulus *et al.* experimental results. Therefore, when analytical tools are unavailable or the structure geometry is complex, the rate of frequency shift from the FEM tool can be combined with the RFC model to calculate the remaining life, as shown in Fig. 11.

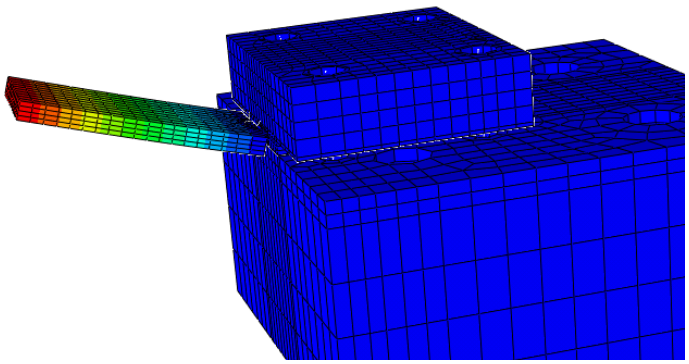

Fig. 12 First mode for crack extension, a=0.000in natural frequency shift

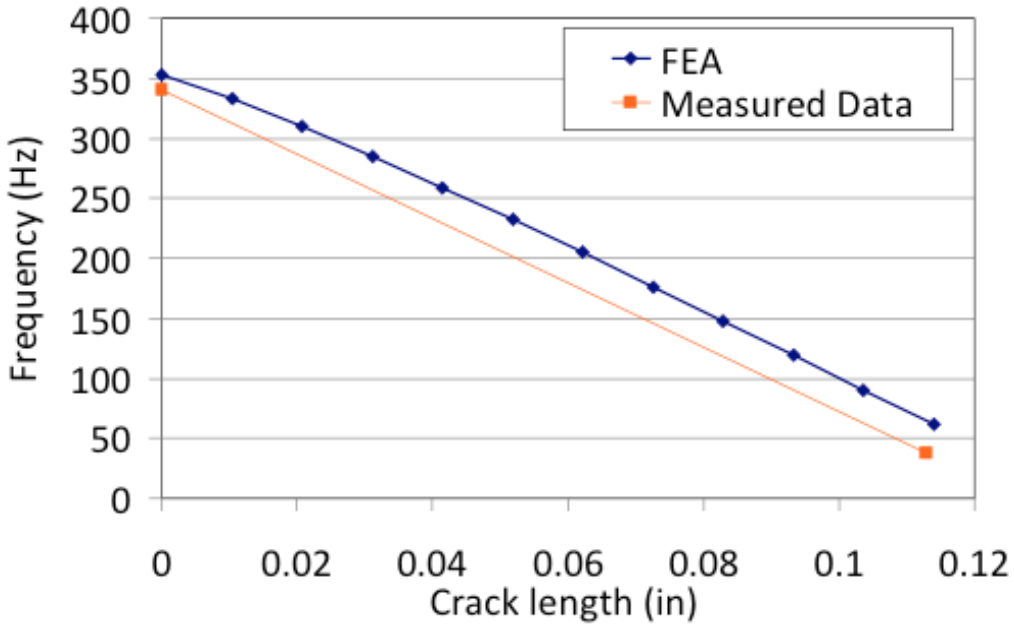

Fig. 13 FEM and experimental

The second computational analysis consisted of predicting the stress intensity factors for crack extensions: a=0.0000, 0.0206, 0.0310 and 0.0516 in, as shown in Fig. 14. After a=0.0516, the beam started to experience excessive plasticity, which meant the use of the stress intensity factor was no longer possible, but the experiment was conducted to full failure. The stress intensity factor was calculated by applying a static load at the tip of the

beam that was equivalent to the rms dynamic load obtained from the experiments performed by Paulus *et al.* [10]. For the zero crack case, both FEM and analytical methods were used to calculate the K_I for each node along the crack front-line, which consisted of 21 nodes. The analytic stress intensity was determined using handbook calculations as described in [10]. The distribution of the stress across the cross section was required to determine the stress intensity factor. This distribution of stress was determined using the stress concentration factor as determined by FEM. An average K_I was calculated for each node on the crack front-line. Eighteen contours (rings) in the spider-web mesh were included in the calculations to insure that the *J*-contour integral was not domain dependent (or contour dependent). This is because the stress intensity factors have the same domain dependence features as the *J*-contour integral. Numerical tests suggest that the estimate from the first ring of elements adjoining the crack front does not provide a high accuracy result [21].

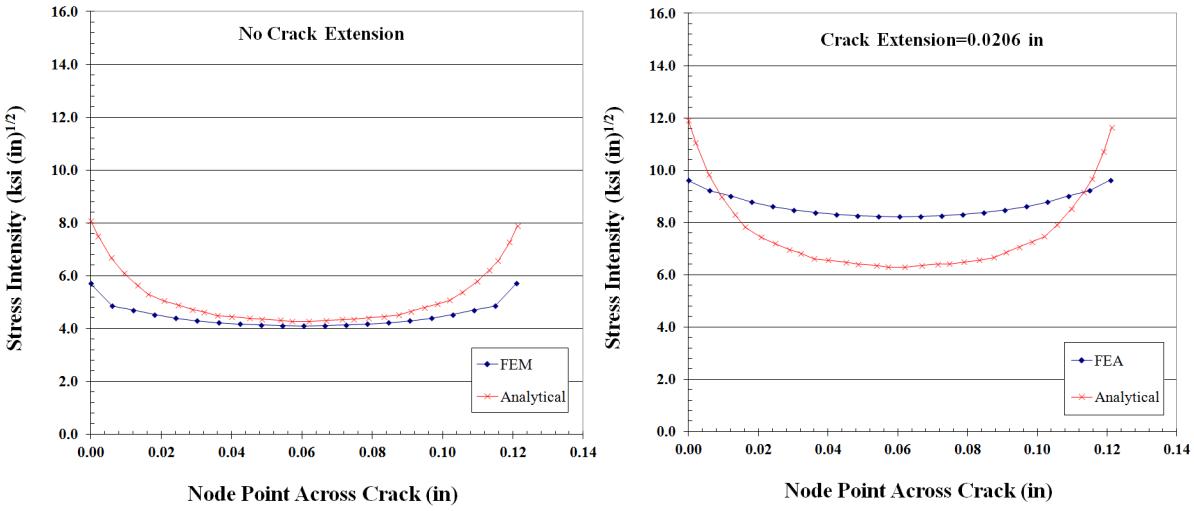

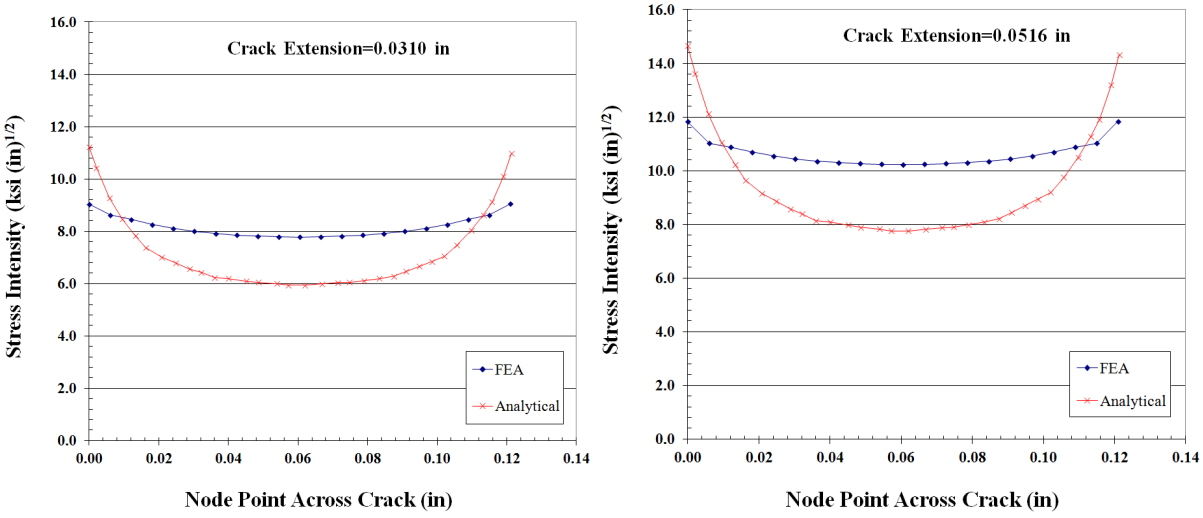

Fig. 14 K_I along the crack front for various crack extensions

The K_I values obtained from FEM model were consistent with the analytical model, especially towards the center of the crack front-line for a=0.0000in, as shown in Fig. 14. There was a slight deviation at the surface nodes. For the other crack extensions, the FEM and analytical K_I values were in close proximity to each other and maintained the same trend. Ultimately, the RFC model required a root-mean-square stress intensity factor, $K_{I,rms}$, as shown in Fig. 11. Thus, $K_{I,rms}$ is calculated for both analytical and FEM analyses for each crack extension by averaging the nodal K_I values and listed in Table I. The $K_{I,rms}$ values from the FEM and the analytical model are plotted as a function of the crack extension, as depicted in Fig. 15. It is inferred from Fig. 15 that the FEM $K_{I,rms}$ values are close to the $K_{I,rms}$ values obtained from analytical model. The $K_{I,rms}$ increased as the shift in the natural frequency decreased (or as the crack depth increased).

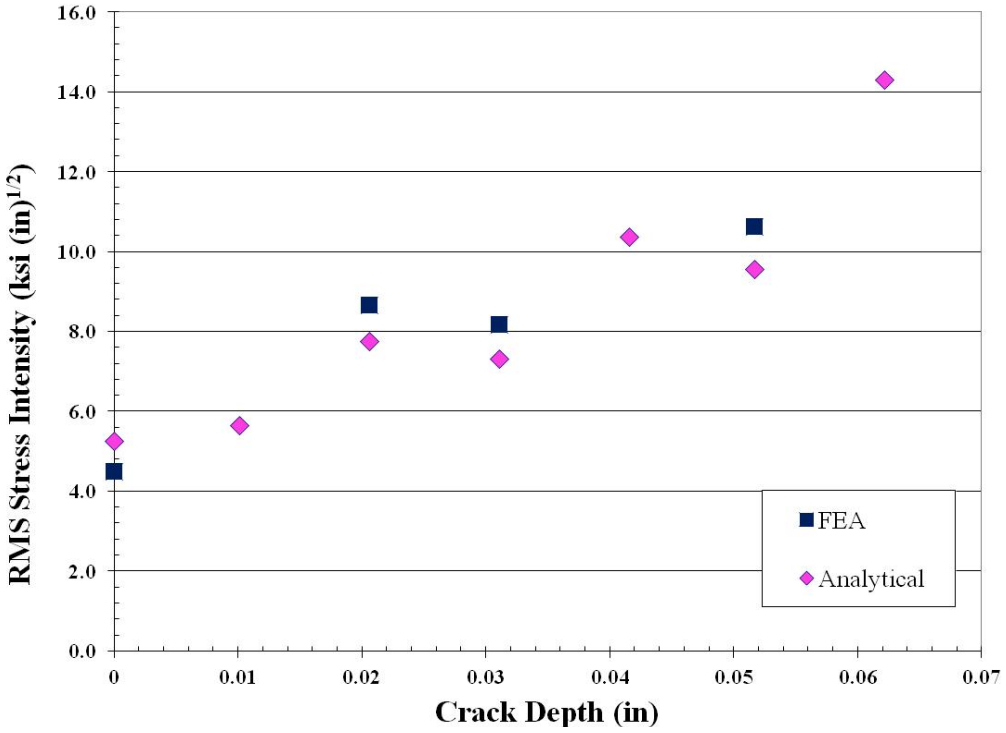

Fig. 15 K_I along the crack front FEM and analytical results

Table I. FEM and analytical $K_{I,rms}$

Crack Extension (in)	$K_{I,rms}$ (ksi-in$^{1/2}$) FEM	$K_{I,rms}$ (ksi-in$^{1/2}$) Analytical
0	4.49	5.26
0.0206	8.67	7.77
0.031	8.16	7.32
0.0516	10.63	9.56

Conclusion

This study provided a general virtual model that combined FEM with RFC. This model was used to predict change in the natural frequency, thus estimating fatigue life, using only frequency domain information. Execution of the model required only the input power spectral density, damping factor and material properties. Integrating the FEM and the RFC model allows the model to be extrapolated to more complex geometries for which closed stress intensity values are not available.

The FEM further demonstrated the validity of the assumption of a linear relationship between crack depth and natural frequency over limited crack lengths. Although this assumption was used for the closed form solution of the RFC model, use of the FEM allows this assumption to be relaxed in lieu of FEM results. The stress intensity quantities as a function of the crack growth are extracted from the FEM using the *J*-contour integral. Reasonably good correlation between the FEM and the analytic model are achieved for the stress intensity and natural frequency. From the model, it can be deduced that the average stress intensity factor increased as the natural frequency decreased. Additional work is needed to conduct experimental and computational time to failure comparison.

The proposed model in this paper may be extended to accelerated life testing, virtual qualification and reliability assessment. It can be used as a degradation model to analyze the relative severities of complex structures under harsh vibration environments. No explicit knowledge of the time history is needed. Thus, structural engineers could harness the flexibility of this model to reasonably predict the life-cycle when the only input is a PSD vibration profile. This approach may reduce the computation time and cost required to run a fully explicit FEM analysis.

References

[1] M. Paulus, “Limitations of the Power Spectral Density as An Indicator of Test Severity”, *Journal of IEST,* 2010.

[2] R.I. Stephens, A. Fatemi, R.R. Stephens and H.O. Fuchs, *Metal Fatigue in Engineering,* 2nd Edition, John Wiley and Sons, 2001.

[3] S. Suresh, *Fatigue of Materials,* 2nd Edition, Cambridge University Press, 2006.

[4] X. Pitoiset and A. Preumont, “Spectral Methods for Multiaxial Random Fatigue Analysis of Metallic Structures”, *International Journal of Fatigue*, 22, 2000, 541–550.

[5] Y. W. Kwon and J. H. Gordis, "Frequency Domain Structural Synthesis Applied to Quasi-Static Crack Growth Modeling", *Shock and Vibration*, 16, 2009, 637-646.

[6] I. A. Ashcroft, V. V. Silberschmidt and B. Echard, "Crack Propagation in a Toughened Epoxy Adhesive under Repeated Impacts", *Shock and Vibration*, 18, 2011, 157-170.

[7] E. Habtour, G. Drake, A. Dasgupta, M. Al-Bassyiouni and C. Choi, “Improved Reliability Testing with Multiaxial Electrodynamics Vibration”, *56th Annual Reliability and Maintainability Symposium Proceedings*, San Jose, CA, January 25-28, 2010.

[8] E. Habtour, C. Choi, M. Osterman and A. Dasgupta, "Novel Approach to Improve Electronics Reliability in the Next Generation of US Army Small Unmanned Ground Vehicles Under Complex Vibration Conditions", *Journal of Failure Analysis and Prevention*, 12, 2012, 86-95.

[9] M.H.A. Bonte, A. deBoer and R. Liebregts, “Prediction of Mechanical Fatigue Caused by Multiple Random Excitations”, *Proceedings of ISMA,* 2004, 697-708.

[10] M. Paulus, E. Habtour and A. Dasgupta, "Life Estimation Model of a Cantilevered Beam Subjected to Complex Random Vibration", *Fatigue & Fracture of Engineering Materials & Structures Journal*, accepted, 2012.

[11] A. Seweryn, "Brittle Fracture Criterion for Structures with Sharp Notches", *Engineering Fracture Mechanics*, 47, 1994, 673–681.

[12] M. Standberg, "Fracture at V-Notches with Contained Plasticity", *Engineering Fracture Mechanics*, 69, 2002, 403–15.

[13] T. T. Anderson, *Fracture Mechanics: Fundamental and Application*, 3rd Edition, CRC Press, Ann Arbor, 2004.

[14] H. Tada, P. C. Paris and G. R. Irwin, *The Stress Analysis of Cracks Handbook*, 3rd Edition, ASME Press, John Wiley & Sons, New York, NY, 2000.

[15] S. S. Quek and G. R. Liu, *Finite Element Method: A Practical Course*, Butterworth-Heinemann, Burlington, MA, 2003.

[16] D. Broek, *Elementary Engineering Fracture Mechanics*, 4th Edition, Kluwer Academic Publishers, Netherlands, 1986.

[17] J. R. Rice, "A Path Independent Integral and the Approximate Analysis of Strain Concentration by Notches and Cracks", *Journal of Applied Mechanics*, 35, 1968, 379-386.

[18] M. Jenssen, J. Zuidema and R. J. H. Wanhill, *Fracture Mechanics*, 2nd Edition, VSSD, Delft, Netherlands, 2006.

[19] G. P. Nikishkov and S. N. Atluri, "Calculation of Fracture Mechanics Parameters for an Arbitrary Three-Dimensional Crack, By the Equivalent Domain Integral Method", International Journal for Numerical Methods in Engineering, 24, 1987, 1801-1821.

[20] T. Irvine, “Optimal Use of the Vibration Response Spectrum for Enveloping Random Data”, *Institute of Environmental Sciences and Technology Proceedings*, 1999.

[21] N. Moes, A. Gravouil and T. Belytschko, “Non-planar 3D Crack Growth by the Extended Finite element and level sets—Part I: Mechanical model”, *International Journal for Numerical Methods in Engineering*, 53, 2002, 2549-2568.

Appendix B: Equation of Motion Development

$$\boldsymbol{R} = v\boldsymbol{i_Y} + (s + w)\boldsymbol{i_Z} + \boldsymbol{R_{local}}$$

The variable s denotes the arc-length along $\boldsymbol{R}$.

$$\boldsymbol{R_{local}} = \eta \boldsymbol{i}_\eta$$

$$\boldsymbol{R} = v\boldsymbol{i_Y} + (s + w)\boldsymbol{i_Z} + \eta \boldsymbol{i}_\eta$$

$$\boldsymbol{i}_\eta = cos(\psi)\boldsymbol{i}_Y + sin(\psi)\boldsymbol{i}_Z$$

Substituting $\boldsymbol{i}_\eta$ into $\boldsymbol{R}$ yields:

$$\boldsymbol{R} = (v + \eta cos(\psi))\boldsymbol{i}_Y + \big(s + w + \eta sin(\psi)\big)\boldsymbol{i_Z}$$

Differentiating $\boldsymbol{R}$ with respect to t:

$$\dot{\boldsymbol{R}} = \big(V_y + \dot{v} - \eta\dot{\psi}sin(\psi)\big)\boldsymbol{i}_Y + \big(\dot{w} + \eta\dot{\psi}\cos\psi\big)\boldsymbol{i_Z} + \boldsymbol{\Omega_{Base}}\times\boldsymbol{R}$$

$$\boldsymbol{\Omega_{Base}}\times\boldsymbol{R} = \begin{bmatrix} \boldsymbol{i_X} & \boldsymbol{i}_Y & \boldsymbol{i}_Z \\ \Omega_X & 0 & 0 \\ 0 & v + \eta\cos(\psi) & s + w + \eta sin(\psi) \end{bmatrix}$$

$$= -\big(s + w + \eta sin(\psi)\big)\Omega_X\boldsymbol{i_Y} + (v + \eta cos(\psi))\Omega_X\boldsymbol{i_Z}$$

Substitute $\boldsymbol{\Omega_{Base}}\times\boldsymbol{R}$ into $\dot{\boldsymbol{R}}$

$$\dot{\boldsymbol{R}} = \big(V_y + \dot{v} - \eta\dot{\psi}sin(\psi)\big)\boldsymbol{i}_Y + \big(\dot{w} + \eta\dot{\psi}\cos\psi\big)\boldsymbol{i_Z} - \big(s + w + \eta sin(\psi)\big)\Omega_X\boldsymbol{i_Y}$$

$$+ (v + \eta cos(\psi))\Omega_X\boldsymbol{i_Z}$$

$$\dot{\boldsymbol{R}} = \Big(V_y + \dot{v} - \eta\dot{\psi}sin(\psi) - s\Omega_X - w\Omega_X - \eta\Omega_X sin(\psi)\Big)\,\boldsymbol{i}_Y$$

$$+ \big(\dot{w} + \eta\dot{\psi}\cos\psi + v\Omega_X + \eta\Omega_X cos(\psi)\big)\boldsymbol{i_Z}$$

$$T = \frac{1}{2}\int_0^L \int_{A_1}^{A_2} \varrho\, \dot{\boldsymbol{R}} \cdot \dot{\boldsymbol{R}}\, dAds + \frac{1}{2} M\left(\dot{\boldsymbol{R}} \cdot \dot{\boldsymbol{R}}\right)\Big|_{s=L}$$

Substituting $\dot{\boldsymbol{R}}$ into the kinetic energy expression.

$$\begin{aligned} T = \frac{1}{2}\int_0^L \int_{\boldsymbol{A_1}}^{\boldsymbol{A_2}} \big[\rho\big(&\dot{v}^2 + 2\dot{v}V_Y + {V_Y}^2 + \dot{w}^2 - 2s\dot{v}\Omega_X - 2sV_Y\Omega_X - 2\dot{v}w\Omega_X - 2V_Y w\Omega_X \\ &+ 2v\dot{w}\Omega_X + s^2{\Omega_X}^2 + v^2{\Omega_X}^2 + 2sw{\Omega_X}^2 + w^2{\Omega_X}^2 + 2\dot{w}\eta\dot{\psi}cos\psi \\ &+ 2\dot{w}\eta\Omega_X cos\psi + 2v\eta\dot{\psi}\Omega_X cos\psi + 2v\eta{\Omega_X}^2 cos\psi + \eta^2\dot{\psi}^2 cos\psi^2 \\ &+ 2\eta^2\dot{\psi}\Omega_X cos\psi^2 + \eta^2{\Omega_X}^2 cos\psi^2 - 2\dot{v}\eta\dot{\psi}sin\psi - 2V_Y\eta\dot{\psi}sin\psi - 2\dot{v}\eta\Omega_X sin\psi \\ &- 2V_Y\eta\Omega_X sin\psi + 2s\eta\dot{\psi}\Omega_X sin\psi + 2w\eta\dot{\psi}\Omega_X sin\psi + 2s\eta{\Omega_X}^2 sin\psi \\ &+ 2w\eta{\Omega_X}^2 sin\psi + \eta^2\dot{\psi}^2 sin\psi^2 + 2\eta^2\dot{\psi}\Omega_X sin\psi^2 + \eta^2{\Omega_X}^2 sin\psi^2\big)\big]\, dAds \\ &+ \frac{1}{2} M[\dot{v}^2 + \dot{w}^2 + v^2\Omega_X^2 + (w+s)^2\Omega_X^2 - 2(s+w)\dot{v}\Omega_X + 2v\dot{w}\Omega_X]\Big|_{s=L} \\ &+ \frac{1}{2} J\left(\Omega_X + \dot{\psi}\right)^2\Big|_{s=L} \end{aligned}$$

Set:

$$\rho = \int_{A_1}^{A_2} \varrho\, dA \qquad J_1 = \int_{A_1}^{A_2} \varrho\, \eta dA \qquad J_2 = \int_{A_1}^{A_2} \varrho\, \eta^2 dA$$

Since the reference point coincides with the mass centroid and η is a principal axis of the differential beam element, J_1 is set equal to zero.

Expand and rearrange:

$$T = \frac{1}{2}\int_0^L \Big[\rho\big(\dot{v}^2 + 2\dot{v}V_Y + {V_Y}^2 + \dot{w}^2 - 2s\dot{v}\Omega_X - 2(s+w)V_Y\Omega_X - 2\dot{v}w\Omega_X + 2v\dot{w}\Omega_X$$

$$+ v^2{\Omega_X}^2 + (w+s)^2{\Omega_X}^2\big) + J_2\big(\Omega_X + \dot{\psi}\big)^2\Big]ds$$

$$+ \frac{1}{2}M\big[\dot{v}^2 + 2\dot{v}V_Y + {V_Y}^2 + \dot{w}^2 - 2s\dot{v}\Omega_X - 2(s+w)V_Y\Omega_X - 2\dot{v}w\Omega_X$$

$$+ 2v\dot{w}\Omega_X + v^2{\Omega_X}^2 + (w+s)^2{\Omega_X}^2\big]\Big|_{s=L} + \frac{1}{2}J\big(\Omega_X + \dot{\psi}\big)^2\Big|_{s=L}$$

The local stress and strain geometry contributions are utilized to account for the geometric nonlinearity (Nayfeh and Pia, 2004). According to the Euler-Bernoulli beam theory plane sections perpendicular to the undeformed reference axis remain plane and perpendicular to the deformed reference axis. The local displacement can be expressed as follows:

$$\boldsymbol{U} = u_\eta \boldsymbol{i_\eta} + u_\zeta \boldsymbol{i_\zeta}$$

where

$$u_\zeta = u_\zeta^o - \eta sin\psi \qquad\qquad u_\eta = u_\eta^o - \eta(1 - cos\psi)$$

where u_ζ^o and u_η^o are the displacement of the reference point on the observed element with respect to the ζ and η the local coordinate system and ψ is the rotation angle of the element. Since the local coordinate system is assigned to the observed element, the displacement of the reference point is:

$$u_\zeta^o = 0 \qquad\qquad u_\eta^o = 0 \qquad\qquad \psi = \frac{\partial u_\eta^o}{\partial s} = 0$$

The local displacement,u_ζ, is defined on the deformed local reference line ζ, thus:

$$\frac{\partial u_\zeta^o}{\partial s} = e$$

Differentiating the local displacement vector, with respect to s and assuming small local rotation angle yields:

$$\frac{\partial \boldsymbol{U}}{\partial s} = \frac{\partial u_\eta}{\partial s}\boldsymbol{i_\eta} + u_\eta \frac{\partial \boldsymbol{i_\eta}}{\partial s} + \frac{\partial u_\zeta}{\partial s}\boldsymbol{i_\zeta} + u_\zeta \frac{\partial \boldsymbol{i_\zeta}}{\partial s}$$

$$\frac{\partial u_\zeta}{\partial s} = e - \eta\psi' cos\psi = e - \eta\psi' \qquad \frac{\partial u_\eta}{\partial s} = -\eta\psi' sin\psi = 0$$

Therefore,

$$\frac{\partial \boldsymbol{U}}{\partial s} = (e - \eta\psi')\boldsymbol{i_\zeta}$$

Differentiating the local displacement vector, $\boldsymbol{U}$, with respect to η and assuming small local rotation angle yields:

$$\frac{\partial \boldsymbol{U}}{\partial \eta} = \frac{\partial u_\eta}{\partial \eta}\boldsymbol{i_\eta} + u_\eta \frac{\partial \boldsymbol{i_\eta}}{\partial \eta} + \frac{\partial u_\zeta}{\partial \eta}\boldsymbol{i_\zeta} + u_\zeta \frac{\partial \boldsymbol{i_\zeta}}{\partial \eta}$$

$$\frac{\partial u_\zeta}{\partial \eta} = -sin\psi = 0 \qquad \frac{\partial u_\eta}{\partial \eta} = cos\psi - 1 = 0$$

Therefore, the strains can be expressed as follows:

$$\varepsilon_{\zeta\zeta} = \frac{\partial \boldsymbol{U}}{\partial s} \cdot \boldsymbol{i_\zeta} = (e - \eta\psi')\boldsymbol{i_\zeta} \cdot \boldsymbol{i_\zeta} = e - \eta\psi'$$

$$\varepsilon_{\zeta\eta} = \frac{\partial \boldsymbol{U}}{\partial s} \cdot \boldsymbol{i_\eta} + \frac{\partial \boldsymbol{U}}{\partial \eta} \cdot \boldsymbol{i_\zeta} = 0$$

$$\varepsilon_{\eta\eta} = \varepsilon_{\xi\xi} = \varepsilon_{\eta\xi} = 0$$

The strain along the elastic axis, e, and the rotation angle, ψ, are related to u and v:

$$e = \sqrt{(1+w')^2 + v'^2} - 1$$

$$cos\psi = \frac{1+w'}{1+e} \qquad sin\psi = \frac{v'}{1+e}$$

The beam is assumed to be inextensional, which is typically true for isotropic elastic structures with an axial stiffness much larger than tension. The longitudinal motions have much smaller amplitude and much higher axial natural frequency; thus the longitudinal motion is neglected (i.e. e<<1). Therefore, the strain along the axial direction is:

$$e = 0 = \sqrt{(1+w')^2 + v'^2} - 1$$

The inextensionality criterion reduces the dependent variables from two to one. Therefore,

$$w' = \sqrt{1 - v'^2} - 1$$

Thus:

$$cos\psi = 1 + w' \qquad sin\psi = v'$$

Performing Taylor's expansion up to cubic nonlinearities and assuming that w and v are small but finite yield:

$$w' \approx -\frac{1}{2}v'^2 \qquad w = -\frac{1}{2}\int_0^\zeta v'^2 ds$$

$$\dot{w} = -\frac{1}{2}\frac{\partial}{\partial t}\left(\int_0^\zeta v'^2 ds\right)$$

$$\dot{w}^2 = \frac{1}{4}\left(\frac{\partial}{\partial t}\int_0^\zeta v'^2 ds\right)^2$$

$$cos\psi = 1 - \frac{1}{2}v'^2 \qquad sin\psi = v' \qquad \psi = \tan^{-1}\left(\frac{sin\psi}{cos\psi}\right)$$

$$\psi = \tan^{-1}\left(\frac{v'}{1+w'}\right) = v' - w'v' + w'^2v' - \frac{1}{3}v'^3 + \cdots$$

Substitute u' into ψ:

$$\psi \approx v' + \frac{1}{6}v'^3$$

Taking the temporal and spatial derivatives yield:

$$\dot{\psi} \approx \dot{v}' + \frac{1}{2}\dot{v}'v'^2 \qquad \dot{\psi}^2 \approx \dot{v}'^2 + \dot{v}'^2v'^2$$

The normalized curvature can be expressed as follows (Nayfeh and Pai, 2004):

$$\rho_\zeta = \psi' = v'' + \frac{1}{2}v''v'^2$$

$$\rho_\zeta{}^2 = \left(v'' + \frac{1}{2}v''v'^2\right)^2 = v''^2 + v''^2v'^2 + \frac{1}{4}v''^2v'^4 \approx v''^2 + v''^2v'^2$$

The beam strain energy for isotropic beam, which includes strains due to extension, bending and torsion, is as follows:

$$\Pi = \frac{1}{2}\int_0^L \left(EAe^2 + EI\rho_\zeta^2\right)ds + \frac{1}{2}cGJ\int_0^l \psi'^2 ds - \rho g\int_0^l w ds - Mgw_{tip}$$

Neglecting torsion and applying the inextensionality reduce the strain energy to:

$$\Pi = \frac{1}{2}\int_0^L EI\rho_\zeta^2 ds - \frac{1}{2}\rho g\int_0^L\int_0^\zeta v'^2 ds\, d\zeta - \frac{1}{2}Mg\int_0^L v'^2 ds$$

$$\int_0^L\int_0^\zeta v'^2 ds\, d\zeta = \int_0^L\int_s^L v'^2 d\zeta\, ds = \int_0^L\int_s^L d\zeta v'^2\, ds = \int_0^L (L-s)v'^2 ds$$

The potential energy can be expressed as follows:

$$\Pi = \frac{EI}{2}\int_0^L (v''^2 + v''^2 v'^2)ds - \frac{1}{2}\rho g \int_0^L (L-s)v'^2 ds - \frac{1}{2}Mg\int_0^L v'^2 ds$$

Substitute w and ψ into the kinetic energy equation:

$$\begin{aligned} T = \frac{1}{2}\int_0^L \Bigg[& \rho\left(\dot{v}^2 + 2\dot{v}V_Y + {V_Y}^2 + \frac{1}{4}\left(\frac{\partial}{\partial t}\int_0^\zeta v'^2 ds\right)^2 + \left(\int_0^\zeta v'^2 ds - 2s\right)V_Y\Omega_X \right. \\ & + \left(\int_0^\zeta v'^2 ds - 2s\right)\dot{v}\Omega_X - \frac{\partial}{\partial t}\left(\int_0^\zeta v'^2 ds\right)v\Omega_X + v^2{\Omega_X}^2 \\ & \left. + \left(s - \frac{1}{2}\int_0^\zeta v'^2 ds\right)^2 {\Omega_X}^2\right) + J_2(\Omega_X^2 + 2\Omega_X\dot{v}' + \Omega_X\dot{v}'v'^2 + \dot{v}'^2 + \dot{v}'^2 v'^2)\Bigg] ds \\ & + \frac{1}{2}M\Bigg[\dot{v}^2 + 2\dot{v}V_Y + {V_Y}^2 + \frac{1}{4}\left(\frac{\partial}{\partial t}\int_0^\zeta v'^2 ds\right)^2 + \left(\int_0^\zeta v'^2 ds - 2s\right)V_Y\Omega_X \\ & + \left(\int_0^\zeta v'^2 ds - 2s\right)\dot{v}\Omega_X - \frac{\partial}{\partial t}\left(\int_0^\zeta v'^2 ds\right)v\Omega_X + v^2{\Omega_X}^2 \\ & \left. + \left(s - \frac{1}{2}\int_0^\zeta v'^2 ds\right)^2 {\Omega_X}^2\Bigg]\right|_{s=L} \\ & + \frac{1}{2}J(\Omega_X^2 + 2\Omega_X\dot{v}' + \Omega_X\dot{v}'v'^2 + \dot{v}'^2 + \dot{v}'^2 v'^2)\Big|_{s=L} \end{aligned}$$

The approximate solutions are assumed in the form:

$$v(t,z) = \sum_{j=1}^{N} q_j(t)Y_j(z)$$

where the trial functions, Y_j, are known independent comparison function from a complete set and denote the undamped linear mode shapes and q_j denotes the generalized modal coordinates, (Meirovitch, 2001). For single mode the assumed solution becomes:

$$v(t,z) = q(t)Y(z)$$

Substitute in the kinetic energy equation and simplify (details provided in Appendix C):

$$a_1\ddot{q} + a_2 q^2\ddot{q} + a_2 q\dot{q}^2 + a_3\dot{\Omega}_X q^2 + (a_4 - a_5 V_Y \Omega_X - a_6\Omega_X^2)q + (a_7 - a_8\Omega_X^2)q^3 = a_9\dot{V}_Y + a_{10}\dot{\Omega}_X$$

The inertial coefficient including the rotary inertia (or effective mass) is:

$$a_1 = \rho\int_0^L Y^2 ds + J_2\int_0^L Y'^2 ds + MY^2|_{s=L} + JY'^2|_{s=L}$$

The nonlinear inertial coefficients including tip rotary inertias are :

$$a_2 = \rho\int_0^L \left(\int_0^\zeta Y'^2 ds\right)^2 ds + J_2\int_0^L Y'^4 ds + M\left(\int_0^\zeta Y'^2 ds\right)^2\Big|_{s=L} + JY'^4|_{s=L}$$

$$a_3 = \frac{1}{2}\left(-\rho\int_0^L Y\int_0^\zeta Y'^2 ds\, ds - MY\int_0^\zeta Y'^2 ds\Big|_{s=L} + J_2\int_0^L Y'^3 ds + JY'^3|_{s=L}\right)$$

The first order stiffness coefficient s(or effective elastic stiffness) are:

$$a_4 = EI\int_0^L Y''^2 ds - \rho g\left(\int_0^L (L-s)Y'^2 ds\right) - Mg\left(\int_0^L Y'^2 ds\right)$$

$$a_5 = 2\rho\int_0^L\int_0^\zeta Y'^2 ds\, ds + 2M\int_0^\zeta Y'^2 ds\Big|_{s=L}$$

$$a_6 = \rho\int_0^L Y^2 ds - \frac{1}{2}\rho\int_0^L (L^2 - s^2)Y'^2 ds + MY^2|_{s=L} - \frac{1}{2}M(L^2 - s^2)Y'^2\Big|_{s=L}$$

The third order nonlinear geometric stiffness coefficients:

$$a_7 = 2EI\int_0^L Y''^4 ds$$

$$a_8 = \frac{1}{2}\left(\rho\int_0^L\left(\int_0^\zeta Y'^2 ds\right)^2 ds + \frac{1}{2}M\left(\int_0^\zeta Y'^2 ds\right)^2\Big|_{s=L}\right)$$

and the base excitation inertial coefficients are:

$$a_9 = \rho\int_0^L Y ds + MY|_{Z=L}$$

$$a_{10} = -\rho\int_0^L sY ds - MsY|_{Z=L} + J_2\int_0^L Y' ds + JY'|_{s=L}$$

Equation of motion is:

$$a_1\ddot{q} + a_2 q^2\ddot{q} + a_2 q\dot{q}^2 + a_3\dot{\Omega}_X q^2 + (a_4 - a_5 V_Y\Omega_X - a_6\Omega_X^2)q + (a_7 - a_8\Omega_X^2)q^3 = a_9\dot{V}_Y + a_{10}\dot{\Omega}_X$$

Dividing by α_1 yields:

$$\ddot{q} + \beta_2 q^2\ddot{q} + \beta_2 q\dot{q}^2 + \beta_3\dot{\Omega}_X q^2 + (\beta_4 - \beta_5 V_Y\Omega_X - \beta_6\Omega_X^2)q + (\beta_7 - \beta_8\Omega_X^2)q^3 = \beta_9\dot{V}_Y + \beta_{10}\dot{\Omega}_X$$

$$\beta_2 = \frac{a_2}{a_1}\ \ \beta_3 = \frac{a_3}{a_1}\quad \beta_4 = \frac{a_4}{a_1}\ \ \beta_5 = \frac{a_5}{a_1}\ \ \beta_6 = \frac{a_6}{a_1}$$

$$\beta_7 = \frac{a_7}{a_1}\ \ \beta_8 = \frac{a_8}{a_1}\ \ \beta_9 = \frac{a_9}{a_1}\ \ \beta_{10} = \frac{a_{10}}{a_1}$$

$$(1 + \beta_2 q^2)\ddot{q} + \beta_2 q\dot{q}^2 + \beta_3\dot{\Omega}_X q^2 + (\beta_4 - \beta_5 V_Y\Omega_X - \beta_6\Omega_X^2)q + (\beta_7 - \beta_8\Omega_X^2)q^3 = \beta_9\dot{V}_Y + \beta_{10}\dot{\Omega}_X$$

$$\gamma = (1 + \beta_2 q^2)$$

Dividing by γ yields:

$$\ddot{q} + \frac{\beta_2}{\gamma} q\dot{q}^2 + \frac{\beta_3}{\gamma} \dot{\Omega}_X q^2 + \frac{(\beta_4 - \beta_5 V_Y \Omega_X - \beta_6 \Omega_X^2)}{\gamma} q + \frac{(\beta_7 - \beta_8 \Omega_X^2)}{\gamma} q^3 = \frac{\beta_9}{\gamma} \dot{V}_Y + \frac{\beta_{10}}{\gamma} \dot{\Omega}_X$$

Appendix C: *Euler-Lagrangian Development*

Expand the kinetic energy and rearrange:

$$T = \frac{1}{2}\int_0^L \Bigg[\rho\Bigg(\dot{v}^2 + 2\dot{v}V_Y + {V_Y}^2 + \frac{1}{4}\left(\frac{\partial}{\partial t}\int_0^\zeta v'^2 ds\right)^2 + \left(\int_0^\zeta v'^2 ds - 2s\right)V_Y\Omega_X$$
$$+ \left(\int_0^\zeta v'^2 ds - 2s\right)\dot{v}\Omega_X - \frac{\partial}{\partial t}\left(\int_0^\zeta v'^2 ds\right)v\Omega_X + v^2{\Omega_X}^2$$
$$+ \left(s - \frac{1}{2}\int_0^\zeta v'^2 ds\right)^2 {\Omega_X}^2\Bigg) + J_2(\Omega_X^2 + 2\Omega_X\dot{v}' + \Omega_X\dot{v}'v'^2 + \dot{v}'^2 + \dot{v}'^2v'^2)\Bigg] ds$$
$$+ \frac{1}{2}M\Bigg[\dot{v}^2 + 2\dot{v}V_Y + {V_Y}^2 + \frac{1}{4}\left(\frac{\partial}{\partial t}\int_0^\zeta v'^2 ds\right)^2 + \left(\int_0^\zeta v'^2 ds - 2s\right)V_Y\Omega_X$$
$$+ \left(\int_0^\zeta v'^2 ds - 2s\right)\dot{v}\Omega_X - \frac{\partial}{\partial t}\left(\int_0^\zeta v'^2 ds\right)v\Omega_X + v^2{\Omega_X}^2$$
$$+ \left(s - \frac{1}{2}\int_0^\zeta v'^2 ds\right)^2 {\Omega_X}^2\Bigg]\Bigg|_{s=L}$$
$$+ \frac{1}{2}J(\Omega_X^2 + 2\Omega_X\dot{v}' + \Omega_X\dot{v}'v'^2 + \dot{v}'^2 + \dot{v}'^2v'^2)\Big|_{s=L}$$

Substitute $v(t,z) = q(t)Y(z)$ into the kinetic energy equation:

$$T = \frac{1}{2}\int_0^L \left[\rho\left(\dot{q}^2Y^2 + 2\dot{q}YV_Y + {V_Y}^2 + \frac{1}{4}\left(\frac{\partial}{\partial t}\int_0^\zeta q^2Y'^2 ds\right)^2 + \left(q^2\int_0^\zeta Y'^2 ds - 2s\right)V_Y\Omega_X\right.\right.$$

$$+ \left(q^2\int_0^\zeta Y'^2 ds - 2s\right)\dot{q}Y\Omega_X - \frac{\partial}{\partial t}\left(q^2\int_0^\zeta Y'^2 ds\right)qY\Omega_X + q^2Y^2\Omega_X^2 + s^2{\Omega_X}^2$$

$$- sq^2\int_0^\zeta Y'^2 ds\,{\Omega_X}^2 + \frac{1}{4}q^4\left(\int_0^\zeta Y'^2 ds\right)^2{\Omega_X}^2\Big)$$

$$\left. + J_2(\Omega_X^2 + 2\Omega_X\dot{q}Y' + \Omega_X\dot{q}q^2Y'^3 + \dot{q}^2Y'^2 + \dot{q}^2q^2Y'^4)\right]ds$$

$$+ \frac{1}{2}M(inertial\ components)\Big|_{s=L} + \frac{1}{2}J(rotational\ components)\Big|_{s=L}$$

$$T = \frac{1}{2}\int_0^L \left[\rho\left(\dot{q}^2Y^2 + 2\dot{q}YV_Y + {V_Y}^2 + q^2\dot{q}^2\left(\int_0^\zeta Y'^2 ds\right)^2 + q^2\left(\int_0^\zeta Y'^2 ds\right)V_Y\Omega_X - 2sV_Y\Omega_X\right.\right.$$

$$+ \left(\int_0^\zeta Y'^2 ds\right)q^2\dot{q}Y\Omega_X - 2s\dot{q}Y\Omega_X - 2q^2\dot{q}\left(\int_0^\zeta Y'^2 ds\right)Y\Omega_X + q^2Y^2\Omega_X^2$$

$$+ s^2{\Omega_X}^2 - \left(\int_0^\zeta Y'^2 ds\right)sq^2{\Omega_X}^2 + \frac{1}{4}\left(\int_0^\zeta Y'^2 ds\right)^2 q^4{\Omega_X}^2\Big)$$

$$\left. + J_2(\Omega_X^2 + 2\Omega_X\dot{q}Y' + \Omega_X\dot{q}q^2Y'^3 + \dot{q}^2Y'^2 + \dot{q}^2q^2Y'^4)\right]ds$$

$$+ \frac{1}{2}M(inertial\ components)\Big|_{s=L} + \frac{1}{2}J(rotational\ components)\Big|_{s=L}$$

$$T = \frac{1}{2}\rho\dot{q}^2\int_0^L Y^2 ds + \rho\dot{q}V_Y\int_0^L Y ds + \frac{1}{2}\rho L{V_Y}^2 + \frac{1}{2}\rho q^2\dot{q}^2\int_0^L\left(\int_0^\zeta Y'^2 ds\right)^2 ds$$

$$+\frac{1}{2}\rho q^2 V_Y\Omega_X\int_0^L\int_0^\zeta Y'^2 ds\, ds - \frac{1}{2}\rho L^2 V_Y\Omega_X - \frac{1}{2}\rho q^2\dot{q}\Omega_X\int_0^L Y\int_0^\zeta Y'^2 ds\, ds$$

$$-\rho\dot{q}\Omega_X\int_0^L sY ds + \frac{1}{2}\rho q^2\Omega_X^2\int_0^L Y^2 ds + \frac{1}{6}\rho L^3{\Omega_X}^2$$

$$-\frac{1}{2}\rho q^2{\Omega_X}^2\int_0^L s\int_0^\zeta Y'^2 ds\, ds + \frac{1}{8}\rho q^4{\Omega_X}^2\int_0^L\left(\int_0^\zeta Y'^2 ds\right)^2 ds + \frac{1}{2}J_2 L\Omega_X^2$$

$$+J_2\dot{q}\Omega_X\int_0^L Y' ds + \frac{1}{2}J_2\dot{q}q^2\Omega_X\int_0^L Y'^3 ds + \frac{1}{2}J_2\dot{q}^2\int_0^L Y'^2 ds$$

$$+\frac{1}{2}J_2 q^2\dot{q}^2\int_0^L Y'^4 ds + \frac{1}{2}M(inertial\ components)\Big|_{s=L}$$

$$+\frac{1}{2}J(rotational\ components)\Big|_{s=L}$$

$$T = \frac{1}{2}\rho\dot{q}^2\int_0^L Y^2 ds + \rho\dot{q}V_Y\int_0^L Y ds + \frac{1}{2}\rho L{V_Y}^2 + \frac{1}{2}\rho q^2\dot{q}^2\int_0^L\left(\int_0^\zeta Y'^2 ds\right)^2 ds$$

$$+\frac{1}{2}\rho q^2 V_Y\Omega_X\int_0^L\int_0^\zeta Y'^2 ds\, ds - \frac{1}{2}\rho L^2 V_Y\Omega_X - \frac{1}{2}\rho q^2\dot{q}\Omega_X\int_0^L Y\int_0^\zeta Y'^2 ds\, ds$$

$$-\rho\dot{q}\Omega_X\int_0^L sY ds + \frac{1}{2}\rho q^2\Omega_X^2\int_0^L Y^2 ds + \frac{1}{6}\rho L^3{\Omega_X}^2$$

$$-\frac{1}{4}\rho q^2\Omega_X^2\int_0^L (L^2 - s^2)Y'^2 ds + \frac{1}{8}\rho q^4{\Omega_X}^2\int_0^L\left(\int_0^\zeta Y'^2 ds\right)^2 ds + \frac{1}{2}J_2\Omega_X^2 L$$

$$+J_2\Omega_X\dot{q}\int_0^L Y' ds + \frac{1}{2}J_2\Omega_X\dot{q}q^2\int_0^L Y'^3 ds + \frac{1}{2}J_2\dot{q}^2\int_0^L Y'^2 ds$$

$$+\frac{1}{2}J_2\dot{q}^2q^2\int_0^L Y'^4 ds + \frac{1}{2}M(inertial\ components)\Big|_{s=L}$$

$$+\frac{1}{2}J(rotational\ components)\Big|_{s=L}$$

$$T = \frac{1}{2}\rho\dot{q}^2\int_0^L Y^2 ds + \rho\dot{q}V_Y\int_0^L Y ds + \frac{1}{2}\rho L{V_Y}^2 + \frac{1}{2}\rho q^2\dot{q}^2\int_0^L\left(\int_0^\zeta Y'^2 ds\right)^2 ds$$

$$+\frac{1}{2}\rho q^2 V_Y\Omega_X\int_0^L\int_0^\zeta Y'^2 ds\, ds - \frac{1}{2}\rho L^2 V_Y\Omega_X - \frac{1}{2}\rho q^2\dot{q}\Omega_X\int_0^L Y\int_0^\zeta Y'^2 ds\, ds$$

$$-\rho\dot{q}\Omega_X\int_0^L sY ds + \frac{1}{2}\rho q^2\Omega_X^2\int_0^L Y^2 ds + \frac{1}{6}\rho L^3\Omega_X^2$$

$$-\frac{1}{4}\rho q^2\Omega_X^2\int_0^L (L^2 - s^2)Y'^2 ds + \frac{1}{8}\rho q^4\Omega_X^2\int_0^L\left(\int_0^\zeta Y'^2 ds\right)^2 ds + \frac{1}{2}J_2\Omega_X^2 L$$

$$+J_2\Omega_X\dot{q}\int_0^L Y' ds + \frac{1}{2}J_2\Omega_X\dot{q}q^2\int_0^L Y'^3 ds + \frac{1}{2}J_2\dot{q}^2\int_0^L Y'^2 ds$$

$$+\frac{1}{2}J_2\dot{q}^2q^2\int_0^L Y'^4 ds + \frac{1}{2}M\dot{q}^2Y^2\Big|_{s=L} + M\dot{q}V_Y Y|_{s=L} + \frac{1}{2}M{V_Y}^2\Big|_{s=L}$$

$$+\frac{1}{2}Mq^2\dot{q}^2\left(\int_0^\zeta Y'^2 ds\right)^2\Big|_{s=L} + \frac{1}{2}Mq^2V_Y\Omega_X\int_0^\zeta Y'^2 ds\Big|_{s=L} - \frac{1}{2}MLV_Y\Omega_X$$

$$+\frac{1}{2}Mq^2\Omega_X^2Y^2\Big|_{s=L}$$

$$+\frac{1}{8}Mq^4\Omega_X^2\left(\int_0^\zeta Y'^2 ds\right)^2\Big|_{s=L} - \frac{1}{4}Mq^2\Omega_X^2\left((L^2 - s^2)Y'^2\right)\Big|_{s=L} + \frac{1}{6}Ms^2\Omega_X^2\Big|_{s=L}$$

$$-M\dot{q}\Omega_X sY|_{s=L} - \frac{1}{2}Mq^2\dot{q}\Omega_X Y\int_0^\zeta Y'^2 ds\Big|_{s=L}$$

$$+\frac{1}{2}J\left(\Omega_X^2 + 2\Omega_X\dot{q}Y' + \Omega_X\dot{q}q^2Y'^3 + \dot{q}^2Y'^2 + \dot{q}^2q^2Y'^4\right)\Big|_{s=L}$$

Collect the generalized coordinates:

$$T = \frac{1}{2}\left[\rho\int_0^L Y^2 ds + J_2\int_0^L Y'^2 ds + MY^2|_{Z=L} + JY'^2|_{s=L}\right]\dot{q}^2$$

$$+\frac{1}{2}\left[\rho\int_0^L\left(\int_0^\zeta Y'^2 ds\right)^2 ds + J_2\int_0^L Y'^4 ds + M\left(\int_0^\zeta Y'^2 ds\right)^2\Bigg|_{s=L}\right.$$

$$\left.+JY'^4|_{Z=L}\right]q^2\dot{q}^2 + \left[\rho\int_0^L Y ds + MY|_{s=L}\right]\dot{q}V_Y$$

$$+\left[-\rho\int_0^L sY ds - MsY|_{s=L} + J_2\int_0^L Y' ds + JY'|_{s=L}\right]\dot{q}\Omega_X$$

$$+\frac{1}{2}\left[\rho\int_0^L\int_0^\zeta Y'^2 ds\, ds + M\int_0^\zeta Y'^2 ds\Big|_{s=L}\right]q^2 V_Y\Omega_X$$

$$+\frac{1}{2}\left[-\rho\int_0^L Y\int_0^\zeta Y'^2 ds\, ds - MY\int_0^\zeta Y'^2 ds\Big|_{s=L} + J_2\int_0^L Y'^3 ds\right.$$

$$\left.+JY'^3\big|_{s=L}\right]q^2\dot{q}\Omega_X$$

$$+\frac{1}{2}\left[\rho\int_0^L Y^2 ds - \frac{1}{2}\rho\int_0^L (L^2 - s^2)Y'^2 ds\right.$$

$$\left.+MY^2|_{s=L} - \frac{1}{2}Mq^2\Omega_X^2\big((L^2 - s^2)Y'^2\big)\Big|_{s=L}\right]q^2\Omega_X^2$$

$$+\frac{1}{8}\left[\rho\int_0^L\left(\int_0^\zeta Y'^2 ds\right)^2 ds + M\left(\int_0^\zeta Y'^2 ds\right)^2\Bigg|_{s=L}\right]q^4\Omega_X^2 + \frac{1}{2}[\rho L + M|_{s=L}]V_Y{}^2$$

$$+\frac{1}{2}[-\rho L^2 - ML]V_Y\Omega_X + \frac{1}{2}\left[\frac{1}{3}\rho L^3 + \frac{1}{3}Ms^2\Big|_{s=L} + J_2 L + J|_{s=L}\right]\Omega_X^2$$

Set:

$$\alpha_1 = \rho\int_0^L Y^2 ds + J_2\int_0^L Y'^2 ds + MY^2|_{Z=L} + JY'^2|_{Z=L}$$

$$\alpha_2 = \rho \int_0^L \left(\int_0^\zeta Y'^2 ds \right)^2 ds + J_2 \int_0^L Y'^4 ds + M \left(\int_0^\zeta Y'^2 ds \right)^2 \Big|_{Z=L} + JY'^4|_{Z=L}$$

$$\alpha_3 = \rho \int_0^L Y ds + MY|_{Z=L}$$

$$\alpha_4 = -\rho \int_0^L sY ds - MsY|_{Z=L} + J_2 \int_0^L Y' ds + JY'|_{Z=L}$$

$$\alpha_5 = \rho \int_0^L \int_0^\zeta Y'^2 ds\, ds + M \int_0^\zeta Y'^2 ds \Big|_{Z=L}$$

$$\alpha_6 = -\rho \int_0^L Y \int_0^\zeta Y'^2 ds\, ds - MY \int_0^\zeta Y'^2 ds \Big|_{Z=L} + J_2 \int_0^L Y'^3 ds + JY'^3|_{Z=L}$$

$$\alpha_7 = \rho \int_0^L Y^2 ds - \frac{1}{2}\rho \int_0^L (L^2 - s^2) Y'^2 ds + MY^2|_{Z=L} - \frac{1}{2} M\left((L^2 - s^2)Y'^2\right)\Big|_{Z=L}$$

$$\alpha_8 = \rho \int_0^L \left(\int_0^\zeta Y'^2 ds \right)^2 ds + M \left(\int_0^\zeta Y'^2 ds \right)^2 \Big|_{Z=L}$$

$$\alpha_9 = \rho L + M|_{Z=L}$$

$$\alpha_{10} = -\rho L^2 - ML$$

$$\alpha_{11} = \frac{1}{3}\rho L^3 + \frac{1}{3} M s^2 \Big|_{s=L} + J_2 L + J|_{Z=L}$$

Substitute into the kinetic energy:

$$T = \frac{1}{2}\alpha_1 \dot{q}^2 + \frac{1}{2}\alpha_2 q^2 \dot{q}^2 + \alpha_3 \dot{q} V_Y + \alpha_4\, \dot{q}\Omega_X + \alpha_5 q^2 V_Y \Omega_X + \frac{1}{2}\alpha_6 q^2 \dot{q}\Omega_X + \frac{1}{2}\alpha_7 q^2 \Omega_X^2$$

$$+ \frac{1}{8}\alpha_8 q^4 \Omega_X^2 + \frac{1}{2}\alpha_9 {V_Y}^2 + \frac{1}{2}\alpha_{10} V_Y \Omega_X + \frac{1}{2}\alpha_{11} \Omega_X^2$$

$$\frac{\partial T}{\partial q} = \alpha_2 q\dot{q}^2 + 2\alpha_5 q V_Y \Omega_X + \alpha_6 q\dot{q}\Omega_X + \alpha_7 q\Omega_X^2 + \frac{1}{2}\alpha_8 q^3\Omega_X^2$$

$$\frac{\partial T}{\partial \dot{q}} = \alpha_1\dot{q} + \alpha_2 q^2\dot{q} + \alpha_3 V_Y + \alpha_4\,\Omega_X + \frac{1}{2}\alpha_6 q^2\Omega_X$$

$$\Pi = \frac{EI}{2}\int_0^L (q^2 Y''^2 + q^4 Y''^2 Y'^2)ds - \frac{1}{2}\rho g q^2\int_0^L (L-s)Y'^2 ds - \frac{1}{2}Mgq^2\int_0^L Y'^2 ds$$

$$\frac{\partial \Pi}{\partial q} = EI\left(\int_0^L Y''^2 ds\right)q + 2EI\left(\int_0^L Y''^2 Y'^2 ds\right)q^3 - \rho g\left(\int_0^L (L-s)Y'^2 ds\right)q$$

$$- Mg\left(\int_0^L Y'^2 ds\right)q$$

Set:

$$\alpha_{12} = EI\int_0^L Y''^2 ds - \rho g\left(\int_0^L (L-s)Y'^2 ds\right) - Mg\left(\int_0^L Y'^2 ds\right)$$

$$\alpha_{13} = 2EI\int_0^L Y''^2 Y'^2 ds$$

$$\frac{\partial \Pi}{\partial q} = \alpha_{12} q + \alpha_{13} q^3 \qquad \frac{\partial \Pi}{\partial \dot{q}} = 0$$

$$\frac{\partial L}{\partial q} = \frac{\partial T}{\partial q} - \frac{\partial \Pi}{\partial q}$$

$$\frac{\partial L}{\partial q} = \alpha_2 q\dot{q}^2 + 2\alpha_5 q V_Y \Omega_X + \alpha_6 q\dot{q}\Omega_X + \alpha_7 q\Omega_X^2 + \frac{1}{2}\alpha_8 q^3\Omega_X^2 - \alpha_{12} q - \alpha_{13} q^3$$

$$\frac{\partial L}{\partial \dot{q}} = \frac{\partial T}{\partial \dot{q}} - \frac{\partial \Pi}{\partial \dot{q}}$$

$$\frac{\partial L}{\partial \dot{q}} = \alpha_1\dot{q} + \alpha_2 q^2\dot{q} + \alpha_3 V_Y + \alpha_4\,\Omega_X + \frac{1}{2}\alpha_6 q^2\Omega_X$$

$$\frac{\partial}{\partial t}\left(\frac{\partial L}{\partial \dot{q}}\right) = \alpha_1\ddot{q} + 2\alpha_2 q\dot{q}^{\mathbf{2}} + \alpha_2 q^2\ddot{q} + \alpha_3\dot{V}_Y + \alpha_4\dot{\Omega}_X + \alpha_6 q\dot{q}\Omega_X + \frac{1}{2}\alpha_6 q^2\dot{\Omega}_X$$

$$\frac{\partial}{\partial t}\left(\frac{\partial L}{\partial \dot{q}}\right) - \frac{\partial L}{\partial q} = 0$$

$$= \alpha_1\ddot{q} + 2\alpha_2 q\dot{q}^{\mathbf{2}} + \alpha_2 q^2\ddot{q} + \alpha_3\dot{V}_Y + \alpha_4\dot{\Omega}_X + \alpha_6 q\dot{q}\Omega_X + \frac{1}{2}\alpha_6 q^2\dot{\Omega}_X - \alpha_2 q\dot{q}^2$$

$$- 2\alpha_5 q V_Y\Omega_X - \alpha_6 q\dot{q}\Omega_X - \alpha_7 q\Omega_X^2 - \frac{1}{2}\alpha_8 q^3\Omega_X^2 + \alpha_{12}q + \alpha_{13}q^3$$

Simplify

$$0 = \alpha_1\ddot{q} + \alpha_2 q\dot{q}^{\mathbf{2}} + \alpha_2 q^2\ddot{q} + \alpha_3\dot{V}_Y + \alpha_4\dot{\Omega}_X + \frac{1}{2}\alpha_6 q^2\dot{\Omega}_X - 2\alpha_5 q V_Y\Omega_X - \alpha_7 q\Omega_X^2$$

$$- \frac{1}{2}\alpha_8 q^3\Omega_X^2 + \alpha_{12}q + \alpha_{13}q^3$$

$$\alpha_1\ddot{q} + \alpha_2 q^2\ddot{q} + \alpha_2 q\dot{q}^{\mathbf{2}} + \frac{1}{2}\alpha_6\dot{\Omega}_X q^2 + (\alpha_{12} - 2\alpha_5 V_Y\Omega_X - \alpha_7\Omega_X^2)q + \left(\alpha_{13} - \frac{1}{2}\alpha_8\Omega_X^2\right)q^3$$

$$= -\alpha_3\dot{V}_Y - \alpha_4\dot{\Omega}_X$$

The inertial coefficient including the rotary inertia (or effective mass) is:

$$a_1 = \alpha_1 = \rho\int_0^L Y^2 ds + J_2\int_0^L Y'^2 ds + MY^2|_{s=L} + JY'^2|_{s=L}$$

The nonlinear inertial coefficients including tip rotary inertias are:

$$a_2 = \alpha_2 = \rho\int_0^L \left(\int_0^\zeta Y'^2 ds\right)^2 ds + J_2\int_0^L Y'^4 ds + M\left(\int_0^\zeta Y'^2 ds\right)^2\Bigg|_{s=L} + JY'^4|_{s=L}$$

$$a_3 = \frac{1}{2}\alpha_6 = \frac{1}{2}\left(-\rho\int_0^L Y\int_0^\zeta Y'^2 ds\, ds - MY\int_0^\zeta Y'^2 ds\Big|_{s=L} + J_2\int_0^L Y'^3 ds + JY'^3|_{s=L}\right)$$

The first order stiffness coefficients (or effective elastic stiffness) are:

$$a_4 = \alpha_{12} = EI\int_0^L Y''^2 ds - \rho g\left(\int_0^L (L-s)Y'^2 ds\right) - Mg\left(\int_0^L Y'^2 ds\right)$$

$$a_5 = 2\alpha_5 = 2\rho\int_0^L\int_0^\zeta Y'^2 ds\, ds + 2M\int_0^\zeta Y'^2 ds\Big|_{s=L}$$

$$a_6 = \alpha_7 = \rho\int_0^L Y^2 ds - \frac{1}{2}\rho\int_0^L (L^2-s^2)Y'^2 ds + MY^2|_{Z=L} - \frac{1}{2}M(L^2-s^2)Y'^2\Big|_{s=L}$$

The third order nonlinear geometric stiffness coefficients:

$$a_7 = \alpha_{13} = 2EI\int_0^L Y''^2 Y'^2 ds$$

$$a_8 = \frac{1}{2}\alpha_8 = \frac{1}{2}\left(\rho\int_0^L\left(\int_0^\zeta Y'^2 ds\right)^2 ds + \frac{1}{2}M\left(\int_0^\zeta Y'^2 ds\right)^2\Big|_{s=L}\right)$$

And the base excitation inertial coefficients are:

$$a_9 = \alpha_3 = \rho\int_0^L Y ds + MY|_{s=L}$$

$$a_{10} = \alpha_4 = -\rho\int_0^L sY ds - MsY|_{Z=L} + J_2\int_0^L Y' ds + JY'|_{s=L}$$

Equation of motion is:

$$a_1\ddot{q} + a_2 q^2\ddot{q} + a_2 q\dot{q}^2 + a_3\dot{\Omega}_X q^2 + (a_4 - a_5 V_Y\Omega_X - a_6\Omega_X^2)q + (a_7 - a_8\Omega_X^2)q^3 = a_9\dot{V}_Y + a_{10}\dot{\Omega}_X$$

Chapter 9 Bibliography

References presented here are in the order used. As each chapter is meant to be a standalone paper, the references for each chapter are contained within that chapter.

E. Habtour, C. Choi, G. Drake, A. Dasgupta, and M. Al- Bassyiouni, “Improved reliability testing with multiaxial electrodynamics vibration,” in *Proceedings of the 56th Annual Reliability and Maintainability Symposium*, San Jose, CA, USA, 2010.

Ernst, M., E. Habtour, A. Dasgupta, M. Pohland, M. Robeson, and M. Paulus. "Comparison of Electronic Component Durability Under Uniaxial and Multiaxial Random Vibrations." *Journal of Electronics Packaging* 137.1, 2015.

W. E. Whiteman and M. S. Berman, “Fatigue failure results for multi-axial versus uniaxial stress screen vibration testing,” *Shock and Vibration*, vol. 9, no. 6, pp. 319–328, 2002.

Nayfeh, A. H. *Introduction to Perturbation Techniques*. New York: Wiley, 1981.

Balachandran, B., and E. B. Magrab. *Vibrations*. 2nd ed. Toronto, Canada: Cengage Learning, 2009.

Virgin, L. N. *Introduction to Experimental Nonlinear Dynamics: A Case Study in Mechanical Vibration*. Cambridge, U.K.: Cambridge UP, 2000.

L. G. Villanueva, R. B. Karabalin, M. H. Matheny, D. Chi, J. E. Sader, and M. L. Roukes, “Nonlinearity in nanomechanical cantilevers,” *Physical Review B*, vol. 87, Article ID 024304, 2013.

Hamdan, M. N., and M. H. F. Dado. "Large Amplitude Free Vibrations Of A Uniform Cantilever Beam Carrying An Intermediate Lumped Mass And Rotary Inertia." *Journal of Sound and Vibration* 206.2 (1997): 151-168.

Erwin, S., I., "In Damage Control Mode, Army Builds Future Network of Combat Brigades", National Defense, (Jul.) 2010.

Steinberg, D., *Vibration Analysis for Electronic Equipment*, 3rd Edition, Wiley Inter-Science, New York, NY, 2000.

Pitarresi J. and Primavera A., "Comparison of Vibration Modeling Techniques for Printed Circuit Cards", *ASME Journal of Electronic Packaging,* 1991, **114**, 378–383.

Jones, R. M., *Mechanics of Composite Materials*, 2nd Edition, Taylor and Francis Group, New York, NY, 1999.

Barker, D. B., and Chen, Y. S., "Modeling Vibration Restrain of Wedge Lock Card Guides", *ASME Annual Meeting,* 92-WA/EEP-16, (Nov.) 1992, Anaheim, CA.

Li, R. S., "A Methodology for Fatigue Prediction of Electronic Components under Random Vibration Load," *Journal of Electronic Packaging, ASME,* 2001, Vol. 123, pp. 394-400.

C. Choi, M. Al-Bassyiouni, A. Dasgupta and M. Osterman, "PoF Issues in Multi-DoF Vibration Testing: ED Shakers and RS Shakers", *IEEE ASTR09 Workshop*, New Jersey, Oct. 2009.

J. E. Shigley and C. R. Mischke, *Mechanical Engineering Design*, McGraw-Hill, Boston, Ma, USA, 6th edition, 2001.

N. E. Dowling, *Mechanical Behavior of Materials: Engineering Methods for Deformation, Fracture, and Fatigue*, Prentice Hall, Upper Saddle River, NJ, USA, 2nd edition, 1999.

I. Elishakoff, “Generalized Eringen problem: influence of axial force on random vibration response of simply supported beam,” *Structural Safety*, vol. 4, no. 4, pp. 255–265, 1987.

C. Leser, L. Juneja, S. Thangjitham, and N. E. Dowling, “On multi-axial random fatigue load modeling,” SAE Technical Chapter 980696, Society of Automotive Engineering, 1996.

Y. Liu and S. Mahadevan, “Multiaxial high-cycle fatigue criterion and life prediction for metals,” *International Journal of Fatigue*, vol. 27, no. 7, pp. 790–800, 2005.

X. Pitoiset, A. Preumont, and A. Kernilis, “Tools for a multiaxial fatigue analysis of structures submitted to random vibrations,” in *Proceedings of the European Conference on Spacecraft Structures Materials and Mechanical Testing*, Braunschweig, Germany, November 1998.

D. J. Segalman, C. W. G. Fulcher, G. M. Reese, and R. V. Field Jr., “Efficient method for calculating rms von Mises stress in a random vibration environment,” *Journal of Sound and Vibration*, vol. 230, no. 2, pp. 393–410, 2000.

D. Socie and G. Marquis, *Multiaxial Fatigue*, Society of Automotive Engineers, Warrendale, Pa, USA, 2000.

K. A. Sweitzer, *Random Vibration Response Statistics for Fatigue Analysis of Nonlinear Structures [Ph.D. thesis]*, University of Southampton, Southampton, UK, 2006.

M. Paulus, A. Dasgupta, and E. Habtour, “Life estimation model of a cantilevered beam subjected to complex random vibration,” *Fatigue and Fracture of Engineering Materials and Structures*, vol. 35, no. 11, pp. 1058–1070, 2012.

R. M. French, R. Handy, and H. L. Cooper, “A comparison of simultaneous and sequential single-axis durability testing,” *Experimental Techniques*, vol. 30, no. 5, pp. 32–37, 2006.

W. E. Whiteman and M. Berman, “Inadequacies in uniaxial stress screen vibration testing,” *Journal of the Institute of Environmental Sciences and Technology*, vol. 44, no. 4, pp. 20– 23, 2001.

E. Habtour, C. Choi, M. Osterman, and A. Dasgupta, “Novel approach to improve electronics reliability in the next generation of US army small unmanned ground vehicles under complex vibration conditions,” *Journal of Failure Analysis and Prevention*, vol. 12, no. 1, pp. 86–95, 2012.

C. J. Dodds and C. H. Ward, “The ubiquitous four-poster,” *Engineering Integrity Society*, vol. 16, no. 1, pp. 17–23, 2005.

C. M. Awate, S. M. Panse, and C. J. Dodds, “Validation of an accelerated test on a four-post road simulator,” Chapter 2007-26- 070, Society of Automotive Engineering, pp. 761–767, 2007.

C. J. Dodds and A. R. Plummer, “Laboratory road simulation for full vehicle testing a review,” in *Proceedings of the Symposium on International Automotive Technology*, 2001.

J. C. Delamotte, R. F. Nascimento, and J. R. F. Arruda, “Simple models for the dynamic modeling of rotating tires,” *Shock and Vibration*, vol. 15, no. 3-4, pp. 383–393, 2008.

C. Q. Liu, “Combination of an improved FRF-based substructure synthesis and power flow method with application to vehicle axle noise analysis,” *Shock and Vibration*, vol. 15, no. 1, pp. 51–60, 2008.

N. W. M. Bishop, “Vibration fatigue analysis in the finite element environment,” in *Proceedings of the 16th Encuentro del Grupo Espan˜ol de Fractura*, Torremolinos, Spain, 1999.

M. H. A. Bonte, A. De Boer, and R. Liebregts, "Prediction of mechanical fatigue caused by multiple random excitations," in *Proceedings of the ISMA Conference*, pp. 697–708, September 2004.

M. H. A. Bonte, A. de Boer, and R. Liebregts, "Determining the von Mises stress power spectral density for frequency domain fatigue analysis including out-of-phase stress components," *Journal of Sound and Vibration*, vol. 302, no. 1-2, pp. 379–386, 2007.

P. H. Wirsching, T. L. Paez, and K. Ortiz, *Random Vibrations: Theory and Practice*, John Wiley and Sons, New York, NY, USA, 1995.

T. Dirlik, *Application of Computers in Fatigue Analysis [Ph.D. thesis]*, University of Warwick, Warwick, UK, 1985.

D. A. Thomas, K. Avers, and M. Pecht, "The "troublenotidentified" phenomenon in automotive electronics," *Microelectronics Reliability*, vol. 42, no. 4-5, pp. 641–651, 2002.

D. H. Hodges and G. A. Pierce, *Introduction to Structural Dynamics and Aeroelasticity*, 2nd edition, 2011.

J. M. Sater, C. R. Crowe, R. Antcliff, and A. Das, "An assessment of smart Air and space structures: demonstrations and technology," IDA Report P-3552, Log: H 00-002035, Institute for Defense Analysis, Alexandria, Va, USA, 2000.

M. R. M. C. Da Silva, "Non-linear flexural-flexural-torsional- extensional dynamics of beams-I. Formulation," *International Journal of Solids and Structures*, vol. 24, no. 12, pp. 1225–1234, 1988.

M. R. M. Crespo Da Silva and C. L. Zaretzky, "Nonlinear flexural-flexural-torsional interactions in beams including the effect of torsional dynamics. I: primary resonance,"

Nonlinear Dynamics, vol. 5, no. 1, pp. 3–23, 1994.

E. H. Dowell, "Damping in beams and plates due to slipping at the support boundaries," *Journal of Sound and Vibration*, vol. 105, no. 2, pp. 243–253, 1986.

D. H. Hodges and E. H. Dowell, "Nonlinear equations of motion for the elastic bending and torsion of twisted nonuniform rotor blades," NASA Technical Notes NASA TN D-7818, 1974.

D. S. Whithead, "The analysis of blade vibration due to random excitation," Tech. Rep. 3253, United Kingdom Ministry of Aviation: Aeronautical Research Council Reports and Memoranda, London, UK, 1960.

M. Aykan and M. Celik, "Vibration fatigue analysis and multi- axial effect in testing of aerospace structures," *Mechanical Systems and Signal Processing*, vol. 23, no. 3, pp. 897–907, 2009.

G. V. Chary, E. Habtour, and G. S. Drake, "Improving the reliability in the next generation of US army platforms through physics of failure analysis," *Journal of Failure Analysis and Prevention*, vol. 12, no. 1, pp. 75–58, 2012.

Y. Zhou, M. Al-Bassyiouni, and A. Dasgupta, "Vibration durability assessment of sn3.0ag0.5cu and sn37pb solders under harmonic excitation," *Journal of Electronic Packaging*, vol. 131, no. 1, 2009.

J. H. Lau, *Solder Joint Reliability, Theory and Applications*, Van Nostrand Reinhold, New York, NY, USA, 1990.

J. Lau, K. Gratalo, E. Schneider, T. Marcotte, and T. Baker, "Solder joint reliability of large plastic ball grid array assemblies under bending, twisting, and vibration conditions," *Circuit*

World, vol. 22, no. 1, pp. 27–32, 1995.

J. H. Lau and P. Yi, *Solder Joint Reliability, of BGA, CSP, Flip Chip and Fine Pitch SMT Assemblies*, McGraw-Hill, New York, NY, USA, 1997.

X. Liu, V. K. Sooklal, M. A. Verges, and M. C. Larson, "Experimental study and life prediction on high cycle vibration fatigue in BGA packages," *Microelectronics Reliability*, vol. 46, no. 7, pp. 1128–1138, 2006.

X. Yang, Y. Luo, and Q. Gao, "Constitutive modeling on time-dependent deformation behavior of 96.5Sn-3.5Ag solder alloy under cyclic multiaxial straining," *Journal of Electronic Packaging*, vol. 129, no. 1, pp. 41–47, 2007.

Y. Zhou, M. Al-Bassyiouni, and A. Dasgupta, "Harmonic and random vibration durability of SAC305 and Sn37Pb solder alloys," *IEEE Transactions on Components and Packaging Technologies*, vol. 33, no. 2, pp. 319–328, 2010.

J. Gu, D. Barker, and M. Pecht, "Prognostics implementation of electronics under vibration loading," *Microelectronics Reliability*, vol. 47, no. 12, pp. 1849–1856, 2007.

D. B. Barker, Y. S. Chen, and A. Dasgupta, "Estimating the vibration fatigue life of quad leaded surface mount components," *Journal of Electronic Packaging*, vol. 115, no. 2, pp. 195–200, 1993.

R. S. Li, "A methodology for fatigue prediction of electronic components under random vibration load," *Journal of Electronic Packaging*, vol. 123, no. 4, pp. 394–400, 2001.

E. Martynenko, W. Zhou, A. Chudnovsky, R. S. Li, and L. Poglitsch, "High cycle fatigue resistance and reliability assessment of flexible printed circuitry," *Journal of Electronic Packaging*, vol. 124, no. 3, pp. 254–259, 2002.

S. Mathew, D. Das, M. Osterman, M. Pecht, R. Ferebee, and J. Clayton, "Virtual remaining life assessment of electronic hardware subjected to shock and random vibration life cycle loads," *Journal of the Institute of Environmental Sciences and Technology*, vol. 50, no. 1, pp. 86–97, 2007.

S. Shetty, V. Lehtinen, A. Dasgupta, V. Halkola, and T. Reinikainen, "Fatigue of chip scale package interconnects due to cyclic bending," *Journal of Electronic Packaging*, vol. 123, no. 3, pp. 302–308, 2001.

M. Ernst, C. Choi, A. Dasgupta, and E. Habtour, "Physics of failure models for multiaxial vibration fatigue in electronics assemblies," in *Proceedings of the Accelerated Stress Testing and Reliability Workshop*, Ontario, Canada, 2012.

A. C. Eringen, "Response of beams and to random loads," *Journal of Applied Mechanics*, vol. 24, pp. 46–52, 1957.

R. E. Herbert, "Random vibrations of a nonlinear elastic beam," *Journal of the Acoustical Society of America*, vol. 36, no. 11, pp. 2090–2094, 1964.

I. Elishakoff and D. Livshits, "Some closed-form solutions in random vibration of Bernoulli-Euler beams," *International Journal of Engineering Science*, vol. 22, no. 11-12, pp. 1291–1301, 1984.

I. Elishakoff, J. Fang, and R. Caimi, "Random vibration of a nonlinearly deformed beam by a new stochastic linearization technique," *International Journal of Solids and Structures*, vol. 32, no. 11, pp. 1571–1584, 1995.

R. A. I. brahimand, R. J. Somnay, "Nonlinear dynamic analysis of an elastic beam isolator sliding on frictional supports," *Journal of Sound and Vibration*, vol. 308, no. 3–5, pp. 735–

757, 2007.

C.-H. Ho, R. A. Scott, and J. G. Eisley, "Non-planar, non-linear oscillations of a beam-I. Forced motions," *International Journal of Non-Linear Mechanics*, vol. 10, no. 2, pp. 113–127, 1975.

C.-H. Ho, R. A. Scott, and J. G. Eisley, "Non-planar, non-linear oscillations of a beam II. Free motions," *Journal of Sound and Vibration*, vol. 47, no. 3, pp. 333–339, 1976.

M. R. M. Crespo da Silva and C. C. Glynn, "Nonlinear flexural-flexural-torsional dynamics of inextensional beams. I: equations of motion," *Journal of Structural Mechanics*, vol. 6, no. 4, pp. 437–448, 1978.

M. R. M. Crespo de Silva and C. C. Glynn, "Nonlinear flexural- flexural-torsional dynamics of inextensional beams. II: forced motions," *Journal of Structural Mechanics*, vol. 6, no. 4, pp. 449– 461, 1978.

M. R. M. C. Da Silva, "Non-linear flexural-flexural-torsional- extensional dynamics of beams-II. Response analysis," *International Journal of Solids and Structures*, vol. 24, no. 12, pp. 1235– 1242, 1988.

A. H. Nayfeh and P. F. Pai, "Non-linear non-planar parametric responses of an inextensional beam," *International Journal of Non-Linear Mechanics*, vol. 24, no. 2, pp. 139–158, 1989.

P. F. Pai and A. H. Nayfeh, "Non-linear non-planar oscillations of a cantilever beam under lateral base excitations," *International Journal of Non-Linear Mechanics*, vol. 25, no. 5, pp. 455– 474, 1990.

C. L. Zaretzky and M. R. M. Crespo da Silva, "Nonlinear flexural-flexural-torsional interactions in beams including the effect of torsional dynamics. II: combination resonance,"

Non- linear Dynamics, vol. 5, no. 2, pp. 161–180, 1994.

H. N. Arafat, A. H. Nayfeh, and C.-M. Chin, "Nonlinear non- planar dynamics of parametrically excited cantilever beams," *Nonlinear Dynamics*, vol. 15, no. 1, pp. 31–61, 1998.

A. H. Nayfeh and H. N. Arafat, "Investigation of subcombination internal resonances in cantilever beams," *Shock and Vibration*, vol. 5, pp. 289–296, 1998.

A. H. Nayfeh and H. N. Arafat, "Nonlinear response of cantilever beams to combination and subcombination resonances," *Shock and Vibration*, vol. 5, no. 5-6, pp. 277–288, 1998.

H. N. Arafat, *Nonlinear Dynamic Analysis of Cantilever Beam [Ph.D. thesis]*, Virginia Polytechnic Institute and State University, Blacksburg, Va, USA, 1999.

J. R. Banerjee, "Explicit analytical expressions for frequency equation and mode shapes of composite beams," *International Journal of Solids and Structures*, vol. 38, no. 14, pp. 2415–2426, 2001.

P. Malatkar and A. H. Nayfeh, "On the transfer of energy between widely spaced modes in structures," *Nonlinear Dynamics*, vol. 31, no. 2, pp. 225–242, 2003.

P. Malatkar, and A. H. Nayfeh, "A parametric identification technique for single-degree-of-freedom weakly nonlinear systems with cubic nonlinearities," *Journal of Vibration and Control*, vol. 9, no. 3-4, pp. 317–336, 2003.

P. Malatkar, *Nonlinear Vibrations of Cantilever Beams and Plates [Ph.D. thesis]*, Virginia Polytechnic Institute and State University, Blacksburg, Va, USA, 2003.

T. J. Anderson, B. Balachandran, and A. H. Nayfeh, "Nonlinear resonances in a flexible cantilever beam," *Journal of Vibration and Acoustics*, vol. 116, no. 4, pp. 480–484, 1994.

J. Dugundji, and V. Mukhopadhyay, “Lateral bending-torsion vibrations of a thin beam under parametric excitation,” *Journal of Applied Mechanics*, vol. 40, no. 3, pp. 693–698, 1973.

D. M. Tang and E. H. Dowell, “Damping in beams and plates due to slipping at the support boundaries. Part 2: numerical and experimental study,” *Journal of Sound and Vibration*, vol. 108, no. 3, pp. 509–522, 1986.

C. W. S. To, “Vibration of a cantilever beam with a base excitation and tip mass,” *Journal of Sound and Vibration*, vol. 83, no. 4, pp. 445–460, 1982.

M. P. Cartmell and J. W. Roberts, “Simultaneous combination resonances in a parametrically excited cantilever beam,” *Strain*, vol. 23, no. 3, pp. 117–126, 1987.

B. Balachandran and A. H. Nayfeh, “Nonlinear motions of beam-mass structure,” *Nonlinear Dynamics*, vol. 1, no. 1, pp. 39– 61, 1990.

B. Balachandran, and A. H. Nayfeh, “Observations of modal interactions in resonantly forced beam-mass structures,” *Nonlinear Dynamics*, vol. 2, no. 2, pp. 77–117, 1991.

J. W. Jaworski, and E. H. Dowell, “Free vibration of a cantilevered beam with multiple steps: comparison of several theoretical methods with experiment,” *Journal of Sound and Vibration*, vol. 312, no. 4-5, pp. 713–725, 2008.

M. Ansari, E. Esmailzadeh, and N. Jalili, “Coupled vibration and parameter sensitivity analysis of rocking-mass vibrating gyroscopes,” *Journal of Sound and Vibration*, vol. 327, no. 3–5, pp. 564–583, 2009.

A. M. Wickenheiser, “Design optimization of linear and non- linear cantilevered energy harvesters for broadband vibrations,” *Journal of Intelligent Material Systems and Structures*, vol. 22, no. 11, pp. 1213–1225, 2011.

M. Ansari, E. Esmailzadeh, and N. Jalili, “Exact frequency analysis of a rotating cantilever beam with tip mass subjected to torsional-bending vibrations,” *Journal of Vibration and Acoustics*, vol. 133, no. 4, Article ID 041003, 2011.

A. Erturk and D. J. Inman, “Parameter identification and optimization in piezoelectric energy harvesting: analytical relations, asymptotic analyses, and experimental validations,” *Proceedings of the Institution of Mechanical Engineers. Part I: Journal of Systems and Control Engineering*, vol. 225, no. 4, pp. 485–496, 2011.

A. Erturk, “Assumed-modes modeling of piezoelectric energy harvesters: Euler-Bernoulli, Rayleigh, and Timoshenko models with axial deformations,” *Computers and Structures*, vol. 106- 107, pp. 214–227, 2012.

M. Esmaeili, N. Jalili, and M. Durali, “Dynamic modeling and performance evaluation of a vibrating beam microgyroscope under general support motion,” *Journal of Sound and Vibration*, vol. 301, no. 1-2, pp. 146–164, 2007.

S. C. Stanton, C. C. McGehee, and B. P. Mann, “Nonlinear dynamics for broadband energy harvesting: investigation of a bistable piezoelectric inertial generator,” *Physica D: Nonlinear Phenomena*, vol. 239, no. 10, pp. 640–653, 2010.

C. P. Green and J. E. Sader, “Torsional frequency response of cantilever beams immersed in viscous fluids with applications to the atomic force microscope,” *Journal of Applied Physics*, vol. 92, no. 10, pp. 6262–6274, 2002.

S. C. Stanton, A. Erturk, B. P. Mann, E. H. Dowell, and D. J. Inman, “Nonlinear nonconservative behavior and modeling of piezoelectric energy harvesters including proof mass effects,” *Journal of Intelligent Material Systems and Structures*, vol. 23, no. 2, pp. 183–

199, 2012.

S. C. Stanton, B. A. M. Owens, and B. P. Mann, “Harmonic balance analysis of the bistable piezoelectric inertial generator,” *Journal of Sound and Vibration*, vol. 331, no. 15, pp. 3617–3627, 2012.

H. J. R. Westra, D. M. Karabacak, S. H. Brongersma, M. Crego- Calama, H. S. J. Van Der Zant, and W. J. Venstra, “Interactions between directly- and parametrically-driven vibration modes in a micromechanical resonator,” *Physical Review B: Condensed Matter and Materials Physics*, vol. 84, no. 13, Article ID 134305, 2011.

K. Wolf, and O. Gottlieb, “Nonlinear dynamics of a cantilever beam actuated by piezoelectric layers in symmetric and asymmetric configuration,” Tech. Rep. ETR-2001-02, Institute of Technology, Haifa, Israel, 2001.

V. Kumar, J. K. Miller, and J. F. Rhoads, “Nonlinear parametric amplification and attenuation in a base-excited cantilever beam,” *Journal of Sound and Vibration*, vol. 330, no. 22, pp. 5401– 5409, 2011.

J. F. Rhoads, N. J. Miller, S. W. Shaw, and B. F. Feeny, “Mechanical domain parametric amplification,” *Journal of Vibration and Acoustics*, vol. 130, no. 6, Article ID 061006, 2008.

S. F. Ali, S. Adhikari, M. I. Friswell, and S. Narayanan, “The analysis of piezomagnetoelastic energy harvesters under broadband random excitations,” *Journal of Applied Physics*, vol. 109, no. 7, Article ID 074904, 2011.

G. Wu, H. J., K. Hansen et al., “Origin of nanomechanical cantilever motion generated from biomolecular interactions,” *Proceedings of the National Academy of Sciences of the United States of America*, vol. 98, no. 4, pp. 1560–1564, 2001.

K. S. Hwang, J. H. Lee, J. Park, D. S. Yoon, J. H. Park, and T. S. Kim, "In-situ quantitative analysis of a prostate-specific antigen (PSA) using a nanomechanical PZT cantilever," *Lab on a Chip: Miniaturisation for Chemistry and Biology*, vol. 4, no. 6, pp. 547– 552, 2004.

J. Dorignac, A. Kalinowski, S. Erramilli, and P. Mohanty, "Dynamical response of nanomechanical oscillators in immiscible viscous fluid for in Vitro biomolecular Recognition," *Physical Review Letters*, vol. 96, no. 18, Article ID 186105, 2006.

A. Salehi-Khojin, S. Bashash, and N. Jalili, "Modeling and experimental vibration analysis of nanomechanical cantilever active probes," *Journal of Micromechanics and Microengineering*, vol. 18, no. 8, Article ID 085008, 2008.

V. Seena, A. Fernandes, P. Pant, S. Mukherji, and V. R. Rao, "Polymer nanocomposite nanomechanical cantilever sensors: material characterization, device development and application in explosive vapour detection," *Nanotechnology*, vol. 22, no. 29, Article ID 295501, 2011.

S. Suresh, *Fatigue of Materials*, Cambridge University Press, Cambridge, UK, 2nd edition, 1998.

D. Segalman, G. Reese, R. Field Jr., and C. Fulcher, "Estimating the probability distribution of von Mises stress for structures undergoing random excitation," *Journal of Vibration and Acoustics*, vol. 122, no. 1, pp. 42–48, 2000.

S. Sarkani, D. P. Kihl, and J. E. Beach, "Fatigue of welded joints under narrowband non-Gaussian loadings," *Probabilistic Engineering Mechanics*, vol. 9, no. 3, pp. 179–190, 1994.

D. Radaj, C. M. Sonsino, and W. Fricke, *Fatigue Assessment of Welded Joints By Local Approaches*, Woodhead Publishing Limited, Cambridge, UK, 2006.

A.Z. Palmgren,“Die Lebensdauer VonKugellagern,” *Zeitschriyt Des Vereines Der Deutschen Ingenioeren*, vol. 68, pp. 339–341, 1924.

M. A. Miner, “Cumulative damage in fatigue,” *Journal of Applied Mechanics*, vol. 12, no. 3, pp. 159–164, 1945.

J. W. Miles, “On structural fatigue under random loading,” *Journal of the Aeronautical Sciences*, vol. 21, no. 11, pp. 753–762, 1957.

S. H. Crandall, “Zero crossings, peaks, and other statistical measures of random responses,” *Journal of the Acoustical Society of America*, vol. 35, no. 11, pp. 1693–1699, 1963.

Y. K. Lin, “Probability distributions of stress peaks in linear and nonlinear structures,” *AIAA Journal*, vol. 1, no. 5, pp. 1133–1138, 1963.

J. S. Bendat, “Probability functions for random responses- prediction of peaks, fatigue damage, and catastrophic failures,” NASA CR-33, N64-17990, 1964.

S. O. Rice, “Mathematical analysis of random noise,” Selected Chapters on Noise and Stochastic Processes, Dover, New York, NY, USA, 1954.

N. W. M. Bishop, *The Use of Frequency Domain Parameters to Predict Structural Fatigue [Ph.D. thesis]*, University of Warwick, 1988.

N. W. M. Bishop and F. Sherratt, “Theoretical solution for the estimation of “rainflow” ranges from power spectral density data,” *Fatigue and Fracture of Engineering Materials and Structures*, vol. 13, no. 4, pp. 311–326, 1990.

K. Upadhyayula, and A. Dasgupta, “Physics-of-failure guidelines for accelerated qualification of electronic systems,” *Quality and Reliability Engineering International*, vol. 14, no. 6, pp. 433-447, 1998.

E. Habtour, M. Paulus, and A. Dasgupta, "Modeling approach for predicting the rate of frequency change of notched beam exposed to Gaussian random excitation," *Shock and Vibration*, 2013.

Y. Lu, *Random Vibration Analysis of Higher-Order Nonlinear Beams and Composite Plates with Applications of ARMA Models [Ph.D. thesis]*, Virginia Polytechnic Institute and State University, Blacksburg, Va, USA, 2008.

T. Łagoda, E. Macha, and A. Niesłony, "Fatigue life calculation by means of the cycle counting and spectral methods under multiaxial random loading," *Fatigue and Fracture of Engineering Materials and Structures*, vol. 28, no. 4, pp. 409–420, 2005.

X. Pitoiset and A. Preumont, "Spectral methods for multiaxial random fatigue analysis of metallic structures," *International Journal of Fatigue*, vol. 22, no. 7, pp. 541-550, 2000.

X. Pitoiset, I. Rychlik, and A. Preumont, "Spectral methods to estimate local multiaxial fatigue failure for structures under- going random vibrations," *Fatigue and Fracture of Engineering Materials and Structures*, vol. 24, no. 11, pp. 715–727, 2001.

A. Carpinteri, E. Macha, R. Brighenti, and A. Spagnoli, "Expected principal stress directions under multiaxial random loading. Part I: theoretical aspects of the weight function method," *International Journal of Fatigue*, vol. 21, no. 1, pp. 83– 88, 1999.

A. Carpinteri, R. Brighenti, E. Macha, and A. Spagnoli, "Expected principal stress directions under multiaxial random loading. Part II: numerical simulation and experimental assessment through the weight function method," *International Journal of Fatigue*, vol. 21, no. 1, pp. 89–96, 1999.

Y. Liu and S. Mahadevan, "A unified multiaxial fatigue damage model for isotropic and

anisotropic materials," *International Journal of Fatigue*, vol. 29, no. 2, pp. 347–359, 2007.

Y. Liu, *Stochastic Modeling of Multiaxial Fatigue and Fracture [Ph.D. thesis]*, Vanderbilt University, Nashville, Tn, USA, 2006.

S. Lambert, E. Pagnacco, and L. Khalij, "A probabilistic model for the fatigue reliability of structures under random loadings with phase shift effects," *International Journal of Fatigue*, vol. 32, no. 2, pp. 463–474, 2010.

C. Braccesi, F. Cianetti, G. Lori, and D. Pioli, "An equivalent uniaxial stress process for fatigue life estimation of mechanical components under multiaxial stress conditions," *International Journal of Fatigue*, vol. 30, no. 8, pp. 1479–1497, 2008.

C. Braccesi, F. Cianetti, G. Lori, and D. Pioli, "The frequency domain approach in virtual fatigue estimation of non-linear systems: the problem of non-Gaussian states of stress," *International Journal of Fatigue*, vol. 31, no. 4, pp. 766–775, 2008.

G. Allegri and X. Zhang, "On the inverse power laws for accelerated random fatigue testing," *International Journal of Fatigue*, vol. 30, no. 6, pp. 967–977, 2008.

Z. Lei and C. Qiu, "A dynamic stochastic finite element method based on dynamic constraint mode," *Computer Methods in Applied Mechanics and Engineering*, vol. 161, no. 3-4, pp. 245– 255, 1998.

S. I. McNeill, "A method for determining the fatigue critical plane for biaxial random vibration in the frequency domain: technical Note," *Fatigue and Fracture of Engineering Materials and Structures*, vol. 33, no. 6, pp. 390–394, 2010.

T. Lagoda, E. Macha, and W. Bedkowski, "Critical plane approach based on energy concepts: application to biaxial random tension-compression high-cycle fatigue regime,"

Inter- national Journal of Fatigue, vol. 21, no. 5, pp. 431–443, 1999.

P. A. Tibbits, "Application of algorithms for percentiles of von Mises stress from combined random vibration and static loadings," *Journal of Vibration and Acoustics*, vol. 133, no. 4, Article ID 044502, 2011.

H. Guechichi, S. Benkabouche, A. Amrouche, and M. Benkhettab, "A high fatigue life prediction methodology under constant amplitude multiaxial proportional loadings," *Materials Science and Engineering A*, vol. 528, no. 13-14, pp. 4789–4798, 2011.

D. Gregory, F. Bitsy, and D. O. Smallwood, "Comparison of the response of a simple structure to single axis and multiple axis random vibration inputs," in *Proceedings of the 79th Shock and Vibration Symposium*, Orlando, Fl, USA, 2008.

U. Fullekrug, "Utilization of multi-axial shaking tables for the modal identification of structures," *Philosophical Transactions of the Royal Society A: Mathematical, Physical and Engineering Sciences*, vol. 359, no. 1786, pp. 1753-1770, 2001.

D. E. Newland, *An Introduction to Random Vibrations, Spectral and Wavelet Analysis*, Dover, Mineola, NY, USA, 2005.

T. Dahlberg, "The effect of modal coupling in random vibration analysis," *Journal of Sound and Vibration*, vol. 228, no. 1, pp. 157-176, 1999.

E. Habtour, M. Pohland, and A. Dasgupta, "Dynamic characterization of circuit card assemblies using multi-degree-of- freedom random vibration," in *Proceedings of the Accelerated Stress Testing and Reliability Workshop*, San Francisco, Ca, USA, 2011.

L. Meirovitch, *Principles and Techniques of Vibrations*, Prentice Hall, Upper Saddel River, NJ, USA, 1997.

M. Cesnik, J. Slavic, and M. Boltezar, “Uninterrupted and accelerated vibrational fatigue testing with simultaneous monitoring of the natural frequency and damping,” *Journal of Sound and Vibration*, vol. 331, pp. 5370-5382, 2012.

A. Perkins, and S. K. Sitaraman, “Analysis and prediction of vibration-induced solder joint failure for a ceramic column grid array package,” *Journal of Electronic Packaging*, vol. 130, no. 1, 2008.

C. Rainieri, G. Fabbrocino, and E. Cosenza, “Near real-time tracking of dynamic properties for standalone structural health monitoring systems,” *Mechanical Systems and Signal Processing*, vol. 25, no. 8, pp. 3010-3026, 2011.

R.-J. Wang and D.-G. Shang, “Fatigue life prediction based on natural frequency changes for spot welds under random loading,” *International Journal of Fatigue*, vol. 31, no. 2, pp. 361-366, 2009.

Y. J. Yan, L. Cheng, Z. Y. Wu, and L. H. Yam, “Development in vibration-based structural damage detection technique,” *Mechanical Systems and Signal Processing*, vol. 21, no. 5, pp. 2198-2211, 2007.

Dixon, M. C. The Maintenance Costs of Aging Aircraft: Insights from Commercial Aviation, Rand Publishing, Arlington, VA, 2006.

Dimarogonas, Andrew D. "Vibration of Cracked Structures: A State of the Art Review." *Engineering Fracture Mechanics* 55.5 (1996): 831-57.

Doebling, S. W., Farrar, C. R., Prime, M. B., and Shevitz, D. W., "Damage Identification and Health Monitoring of Structural and Mechanical Systems from Changes in their Vibration Characteristics: A Literature Review, Los Alamos National Laboratory report LA-13070-

MS, 1996.

Zwink, B. R. "Nondestructive Evaluation of Composite Material Damage Using Vibration Reciprocity Measurements." *Journal of Vibration and Acoustics* 134.4 (2012): 041013-1-41013-8.

Wang, D., Q. Maio, Q. Zhou, and G. Zhou. "An Intelligent Prognostic System for Gear Performance Degradation Assessment and Remaining Useful Life Estimation." *Journal of Vibration and Acoustics* 137.2 (2015): 021004-1-21004-12.

Staszewski, W. J., C. Boller, and Geoffrey R. Tomlinson. *Health Monitoring of Aerospace Structures: Smart Sensor Technologies and Signal Processing*. West Sussex, England: Hoboken, NJ, 2004.

Farrar, C. R., and K. Worden. *Structural Health Monitoring: A Machine Learning Perspective*. Chichester, West Sussex, U.K.: Wiley, 2013.

Worden, K., and Geoffrey R. Tomlinson. *Nonlinearity in Structural Dynamics: Detection, Identification, and Modelling*. Bristol: Institute of Physics, 2001.

Habtour, E., C. Choi, M. Osterman, and A. Dasgupta. "Novel Approach to Improve Electronics Reliability in the Next Generation of US Army Small Unmanned Ground Vehicles Under Complex Vibration Conditions." *Journal of Failure Analysis and Prevention* 12.1 (2012): 86-95.

Salawu, O. S., 1997a, “Detection of Structural Damage Through Changes in Frequency: A Review,” *Engineering Structures*, Vol. 19, No. 9, pp. 718-723.

Sun, Z., B. Rocha, K. Wu, and N. Mrad. "A Methodological Review of Piezoelectric Based Acoustic Wave Generation and Detection Techniques for Structural Health Monitoring."

International Journal of Aerospace Engineering 2013 (2013): 1-22.

Venstra, W. J., H. J. R. Westra, and H. S. J. Van Der Zan. "Mechanical Stiffening, Bistability, and Bit Operations in a Microcantilever." *Applied Physics Letters* 97.12 (2010): 193107.

Kacem, N., J. Arcamone, F. Perez-Murano, and S. Hentz. "Dynamic Range Enhancement of Nonlinear Nanomechanical Resonant Cantilevers for Highly Sensitive NEMS Gas/mass Sensor Applications." *Journal of Micromechanics and Microengineering* 20.4 (2010): 045023.

Dowell, E. "Damping in Beams and Plates Due to Slipping at the Support Boundaries." *Journal of Sound and Vibration* 105.2 (1986): 243-53.

Habtour, E., W. Connon, M. F. Pohland, S. C. Stanton, and M. Paulus. "Review of Response and Damage of Linear and Nonlinear Systems under Multiaxial Vibration." *Shock and Vibration*, vol. 2014, Article ID 294271, 2014-a. doi:10.1155/2014/294271.

Zaitsev, S., A. K. Pandey, O. Shtempluck, and E. Buks. "Forced and Self-excited Oscillations of an Optomechanical Cavity." *Physical Review E* 84 (2011): 046605.

Crespo Da Silva, M. R. M. and C. L. Zaretzky. "Nonlinear Flexural-Flexural-Torsional Interactions in Beams Including the Effect of Torsional Dynamics. I: Primary Resonance." *Nonlinear Dynamics* 5.1 (1994): 3-23.

Glaz, B., Friedmann, P. P., and Liu, L., "Vibration Reduction and Performance Enhancement of Helicopter Rotors Using an Active/Passive Approach," AIAA Chapter 2008-2178, Proceedings of the 49thAIAA/ASME/ ASCHE/AHS/ASC Structures, Structural Dynamics & Materials Conference, Schaumburg, IL, April 2008.

Lifshitz, R., M. C. Cross. “Nonlinear Dynamics of Nanomechanical and Micromechanical Resonators.” edited by: Schuster, H. G. *Reviews of Nonlinear Dynamics and Complexity.* Vol. I. Weinheim: Wiley-VCH, 2008.

Lifshitz, R., E. Kenig, and M. C. Cross. "Collective Dynamics in Arrays of Coupled Nonlinear Resonators." edited by: Dykman, M. I. *Fluctuating Nonlinear Oscillators: From Nanomechanics to Quantum Superconducting Circuits*. Oxford: Oxford UP, 2012.

Glaz, B., Friedmann, P. P., Liu, L., Kumar, D., and Cesnik, C. E. S., "The AVINOR Aeroelastic Simulation Code and its Application to Reduced Vibration Composite Rotor Blade Design," AIAA Chapter 2009-2601, Proceedings of the 50th AIAA/ASME/ASCHE/AHS/ASC Structures, Structural Dynamics & Materials Conference, Palm Springs, CA, May 2009.

Jordan, D. W., and P. Smith. *Nonlinear Ordinary Differential Equations: An Introduction for Scientists and Engineers*. 4th ed. Oxford England: Oxford UP, 2007.

Ismail, F., A. Ibrahim, and H.R. Martin. "Identification of Fatigue Cracks from Vibration Testing." *Journal of Sound and Vibration* 140.2 (1990): 305-17.

Hollkamp, J. J., R. W. Gordon, and S. M. Spottswood. "Nonlinear Modal Models for Sonic Fatigue Response Prediction: A Comparison of Methods." *Journal of Sound and Vibration* 284.3-5 (2005): 1145-163.

Chondros, T. G., A. D. Dimarogonas, and J. Yao. "Vibration Of A Beam With A Breathing Crack." *Journal of Sound and Vibration* 239.1 (2001): 57-67.

Shen, M. H., and Y. C. Chu. "Vibrations of Beams with a Fatigue Crack." *Computers & Structures* 45.1 (1992): 79-93.

Ruotolo, R., C. Surace, P. Crespo, and D. Storer. "Harmonic Analysis of the Vibrations of a Cantilevered Beam with a Closing Crack." *Computers & Structures* 61.6 (1996): 1057-074.

Tsyfansky, S.l., and V.I. Beresnevich. "Non-Linear Vibration Method For Detection Of Fatigue Cracks In Aircraft Wings." *Journal of Sound and Vibration* 236.1 (2000): 49-60.

Pugno, N., C. Surace, and R. Ruotolo. "Evaluation Of The Non-Linear Dynamic Response To Harmonic Excitation Of A Beam With Several Breathing Cracks." *Journal of Sound and Vibration* 235.5 (2000): 749-62.

Saavedra, P. N., and L. A. Cuitino. "Crack Detection and Vibration Behavior of Cracked Beams." *Computers & Structures* 79.16 (2001): 1451-459.

Loutridis, S., E. Douka, and L. J. Hadjileontiadis. "Forced Vibration Behaviour and Crack Detection of Cracked Beams Using Instantaneous Frequency." *NDT & E International* 38.5 (2005): 411-19.

Ihn, J. B., and F. Chang. "Detection and Monitoring of Hidden Fatigue Crack Growth Using a Built-in Piezoelectric Sensor/actuator Network: I. Diagnostics." *Smart Materials and Structures* 13.3 (2004): 609-20.

Ryles, M., F. H. Ngau, I. Mcdonald, and W. J. Staszewski. "Comparative Study of Nonlinear Acoustic and Lamb Wave Techniques for Fatigue Crack Detection in Metallic Structures." *Fatigue & Fracture of Engineering Materials & Structures* 31.8 (2008): 674-83.

Priya S, Viehland D, Carazo A. High-power reso- nant measurements of piezoelectric materials: importance of elastic nonlinearities. Journal of Applied Physics 90.3 (2001): 1469–1479.

Yu S, He S and Li W. Theoretical and experimental studies of beam bimorph piezoelectric

power harvesters. Journal of Mechanics and Materials of Structures 5.3 (2010): 427–445.

Nayfeh, A. H., and P. F. Pai. *Linear and Nonlinear Structural Mechanics*. Hoboken, NJ: Wiley-Interscience, 2004.

Zavodney, L. D., and A. H. Nayfeh. "The Non-linear Response of a Slender Beam Carrying a Lumped Mass to a Principal Parametric Excitation: Theory and Experiment." *International Journal of Non-Linear Mechanics* 24.2 (1989): 105-25.

Meirovitch, L. *Fundamentals of Vibrations*. Boston: McGraw-Hill, 2001.

Hsiao, K.m., and R.t. Yang. "Effect Of Member Initial Curvature On A Flexible Mechanism Response." *Journal of Sound and Vibration* 190.2 (1996): 177-94.

Oliver, W. C., and G. M. Pharr. “An improved technique for determining hardness and elastic modulus using load and displacement sensing indentation experiments.” *Journal of Materials Research*, Vol. 7, No. 6 (1992): 1564-83.

Taylor, M. D., K. S. Choi, X. Sun, D. K. Matlock, C. E. Packard, L. Xu, F. Barlat. “Correlations between nanoindentation hardness and macroscopic mechanical properties in DP980 steels.” *Materials Science & Engineering A*. Vol. 597 (2014): 431-39.

Saha, R., and W. D. Nix. “Effects of the substrate on the determination of thin film mechanical properties by nanoindentation.” *Acta Materialia* 50 (2002): 23-38.

Gregory, J. R., and S. M. Spearing. “Nanoindentation of neat and *in situ* polymers in polymer-matrix composites.” *Composites Science and Technology 65.3-4* (2005): 595-607.

Gershon, A. L., D. P. Cole, A. K. Kota, and H. A. Bruck. “Nanomechanical characterization of dispersion and its effects in nano-enhanced polymers and polymer composites.” *Journal of Materials Science* 45 (2010): 6353-6364.

Cole, D. P. and K. S. Strawhecker. “An improved instrumented indentation technique for single microfibers.” *Journal of Materials Research* 29.9 (2014): 1104-1112.

Cole, D. P., A. L. M. Reddy, M. G. Hahm, R. McCotter, A. H. C. Hart, R. Vajtai, P. M. Ajayan, S. P. Karna, and M. L. Bundy. “Electromechanical properties of polymer electrolyte-based stretchable supercapacitors.” *Advanced Energy Materials* 4 (2014): 1300844.

Klesnil, M., and P. Lukáš. *Fatigue of Metallic Materials*. Amsterdam: Elsevier, 1992.

Kang, S.K., Y-S. Jung, B-G. Yoo, J-I. Jang, and Y-K. Lee. "Orientation-dependent Indentation Modulus and Yielding in a High Mn Twinning-induced Plasticity Steel." *Materials Science and Engineering: A* 532 (2012): 500-04.

Sangid, M. D. "The Physics of Fatigue Crack Initiation." *International Journal of Fatigue* 57 (2013): 58-72.

Cartmell, M. *Introduction to Linear, Parametric, and Nonlinear Vibrations*. London: Chapman and Hall, 1990.

Carrella, A., and D.J. Ewins. "Identifying and Quantifying Structural Nonlinearities in Engineering Applications from Measured Frequency Response Functions." *Mechanical Systems and Signal Processing* 25.3 (2011): 1011-027.

Dowell, E. "Damping in Beams and Plates Due to Slipping at the Support Boundaries." *Journal of Sound and Vibration* 105.2 (1986): 243-53.

Hodges,D. H., "Nonlinear Equations for Dynamics of Pre-twisted Beams Undergoing Small Strains and Large Rotations," NASA TP 2470, May 1985.

Chung, J., and H. H. Yoo. "Dynamic Analysis Of A Rotating Cantilever Beam By Using The Finite Element Method." *Journal of Sound and Vibration* 249.1 (2002): 147-64.

Bauchau, O. A., and Hong, C. H., "Finite Element Approach to Rotor Blade Modeling," *Journal of the American Helicopter Society,* Vol. 32, No. 1, 1987, pp. 60-67.

Hodges, D. H., "Review of Composite Rotor Blade Modeling," *AIAA Journal,* Vol.3, No. 82, 1990, p.561-565.

Yigit, A., R. Scott, and A. Galipulsoy. "Flexural Motion of a Radially Rotating Beam Attached to a Rigid Body." *Journal of Sound and Vibration* 121.2 (1988): 201-10.

Liao, C., and Y. Y. Dang. "Structural Characteristics of Spinning Pretwisted Orthotropic Beams." *Computers & Structures* 45.4 (1992): 715-31.

Chen, W. R. "On the Vibration and Stability of Spinning Axially Loaded Pre-twisted Timoshenko Beams." *Finite Elements in Analysis and Design* 46.11 (2010): 1037-047.

Smith, C., and H. Baruh. "Dominance of Stiffening Effects for Rotating Flexible Beams." *Journal of Guidance, Control, and Dynamics* 14.5 (1991): 1072-074.

Baruh, H. *Analytical Dynamics*. Boston, MA: WCB/McGraw-Hill, 1999.

Nayfeh, A. H. and D. T. Mook, *Nonlinear Oscillations,* Wiley-VCH, New York, 1995.

Cole, D. P., H. A. Bruck, and A. L. Roytburd. “Nanoindentation studies of graded shape memory alloy thin films processed using diffusion modification.” *Journal of Applied Physics* 103 (2008): 064315.

Cole, D. P., H. Jin, W. Lu, A. L. Roytburd, and H. A. Bruck. “Reversible nanoscale deformation in compositionally graded shape memory alloy films.” *Applied Physics Letters* 94 (2009): 193114.

Cole, D. P., Bruck, H. A., Roytburd, A. L., “Nanomechanical characterisation of graded NiTi

films fabricated through diffusion modification," *Strain* 45 (2009): 232-237.

Villarino de Castro, D. B., J. M. Ventura, C. O. F. T. Ruckert, D. Spinelli, W. W. B. Filho. "Influence of phosphorus content and quenching/tempering temperature on fracture toughness and fatigue life of SAE 5160 Steel." *Materials Research* 13(4) (2010): 445-455.

Mura, T. *Micromechanics of Defects in Solids*. The Hague: Nijhoff, 1982.

Charsley, P., and M.P.E. Desvaux. "The Behaviour of Copper-12% Aluminium under Simple Reversed Stresses." *Materials Science and Engineering,* 4.4 (1969): 211-20.

Tanaka, K., and T. Mura. "A Theory of Fatigue Crack Initiation at Inclusions." *Metallurgical Transactions A* 13.1 (1982): 117-23

Habtour, E., Cole, D. P., Riddick, J. C., Weiss, V., Robeson, Sridharan, R., and Dasgupta, A., "Detection of Fatigue Damage Precursor Using a Nonlinear Vibration Approach", *Journal of Structural Health Monitoring*, (under review).

Habtour, E., Cole, D., Sridharan, R., and Dasgupta, A., M., "Utilizing Nonlinear Dynamic Parameters and Micromechanics to Enhance Damage Precursor Detection", *10th International Workshop on Structural Health Monitoring (IWSHM) Proceedings,* Stanford, CA, September 1-3, 2015, (Accepted).

Wang, R. J., J. X. Li, Y. J. Su, L. J. Qiao, and A. A. Volinsky. "Changes of Work Function in Different Deformation Stage for 2205 Duplex Stainless Steel by SKPFM." *Procedia Materials Science* 3 (2014): 1736-741.

Habtour, E., Cole, D., and Dasgupta, A., "Local Mechanical Characterization of Structural Damage Precursor", *ASME 2015 Conference on Smart Materials, Adaptive Structures and*

Intelligent Systems (SMASIS2015) Proceedings, Colorado Springs, Colorado, September 21-23, 2015. (Accepted).

Paulus, M., "Limitations of the Power Spectral Density as An Indicator of Test Severity",

Stephens, R.I., A. Fatemi, R.R. Stephens and H.O. Fuchs, *Metal Fatigue in Engineering,* 2nd Edition, John Wiley and Sons, 2001.

Y. W. Kwon and J. H. Gordis, "Frequency Domain Structural Synthesis Applied to Quasi-Static Crack Growth Modeling", *Shock and Vibration*, 16, 2009, 637-646.

Ashcroft, I. A., V. V. Silberschmidt and B. Echard, "Crack Propagation in a Toughened Epoxy Adhesive under Repeated Impacts", *Shock and Vibration*, 18, 2011, 157-170.

Seweryn, A., "Brittle Fracture Criterion for Structures with Sharp Notches", *Engineering Fracture Mechanics*, 47, 1994, 673–681.

Standberg, M., "Fracture at V-Notches with Contained Plasticity", *Engineering Fracture Mechanics*, 69, 2002, 403–15.

Anderson, T. T., *Fracture Mechanics: Fundamental and Application*, 3rd Edition, CRC Press, Ann Arbor, 2004.

Tada, H., P. C. Paris and G. R. Irwin, *The Stress Analysis of Cracks Handbook*, 3rd Edition, ASME Press, John Wiley & Sons, New York, NY, 2000.

Quek S. S., and G. R. Liu, *Finite Element Method: A Practical Course*, Butterworth-Heinemann, Burlington, MA, 2003.

Broek, D., *Elementary Engineering Fracture Mechanics*, 4th Edition, Kluwer Academic Publishers, Netherlands, 1986.

Rice, J. R., "A Path Independent Integral and the Approximate Analysis of Strain Concentration by Notches and Cracks", *Journal of Applied Mechanics*, 35, 1968, 379-386.

Jenssen, M., J. Zuidema and R. J. H. Wanhill, *Fracture Mechanics*, 2nd Edition, VSSD, Delft, Netherlands, 2006.

Nikishkov, G. P., and S. N. Atluri, "Calculation of Fracture Mechanics Parameters for an Arbitrary Three-Dimensional Crack, By the Equivalent Domain Integral Method", International Journal for Numerical Methods in Engineering, 24, 1987, 1801-1821.

Irvine, T., "Optimal Use of the Vibration Response Spectrum for Enveloping Random Data", *Institute of Environmental Sciences and Technology Proceedings*, 1999.

Moes, N., A. Gravouil and T. Belytschko, "Non-planar 3D Crack Growth by the Extended Finite element and level sets—Part I: Mechanical model", *International Journal for Numerical Methods in Engineering*, 53, 2002, 2549-2568.